Interactions of imidazole derived urea compounds and their transition metal complexes with selected anions

Maya Asyikin Mohamad Arif

Department of Chemistry
Durham University
2019

This dissertation is submitted in partial fulfilment of the requirements for the degree of

Doctor of Philosophy

Interactions of imidazole derived urea compounds and their transition metal complexes with selected anions

Maya Asyikin Mohamad Arif, Durham University

Abstract

Anions play important roles in various chemical, biological and environmental processes, hence there is a significant interest in designing artificial anion receptors that can bind or sense anions. In this study, a range of anion receptor compounds derived from imidazole ureas has been synthesised using organic (triethylbenzene and mesitylcalixarene) and metal-organic (Ru(II), Pt(II) and Pd(II)) scaffolds and ^{1}H NMR spectroscopy was used extensively to assess the anion binding and self-assembly properties of the receptor compounds.

The cation and anion binding properties of the free imidazole urea ligands using different types of transition metals as well as anions is discussed in Chapter 2. The imidazole urea compounds bind to transition metals namely Cu(II), Co(II) and Ni(II) in unidentate fashion and show hydrogen bonding interactions with the anions at the urea NH. The self-assembly properties of these imidazole urea compounds has been studied by gelation experiments in which silver(I) complexes of these ligands, particularly the silver(I) complex of an imidazole urea bearing a dodecyl terminal group can form a gel at 2% (w/v) due to the combination of hydrogen bonding, van der Waals and solvophobic interactions.

In Chapter 4, a new series of organic-based derivatives of these ligands have also been prepared using triethylbenzene and mesitylcalixarene scaffolds and they were found to show weak interactions with halide ions in a competitive solvent, DMSO and exhibit acid-base reactions with basic anions such as fluoride and acetate.

In Chapters 5 and 6, the synthesis of metal-based imidazole urea derivatives using ruthenium(II), platinum(II) and palladium(II) precursors is described. During the course of the experiments, a number of interesting, and in some cases, unexpected results were

found. Tripodal ruthenium(II)-based derivative in which the ruthenium(II) centre is linked to three imidazole urea ligands, have also been prepared and show interaction only with basic anions such as fluoride, acetate and benzoate. On the other hand, Pt(II) and Pd(II) complexes of imidazole ureas have shown a tendency to self-aggregate forming oligomers and also show interactions with basic anions such as fluoride and acetate through deprotonation.

Finally, although the anion binding and self-assembly properties of these receptors were not fully understood, it is suggested that the complex behaviour of these organic and metal-based derivatives could be due to the multiple intramolecular and intermolecular interactions of the molecule.

Table of contents

Abbreviations and Symbols

AFM	Atomic force microscopy
ADP	Adenosine diphosphate
AMP	Adenosine monophosphate
ATP	Adenosine triphosphate
CD_3CN	Deuterated acetonitrile
$CDCl_3$	Deuterated chloroform
CMP	Cytidine monophosphate
DFT	Density functional theory
DMSO	Dimethyl sulfoxide
DOSY	Diffusion-ordered Spectroscopy
Dppe	1,2-bis(diphenylphosphino)ethane
ESI-MS	Electrospray ionisation mass spectrometry
ESIPT	Excited-stated intramolecular proton transfer
FT-IR	Fourier-transfer infrared spectroscopy
GMP	Guanosine monophosphate
GTP	Guanosine triphosphate
HRMS	High resolution mass spectrometry
LMWG	Low-molecular-weight gelator
MeOH-d_4	Deuterated methanol
MLCT/LMCT	Metal-ligand charge transfer/ Ligand-metal charge transfer
NMR	Nuclear magnetic resonance
SC-XRD	Single-crystal X-ray diffraction
SEM	Scanning electron microscopy
TEM	Transmission electron microscopy
UV-vis	Ultraviolet-visible spectroscopy
VT	Variable temperature
XB	Halogen bonding
$H_2PO_4^-$	Dihydrogen phosphate

$H_4P_2O_7$	Pyrophosphoric Acid
NH_4PF_6	Ammonium hexafluorophosphate
mV	milivolt
G'*, *G"	Storage and loss moduli
ppm	Part per million
TBA	tetrabutylammonium

List of Figures

List of Tables and Schemes

Statement of copyright

Declaration

This work has not been submitted in substance for any other degree or award at this or any other university or place of learning, nor is being submitted concurrently in candidature for any degree or other award. Crystallographic data for structures **2.1, 2.4, 2.6, 2.7, 2.9, 2.10 and 2.11** were collected and processed by Dr Dmitry Yufit. DOSY NMR, Solid-state NMR and TEM were performed by Dr Juan Aguilar Malavia, Dr David Apperley and Dr Budhika Mendis, respectively. All other results are the product of independent work and investigation by the author.

Acknowledgements

First and foremost, I would like to thank my supervisor, Professor Jonathan Steed, for his help, guidance and direction these past few years, and for giving me the constant encouragement to complete the thesis. A big thank you also goes to the Durham University technical and analytical staff, particularly Dr Juan Aguliar-Malavia, Dr Raquel Vidal, Dr Dmitry Yufit, Dr Jackie Mosely, Dr Aileen Congreve, Dr Buddhika and Mr. Leon Bowen for their assistance in data acquiring and interpretation. I also need to thank everyone in the Steed group, past and present for being a great company during my PhD years.

I must also thank my husband and my son, for being there with me, through thick and thin for these past few years. Also to my parents and family, for their never ending support over the years.

Finally, I would like to thank Government of Malaysia and University Malaysia Sarawak for the funding and Durham Chemistry for providing excellent facilities for my research.

Chapter 1

Anion receptors based on organic and metal-organic host scaffolds

1.1 Introduction to Anion Recognition

The past twenty years have seen increasingly rapid advances in the field of anion binding and sensing. The development of artificial anion receptors has received significant attention due to the important roles anions play in chemical, biological and environmental processes.[1–4] For instance, anion such as fluoride[2] have been shown to play a dual role; being considered as a pollutant anion at high concentration on one hand and at the same time useful in a human diet.

Recognition of other anions such as cyanide,[5] sulphate[2,6] and nitrate[7] also has been widely explored due to the harmful effects of high concentrations of these anions to the environment. Another toxic detrimental anion such as cyanide ion can cause poisoning in the environment even though at relatively low concentration. Despite its toxicity, it is still widely used in the production of synthetic fibres, resins and herbicides as well as being utilised in mining industries, and particularly in gold separation which possesses great risk in the contamination of drinking water.[8]

Conversely, there are also anions that are essential in biological processes such as carboxylates.[1] For instance, levels of multi-carboxylate anions such lactate and citrate in the human body can provide vital information on serious diseases, for example, the changes in citrate levels can be associated with kidney dysfunction and prostate cancer,[9] while high level of lactate can contribute to the growth and progression of cancer cells.[10,11]

Excess concentration of phosphate ion in chronic kidney disease patients (CKD) can cause hyper- and hypophosphatemia that is associated with severe cardiovascular and kidney problems.[12–14] Disregulation of chloride transport in cells can be associated with diseases such as Dent's disease, osteoporosis, Bartter's syndrome and idiopathic epilepsy.[15]

Despite the popularity of anion recognition, the design of synthetic anion receptors remains a great challenge for several reasons. First, anions are larger than isoelectronic cations, with a lower charge-to-radius ratio thus resulting in less effective electrostatic binding. Anions are also prone to bind to protic solvent making it a challenge to recognise them in water for instance. Additionally, some anions may be pH sensitive; therefore to design a particular anion receptor, the pH of the solution should also be taken into consideration to achieve the maximum interaction between the host and the guest anions. In designing a supramolecular host for both natural and artificial systems, a host should show high selectivity and be capable of discriminating between one guest and another.

The affinity of a host for a particular receptor can be determined by its binding constant, *K,* which represents the thermodynamic equilibrium constant for the binding process, Host + Guest $\rightleftharpoons$ (Host.Guest):[16]

$$K = \frac{[\text{Host} \,.\, \text{Guest}]}{[\text{Host}] \times [\text{Guest}]}$$

The selectivity of a particular host can be determined from the ratio of binding constant of one guest over another:

$$\text{Selectivity} = \frac{K_{\text{guest 1}}}{K_{\text{guest 2}}}$$

Basic concepts such as the lock and key analogy,[17] preorganisation and complementarity[16] as well as knowledge on the interaction between host and guest can be exploited to manipulate the selectivity of a particular host. Another type of selectivity is known as kinetic selectivity, which relates to the transformation of the competing substances along the reaction path such as an enzymatic catalysis process. In this case, a system is said to be selective for the guest that transforms fastest, rather than the one that is bound the strongest.[16]

There are two types of anion receptors that have been extensively reviewed; neutral receptors and positively-charged receptors. In neutral receptors which are usually based on amides,[18,19] ureas,[20–22] thioureas,[20,23,24] squaramides[25] and pyrroles,[26] the main interactions normally occur *via* effective hydrogen bonding and in some cases through deprotonation of the hydrogen bonding donor. In contrast, positively charged anion

receptors exploiting pyridinium,[22,27,28] imidazolium[29,30] and ammonium[31–34] units interact with anions mainly *via* electrostatic interactions. The detailed literature on the recognition pathways of anions by these types of host molecules are discussed in the following section.

1.2 Types of interactions in anion recognition

1.2.1 Hydrogen bonds

Of all the interactions, hydrogen bonding is the most common and has been demonstrated in the work of many researchers.[35–38] Hydrogen bonding is mainly exploited due to its relative strength (10-30 kJ mol^{-1}) and it allows the possibility of designing receptors with specific shapes.[35] A considerable amount of literature has been published on anion hosts that contain hydrogen bond donor units in their molecules such as amides,[39] sulphonamides,[39] ureas,[40] imidazoles,[29,41] pyrroles,[42,43] thioureas[24] and squaramides.[25]

Chiral macrocycles **1.1-1.3** featuring amide and sulphonamide as anion-binding sites have been described by Ema and co-workers.[39] These systems have multiple H-bonding sites and a fluorescent binaphthyl moiety that enables the recognition process to be monitored using cost effective UV/Vis and fluorescent methods. Electrospray ionization (ESI) mass spectrometry was employed to determine the binding of the anions to the receptor while the binding affinities were determined from ^{1}H NMR titration experiments in DMSO-d_6. NMR data proved that deprotonation occurs at the NH group of the nitrobenzamide and sulphonamide of **1-3**.

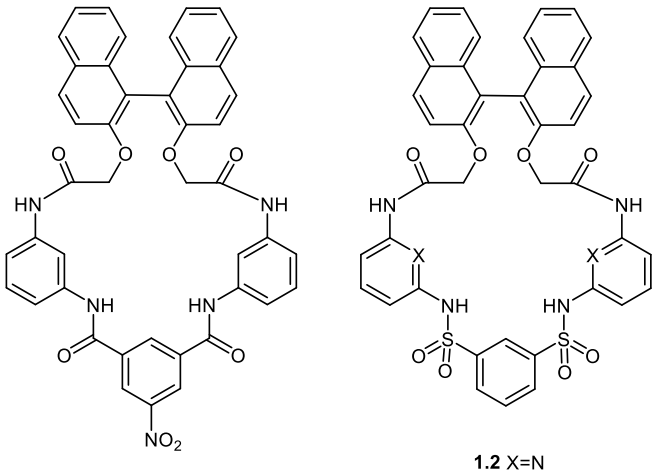

Recognition of anions by receptor **1.1** has been observed from significant colour changes upon addition of strongly basic anions such as F^-, N_3^-, AcO^-, CN^- and $H_2PO_4^-$. Of all the anions tested, only CN^- ion showed a very distinct colour change from colourless to deep reddish purple indicated that **1.1** could be used to selectively recognise CN^- ion. In contrast, receptors **1.2** and **1.3** did not show any colour changes, but experienced fluorescence quenching upon addition of the respective anions. Additionally, receptors **1.2** and 1.**3** can be utilised to discriminate N_3^- ion as they showed different intensity in the fluorescence quenching. The recognition abilities of these receptors were then extended toward biologically important molecules namely AMP, ADP, ATP, CMP, GMP, H_3PO_4 (Pi) and $H_4P_2O_7$ (PPi) (Figure 1.1). A sensor array using receptor **1.2** and **1.3** has also been developed, and can discriminate the seven respective phosphates in an aqueous DMSO solution with 100% classification accuracy.

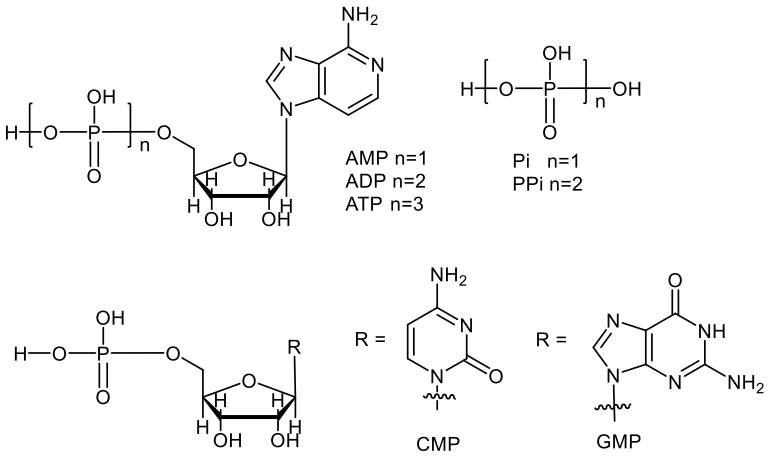

Figure 1.1 Molecular structures of seven respective phosphates used in the study of molecular recognition properties of receptors **1.1**-**1.3**.

Recently, Davis and co-workers reported the synthesis of steroidal squaramide receptor, **1.4**. The presence of squaramide units contribute to a greater acidity, therefore a stronger hydrogen bond donor compared to that of ureas and thioureas as well as converging N-H groups that are suitable for anion capturing. Receptor **1.4** displayed a very high chloride ion affinity in chloroform with binding constant greater than 10^{14} M^{-1}, among the highest reported for anion recognition by electroneutral synthetic receptors.[44] In addition, **1.4** also binds bromide, iodide and nitrate anions at lower binding constants of 1.6 x 10^{13} M^{-1}, 3.9 x 10^{11} M^{-1} and 1.5 x 10^{13} M^{-1}, respectively.

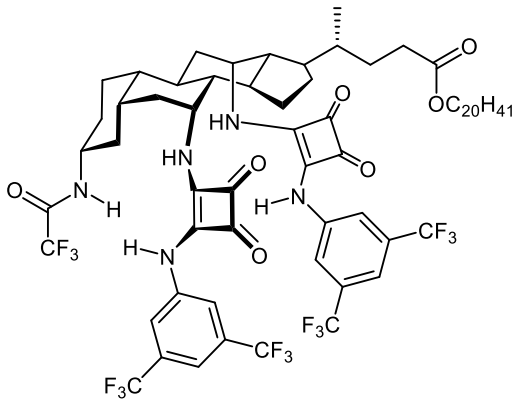

1.4

1.2.2 Electrostatic interaction and hydrogen bonds

Effective sensors for anions can also be produced through a combination of electrostatic and hydrogen bond interactions. By this, recently, the Beer group has reported the synthesis and anion binding properties of two redox-active imidazoliophane isomers **1.5** (*syn*) and **1.6** (*anti*).[45] As evidenced by spectrophotometric titration, **1.5** was found to form 1:1 complexes in acetonitrile with I^- (K_a = 423(42) M^{-1}), Br^- (K_a = 125(7) M^{-1}) and Cl^- (K_a = 79(5) M^{-1}). Investigation through Osteryoung square-wave voltammetry (OSWV) in acetonitrile for receptor **1.5** revealed "two wave behaviour" associated with the emergence of a new wave at more negative potential and disappearance of the wave corresponded to the free receptor. Upon addition of halides ion (I^-, Br^- and Cl^-), a new oxidation peak also has been observed. In contrast, the *anti* isomer **1.6** did not show any significant changes upon the addition of halides in both experiments.

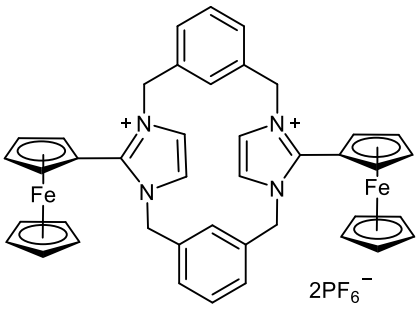

1.5^{2+} $2PF_6^-$ (syn)
1.6^{2+} $2PF_6^-$ (anti)

1.2.3 Anion-π and lone pair electron-π interaction

Tetraoxacalix[2]arene[2]triazine **1.7**, an example of electron-deficient macrocyclic host was produced by the Wang group in 2013.[7] The single crystal X-ray structure determination of this system revealed two opposing triazine rings moieties that serve as a pair of tweezers, interacting with the anions through cooperative anion-π and lone pair electron-π interactions (Figure 1.2). The interaction is established by the short distances of anions to the centroid or the plane of the triazine ring. It is also worth noting that from the X-ray structures of the anion complexes, there is no evidence of hydrogen bonding interactions between anions and arene C-H moieties, which confirms that the host interacts with the anion guest solely through anion-π and lone pair electron-π interactions. Fluorescent titration experiments in acetonitrile shows that the receptor forms the strongest complex (1:1) with NO_3^- (K_a = 16950 M^{-1}), followed by Cl^- (K_a = 4246 M^{-1}), BF_4^- (K_a = 673 M^{-1}), PF_6^- (K_a = 291 M^{-1}) and SCN^- (K_a = 239 M^{-1}).

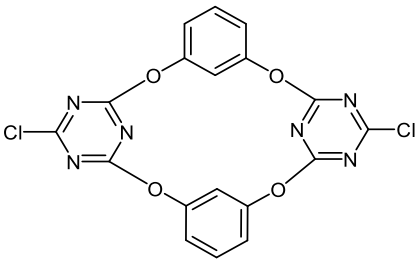

1.7

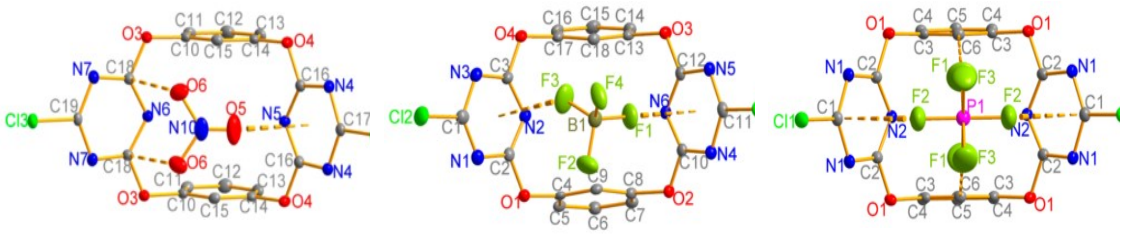

(a) (b) (c)

Figure 1.2 Single crystal X-ray structures of a) Et_4N^+(**1.7**.NO_3^-) b) Et_4N^+(**1.7**.BF_4^-) c) Et_4N^+(**1.7**.PF_6^-)[7]. Reproduced with permission from reference 7.

1.2.4 Halogen bonding

The term halogen bonding is used to describe the non-covalent interaction or weak electrostatic attraction between an electron deficient, positively polarised atom (halogen) and Lewis base (O, S, N, etc.).[46] Halogen bonding (XB) shows similar characteristic in comparison with hydrogen bonding particularly regarding stringent directionality and bond strength.[35] So far this interaction has only been widely exploited in solid state crystal engineering[46] compared to solution phase applications, particularly in solution phase anion recognition.

Work by Raatikainen and co-workers has demonstrated the excellent halogen bond (XB) donor abilities in the solid states of bipodal and tripodal cationic ligands having 2-iodoimidazolium units **1.8** and **1.9.** Suitable crystals of **1.8** and **1.9** for X-ray crystallography have been obtained in the form of **1.8**•$(Br^-)_2$, **1.8**$_2$•$Br^-(CF_3SO_3^-)_2$•H_2O and **1.9**•$(Br^-)_3(CH_3CN)_2$. In this study, the halogen bond donor abilities were measured using "normalised contact", N_c which is defined as follows:[47,48]

$$N_c = D_{ij} / (rvdW_i + rP_j)$$

Where, D_{ij} = experimental distance between the atom i and anion j

$rvdW_i$ = van der Waals radius for atom i

rP_j = Pauling radius for anion j

X-ray data of **1.8**•$(Br^-)_2$ and **1.9**•$(Br^-)_3(CH_3CN)_2$ both revealed that iodine is strongly bonded to Br^- *via* a linear, short and charge-assisted XB with I-Br^- distance of 3.041 and 3.047 Å, respectively and N_c value of 0.78.

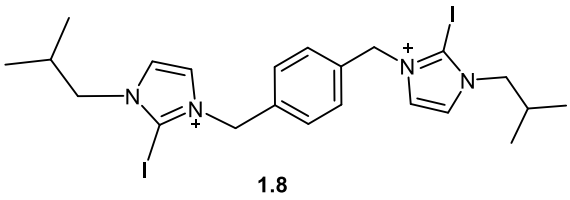

1.8

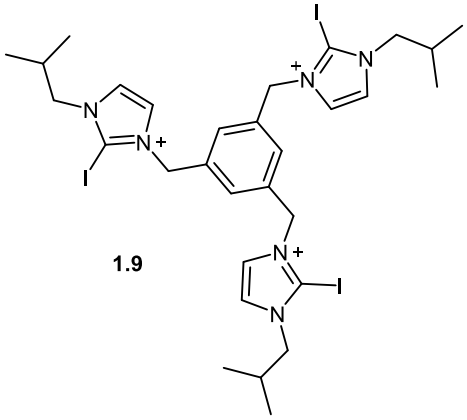

1.9

Also, an elegant example of catenane host system, **1.10**-**1.11** exploiting halogen and hydrogen bond for anion recognition in solution phase has been described by Gilday and Beer.[49]

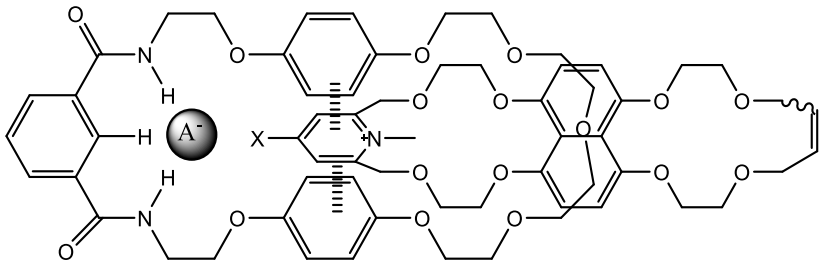

1.10 · Br X = Br A^- = Br^-

1.11 · I X = I A^- = I^-

In order to study the anion binding properties of this system, the halide hosts underwent anion exchange to afford **1.10.**PF_6 and **1.11.**PF_6 on addition of aqueous NH_4PF_6. The binding of these compounds were evaluated using ^{1}H NMR spectroscopic titrations in a mixture of [D]chloroform/[D_4]MeOH 1:1. Both of the compounds showed strongest affinity toward iodide, I^- ion (K_a = 220 and 340 M^{-1}) in comparison with Cl^- and Br^- ions particularly due to greater halogen-bond-donor ability of the iodine atom compared with two other anions. In contrast, both of these compounds did not show any complexation with AcO^- ion. Contrary to expectations based on anion basicity, it was found that the trend in anion selectivity of these compounds is in the order, $I^- > Br^- > Cl^-$.

The author concluded that the contradictory results was due to a few possible reasons, first the interlocked binding domains are more appropriate for larger anions such as I^-. Secondly, in the competitive protic solvent mixture, the Cl^- ion is more prone to desolvation effect that accounted for the lower affinity. With respect to halogen bonding interactions, the larger halide anions experience greater degree of charge-transfer type reaction between the respective catenane's bromo- and iodopyridinium halogen-bond-donor motif.

Latest work reported by Ghosh and co-workers described the synthesis and anion binding behaviour of compound **1.12** (halogen bonding analogue) and compound **1.13** (hydrogen bonding analogue).[50] In acetonitrile solution, compound **1.12** has high selectivity toward dihydrogenphosphate ($H_2PO_4^-$) anion even in the presence of ten equivalents of other competitive anions and able to detect $H_2PO_4^-$ ion at a very low concentration of 0.018 μM. On the other hand, the hydrogen bond analogue, **1.13**, albeit showing similar binding behaviour, binds $H_2PO_4^-$ significantly weaker than that of **1.12**.[50] As shown by X-ray crystal structure, **1.12** interacts with $H_2PO_4^-$ ion through solitary C-I…..anion halogen bonding interactions.

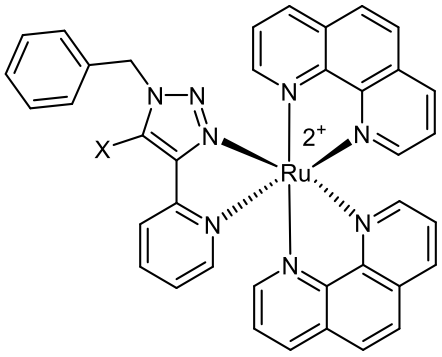

1.12 $[PF_6]_2$: X = I
1.13 $[PF_6]_2$: X = H

1.2.5 Metal or Lewis acid coordination

Lewis acids or metal centres are able to from bonds with anions by overlapping of orbitals due to their electron deficient nature. Taking advantage of this feature, many macrocyclic hosts containing metal centres have been developed. The presence of a metal centre in an anion host facilitates strong interactions[51] as well as addressing the limitation of hydrogen bonding-based receptors in aqueous solvents due to the

competition of anions and solvents at the hydrogen bonding sites.[52] A benzimidazole-based fluorescent sensor described by Saluja and co-workers provides an example of anion sensing through Lewis acid coordination.[53] Cation displacement approach was employed for the recognition of phosphate ion (Figure 1.3).[54] The addition of Cu^{2+} ion to **1.14** at pH 7 led to maximum quenching (association constant, K_a = 5.34 x 10^3 M^{-1}). However, upon addition of PO_4^{3-} anion to Cu(II) complex of **1.14**, the fluorescence intensity of **1.14** was fully restored, which resulted in enhanced fluorescent emission at 420 nm. From fluorescent intensity (time-dependence) experiments, it was revealed that sensor Cu.**1.14** required 9.5 min to achieve equilibrium in the recognition of phosphate anion.

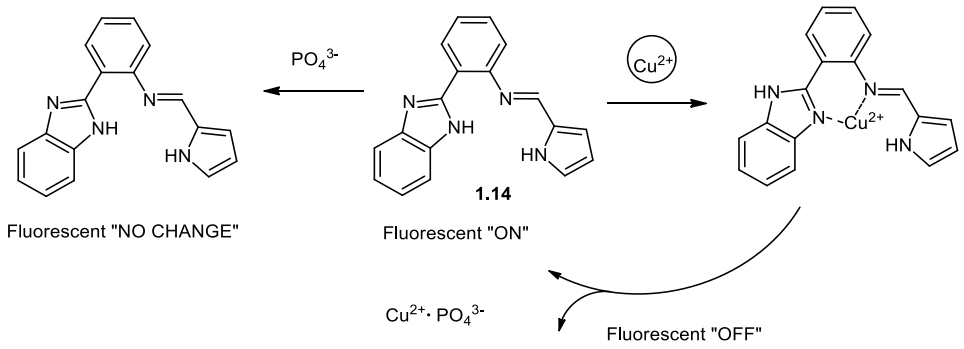

Figure 1.3 Recognition of PO_4^{3-} anion using Cu(II) complex of **1.14** based on cation displacement approach.

1.3 Classes of anion receptors

In the past decades, many classes of anion receptors having different kinds of functionalities have been prepared and reported. Here, we focus on just four classes of anion receptors which are within the scope of this study. The following sections describe detailed examples of anion receptors based-on calixarenes and imidazoles as well as metal-based and ion pair receptors.

1.3.1 Imidazole-based hosts

Imidazoles are a class of heterocyclic compounds that are essential in biological processes, and are common functional groups in structures in the human body, such as histamine and histidine.[55] Due to their amphoteric nature, imidazole compounds can serve as selective and effective anion, cation or neutral molecule sensors that are capable of interacting with a broad range of drugs and proteins. The acidity of the NH proton of imidazole can also be tuned by varying the electronic properties of the substituents attached to the ring. In addition, the presence of a basic nitrogen atom within the ring, which can coordinate to cations, makes imidazole a suitable candidate for the construction of metal-based and ditopic anion receptors.[55] The following sections discuss several examples of imidazole- and benzimidazole-based anion receptors.

1.3.2.1 Imidazole

Elegant examples of imidazolium based receptors namely imidazoliophane, **1.15** and bromoimidizoliophane, **1.16** have been reported by the Beer group.[56] These receptors were then converted to hexafluorophosphate salts upon addition to aqueous NH_4PF_6. This study was conducted to compare the binding affinity between **1.15** and **1.16**, which are hydrogen-bonding receptor and halogen-bonding receptors, respectively. The anion binding properties of both receptors were evaluated using ^{1}H NMR spectroscopy toward fluoride, chloride, bromide and iodide ions (as TBA salts) in CD_3OD/D_2O 9:1.

Receptor **1.15** binds halide weakly (K_a (Cl) = 133 M^{-1}, K_a (Br) = 130 M^{-1}, K_a (I) = 102 M^{-1}), while receptor **1.16**, with addition of bromine atom to its molecular structure, binds anions strongly particularly for bromide ion (K_a (Cl) = <10 M^{-1}, K_a (Br) = 889 M^{-1}, K_a (I) = 184 M^{-1}), which is sevenfold stronger than that of **1.15**. This data also provides an insight into why **1.15** is unable to discriminate the respective anions while **1.16** showed a very high selectivity for bromide. Recognition of bromide ion is accomplished through pure halogen bonding in aqueous media due to the addition of a bromine atom to the macrocyclic framework which enhanced its ability to recognise anions.

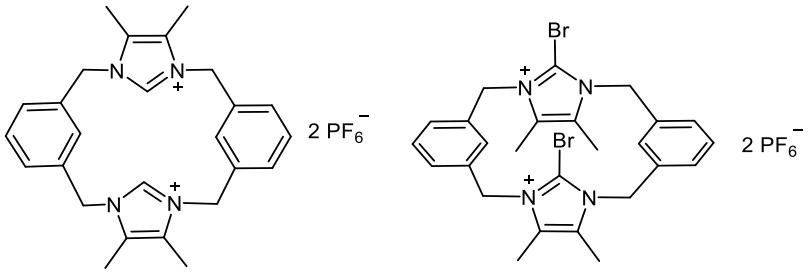

1.15 **1.16**

A year later, a similar series of charged-assisted bidentate chloro-, bromo- and iodo-imidazoliophane receptors were utilised in halogen anion recognition (Cl^-, Br^- and I^-).[57] The anion binding properties of these series have been investigated by means of ^1H NMR spectroscopy, fluorescence spectroscopy, X-ray structural determination as well as computational DFT calculation. Of all the compounds synthesised, only **1.17** and **1.18** showed significant perturbation in the chemical shift of internal naphthalene protons and increase in the fluorescence intensity band upon addition of Br^- and I^- ions (as TBA salt). The author concluded that **1.17** and **1.18** selectively bind I^- and Br^-, respectively *via* pure halogen bonding in aqueous methanolic (CD_3OD:D_2O 9:1) solvent media.

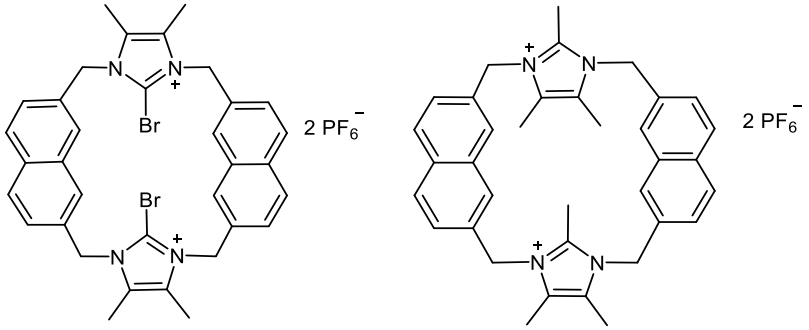

1.17 **1.18**

A pincer-shaped diimidazolium salt **1.19** has been reported by Marullo and co-workers for the selective recognition of dicarboxylate anion.[58] In this molecule, the two cationic groups are arranged in a pincer-like fashion which converges on the anion to allow effective interaction with the guest anions. The binding constants of the anion complexes formed were determined on the basis of ^1H NMR studies showing a 1:1 complex formation. Of all the anions (halide, monocarboxylate and dicarboxylate) tested, **1.19** preferentially binds dicarboxylate anions with the relative binding strength order of fumarate < oxalate < succinate < tartrate. The authors concluded that the flexibility of the alkyl spacer of the dicarboxylate anion greatly influenced the conformation of the dicationic host for maximum interaction with the anions.

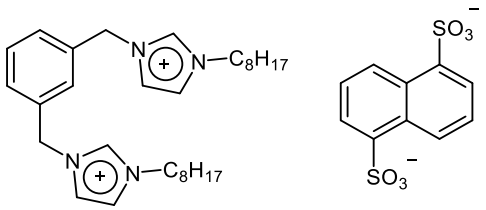

1.19

Water-soluble imidazolium-based receptors **1.20**-**1.22** which selectively recognise monophosphate nucleotide in aqueous solution at physiological pH of 7.4 have been reported by Yousuf and co-workers.[59] Evidence for binding came from fluorescence, ^{1}H NMR spectroscopy and density functional theory (DFT) studies. Receptor **1.20** consists of imidazolium units with bridging benzyl moieties bind AMP strongly through strong H-π interaction with a binding stoichiometry of 1:1. On the other hand, receptor **1.21** preferentially coordinates GTP in a 1:1 fashion. The presence of an electron-withdrawing N atom in acridine moiety of **1.21** strengthens the H-π interaction between **1.21** and GTP which results in fluorescence quenching at physiological pH. In contrast, receptor **1.22** which has naphthalene-imidazolium based cyclic structure selectively recognised pyrophosphate (PPi) in a 2:1 fashion. The recognition process of PPi by **1.22** proceeds through the formation of an excimer due to π-π interactions between the fluorophores.

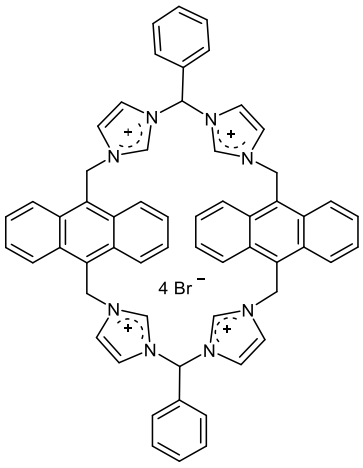

1.20

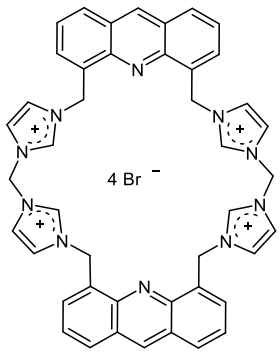

1.21

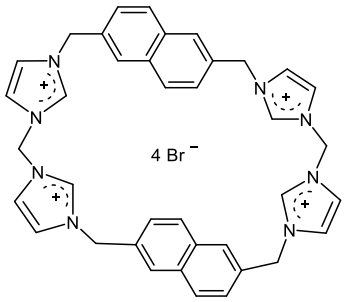

1.22

Additionally, the F^- ion signalling potential of the imidazole NH group also has been described.[41] This sensor **1.23** in CH_3CN:H_2O (9:1, v/v) underwent a colour change from yellow to red, and the intensity of peaks at 550 nm gradually decreased and was replaced by a new peak at 477 nm. The colour change observed is ascribed to charge transfer interaction between fluoride bound NH of imidazole and the electron deficient

nitro group at the *para* position. Fluoride was found to bind in 1:1 fashion to NH group with a binding constant of 1.42 x 10^4 M^{-1}.

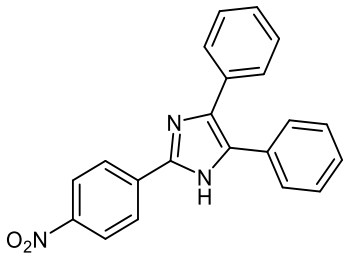

1.23

Cametti and co-workers have synthesised imidazole-based receptors for the assessment of the relative strength of halogen bond (XB) (receptor **1.24**) over hydrogen bond (HB) (receptor **1.25**) and the effect of halogen atom polarisability toward halogen bond strength (receptor **1.26**).[60] ^{1}H NMR titration experiment was carried out in DMSO to determine the binding affinity of **1.24**.I^-, **1.25**.I^- and **1.26**.I^- toward Cl^- ion. Compound **1.24**.I^-, the XB-based receptor showed better affinity for Cl^- ion of more than one order of magnitude compared to HB-based receptor **1.25**.I^-, while compound **1.26**.I^- did not show any interaction with the Cl^- ion, consistent with the generally accepted electrostatic model of XB.[61–63] Binding of **1.24** with AcO^- ion also showed higher affinity than Cl^- and increase in association constant of 10-fold over HB-based receptor **1.25**. In addition, in the case of $H_2PO_4^-$ ion binding, receptor **1.24** also showed greater affinity of 40 times more than receptor **1.25**.

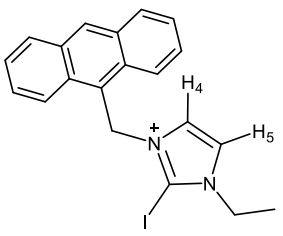

1.24

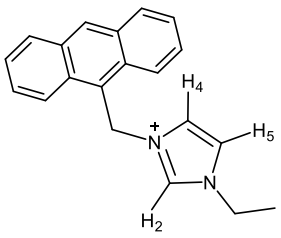

1.25

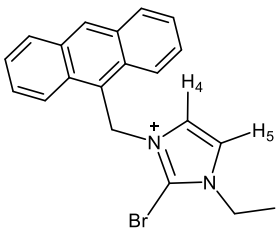

1.26

1.3.2.2 Benzimidazole

A series of benzimidazole-based receptors **1.27-1.31** has been prepared and reported by the Gale group[64] and their binding properties towards various anions were investigated using ^{1}H NMR spectroscopy in DMSO-d_6/0.5% water solution and single crystal X-ray crystallography.

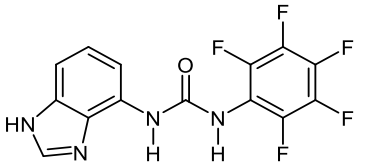

1.27

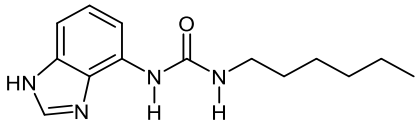

1.28

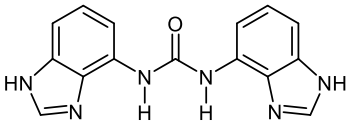

1.29

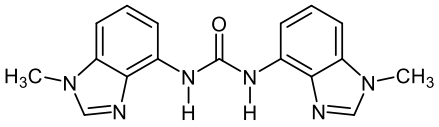

1.30

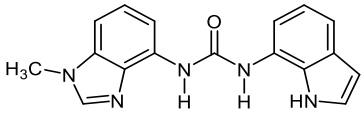

1.31

In the case of compound **1.27**, evidence from ^{1}H NMR titration and single crystal X-ray structure suggested that Cl^- interacts with only one NH group *via* a single hydrogen bond due to the formation of an intramolecular hydrogen bond between the hydrogen bond of urea and benzimidazole nitrogen atom (Figure 1.4a). In contrast, the addition of more basic anions such as SO_4^{2-}, OAc^- and benzoate induced the formation of the other tautomer that allows all three NH groups to interact with the anions as evidenced by the broad resonance observed in ^{1}H NMR spectrum and by the X-ray single crystal structure of benzoate complex of **1.27** (Figure 1.4b).

a) b)

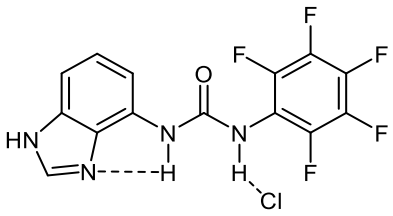

1.27. Cl

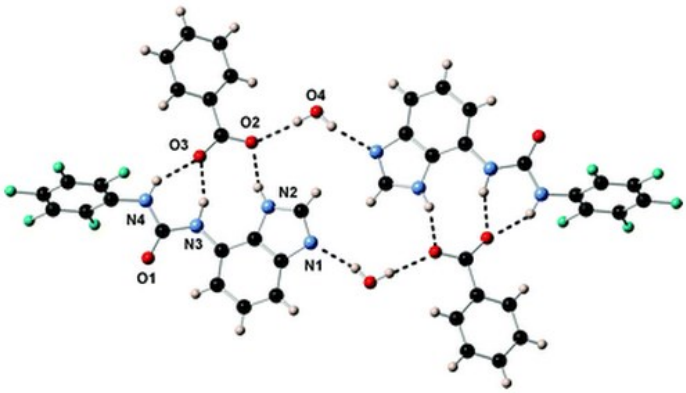

Figure 1.4 a) The conformation of compound **1.27** in the presence of chloride b) The single crystal X-ray structure of the benzoate complex of compound **1.27**.[64] Reproduced with permission from reference 64.

Likewise, receptor **1.28**-**1.31** showed similar results to **1.27** except that receptor **1.30** shows a very high selectivity towards dihydrogen phosphate ion compared to others due to the presence of methyl group in the benzimidazole ring that allows the anions to donate two hydrogen bonds to the benzimidazole groups (Figure 1.5). The authors concluded that tautomeric switching concept offer methods in discriminating different types of anions.

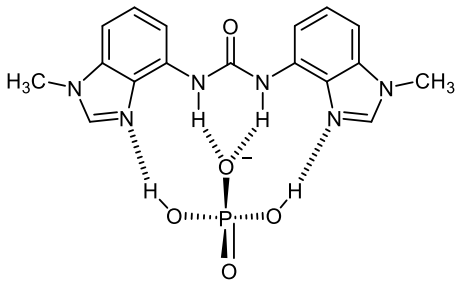

1.30 . $H_2PO_4^-$

Figure 1.5 The proposed binding mode of compound **1.30** with dihydrogen phosphate.

Cyclo[2]bezimidazole, **1.32** has been reported by Abraham and co-workers for the selective recognition of fluoride, bifluoride and oxoanions hydrophosphate and benzoate.[65] The authors suggested that the luminescence 'turn on' upon binding with the anions was caused by the inhibition of an Excited State Intramolecular Proton Transfer Process (ESIPT). In the case of fluoride anion complex, the intensity of the emission peak at 412 nm increased almost 150 times compared to that of free receptor **1.32**. In addition, effective transformation of fluoride into bifluoride, HF_2^-[66] was

confirmed by NMR studies which revealed the formation of a 1:1 complex with HF_2^- with association constant of 100 000 ± 10% M^{-1} and 60-fold turn-on of the luminescence. The smaller Stokes shift of complexed **1.32** than that of free **1.32** also an indicator of ESIPT process inhibition. It was also revealed that the anion binding event is associated with the stabilization of the 1-4H_{in} (**1.33**) tautomer due to the formation of four hydrogen bonds between the NH groups of the molecule and the anion.

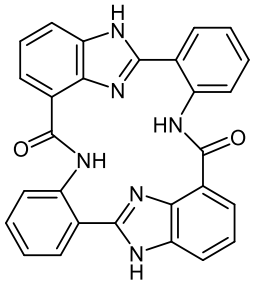

1.32

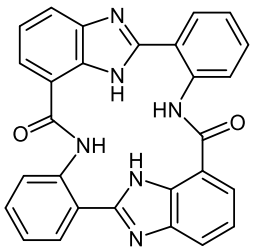

1.33

A strong colorimetric sensor for F^- and CN^- ions based on anthraimidazolediones **1.34** has been prepared by Kumari and co-workers.[67] While **1.34** can recognise both F^- and CN^- ions in organic media, in aqueous CH_3CN (9:1) media, it can only recognise CN^- ion due to the high hydration energy of F^- ion (ΔH_{hyd} = -505 kJ/mol) over CN^- ion (ΔH_{hyd} = -67 kJ/mol). An intramolecular charge-transfer (ICT) process has been addressed to explain the significant red-shifts observed upon addition of F^- and CN^- ions.

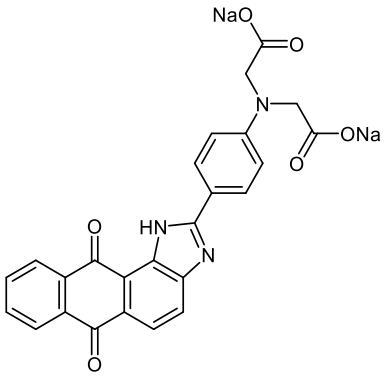

1.34

A chemodosimeter based on benzimidazole **1.35** for selective recognition of F^- ion has been described by Li and co-workers in 2011.[68] The chemodosimeter approach in anion sensing particularly for F^- ion has drawn attention due to its high selectivity and a large spectroscopic shift. Anion binding behaviour was investigated in acetonitrile using fluorescence spectroscopic technique. This receptor can report the presence of F^- ion selectively, based on the fluorescence "turn-on" with 62–fold increase in the emission

intensity to that of free receptor and detection limit of 2.72 x 10^{-6} mol L^{-1}. The addition of F^- ion initiates the cyclisation from pyridinium **1.35** to pyrido[1,2-α]benzimidazole **1.36** confirmed by single crystal X-ray structure. The observed enhancement of fluorescence at 481 nm corresponds to the extended conjugation in compound **1.36**.

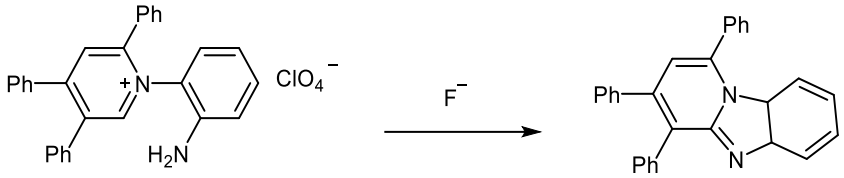

1.35 **1.36**

1.3.2 Pre-organised anion hosts based on organic frameworks

In recent years, there has been an increasing amount of literature on pre-organised anion hosts based on organic frameworks. To name the few, preorganised scaffolds such as calixarene[69–74], trialkylbenzene[28,75–77], tris(2-aminoethyl)amine and tricarboxylic ester trindane have been widely used in templating the anion receptors in such a way that the anions can be encapsulated inside the cavity of the receptor with a high degree of steric fit. The choice of scaffolds used is also very important to enhance the selectivity and affinity of the anion binding. The following subsections will discuss the anion binding properties of two most common scaffold that will be used in this work which are trialkylbenzene and calixarenes.

1.3.2.1 Trialkylbenzene-based hosts

One elegant example of trialkylbenzene-based host is compound **1.37**, which is capable of sensing iodide ion. While there has been much research on the sensing of F^- and Cl^- ions, there has been little information in the recognition of iodide ion, particularly due to its large size and low charge density.[72,78,79] On the basis of this, a benzimidazole-based tripodal receptor **1.37** has been designed to selectively bind iodide ion over a broad concentration range without interference from any other anions.[80] ^{1}H and ^{13}C NMR spectra revealed that **1.37** adopts conformation A (Figure 1.6) which is essential for

strong encapsulation of anions. This receptor is able to selectively coordinate to I^- in CH_3CN/H_2O (99:1, v/v, pH = 7.91) that results in a strong static quenching of the emission at λ_{max} 318 and 408 nm.[55] The NH_2 group of receptor **1.37** binds iodide in 1:1 fashion confirmed by ^1H NMR spectra with binding constant and detection limit of (1.5±0.2) x 10^3 M^{-1} and 7.45 x 10^{-6} M, respectively.

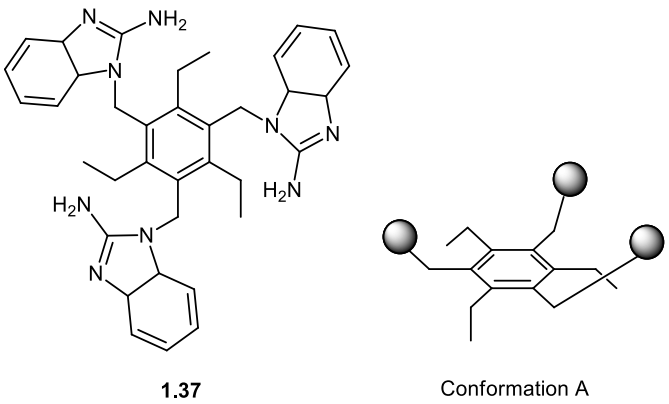

Figure 1.6 Conformation A adopted by **1.37**.

Another example of a trialkylbenzene-based host is compound **1.38**, which consists of triazole and pyrene moiety as the anion and cation binding site and fluorescence signalling unit, respectively. [81] The UV titration experiments have been carried out in the presence of a variety of anions of different topologies, such as the halides, nitrate, sulphates, phosphates, carboxylates and dicarboxylates. Of all the anions tested, citrate is the only ion that can show significant fluorescence changes from green to blue, visually observed by standard UV lamp. Receptor **1.38** selectively binds citrate at 1:1 ratio with an association constant and detection limit of 8.2 × 10^3 M^{-1} and 3.7 × 10^{-6} M.

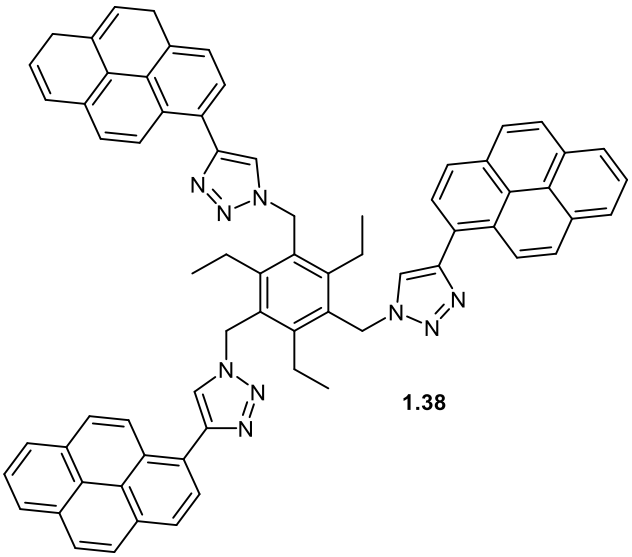

1.38

Another example of trialkylbenzene-based receptor is compound **1.39**, synthesised by Chawla and co-workers[82] showing selectivity towards the sensing of fluoride and acetate ion. The addition of the above-mentioned anions induced the colour changes from colourless to yellow-green, visible by naked-eye. It is postulated that the intermolecular charge transfer (ICT) from the amide pyridinium unit (electron-rich anion binding site) to the nitrobenzene fragment (electron deficient unit) is the driving force of the bathochromic shift, hence the colour changes.

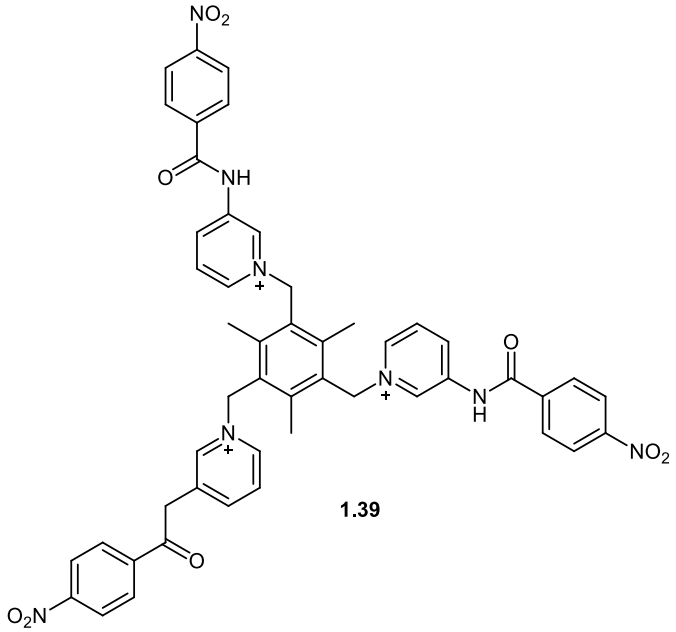

1.39

A 'pin-wheeled' type anion receptors comprise of pyridinium and urea groups, **1.40**-**1.41**, have been extensively studied by Steed and co-workers.[83] ^{1}H NMR titration experiments show that compound **1.40** effectively binds halides (Cl^- and Br^-) and

oxyanions such as NO_3^-, AcO^- and $H_2PO_4^-$) through pyridinium C-H···A- interactions. DFT calculation performed shows that the chloride ion is encapsulated within the cavity through multiple C-H···Cl and N-H···Cl interactions and the capsule is sealed by C-H···π interaction when a *p*-tolyl group is introduced as the end group. On the other hand, compound **1.41**, comprises of two anion binding sites; 3-aminopyridium pocket and urea group interacts with chloride through charge assisted N-H···Cl and is zipped-up by the urea group through α-urea tape motif.

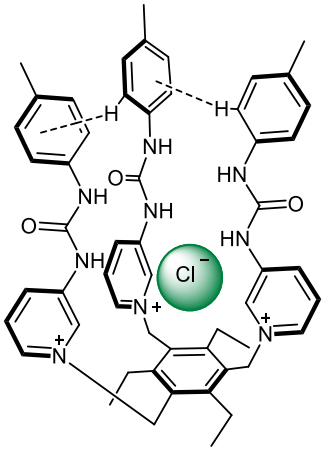

1.40

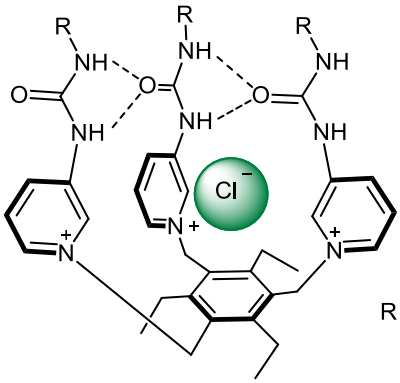

R = n-octyl

1.41

In another work, Ghosh and co-worker has synthesised two elegant tripodal anion receptors based on a hexasubstituted aryl core, **1.42** and **1.43**, which differ from each other on the position of the nitro substituent at *ortho* and *para* position, respectively.[84,85]

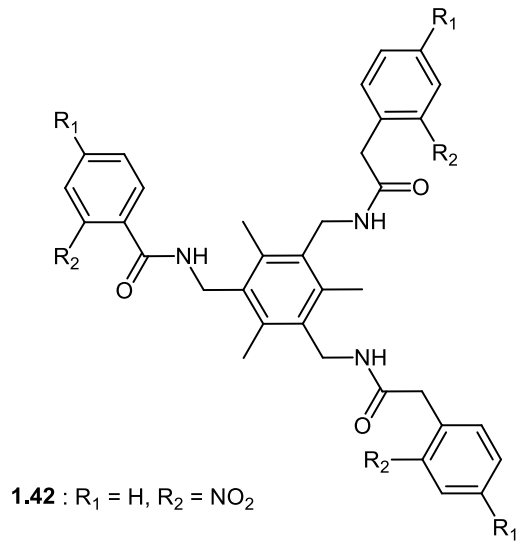

1.42 : R_1 = H, R_2 = NO_2

1.43 : R_1 = NO_2, R_2 = H

Although both of the compounds contain the same cavity, they show different binding modes towards various anions. The addition of anions such as fluoride, chloride, nitrate and acetate (as TBA salt) to compound **1.43** results in the formation of dimeric capsular assembly (Figure 1.7) while in the case of compound **1.42**, only the addition of fluoride ion results in the formation of the dimeric capsular assembly while the rest of the anions (chloride, nitrate and acetate) drive the compound to form a zipper-like assembly (Figure 1.8).

a) b)

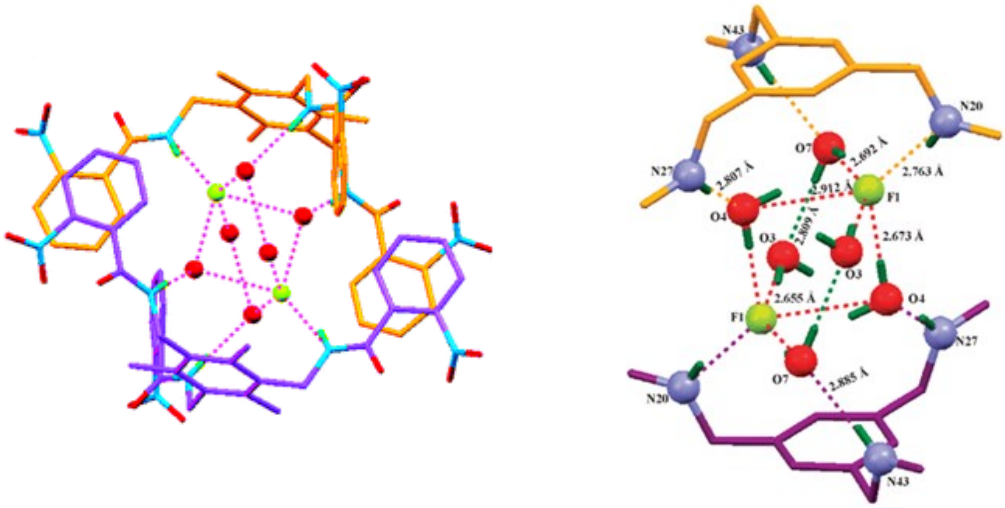

Figure 1.7 a) Formation of a dimeric capsular assembly with fluoride ion and water through hydrogen bonding interactions with receptor **1.42** b) Partial structure of the fluoride complex of **1.43** showing the hydrogen bonding pattern of the $[F_2(H_2O)_6]^{2-}$ cluster and its interactions with **1.43.** Reproduced with permission from reference 84 and 85.

Figure 1.8 shows that, in the presence of nitrate ions, compound **1.42** shows a zipper-like assembly, in contrast with compound **1.43** that prefer to form a dimeric capsular assembly. In compound **1.43**, dimeric capsular assembly is enforced through the CH···O interaction between cleft bound nitrate with the aryl CH that bring the similarly charged anion into close proximity. Conversely, the formation of zipper-like assembly in compound **1.42** was driven by various interactions such as three strong NH···O between amide protons of **1.42** and two oxygen atoms of nitrate and also through one intermolecular CH…O interaction between aryl C-H and another oxygen atom of the nitrate.

a)

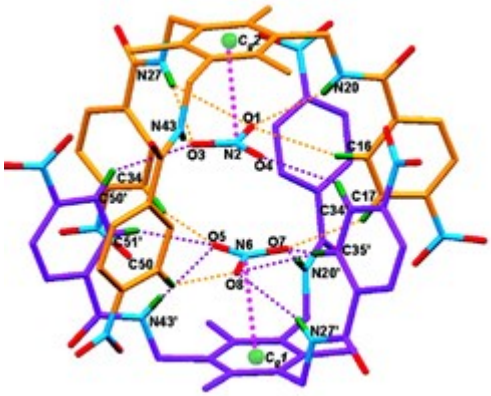

b)

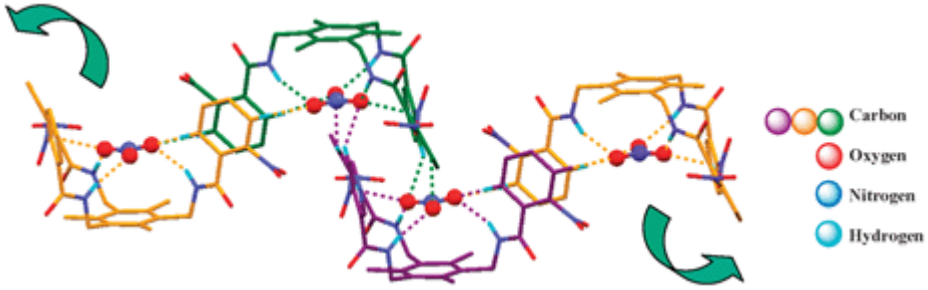

Figure 1.8 a) Formation of a dimeric capsule with encapsulated nitrate ion through hydrogen bonding interactions of nitrate anions with receptor **1.42** b) Formation of a zipper-like assembly with encapsulated nitrate ion through hydrogen bonding interactions of nitrate anions with receptor **1.43**. Reproduced with permission from reference 84 and 85.

In recent work reported by the Davis group, a tris-thiourea compound based on a triethylbenzene core, **1.44** has shown its effectiveness as anion carriers with the value of 0.0019 mol% carrier: lipid, among the lowest value reported in the literature.[86] In comparison with compound **1.45**, **1.44** binds chloride ion 20 times stronger with a binding constant of 8 x 10^8 M^{-1}. Based on the structure of the scaffold, the compactness of the cyclohexane-based system possibly allows some weak interactions between the thiourea group thus favouring non-binding conformation that eventually results in low binding constant. In contrast, the benzene-based scaffold allows the binding groups spread apart and minimise the weak interaction between the binding groups.

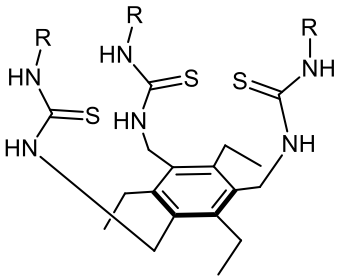

1.44

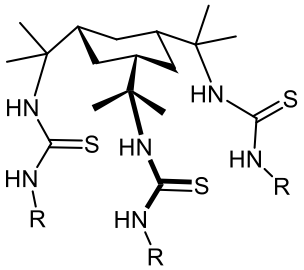

1.45

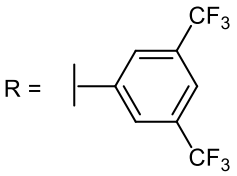

From the single crystal structure of **1.44** + $Me_4N^+Cl^-$, it is revealed that the two molecules of receptor formed a cage that surrounds a cyclic $(Cl^-\cdots H_2O)_2$ dianionic cluster (Figure 1.9) suggesting that the presence of this dimeric species might also be responsible for anion transport.

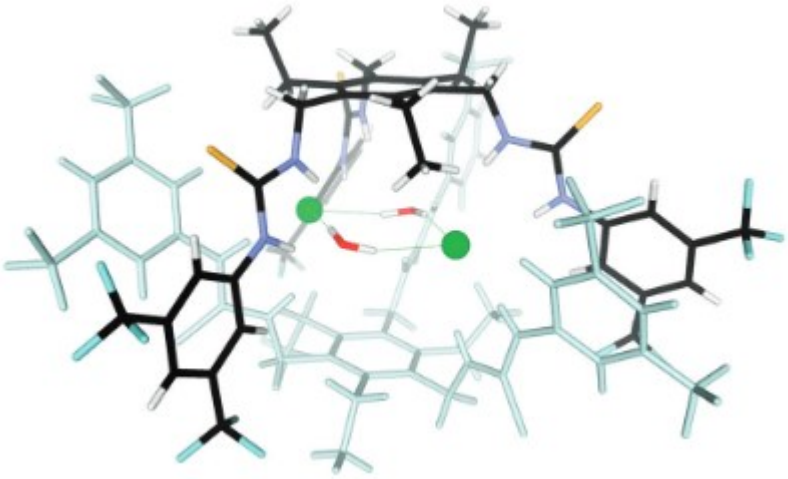

Figure 1.9 Structure of (**1.44**·Cl^-·$H_2O)_2$ as obtained by crystallisation of **1.44** + $Me_4N^+Cl^-$. One molecule of **1.44** is coloured pale cyan, and the two Me_4N^+ cations outside the cavity are omitted for clarity. Reproduced with permission from reference 86.

1.3.2.2 Calixarene-based hosts

There is a wealth of literature on the development of calix-based receptors. As a macrocyclic ligand, calixarenes have an advantage of recognising larger anions due to their medium to large cavity making them suitable host compounds for ionic species. In addition to that, the framework of calixarenes allows the positioning of functional groups which can facilitate the interaction with a guest molecule. Of key recent importance are the tetrameric and pentameric calix[4]imidazolium **1.46** and calix[5]imidazolium **1.47** described by Young Chun and co-workers.[70]

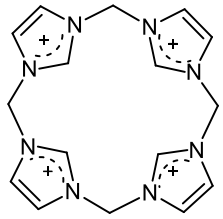

1.46

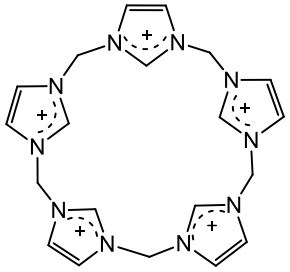

1.47

These receptors were synthesised in a one pot reaction to afford the new type of positively charged imidazolium based homo-calix compounds that were observed as a single crystal structure of calix[4]imidazolium **1.46** in the form of a chloride salt, **1.46**.4Cl.X.H_5O_2 [X=Cl/Br=0.5Cl. 0.5Br] and calix[5]imidazolium **1.47** in the form of a bromide salt, **1.47**.5Br.[F.H_5O_2]. The anion sensing ability of these two receptors has been investigated using fluorescence and NMR spectroscopy as well as theoretical calculations. Receptor **1.46** strongly binds F^- ion over other anions with a binding constant of $8.3x10^4$ M^{-1} in aqueous media in a 1:1 fashion. In contrast, **1.47** can recognise neutral molecule such as C_{60} fullerene *via* π^+-π interaction in aqueous media due to its larger cavity compared to receptor **1.46**.

A ditopic tetrapodal imidazolium-based 1,3-alternate calix[4]arene **1.48** has been reported by Willans and co-workers.[29] This receptor binds Cl^-, $MeCO_2^-$ and malonate^{2-} as 1:1 anion complexes and binds NO_3^- and Br^- in 1:2 fashion. In terms of overall stability constant, the bonds of two equivalent of Cl^-, Br^- and $MeCO_2^-$ with the receptor are equally strong except that in the case of Cl^-, the first equivalent of chlorides shows lower affinity ($K_{12} > K_{11}$) suggesting the positive allosteric effect in which binding of the first

chloride anion facilitates the binding of the second. In contrast, malonate show low binding affinity as the small cavity between the two imidazolium groups could not accommodate the binding of the large size malonate anion.

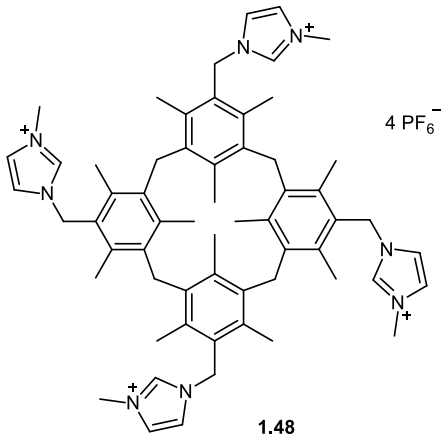

1.48

X-ray crystallography study confirmed the 1,3-alternate conformation of the calixarene core with large amounts of enclathrated solvent. The imidazolium groups were found to adopt either *in* or *out* arrangement that depends on whether they are oriented inwards or outwards towards the calixarene pseudo C_4 axis (Figure 1.10a and 1.10b). For instance, the chloride complexes of **1.48** formed *in-out* and *out-out* conformers that are capable of chelating a single anion in a pincer-like fashion thus enhanced the solution-state binding. In addition to that, the X-ray data also provides information on the binding mechanism between the receptor and anions which mainly occur *via* acidic NCHN groups and sp^2 hybridised imidazolium CH groups . The highlighted feature of this work is the inclusion of an imidazolium group between in-out pair of the chloride complexes which caused distortion of the calixarene framework thus allows edge-to-face π interaction (Figure 1.10c).

Figure 1.10 a) *In-out* and b) *Out-out* binding regions in imidazolium groups in the X-ray crystal structure of the Cl^- salt of **1.48** c) View of molecule **1.48** highlighting the *in-out* geometry and the inclusion of an imidazolium moiety from an adjacent molecule.[29] Reproduced with permission from reference 29.

In 2012, the same group synthesised tetrakis(methyl-imidazolium)calix[4]arene **1.49** and examined its interactions with various anions (Cl^-, Br^-, NO_3^-, AcO^- and PO_4^-).[30] Evidence of binding was obtained from ^1H NMR spectroscopic studies and also from an X-ray single crystal structure. Different modes of interaction were observed upon addition of different types of anions. Downfield shift at C4 and C5 was observed upon addition of Cl^-, Br^-, NO_3^- with Cl^- showed the most pronounced shift, followed by Br^- and NO_3^-. The X-ray crystal structure of **1.49** revealed the interaction of Br^- with the hydroxyl groups on the lower rim of the calix[4]arene (Figure 1.11). While the addition of AcO^- and PO_4^{3-} at one equivalent exhibited a downfield shift of the C2 proton resonance; suggesting the binding of the anion to the imidazolium C2 protons at the upper rim of **1.49**, the second equivalent of these anions interacts with the acidic lower rim causing partial deprotonation of the hydroxyl groups.

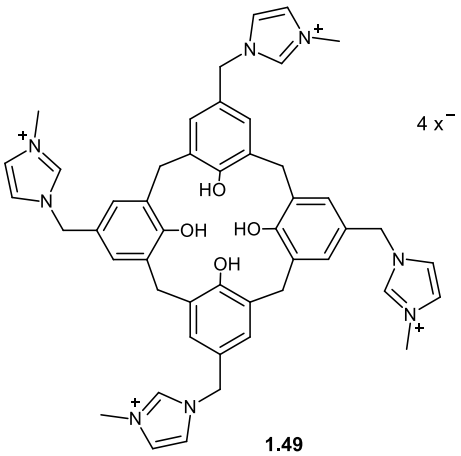

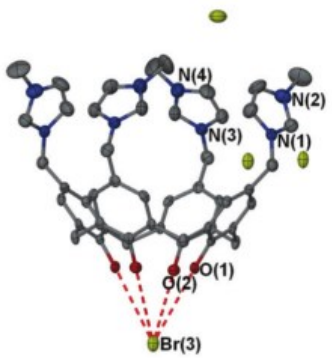

Figure 1.11 Single crystal X-ray structure of **1.49**.Br^-.[30] Reproduced with permission from reference 30.

Receptors **1.50** and **1.51**, derived from bis(N-imidazolyl)calix[4]arene system have been utilised by Dinares and co-workers for anion recognition.[87] Both receptors consist of two imidazole units that are directly bonded to the upper rim of the calixarene structure. The binding affinity of **1.50** and **1.51** was evaluated using ^{1}H NMR spectroscopic titration in acetonitrile. In acetonitrile, anions are bound strongly to **1.50** and **1.51** with a 1:1 and 1:2 host:guest stoichiometry observed, respectively. The binding stoichiometry of 1:2 observed for receptor **1.50** is due to the interference of isopropyl group in the interaction between both imidazolium moieties and the anion, inside the receptor cavity. It is also revealed that receptor **1.50** only formed 1:1 complexes with small anions such as Cl^- and CN^-. Interestingly, both of the receptors showed strong affinity to benzoate anion (K_a = 404 M^{-1} and K_1 = 9374 M^{-1}, K_2 = 429 M^{-1} respectively) over other anions tested, most probably due to a strong $(C\text{-}H)^+\cdots RCO_2^-$ hydrogen bond. Receptor **1.50** also showed strong anion binding to malonate (1:1) with a binding constant of 1142 M^{-1}. The calixarene unit of both receptors was found to adopt a pinched cone conformation with the substituted rings parallel upon anion coordination.[88]

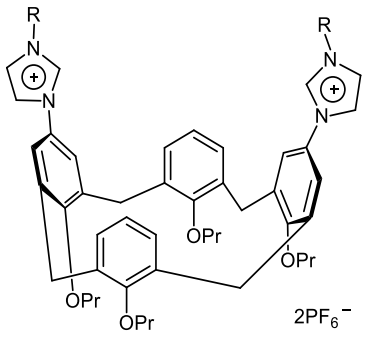

1.50 · $2PF_6^-$ R = *n*-Bu

1.51 · $2PF_6^-$ R = *i*-Pr

Calix[4]arene derivatives consisting of two ferrocenyl imine, **1.52** and two ferrocenyl amine, **1.53** have been described as selective receptors for Cl^- and Br^- ions.[89] A 1:1 adduct was formed with both anions evidenced by cyclic voltammogram and UV/Vis spectra. In comparison with **1.53**, compound **1.52** which is a Schiff base compound showed a greater anodic shift of 202-302 mV. On the other hand, Cl^- complexes of **1.52** and **1.53** produced the largest shift of the ferrocene/ferrocenium redox couple. The recognition process involves the oxidation of ferrocene unit (Fc) to Fc^+ which subsequently binds anions through electrostatic interaction.

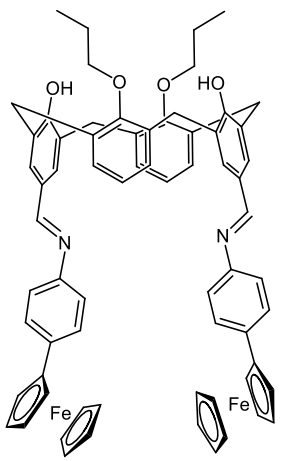

1.52

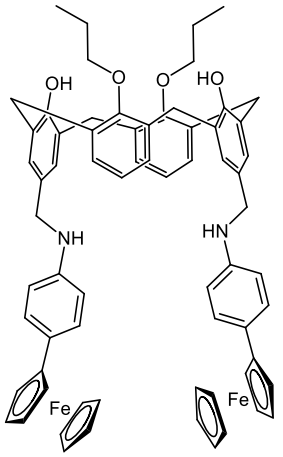

1.53

A series of calix[4]arene based receptors containing squaramide moieties **1.54**-**1.56**[73] has also been utilised for anion recognition *via* the formation of hydrogen bonding in the case of **1.54** and deprotonation of N-H group by strong basic anions in the case of **1.55** and **1.56**. Receptor **1.54** preferentially binds $H_2PO_4^-$ ion (log K_a = 4.72) over F^- ion (log K_a = 4.66) and CH_3COO^- (log K_a = 4.34) in DMSO forming 1:1 anion complex confirmed by UV/Vis spectroscopy and Job's plot. Titration experiment of **1.55** and **1.56** with CH_3COO^- in DMSO showed a bathochromic shift from a shorter wavelength (345 nm) to a longer wavelength (370 nm) due to internal charge transfer (ICT) transition indicated a typical Bronsted acid-base reactions.[90] Receptors **1.54** and **1.55** have potential as colorimetric sensors for F^- and CH_3COO^- ions due to colour changes that are observable by the "naked-eye" caused by direct deprotonation of the N-H group.

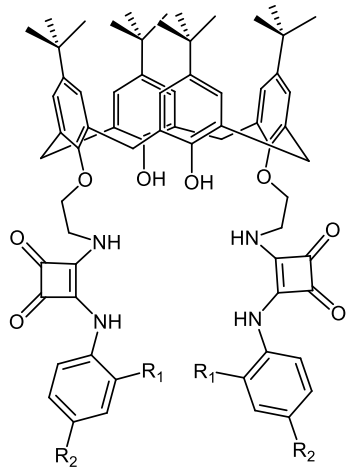

1.54 R_1 = H; R_2 = H
1.55 R_1 = H; R_2 = NO_2
1.56 R_1 = NO_2; R_2 = H

Work by the group of Gotor[91] has produced a BODIPY-based bis(calix[4]pyrrole) **1.57** for recognition and sensing of α,ω-dicarboxylates of different chain length (C2, C5 and C7-C12) as well as naphthalene dicarboxylates (Figure 1.12). In this case, changes in the UV/Vis and the quenching of the fluorescence emission led to the suggestion that **1.57** showed high affinity toward α,ω-dicarboxylates of C9 and C10 chain length, most probably due to the simultaneous coordination of both terminal carboxylate moieties to both calixpyrrole units.

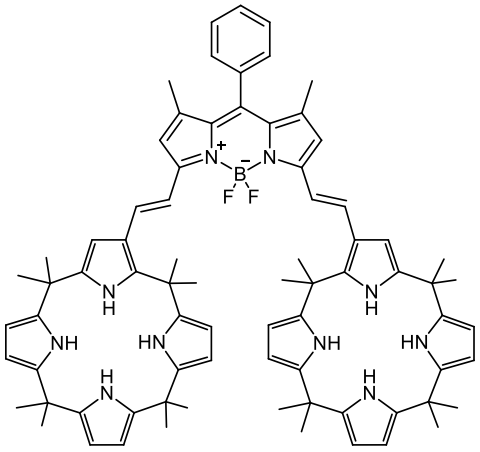

1.57

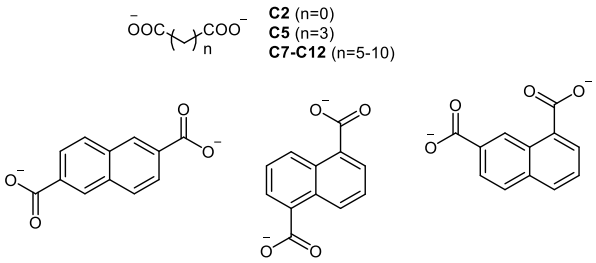

Figure 1.12 The molecular structure of the aliphatic and aromatic dicarboxylates.

Recognition of cyanide ion in CH_3CN/DMSO (3%) is also possible using **1.58**, nitrovinyl substituted calix[4]pyrrole, a dual-functional reaction-based chemosensor.[42] In this system, while the pyrrole N-H groups serve as a hydrogen-bonding site for halide anions such as Cl^- and Br^-, the vinylic nitro group provides a site for the attachment of CN^- ion, proved by the gradual disappearances of vinylic protons signals in ^1H NMR spectrum upon addition of CN^- ion. Nucleophilic additions of CN^- to **1.58** results in compound **1.59** which is unstable and undergoes elimination to form cyanide adduct **1.60**. UV/Vis titration experiments revealed the selectivity of receptor **1.58** toward CN^- ion even in the presence of an excess of other inhibitory anions.

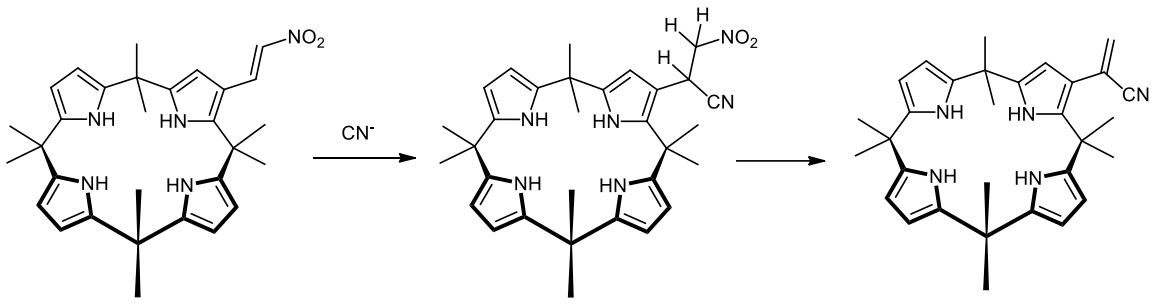

1.58 **1.59** **1.60**

Recently, Chang and co-workers have demonstrated the effect of geometrical isomerism on anion affinity in hexapyrrolic calix[4]pyrrole system using UV/Vis and NMR spectroscopy, X-Ray crystallography and DFT methods.[92] From X-ray single crystal structure analysis, it was confirmed that *trans*-**1.61** adopts a 1,2-alternate conformation while *cis*-**1.61** adopts 1,3-alternate conformation (Figure 1.13).[93] Negative mode ESI MS revealed both isomers bind anions in 1:1 fashion. *Cis*-**1.61** showed greater anion affinity compared to *trans*-**1.61** particularly in the case of chloride (116 times difference), dihydrogen phosphate (6 times difference) and benzoate (126 times difference). While *cis*-**1.61** shows high binding constant (K_{as} >10^4 M^{-1}) and high cross-reactivity,[94] *trans*-**1.61** shows lower binding constants with high selectivity due to the high directionality of the hydrogen bonding. The interaction *cis*-**1.61** and *trans*-**1.61** with fluoride ion were also investigated in solution by ^{1}H NMR titration in acetonitrile. Addition of fluoride to the solution of *trans*-**1.61** caused significant downfield shift of pyrrole NH protons on the side arm suggesting the anion complex was formed *via* hydrogen bonding in contrast with *cis*-**1.61** which formed anion complex *via* anion-π interaction.[95]

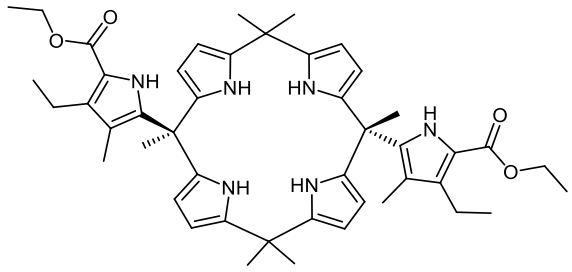

trans-**1.61**

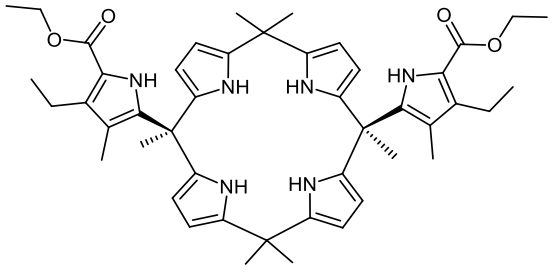

cis-**1.61**

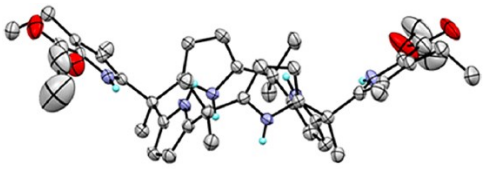

a) *cis*-**27**

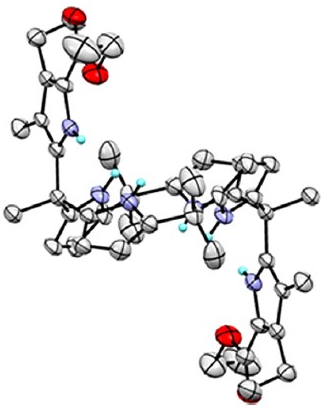

b) *trans*-**1.61**

Figure 1.13 Single crystal X-ray structure of a) *cis*-**1.61** adopting 1,3-alternate conformation b) *trans*-**1.61** adopting 1,2-alternate conformation.[95] Reproduced with permission from reference 95.

1.3.3 Preorganised metal-based receptors.

Recent developments in the field of anion binding and sensing have led to a renewed interest in the construction of metal based receptors. A considerable amount of literature has been published on metal based receptors particularly due to the diversity of their geometries, redox activities, photophysical activities and their abilities to act as Lewis acids.[96] Metal-based receptors exploit a combination of electrostatic attraction coordination and hydrogen bonds to interact with the guest molecules. Therefore, it is often observed that a metal-based receptor employs N-H group as part of their molecular structure which can serve as hydrogen bond donor.

In addition, metal ions also play important roles in the pre-organisation of the host molecules. The presence of metal ions will provide extra binding sites that can improve the selectivity and sensitivity of the host molecules. Moreover, the electron withdrawing characteristic of metals can enhance hydrogen bond donor ability of the host molecules which subsequently increase the strength of host-guest interaction.[97]

A wide range of anion hosts based on metal complexes such as copper(II)[98,99], ruthenium(II)[100], osmium(II)[100,101], rhenium(I)[102], europium(III)[103] has been synthesised and reported. Detailed examples of transition metal-based receptors and lanthanide-based receptors are discussed in the following section.

1.3.3.1 Transition metal-based receptors

The important role of metal ions as structural and signalling elements in anion binding and sensing systems has been demonstrated by the Steed group.[104] As in receptors **1.62a**-**1.62c**, the two anion-binding aminomethylpyridine ligands are organised by the semi-labile Ru(II) centre that acts as a structural core. The receptors bind strongly to Cl^- followed by acetate and nitrate ion in $CDCl_3$ solution forming both 1:1 and 2:1 anion complexes. The binding events of the anions to the hosts was observed through the ^1H NMR resonance of methylene protons Ha and Hb, in which the strongly bound anion, for instance, Cl^- collapsed the resonance to singlet while weakly bound anion such as $CF_3SO_3^-$ did not cause any significant changes even at excess concentration. The authors suggested that in the presence of tightly bound anion, i.e. Cl^-, a more symmetric 16-e^- exchange intermediate was formed from the dissociation of Cl^- driven by the transient anion.

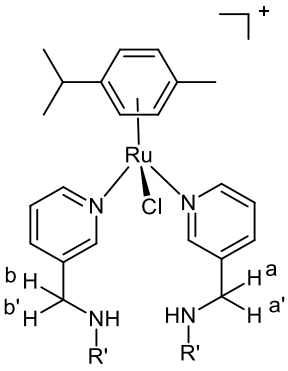

1.62

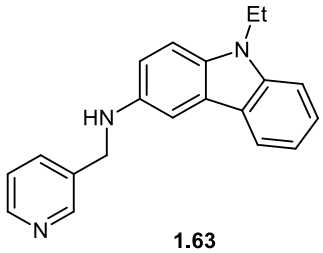

1.63

a R' = Ph
b R' = 4-$C_6H_4NO_2$
c R' = $C_{14}H_{12}N$ (as in ligand **1.63**)

Receptor **1.62c** comprises a carbazole derivative, **1.63** and has been described as a fluorescent anion chemosensor capable of sensing various anions such as Cl^-, Br^-, NO_3^- and $MeCO_2^-$. The presence of these anions resulted in partial quenching of the fluorescence (factor of ≈2.5) and a shift to shorter wavelength (λ = 447 nm for Cl^-, Br^- and $MeCO_2^-$ and λ = 456 nm for NO_3^-). A strong absorption state at λ = 370 nm region was attributed to charge transfer from p-orbital of Cl^- to an orbital localised over the central metal and pyridyl ligands that account for the mechanism for the anion to quench the intraligand charge transfer (ILCT) process.[105]

Another series of potential colourimetric and a fluorometric metal-based sensor for F^-, CN^- and AcO^- ion recognition have been reported by Maity and co-workers.[100] These sensors are an elegant example of Ru(II) and Os(II) complexes **1.65-1.68** derived from terpyridyl-imidazole ligand **1.64**. Anion binding properties were investigated using a combination of techniques such as spectrophotometric, steady-state and time-resolved fluorimetric, ^1H NMR spectroscopic, cyclic voltammetric and single crystal X-ray crystallographic techniques. Time-resolved emission studies revealed that metalloreceptors **1.65-1.68** show longer lifetimes compared to that of **1.64**, their purely organic counterparts[106] due to the presence of ruthenium(II) and osmium(II) that are known to show outstanding photophysical and electrochemical properties.[107] Significant visual colour change, remarkable absorption spectra and emission spectral changes provide evidence that all metalloreceptors **1.65-1.68** can selectively recognise CN^-, F^- and AcO^- in decreasing selectivity trend with lower limit of detection in the range of 10^{-8} M to 10^{-9} M. The authors concluded that the recognition process of selective anions proceeds *via* deprotonation of the imidazole NH proton(s) of the complexes.

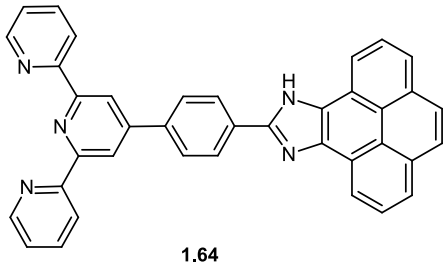

1.64

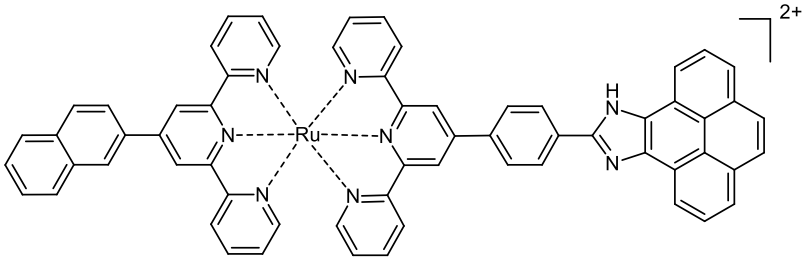

1.65

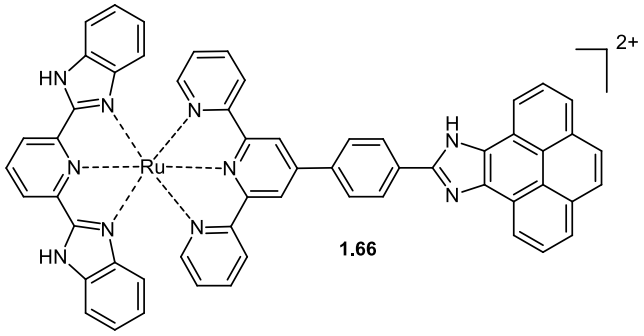

1.66

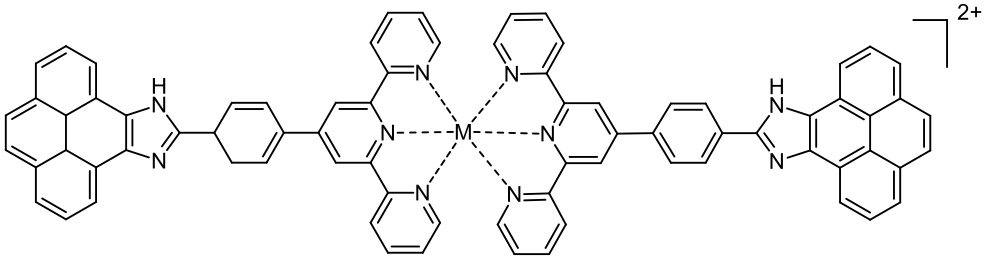

1.67, M = Ru
1.68, M = Os

Further example of metalloreceptor based on Cu(II) ion has been described Goswami and co-workers for the selective sensing of dihydrogen phosphate (DHP) by incorporating Cu(II) ions into receptor **1.69**.[108] In this system, the incorporation of a Cu(II) centre into the organic framework results in an open cavity of the metal template pre-organized macrocyclic receptor **1.70** which allows better encapsulation of DHP ion thus enhancing the selectivity of the Cu(II) complex toward DHP anion over other anions studied (iodide, bromide, chloride, fluoride, acetate, phosphate, nitrate, benzoate, and (-)-mandelate).

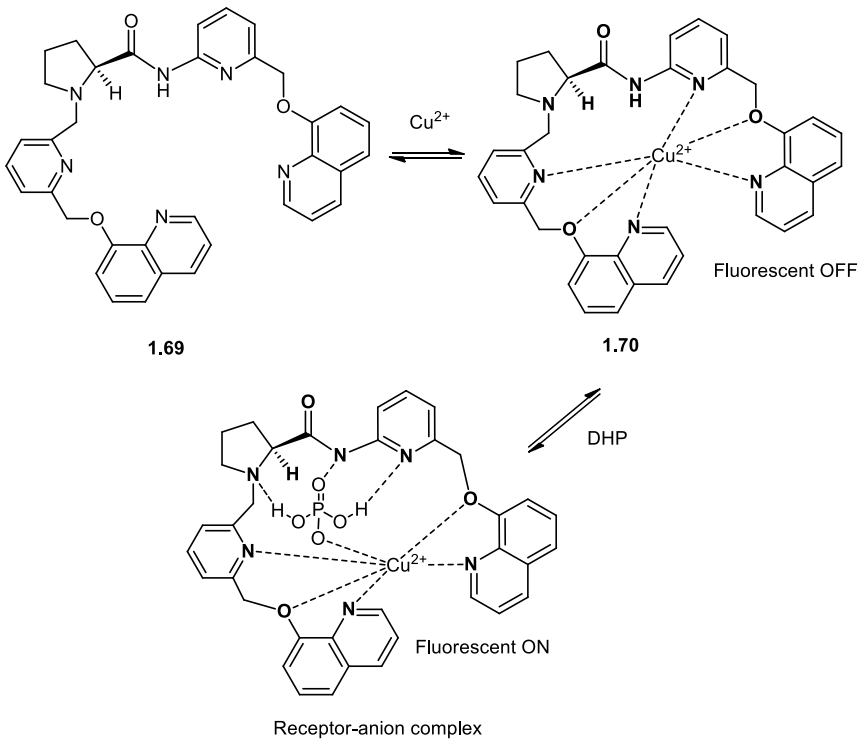

Figure 1.14 Equilibrium process showing the co-operative binding of Cu^{2+} and DHP to receptor **1.69**.[108]

Additionally, Ling and co-workers have described the synthesis of ruthenium(II) polypyridyl complex $[Ru(tpy)(H_4bbdip)]^{2+}$ (tpy = terpyridine, H_4bbdip = 2,6-bis(benzo[1,2-d:4,5-d']diimidazole-2'-yl)pyridine) **1.71** as colorimetric sensor for F^- and OAc^-.[109]

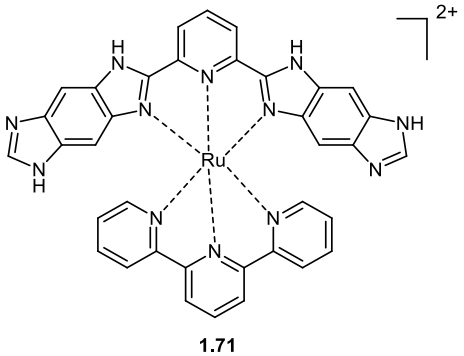

1.71

Significant changes in the absorption spectra of complex **1.72** has been observed upon addition of F^- and OAc^- anions, where the first band at 480 nm was shifted to 507 nm (0-2 equivalent) and shifted progressively to 528 nm upon addition of more than 2 equivalent of the respective anions as well as significant colour changes from yellow to red. The binding interaction between complex **1.72** and anions was investigated by

means of ^{1}H NMR spectroscopy. Upon titration with F^- and OAc^- anions, the chemical shifts of C-H proton around N-H were gradually shifted to upfield, which is correlated with the results of UV/Vis absorption titrations indicated that the binding occurs through hydrogen bonding and proton transfer from N-H to F^- and OAc^-, respectively.

Similarly, Yang and co-workers[110] reported the high selectivity of a ruthenium(II) complex carrying both imidazole and indole groups **1.73** toward AcO^- ion (K_a = 30700 M^{-1}). The addition of 40 µM of AcO^- to the complex solution results in a very significant colour change from yellow to light orange which was not visible upon addition of other anions at the same concentration. It was deduced that AcO^- binds to indole proton of **1.73** in 1:1 stoichiometry *via* hydrogen bonding (Figure 1.15), which was confirmed by significant perturbation of C-H protons around N-H group.

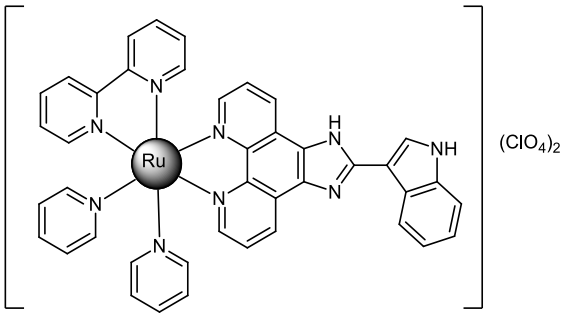

1.72

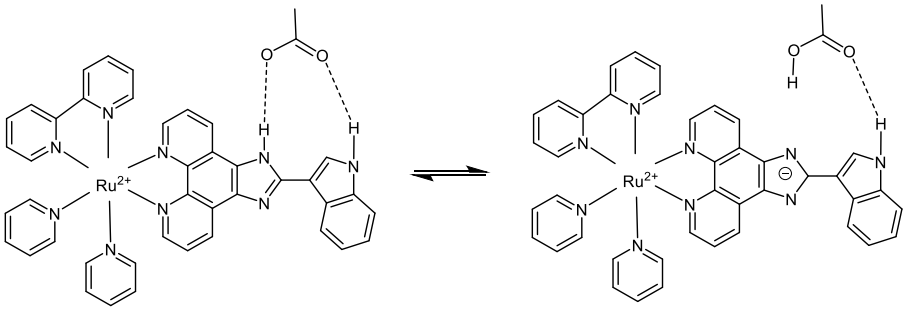

Figure 1.15 Binding of **1.73** to AcO^- *via* hydrogen bonding.

Other work, published by He and co-workers has described the anion binding studies of dinuclear phosphine gold(I) complexes (**1.74-1.76**) with bridging bis(dicyclohexylphosphino)methane auxiliary ligands and various receptor pendant groups toward various anions (F^-, AcO^-, $H_2PO_4^-$, Cl^-, Br^- and I^-).[96]

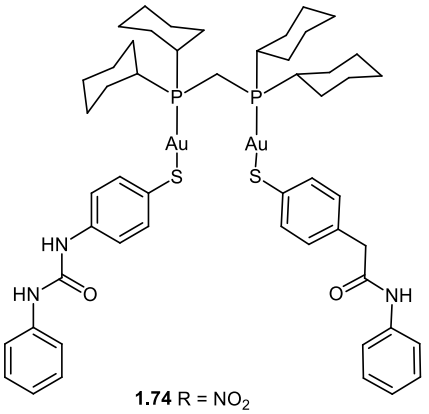

1.74 R = NO_2
1.75 R = H

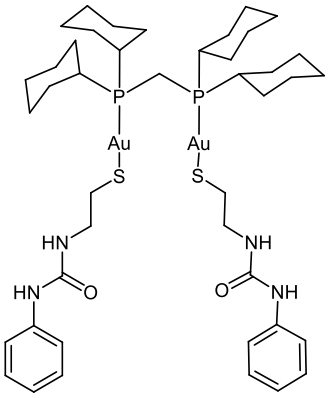

1.76

The anion binding abilities of these complexes were investigated by means of UV/Vis spectrophotometry and NMR spectroscopy. Upon addition of the basic anions (F^-, AcO^- and $H_2PO_4^-$), a significant change in UV/Vis spectra were observed, in contrast with the addition of Cl^-, Br^- or I^-. This is particularly due to the acidity of the hydrogen bond donor that enables it to form a strong hydrogen bond with basic anions. For complex **1.74** and **1.75**, the titration experiments were conducted in DMSO while for complex **1.76**, a less competitive solvent, CH_2Cl_2 was used. Based on the binding constants, all of the complexes showed similar anion selectivity trends of $F^- > AcO^- > H_2PO_4^- > Cl^- \approx Br^- \approx I^-$, which is consistent with the trend in anion basicity.[111]

Ramdass and co-workers have synthesised a range of colorimetric sensors of rhenium(I) complexes containing amide **1.77**, urea **1.78** and thiourea derivatives **1.79** of 2,2-bipyridine ligands.[102]

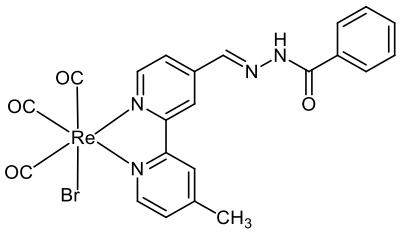

1.77

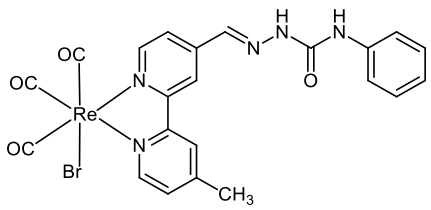

1.78

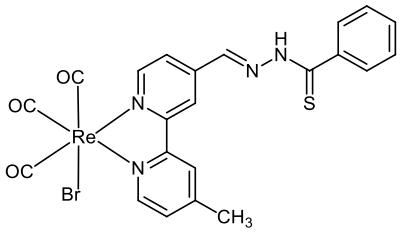

1.79

Compounds **1.77-1.79** showed colour changes from light yellow to red upon addition of anions (CN^-, F^-, CH_3COO^- and $H_2PO_4^-$), in which the intensity of the colour was strongly influenced by the binding constant of the anion complex. All receptors **1.77-1.79** bind strongly to CN^- in acetonitrile with binding constants of 3.0 x 10^4 M^{-1}, 6.5 x 10^4 M^{-1} and 8.7 x 10^4 M^{-1}, respectively. Evidence from ^1H NMR spectroscopy revealed the mechanism of recognition involves deprotonation of the NH protons of the amide/urea /thiourea moiety of the receptors.

A metalla-bowl **1.80** capable of sensing multicarboxylate anions (oxalate, tartrate and citrate) has been reported by Mishra and co-workers.[112] This metalla-bowl consists of two bis-amides as four potential hydrogen-bond donors and two Ru-acceptors as a signalling unit. Overall, all anions formed 1:1 complex with **1.80** in methanol and show increasing complex stability along the series, oxalate (4.0 x 10^4 M^{-1}) < tartrate (5.0 x 10^4 M^{-1}) < citrate (5.5 x 10^4 M^{-1}). Proton NMR titration experiments revealed the strong bidentate H-bonding interaction between amidic N-H and multicarboxylate anions.

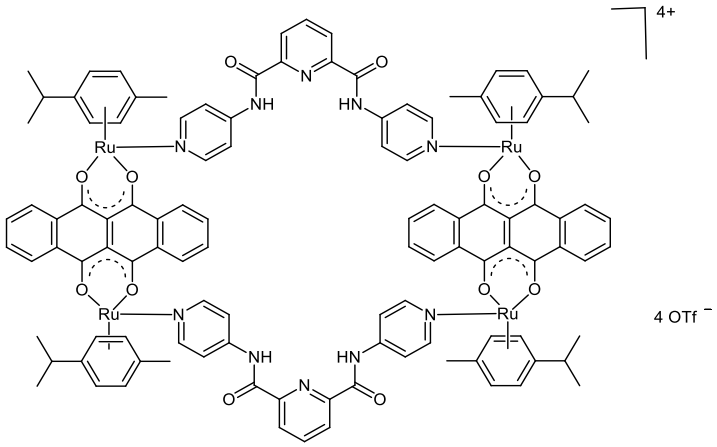

1.80

Furthermore, the Steed group has reported the anion binding ability of acyclic bis(thioureas) **1.81-1.82** and their complexes with ruthenium(II) **1.83-1.84** for selective halide anion sensing (Cl^-, Br^- and I^-).[24] In comparison with the free ligand **1.81-1.82**, both **1.83** and **1.84** bound Cl^- very strongly in acetone with binding constant of more than the value that can be accurately measured by NMR spectroscopic titration.

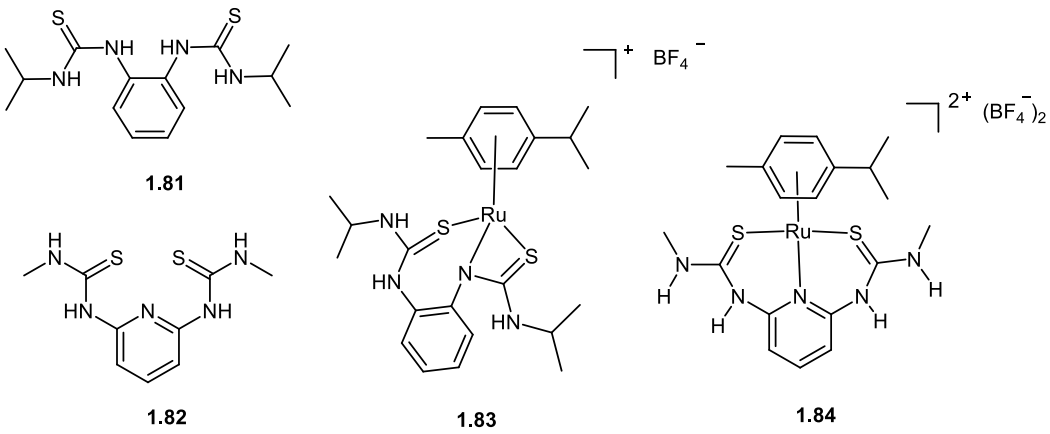

In both cases, the vital role of the coordinating metal was clearly demonstrated particularly in the enhancement of the preorganisation and acidity of the hydrogen-bond donor of bis(thiourea) receptors.[24,113] Additionally, the positive charge imparted by the metal centre contributes to the effectiveness of this receptor over the neutral free ligands. In the case of **1.84**, the presence of the metal inhibits the formation of intramolecular hydrogen bonding from the thiourea NH groups to the pyridyl nitrogen atom in free ligand **1.82** thus allow the Cl^- ion to interact with both thiourea groups.

Complexes **1.85** and **1.86** are water-soluble metallomacrocycles based on flexible imidazole ligand with spacers (as in **1.85**, where M = Pd and spacer = anthracenyl) or linkers (as in **1.86**, where M=Pd and linkers = ferrocene).[114] In these compounds the palladium(II) square planar ion act as a structural element and imparts a positive charge to the receptor. Fluorescence titration of **1.85** carried out in aqueous solution revealed strong fluorescence enhancement induced by HSO_4^- due to the dissociation of H^+ from the HSO_4^- ion. Upon addition of HSO_4^-, the fluorescent is 'turned on' instead of 'turned off' which is in contrast with other reports.[115] Utilisation of 'turned on' system in anion sensing can prevent false response and as well as producing better signal to noise ratio as the detection occurs relative to the dark background.[116] On the other hand, the binding event of receptor **1.86** was investigated using cyclic voltammetric and square wave voltammetric method in acetonitrile. Upon addition of HSO_4^-, obvious changes of the E_p values was observed indicating strongest interaction at the redox centre and subsequent appearance of the second wave at more negative potential confirmed the formation of receptor-anion complex.

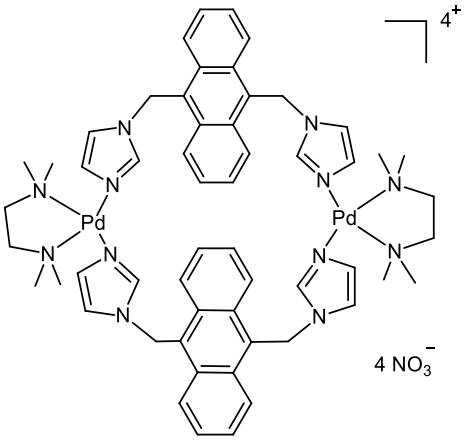

1.85

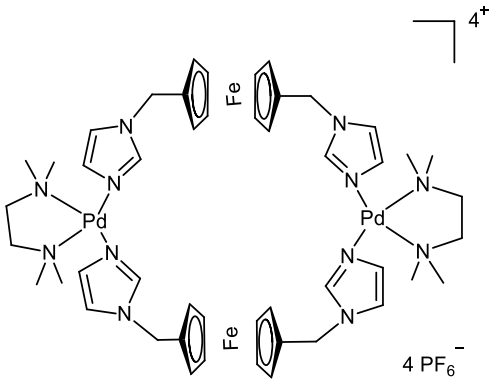

1.86

A benzimidazole-based Co^{3+} receptor **1.87** has been described by Sharma and co-workers capable of distinguishing I^- and HSO_4^- over other anions, using electrochemical and spectroscopic techniques, respectively in MeOH/H_2O (8:2, v/v) solution.[117] Addition of I^- to **1.87** caused a change in the electrochemical signal, $\Delta E_{1/2}$ = 145 mV even in the presence of other anions. On the other hand, the addition of HSO_4^- to **1.87** showed the formation of 1:1 anion complex from hydrogen bond interaction between HSO_4^- and N-H of benzimidazole which is observed using UV/Vis spectroscopy.

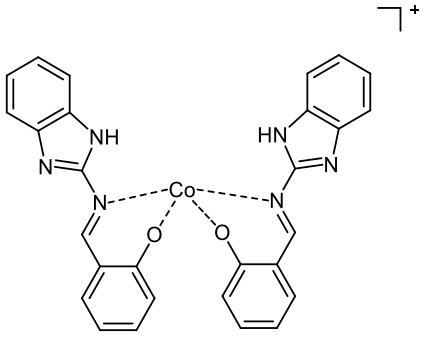

1.87

The recognition of any anions in water has been a challenge in designing anion receptors due to the high hydration energy possessed by anions. A cation displacement approach has been employed by many researchers to overcome this problem. Using this concept, Saluja and co-workers prepared a Cr^{3+} complex of benzimidazole-based compound **1.88** for the detection of F^- and HSO_4^- ion.[118] Fluorescence titration experiments show complex **1.88**.Cr^{3+} binds F^- and HSO_4^- ion in HEPES-buffered CH_3CN/H_2O (8:2, v/v) solution with binding constants of (2.89±0.25)x10^5 and (2.30±0.20)x10^6 M^{-1}, respectively.

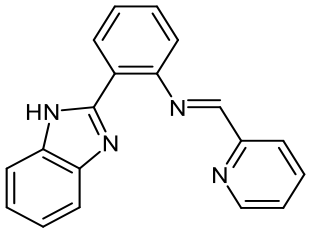

1.88

In 2014, the Yam group reported the syntheses and characterisation of alkenylplatinum(II) complexes with amide-based terpyridine ligands, **1.89** and **1.90**.[119] They chose to study square planar d^8 platinum(II) polypyridine complexes due to the spectroscopic and luminescence properties that these complexes possess as well as the ability of the complexes to self-assemble *via* Pt---Pt and aromatic π---π stacking interactions. The addition of Cl^- or Br^- ions to the acetonitrile solution of **1.89** reduced the intensity and resulted in a slight red shifts at 467 nm that corresponds to the low-energy MLCT/LMCT absorption band. Upon anion inclusion, the electron density of the amide group is enhanced, which allows photoinduced electron transfer that is responsible for the phosphorescence quenching. On the other hand, the phenyl group in **1.89** was replaced with hexyl groups to afford complex **1.90** which has better solubility in a less polar solvent such as acetone. The addition of 0 to 2 equivalent of F^- ion to acetone solution of **1.90** showed similar observation to that of **1.89** except with more pronounced changes, and subsequent addition of F^- ion has resulted in dramatic colour changes from yellow to orange-red.

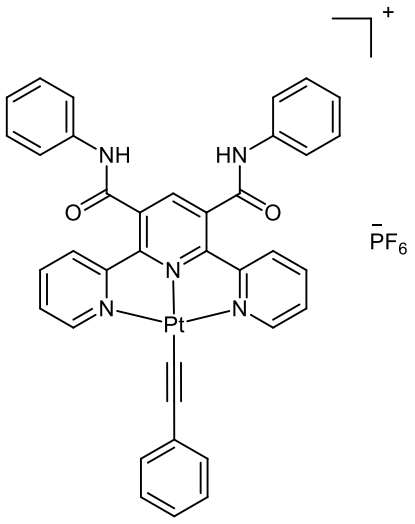

1.89

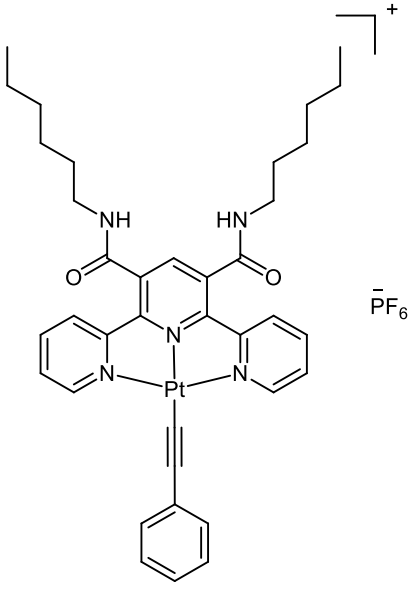

1.90

Another series of platinum(II) terpyridine complexes with amide-, urea- and sulphonamide- containing ligands attached to calixarene scaffold (**1.91**-**1.93**) have also been reported recently.[120]

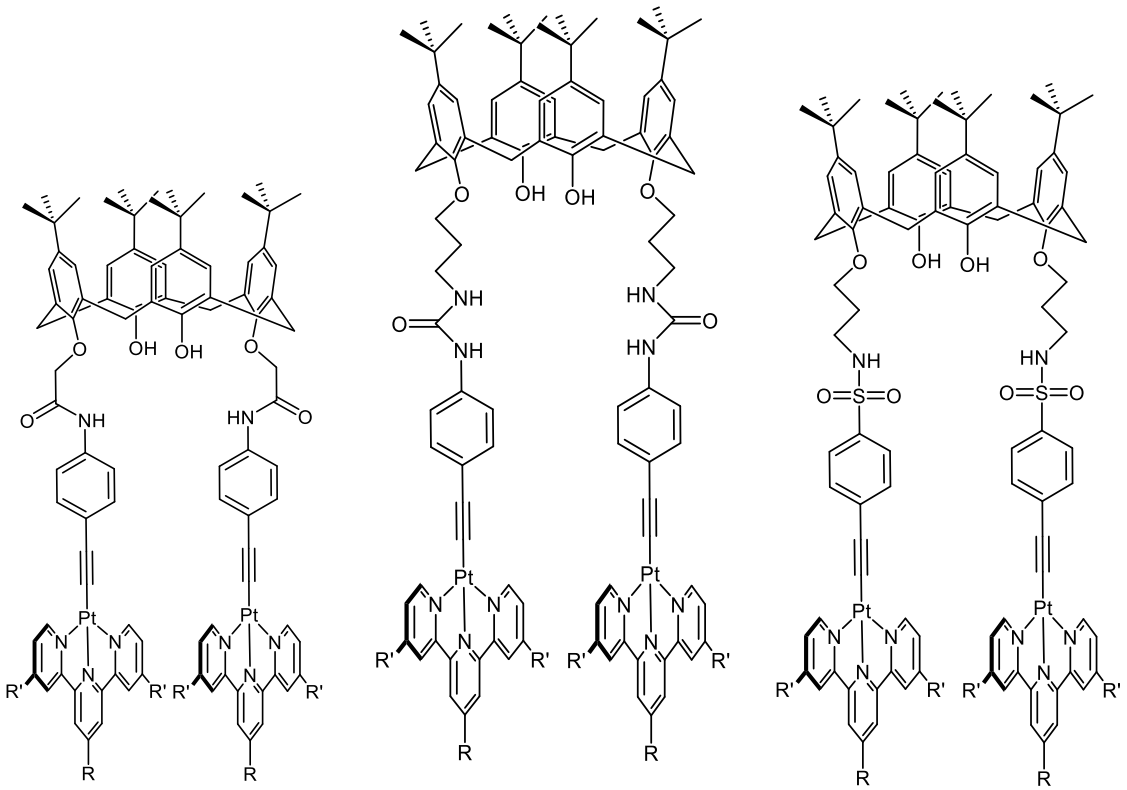

By having a bigger pocket of binding site, complex **1.91** binds $H_2PO_4^-$ ion stronger than complexes **1.92** and **1.93** that show a better encapsulation of a smaller anion such as fluoride due to the smaller cavity. Among all of the complexes, complex **1.92** show significant colourimetric changes upon addition of anions, which can be detected directly by naked eye (Figure 1.16).

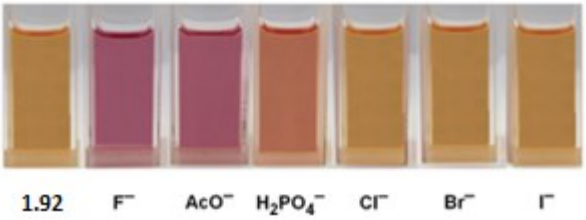

Figure 1.16 Colourimetric changes upon the addition of anions into the yellow solution of complex **1.92**. Reproduced with permission from reference 120.

The anion binding event of complex **1.93** towards F^-, OH^- and $H_2PO_4^-$ has been studied in detail with ^1H NMR titration in dicholoromethane-d_2. The addition of $F^-$and OH^- into the solution of complex **1.93** results in the disappearance of the sulphonamide NH proton, which possibly due to the deprotonation process with the calixarene phenolic proton remain unaffected. In contrast, when titrated with $H_2PO_4^-$ ion, both of the sulphonamide NH and calixarene phenolic proton signals shifted further downfield suggesting the binding of the anion to the binding site instead of deprotonation process. The broadening of the above-mentioned proton signals also suggests the presence of self-aggregation of the molecules.

Platinum-based pincer-type complexes, **1.94** has been reported as an irreversible chemodosimeter for the high selectivity detection of CN^- ion in aqueous solution.[121] This complex can detect CN^- ion despite the presence of up to 20 equivalents of other anions such as F^-, OAc^- and $H_2PO_4^-$. The mechanism of CN^- ion detection is through the displacement of the terpyridine by two CN^- ions (Figure 1.17). The displacement of the terpyridine ligand is confirmed from the fluorescence quenching of complex **1.94** that is observable under the UV-lamp (365 nm).

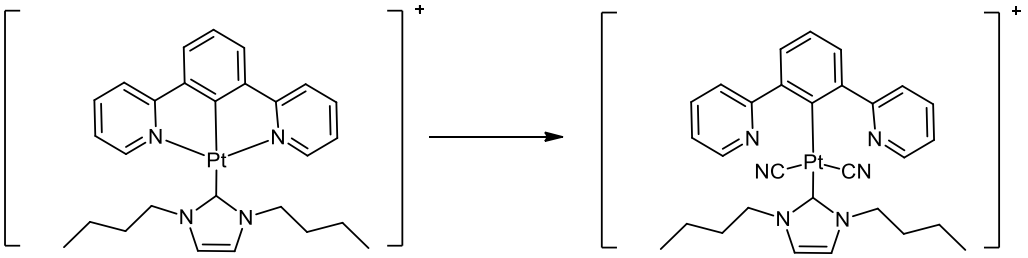

1.94

Figure 1.17 a) Dipyridylbenzene ligand displacement by two CN^- ions b) Quenching of the fluorescence of complex **1.94** under the UV-lamp (365 nm).

1.3.3.2 Lanthanide-based receptors

Apart from transition metals-based metalloreceptors, the past decades have seen the rapid development of lanthanide-organic chromophore complexes in the field of anion recognition, as lanthanide complexes can display sharp and intense emission bands and versatile colour changes upon interaction with anion guests.[103] Additionally, lanthanide complexes can provide strong electrostatic interactions with anions due to their positive charge and oxophilic character.[122] Apart from that, lanthanide complexes can respond to a wide range of analytes through different sensing mechanism. In contrast with transition metal ions, direct excitation of lanthanide ions is inefficient due to their low absorption coefficient, and it is susceptible to interference caused by solvent molecules such as water which subsequently leads to nonradiative deactivation processes.[123] Often attached to lanthanide ions are antenna chromophores or sensitizers which can shift the excitation wavelength of lanthanide to the visible region. Recent reports on lanthanide complexes, particularly Eu^{3+} and Tb^{3+} have discussed the roles of lanthanide complexes in bioanalytical applications.[124–126]

An antenna ligand, 2-(3,4,5-trimethoxyphenyl)imidazo[4,5-f]-1,10-phenanthroline scaffold was utilised by Zheng and co-workers[103] to construct europium-based **1.95** anion sensor.

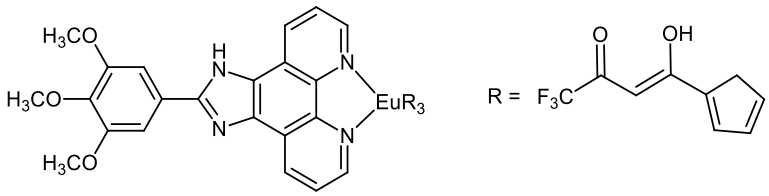

1.95

The photophysical properties of **1.95** were determined *via* UV/Vis and fluorescence spectroscopy in dimethylsulfoxide. The addition of eight equivalents of fluoride ion to complex **1.95** resulted in the disappearance of a peak at 283 nm which corresponded to the aromatic moiety and phenanthroline heterocyclic ring and emergence of a new peak at 294 nm indicated the formation of hydrogen bond between complex **1.95** and F^- ion. The similar effect was also observed upon addition of 3-10 equivalents of acetate ion (as the tetrabutylammonium, TBA salt). Titration of complex **1.95** with five equivalents of

F^-, $H_2PO_4^-$ and AcO^- ions displayed prominent colour changes from pink to purple, blue and green, respectively (Figure 1.18).

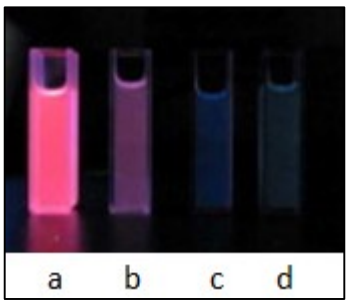

Figure 1.18 Colour changes upon addition of F^-, $H_2PO_4^-$ and AcO^- ions (a: no anion; b: 5 eq. F^-; c: 5 eq. of $H_2PO_4^-$; d: 5 eq. of AcO^-) into the solution of complex **1.95**. Reproduced with permission from reference 103.

Similarly, Butler and co-workers have synthesised series of europium(III) complexes **1.95-1.100** based on triazacyclononane, which were utilised in the recognition of oxy-anions in aqueous media.[125] The ligands consist of two strongly absorbing arylalkynyl-pyridyl chromophores, generating "bright" complexes which are useful in the construction of responsive emissive probes. In this system, the binding of several oxy anions such as carboxylates, lactate and citrate were assessed by means of emission spectral titrimetric analysis. Water molecules were replaced by oxy-anions or amino acid residues (hard donor) to form complexes **1.95-1.100**. The displacement of water molecules causes a change in the spectral fingerprint as well as an increase in the emission intensity. Complexes **1.96-1.99** bind strongly to lactate, benzoate and bicarbonate with binding affinity ranging from log K_a = 3 to 4. Other than oxy-anions, receptor **1.98** binds strongly to fluoride ions in 50% aqueous methanol due to the large steric demand at the metal centre. The hydrophilic characteristic of this complexes enables it to be internalised readily into mammalian cells for staining purposes. The brighter the complexes, the more advantages it can offer in bioanalytical application. Brighter complexes often require less excitation light and lower concentration which will cause less photodamage to the living specimen in the former case and the latter case will minimise disturbances of metal ion homeostasis.[127]

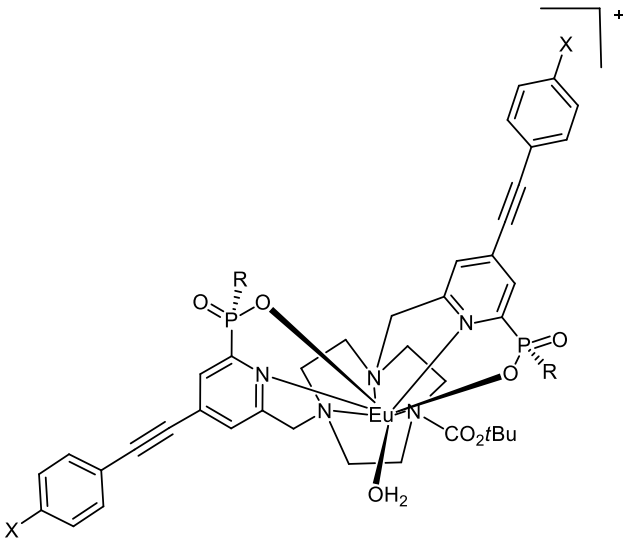

[EuXL^1] **1.96** X = $O(CH_2CH_2O)_3Me$, R = H
[EuXL^2] **1.97** X = CF_3Me, R = Ph
[EuXL^3] **1.98** X= OMe, R = Me
[EuXL^4] **1.99** X = OCH_2COOH, R = Me
[EuXL^5] **1.100** X = $OCH_2CONHCH_2CH(OH)CH(OH)CH(OH)CH(OH)CH_2OH$, R = Me

More sophisticated d-f mixed-metal complexes have been described by Shinoda and co-workers,[124] combining Pt(II) and lanthanide(III) centres to specifically recognize the chirality of succinate anions. In this system, a platinum(II) complex has been attached to the pyridine moieties of cyclen-lanthanide complexes to yield series of mixed-metal complexes **1.101-1.104**. Single crystal X-ray structure determination of complex **1.104** revealed two different metal centres were successfully incorporated into the single complex (Figure 1.19).

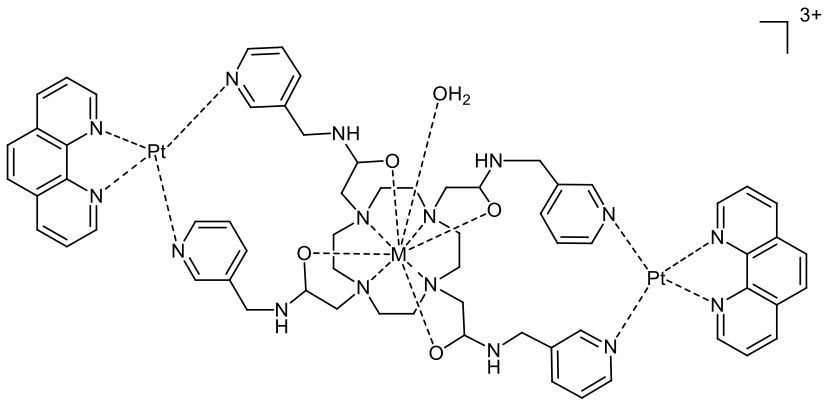

1.101 M= Lu^{3+}
1.102 M= Yb^{3+}

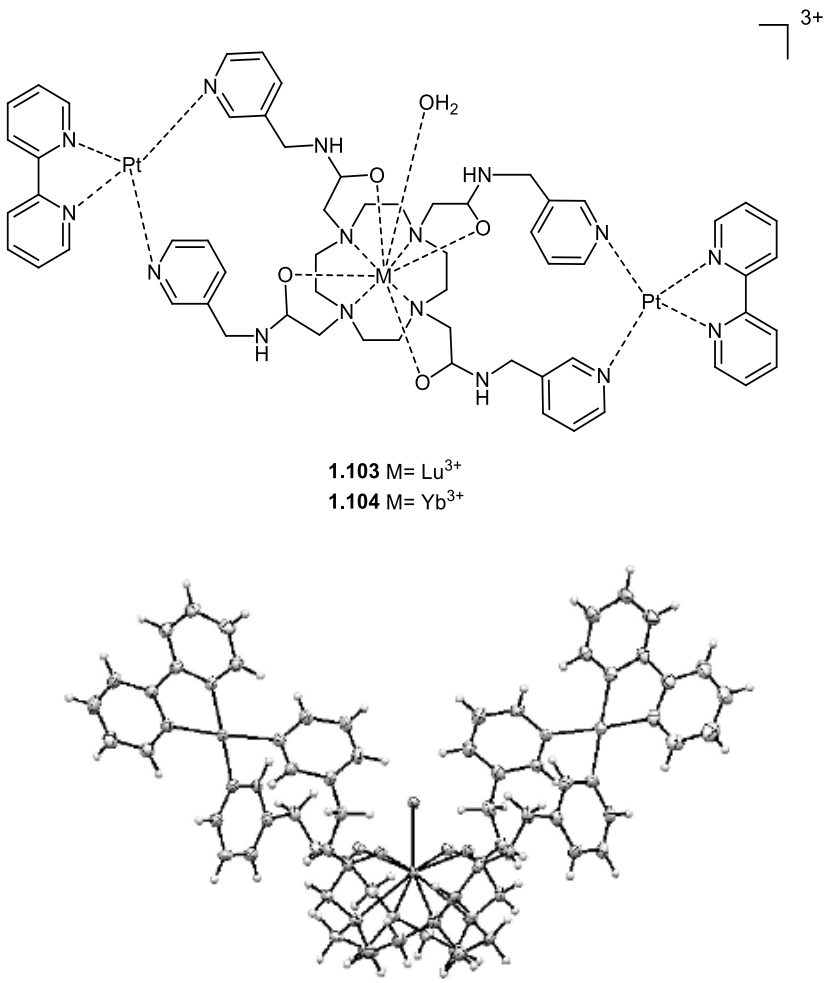

1.103 M= Lu^{3+}
1.104 M= Yb^{3+}

Figure 1.19 Single crystal X-ray structure of complex **1.104**.[124] Reproduced with permission from reference 124.

In this work, circular dichroism (CD) spectroscopy was employed to determine the absolute configuration and enantiomeric excess of monocarboxylate and dicarboxylate anions. In this system, the Pt^{2+} and Ln^{3+} centres formed strong binding with the dicarboxylate anions, proved by selective CD responses governed by the chain length and chirality of the dicarboxylate substrates.

1.3.4 Ion pair receptors

Another class of receptors are ion-pair or ditopic receptors which are designed to simultaneously recognise both anions and cations. The common designs of ion-pair receptors are illustrated in Figure 1.20.[128] The first design emphasises the formation of cascade complex comprises of anions forming a bridge to encapsulate two cations. For

separated ion pair (design b), the cation and anion sites are located further apart in contrast with contact ion pair (design c) where both of sites are nearby.

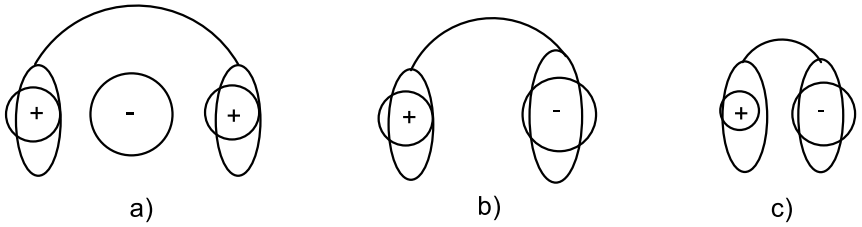

Figure 1.20 Common designs of ditopic receptors: a) Cascade complex b) Heteroditopic receptor for separated ion pairs c) and contact ion pairs.

Oligoether-strapped ion-pair receptor **1.105** synthesised by Park and co-workers is one of an elegant example of its type, consists of both a strong anion-binding site and two possible cation recognition sites.[129] The crystal structure of CsCl complex of receptor **1.105** revealed two complexation modes for cation by the oligoether (A) and within the tetrapyrrolic "cup" of calix[4]pyrrole (B) as shown in Figure 1.21.

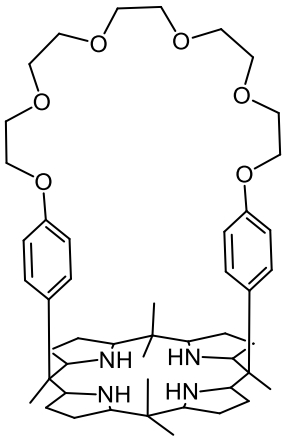

1.105

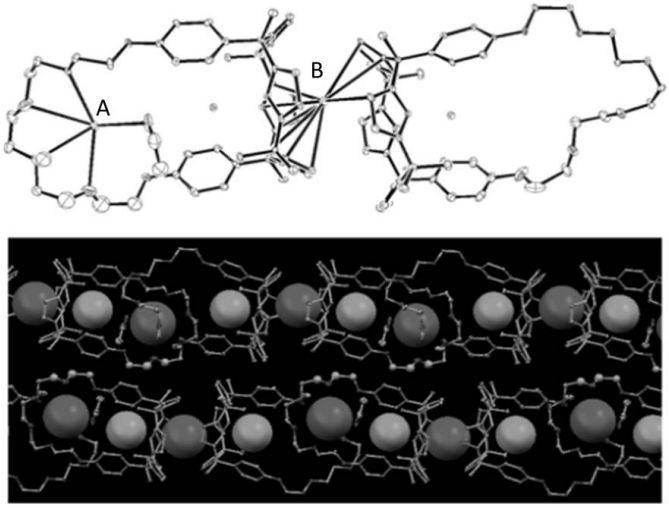

Figure 1.21 Single-crystal X-ray structure of the cesium chloride complex of receptor **1.105**[129] Reproduced with permission from reference 129.

The ^{1}H NMR spectroscopy and isothermal titration calorimetry (ITC) method were employed to determine the binding constant with both methods concurring to give a selectivity series of $F^- > AcO^- > Cl^-$. The binding constant for F^- in CD_3CN is remarkably high which is 4.88 x 10^8 M^{-1}, contributed by hydrogen bond interaction as well as stabilizing anion-π interactions of two phenyl groups presence in the moieties. The effect of counterion has also been studied by treating [**1.105**.F]$^-$ and [**1.105**.Cl]$^-$ with

alkaline metal ion salts namely Li^+, K^+, Na^+ and Cs^+ in a mixture of acetonitrile/methanol (9:1 v/v). Different complexation modes have been observed depending on the metal salts used. Cs^+ ion was proved to bind to the cup of the calix[4]pyrrole moiety forming receptor mediated ion-pair complex for both [**1.105**.F]$^-$ and [**1.105**.Cl]$^-$, confirmed by a significant downfield shift in β-pyrrolic proton signals along with little changes in oligoether moiety. In contrast, the addition of K^+ cation to [**1.105**.F]$^-$ caused a significant downfield shift of ether bridges as well as upfield shift of pyrrole N-H protons indicated that ion pair [K^+.F^-] is bound within the receptor cavity. A similar result was found upon addition of Li^+ cation to [**1.105**.Cl]$^-$.

Similarly, benzocrown-ether-capped ion-pair receptor **1.106**, designed by Park and co-workers formed stable 1:1 complexes with fluoride and chloride ions (as tetraalkylammonium salts) in $CDCl_3$.[130] Formation of two different ion-pair complexes depending on the nature of the cation has been clearly demonstrated as well. Single-crystal structural studies revealed that calix[4]pyrrole moiety of **1.106** adopts a partial cone conformation suitable for cation and anion sensing (Figure 1.22a). On the other hand, CsF complex of **1.106** formed a receptor-shared ion-pair complex in which the fluoride ion is bound tightly inside the cavity, while cesium ion is bound within the calix[4]pyrrole (Figure 1.22b). In contrast, single crystal X-ray structure of LiCl complex of **1.106** revealed the formation of water-separated dimeric ion-pair complex [{**1.106**.LiCl-(H_2O)}$_2$] (Figure 1.22c).

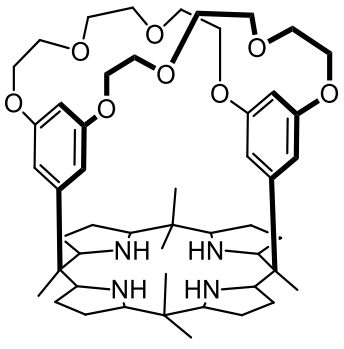

1.106

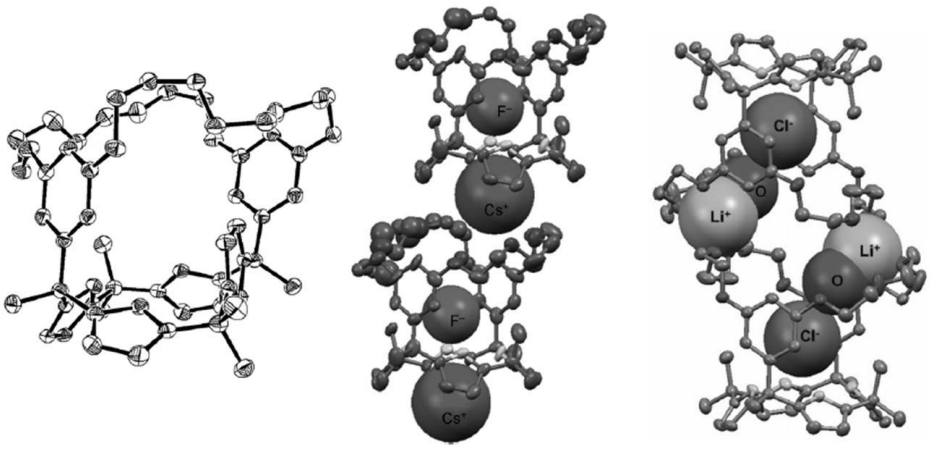

Figure 1.22 a) Partial cone conformation of calix[4]pyrrole moiety of **1.106** b) CsF complex of **1.106** c) LiCl of **1.106**.[130] Reproduced with permission from reference 130.

In 2012, the Beer group reported the synthesis of a heteroditopic receptors comprised of calix[4]-diquinone triazole **1.107** and their interaction with cations (K^+, Na^+ and NH_4^+) and anions (Cl^-, Br^- and I^-).[131] Binding experiments, carried out using ^1H NMR spectroscopy and UV/Vis spectroscopy in 2% D_2O/CD_3CN revealed that **1.107** underwent a conformational change to enable the lower rim oxygen and triazole nitrogen donors to complex with the cation with selectivity trend of Na^+ (460 M^{-1}) > K^+ (155 M^{-1}) > NH_4^+. The anion binding experiments conducted revealed the selectivity trend of Cl^- (178 M^{-1}) > Br^- (67 M^{-1}) > I^- (31 M^{-1}) suggested that bistriazole-isophthalamide cavity of **1.107** is more suitable for the inclusion of Cl^- ion. Compared to the cation-free form of receptor **1.107**, the association constants are significantly enhanced by 3 to 11 times greater for the halides ion in the presence of all cations.

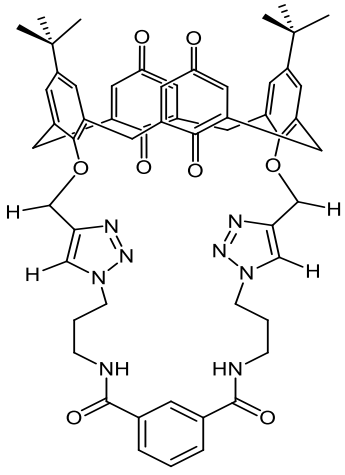

1.107

Recently, a ferrocene-strapped system **1.108-1.110** having an electrochemically-active sensing unit was reported by Alfonso and co-workers.[132] Voltammetric studies of **1.108-1.110** revealed a reversible two-electron oxidation wave at $E_{1/2}$ = 623 mV for **1.108** and one-electron oxidation wave at $E_{1/2}$ = 630 mV and $E_{1/2}$ = 675 mV, for **1.109** and **1.110**, respectively, corresponding to the ferrocene couple. The addition of anions, such as AcO^- and $H_2PO_4^-$ to **1.108-1.110** in acetonitrile, resulted in a cathodic shift of the cyclic voltammetric wave. Conversely, the addition of HSO_4^- results in a slight anodic shift, contributed by the acidic nature of HSO_4^- that promotes a guest-to-host proton transfer reaction accompanied by hydrogen bonding and electrostatic reaction.

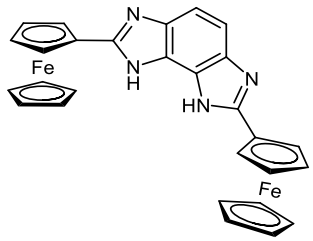

1.108

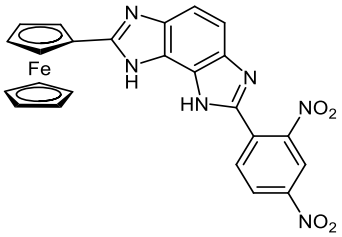

1.109

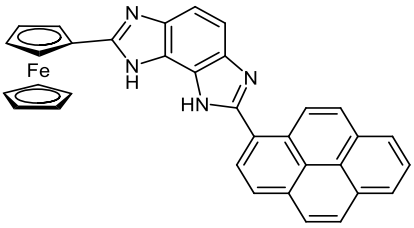

1.110

McConnell and co-workers have studied the ion-pair binding properties of a series of ditopic calix[4]diquinone receptors **1.111-1.115** in acetonitrile.[133] It contains calix[4]arene subunit for cation recognition and diquinone units for anion recognition. Enhanced binding of ion-pairs over 'free ions' was observed for receptor **1.111**, **1.112** and **1.114** (1:1 stoichiometry) showing selectivity trend of the following order; NH_4Cl > KCl > NaCl in 0.5% *v/v* H_2O/CH_3CN. In the case of receptor **1.111** and **1.112**, ^1H NMR spectroscopic titration study carried out in CD_3CN/D_2O (98/2, v/v) shows that the presence of coordinating cation enables chloride ion recognition which could not be achieved in its absence.

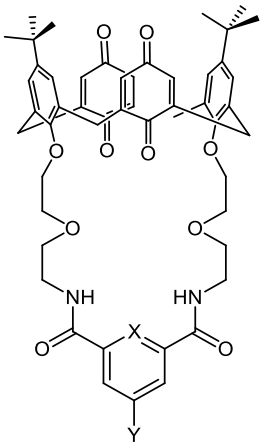

1.111 X = CH, Y = tBu
1.112 X = N, Y = H

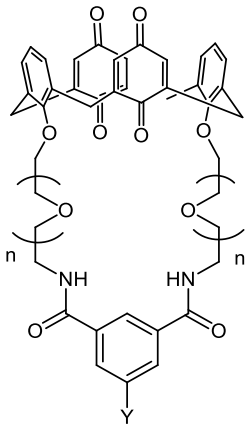

1.113 n = 1, Y = H
1.114 n = 1, Y = NO_2
1.115 n = 2, Y = H

An elegant example of ion-pair receptors **1.116-1.117** based on anion-π interaction has been produced by Chen and co-workers.[134] The ability of these receptors to interact with ion pairs was examined by fluorescence and ^{1}H NMR titration experiments. The titration of fluoride ion with [**1.116**.Zn]$^{2+}$ and [**1.116**.Pb]$^{2+}$ resulted in an enhancement of fluorescence intensity band at 425 nm, with the association constants of 1.53 x 10^5 M^{-1} and 3.71 x 10^3 M^{-1}, respectively. The presence of Zn^{2+} ion has tremendously increased the binding constant more than 23-fold from its parent compound **1.116** (K_a = 6.59 x 10^3 M^{-1}). Additionally, anions such as chloride, bromide and nitrate that were not recognised by **1.116** have successfully bound to [**1.116**.Zn]$^{2+}$ with a binding constant of 7.39 x 10^3 M^{-1}, 1.59 x 10^3 $M^{-1}$and 4.25 x 10^3 M^{-1}, respectively. Likewise, in the presence of metal ions such as K^+, Cs^+, Ca^{2+} and Sr^{2+}, cyanide ion was found to bind to **1.117** with binding constant ranging from 3.46 x 10^3 M^{-1} to 8.36 x 10^3 M^{-1}. The author concluded that the mechanism of ditopic interaction of **1.116** with Zn^{2+} and anion species proceeds *via* interaction of anion with the electron-deficient triazine ring, [anion-**1.116**-Zn]$^{2+}$.

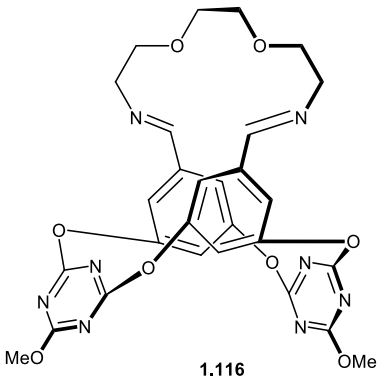

1.116

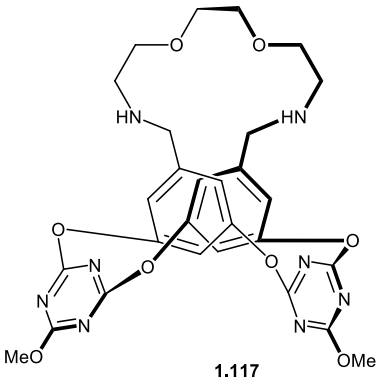

1.117

Another ditopic receptor derived from **1.118** has been reported by the Carreira-Barral group.[98] Spectrophotometric titrations carried out for the Cu(II) complex of **1.118** revealed the formation of anion binding complex with decreasing affinity as follows: $MeCO_2^-$ ~ Cl^- (log K_{11} > 7) > NO_2^- > $H_2PO_4^-$ > Br^- > HSO_4^- > NO_3^- (*log* K_{11} < 2). The single crystal X-ray structure of the [Zn(**1.118**)Cl_2] complex revealed that the ligand adopted 'bent propeller' conformation due to the presence of intramolecular slipped π-π stacking interaction between N atom of the pyridine ring and the benzylurea fragment[135] while chloride anion is coordinated *via* hydrogen-bonding with the NH group of the urea fragment (Figure 1.23a). On the other hand, the single crystal structure of [Cu(**1.118**)NO_3] revealed the interaction between the [Cu(**1.118**)(ONO_2)(OHMe)]$^+$ cation with nitrate ion *via* bifurcated hydrogen bond, forcing the ligand to adopt an 'open wing butterfly' conformation (Figure 1.23b). The addition of different anions leads to different binding stoichiometry, for instance, the addition of HSO_4^- provokes the formation of a 1:1 species, while the addition of other anions such as Cl^-, NO_2^-, $H_2PO_4^-$ and Br^- results in the formation of 1:2 (metal/anion) species.

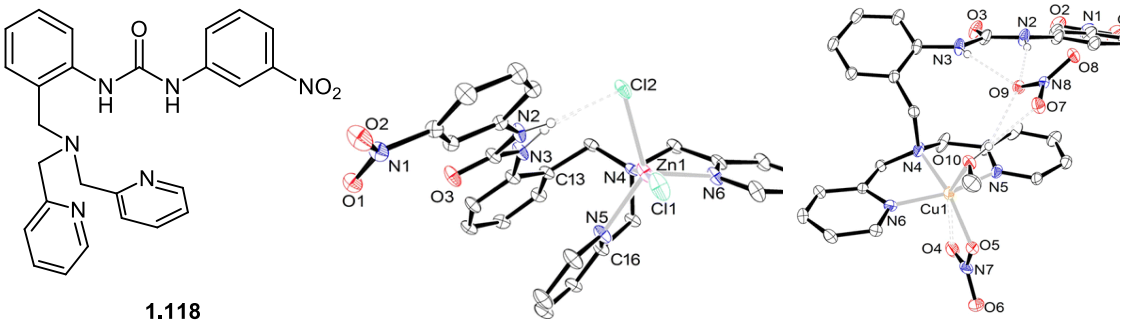

Figure 1.23 a) 'Bent propeller' conformation of [Zn(1.118)Cl_2] b) 'Open wing butterfly' conformation of [Cu(**1.118**)NO_3].[98] Reproduced with permission from reference 98.

Recently, Romanski and Karbarz have reported an ion-pair receptor, **1.119** that is consist of anthraquinone-thiourea unit responsible for anion binding and a crown ether-based cation binding site.[136] In the presence of sodium ion, receptor **1.119** has shown a very high affinity toward Cl^- and Br^- ions which is 3.09 times and 4.28 times, respectively, more strongly associated in comparison with the absence of sodium ion. Upon titration with one equivalent of different salts, namely NaCl, KCl and NH_4Cl, the crown ether unit has shown a high selectivity toward Na^+ ion with binding constant, K = 30900 M^{-1} over K^+ and NH_4^+ ions with binding constant of 6900 M^{-1} and 4450 M^{-1}, respectively. The

authors also suggest that the association of sodium ion to the crown ether unit diminishes the electron density in the phenyl ring linked with the anion binding site, thus reinforces stronger anion binding.

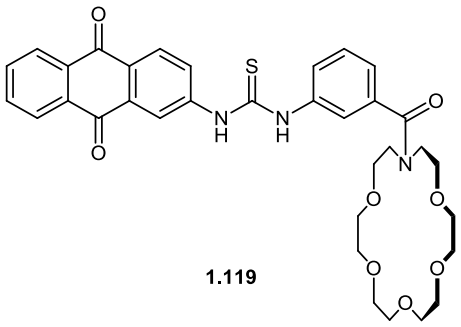

1.119

1.4 Summary

Over recent years, the important progress achieved in anion sensing and binding has been exemplified by numerous systems that have been described in this field. Furthermore, the concept of pure anion binding has been extensively exploited in real-world applications, such as sensing, catalysis and the medicinal use of transmembrane anion transport. It is also anticipated that this research field will continue to grow in the coming years.

1.5 Project Aims and Overview

The aim of this project is to get closer towards fully understanding how imidazole urea derivatives and their transition metal complexes interact with variety of anions in organic solvents. While studies on the interactions of pyridyl urea derivatives and their complexes with various anions have been well-documented, there is very little published research on how imidazole urea interacts with the anions and how the imidazole group contributes in the hydrogen bonding interactions in the molecule. The choice of ligands for the synthesis of these hosts was inspired through the work of Barboiu group in which the imidazole urea synthesised was capable of forming mixed ion–water channel-like superstructures, useful for ion recognition as well as supramolecular transport devices.[137,138]

In the previous sections, we have described different types of anion receptors and how they have been constructed, particularly involving the necessary interactions needed to encapsulate or bind with the respected anions. Of particular interest is the use of electrostatic interaction and hydrogen bonding in the design of anion receptors. Hydrogen bond-based anion receptor such as ureas, amide and thioureas have been well studied due to the high degrees of directionality and are often easy to prepare, although some of them may display poor solubility in less competitive organic solvents. The preparation of imidazole urea compounds and their transition metal complexes as well as their interaction with various anions wil be discussed in detail in Chapter 2 and 3.

On the other hand, when selecting a core to base an anion receptor on, there are merits and weaknesses that need to be accounted for. For instance, ligand frameworks based on organic molecules are highly versatile as well as being more stable as the introduction of the anions will not alter the structure of the receptors. Therefore for this purpose, we decided to use two common organic scaffolds derived from 1,3,5-tribromo-2,4,6-triethylbenzene and tetrakis-*p*-bromomethylated mesityl calix[4]arene (Figure 1.24).

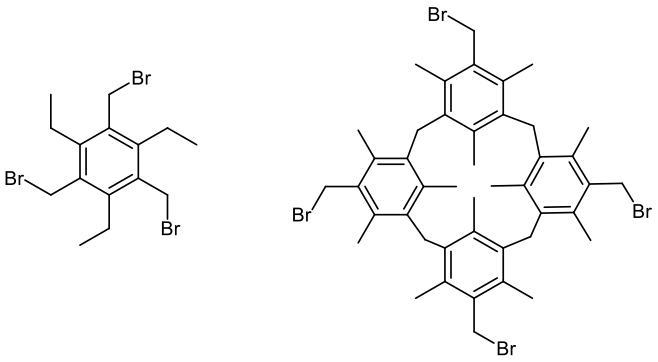

Figure 1.24 Organic scaffolds; 1,3,5-tribromo-2,4,6-triethylbenzene and tetrakis-*p*-bromomethylated mesityl calix[4]arene.

The former is chosen due to the degree of preorganisation that it can offer in which all the three binding arms can be projected in one direction to form a conical conformation. Similarly, the latter can provide similar degree of preorganisation and would be able to encapsulate at least two anions simultaneously. The anion receptor based on the organic scaffolds can be prepared by reacting the desired scaffold with imidazole urea compounds synthesised prior the reaction (Scheme 1.1). The synthesis of these organic-based anion hosts and their binding behaviour towards anions will be discussed in detail in Chapter 4.

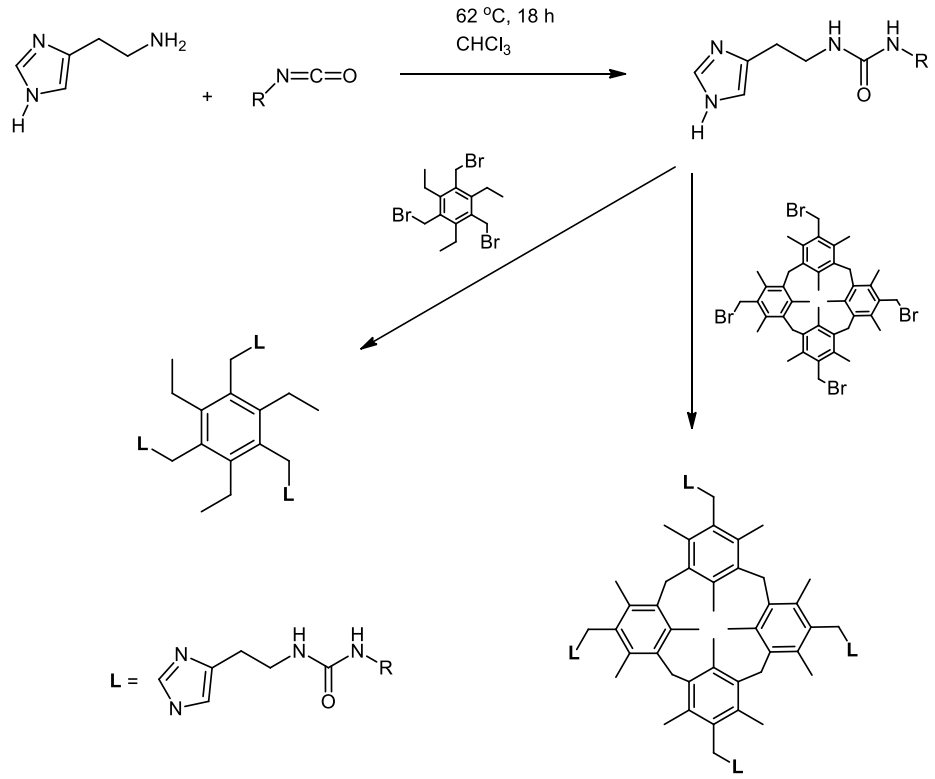

Scheme 1.1 Stepwise synthesis pathway of imidazole urea compounds based on organic scaffold. The ligand is connected to the organic core through N atom and there is a possibility of isomerism.

However, despite the versatility of the organic molecules, one of the drawbacks of using organic scaffold is the reaction is often unpredictable and highly dependent on the nature of their structure in this case, which may lead to the formation of isomers. Thus, another option of using transition metal as the core is also considered in the preparation of the suitable anion receptors. Although metal-based anion receptors are often more predictable in in terms of their geometry, it is highly dependent on the lability of the transition metals. For example, labile transition metals such as copper and cobalt could be easily replaced by anions such as chloride and cyanide. Therefore, we decided to use three different less labile metals namely platinum(II), palladium(II) and ruthenium(II) as a base for the host complexes. For this purpose, we have prepared a series of tripodal [9]ane-S_3-capped Ru(II) complexes (Scheme 1.2) as well as bipodal Pt(II) and Pd(II) complexes using chelating ligands such as ethylenediamine, cyclohexanediamine and 1,2-Bis(diphenylphosphino)ethane (Scheme 1.3).

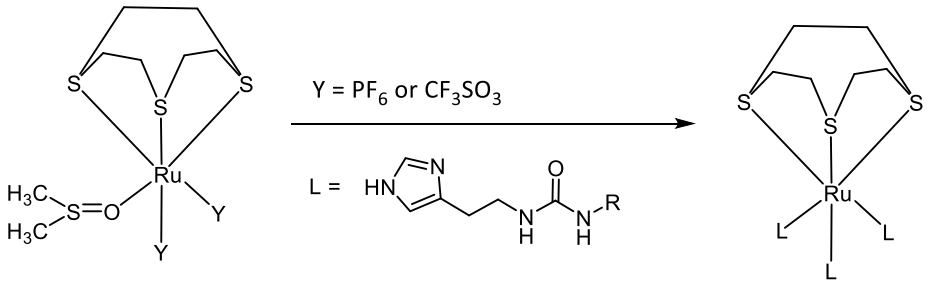

Scheme 1.2 Preparation of ruthenium(II) complexes using mixed ligands system of trithiacyclononane and imidazole urea ligands.

a)

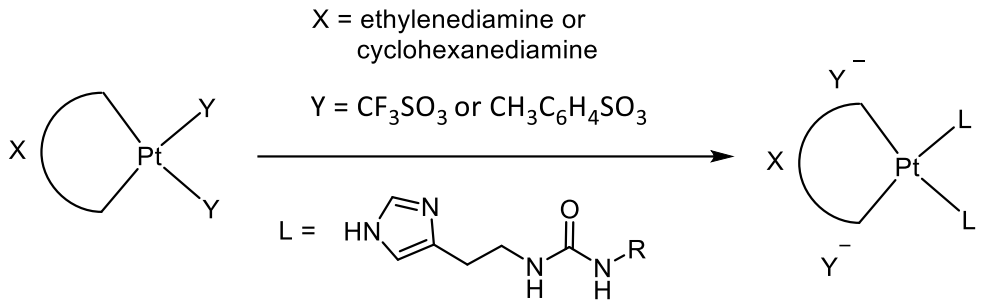

b)

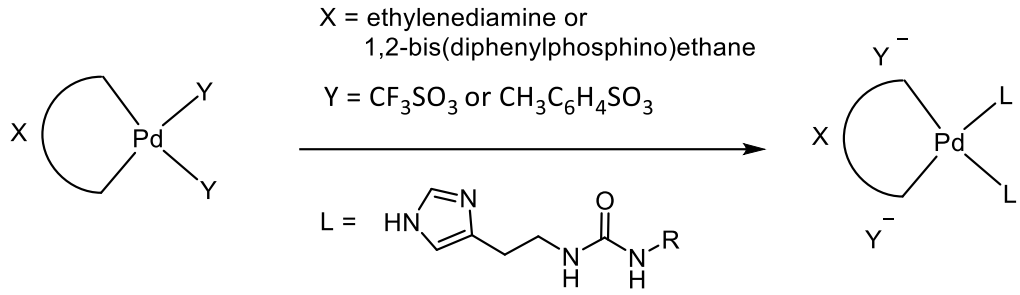

Scheme 1.3 a) Preparation of Pt(II) complexes using mixed ligands system of ethylenediamine or cyclohexanediamine and imidazole urea ligands b) Preparation of Pd(II) complexes using mixed ligands system of ethylenediamine or 1,2-Bis(dipehnylphosphino)ethane (dppe) and imidazole urea ligands.

The synthesis of the transition metal-based anion receptors and their binding behaviour towards selected anions will be investigated using ^{1}H NMR titration spectroscopy where appropriate. Data from the titration experiments will be able to provide information on the degree of pre-organisation and flexibility of the hosts synthesised and is discussed in detail in Chapter 5 and 6.

1.6 References

(1) Swinburne, A. N.; Paterson, M. J.; Fischer, K. H.; Dickson, J.; Wallace, E. V. B.; Belcher, W. J.; Beeby, A.; Steed, J. W. *Chem. Eur. J.* **2010**, *16*, 1480–1492.

(2) Quinn, W.; Saeed, M.; Powell, D. R.; Hossain, M. A. *Int. J. Environ. Res. Public Health* **2010**, *7* (5), 2057–2070.

(3) Gale, P. A.; Busschaert, N.; Haynes, C. J. E.; Karagiannidis, L. E.; Kirby, I. L. *Chem. Soc. Rev.* **2014**, *43* (1), 205–241.

(4) Haynes, C. J. E.; Gale, P. A. *Chem. Commun.* **2011**, *47* (29), 8203–8209.

(5) Liu, Y.; Ai, K.; Cheng, X.; Huo, L.; Lu, L. *Adv. Funct. Mater.* **2010**, *20* (6), 951–956.

(6) Langton, M. J.; Beer, P. D. *Chem. Eur. J.* **2012**, *18* (45), 14406–14412.

(7) Wang, D.-X.; Wang, M.-X. *J. Am. Chem. Soc.* **2013**, *135* (2), 892–897.

(8) G.C. Miller, C. A. Pritsos. In *Cyanide, social, industrial and economic aspects, In: Proceedings of the TMS Annual Meeting*; 2001; pp 73–81.

(9) Costello, L. C.; Franklin, R. B. *Mol. Cancer* **2006**, *5* (17), 1–13.

(10) Hirschhaeuser, F.; Sattler, U. G. A.; Mueller-Klieser, W. *Cancer Res.* **2011**, *71* (22), 6921–6925.

(11) Dhup, S.; Dadhich, R. K.; Porporato, P. E.; Sonveaux, P. *Curr. Pharm. Des.* **2012**, *18* (10), 1319–1330.

(12) Toussaint, N. D.; Pedagogos, E.; Tan, S. J.; Badve, S. V.; Hayley, C. M.; Parkovic, V.; Elder, G. J. *Nephrology* **2012**, *17*, 433–444.

(13) Foley, R. N. *Clin. J. Am. Soc. Nephrol.* **2009**, *4*, 1136–1139.

(14) Zoccali, C.; Ruggenenti, P.; Perna, A.; Leonardis, D.; Tripepi, R.; Tripepi, G.; Mallamaci, F.; Remuzzi, G. *J. Am. Soc. Nephrol.* **2011**, *22*, 1923–1930.

(15) Jentsch, T. J.; Maritzen, T.; Zdebik, A. A. *J. Clin. Invest.* **2005**, *115*, 2039–2046.

(16) Steed, J. W.; Atwood, J. L. *Supramolecular Chemistry, 2nd edition*; John Wiley & Sons, Ltd, 2009.

(17) J.P. Behr. *"The lock-and-Key principle. the State of the Art-100 years on.";* J. Wiley & Sons: Chichester, 1994.

(18) Li, X.; Shen, B.; Yao, X.-Q.; Yang, D. *J. Am. Chem. Soc.* **2007**, *129* (23), 7264–7265.

(19) Santacroce, P. V; Davis, J. T.; Light, M. E.; Gale, P. A.; Iglesias-Sanchez, J. C.; Prados, P.; Quesada, R. *J. Am. Chem. Soc.* **2007**, *129* (7), 1886–1887.

(20) Busschaert, N.; Gale, P. A.; Haynes, C. J. E.; Light, M. E.; Moore, S. J.; Tong, C. C.; Davis, J. T.; Harrell, W. A. *Chem. Commun.* **2010**, *46* (34), 6252–6254.

(21) McNally, B. A.; O'Neil, E. J.; Nguyen, A.; Smith, B. D. *J. Am. Chem. Soc.* **2008**, *130*

(51), 17274–17275.

(22) Engle, J. M.; Carroll, C. N.; Johnson, D. W.; Haley, M. M. *Chem. Sci.* **2012**, *3* (4), 1105.

(23) Andrews, N. J.; Haynes, C. J. E.; Light, M. E.; Moore, S. J.; Tong, C. C.; Davis, J. T.; Harrell Jr., W. A.; Gale, P. A. *Chem. Sci.* **2011**, *2* (2), 256–260.

(24) Soriano, M. L.; Lenthall, J. T.; Anderson, K. M.; Smith, S. J.; Steed, J. W. *Chem. Eur. J.* **2010**, *16* (35), 10818–10831.

(25) Busschaert, N.; Kirby, I. L.; Young, S.; Coles, S. J.; Horton, P. N.; Light, M. E.; Gale, P. A. *Angew. Chem.* **2012**, *51* (18), 4426–4430.

(26) Mahanta, S. P.; Panda, P. K. *Org. Biomol. Chem.* **2014**, *12* (2), 278–285.

(27) Gong, W.; Gao, B.; Bao, S.; Ye, J.; Ning, G. *J. Incl. Phenom. Macrocycl. Chem.* **2011**, *72* (3–4), 481–486.

(28) Filby, M. H.; Dickson, S. J.; Zaccheroni, N.; Prodi, L.; Bonacchi, S.; Montalti, M.; Paterson, M. J.; Humphries, T. D.; Chiorboli, C.; Steed, J. W. *J. Am. Chem. Soc.* **2008**, *130* (12), 4105–4113.

(29) Willans, C. E.; Anderson, K. M.; Potts, L. C.; Steed, J. W. *Org. Biomol. Chem.* **2009**, *7* (13), 2756–2760.

(30) Bullough, E. K.; Kilner, C. A.; Little, M. A.; Willans, C. E. *Org. Biomol. Chem.* **2012**, *10* (14), 2824–2829.

(31) Bazzicalupi, C.; Bencini, A.; Giorgi, C.; Valtancoli, B.; Lippolis, V.; Perra, A. *Inorg. Chem.* **2011**, *50* (15), 7202–7216.

(32) Bazzicalupi, C.; Bencini, A.; Puccioni, S.; Valtancoli, B.; Gratteri, P.; Garau, A.; Lippolis, V. *Chem. Commun.* **2012**, *48* (1), 139–141.

(33) Bencini, A.; Coluccini, C.; Garau, A.; Giorgi, C.; Lippolis, V.; Messori, L.; Pasini, D.; Puccioni, S. *Chem. Commun.* **2012**, *48* (84), 10428–10430.

(34) Hossain, M. A.; Kang, S. O.; Kut, J. A.; Day, V. W.; Bowman-James, K. *Inorg. Chem.* **2012**, *51* (8), 4833–4840.

(35) Beer, P. D.; Gale, P. A. *Angew. Chem.* **2001**, *40* (3), 486–516.

(36) Whitcombe, M. J.; Kirsch, N.; Nicholls, I. A. *J. Mol. Recognit.* **2014**, *27* (6), 297–401.

(37) Qureshi, N.; Yufit, D. S.; Steed, K. M.; Howard, J. A. K.; Steed, J. W. *CrystEngComm* **2014**, *16* (36), 8413.

(38) Ion, L.; Nieto, S.; Pérez, J.; Riera, L.; Riera, V.; Díaz, J.; López, R.; Anderson, K. M.; Steed, J. W. *Inorg. Chem.* **2011**, *50* (17), 8524–8531.

(39) Ema, T.; Okuda, K.; Watanabe, S.; Yamasaki, T.; Minami, T.; Esipenko, N. a; Anzenbacher, P. *Org. Lett.* **2014**, *16* (5), 1302–1305.

(40) Ali, H. D. P.; Kruger, P. E.; Gunnlaugsson, T. *New J. Chem.* **2008**, *32* (7), 1153.

(41) Goswami, S.; Chakrabarty, R. *Eur. J. Chem.* **2011**, *2* (3), 410–415.

(42) Hong, S.-J.; Lee, C.-H. *Tetrahedron Lett.* **2012**, *53* (25), 3119–3122.

(43) Anzenbacher, P.; Liu, Y.; Palacios, M. a; Minami, T.; Wang, Z.; Nishiyabu, R. *Chemistry (Easton).* **2013**, *19* (26), 8497–8506.

(44) Edwards, S. J.; Valkenier, H.; Busschaert, N.; Gale, P. A.; Davis, A. P. *Angew. Chem.* **2015**, *54* (15), 4592–4596.

(45) Caballero, A.; White, N. G.; Beer, P. D. *CrystEngComm* **2014**, *16* (18), 3694.

(46) Metrangolo, P.; Meyer, F.; Pilati, T.; Resnati, G.; Terraneo, G. *Angew. Chem.* **2008**, *47* (33), 6114–6127.

(47) Bondi, A. *J. Phys. Chem* **1964**, *68*, 441–451.

(48) Shannon, R. D. *Acta Crystallogr., Sect. A; Cryst. Phys., Diffr., Theor. Gen. Crystallogr.* **1976**, *A32*, 751–767.

(49) Gilday, L. C.; Beer, P. D. *Chem. Eur. J.* **2014**, *20*, 1–8.

(50) Chowdhury, B.; Sinha, S.; Ghosh, P. *Chem. Eur. J.* **2016**, *22* (50), 18051–18059.

(51) Bhuyan, M.; Katayev, E.; Stadlbauer, S.; Nonaka, H.; Ojida, A.; Hamachi, I.; König, B. *European J. Org. Chem.* **2011**, *2011* (15), 2807–2817.

(52) Gong, W.; Bao, S.; Wang, F.; Ye, J.; Ning, G.; Hiratani, K. *Tetrahedron Lett.* **2011**, *52* (5), 630–634.

(53) Saluja, P.; Kaur, N.; Singh, N.; Jang, D. O. *Tetrahedron Lett.* **2012**, *53* (26), 3292–3295.

(54) Wang, H.; Xue, L.; Jiang, H. *Org. Lett.* **2011**, *13* (15), 3844–3847.

(55) Molina, P.; Tárraga, A.; Otón, F. *Org. Biomol. Chem.* **2012**, *10* (9), 1711–1724.

(56) Caballero, A.; White, N. G.; Beer, P. D. *Angew. Chemie* **2011**, *50* (8), 1845–1848.

(57) Zapata, F.; Caballero, A.; White, N. G.; Claridge, T. D. W.; Costa, P. J.; Félix, V.; Beer, P. D. *J. Am. Chem. Soc.* **2012**, *134* (28), 11533–11541.

(58) Marullo, S.; D'Anna, F.; Cascino, M.; Noto, R. *J. Org. Chem.* **2013**, *78* (20), 10203–10208.

(59) Yousuf, M.; Ahmed, N.; Shirinfar, B.; Miriyala, V. M.; Youn, I. S.; Kim, K. S. *Org. Lett.* **2014**, *16* (8), 2150–2153.

(60) Cametti, M.; Raatikainen, K.; Metrangolo, P.; Pilati, T.; Terraneo, G.; Resnati, G. *Org. Biomol. Chem.* **2012**, *10* (7), 1329–1333.

(61) Legon, A. C. *Phys. Chem. Chem. Phys.* **2010**, *12* (28), 7736–7747.

(62) Cavallo, G.; Metrangolo, P.; Pilati, T.; Resnati, G.; Sansotera, M.; Terraneo, G. *Chem. Soc. Rev.* **2010**, *39* (10), 3772–3783.

(63) Rissanen, K. *CrystEngComm* **2008**, *10* (9), 1107.

(64) Gale, P. A; Hiscock, J. R.; Lalaoui, N.; Light, M. E.; Wells, N. J.; Wenzel, M. *Org. Biomol. Chem.* **2012**, *10* (30), 5909–5915.

(65) Yael Abraham, Husein Salman, K. S. and Y. E. *Chem. Commun.* **2011**, *47*, 6087–6089.

(66) Sharma, R. K.; Fry, J. L. *J. Org. Chem.* **1983**, *48* (12), 2112–2114.

(67) Kumari, N.; Jha, S.; Bhattacharya, S. *J. Org. Chem.* **2011**, *76* (20), 8215–8222.

(68) Li, G.; Gong, W.-T.; Ye, J.-W.; Lin, Y.; Ning, G.-L. *Tetrahedron Lett.* **2011**, *52* (12), 1313–1316.

(69) Willans, C. E.; Anderson, K. M.; Potts, L. C.; Steed, J. W. *Org. Biomol. Chem.* **2009**, *7* (13), 2756–2760.

(70) Chun, Y.; Singh, N. J.; Hwang, I.-C.; Lee, J. W.; Yu, S. U.; Kim, K. S. *Nat. Commun.* **2013**, *4*, 1797.

(71) Lee, C.-H. *Bull. Korean Chem. Soc.* **2011**, *32* (3), 768–778.

(72) Tuntulani, T.; Thavornyutikarn, P.; Poompradub, S.; Jaiboon, N.; Ruangpornvisuti, V.; Chaichit, N.; Asfari, Z.; Vicens, J. *Tetrahedron* **2002**, *58* (52), 10277–10285.

(73) Jin, C.; Zhang, M.; Deng, C.; Guan, Y.; Gong, J.; Zhu, D.; Pan, Y.; Jiang, J.; Wang, L. *Tetrahedron Lett.* **2013**, *54* (8), 796–801.

(74) Filby, Maria. Anion binding host systems based on calix [4] arenes and nanoparticles, Ph.D Dissertation, Durham University, United Kingdom, 2007.

(75) Higashihara, G.; Inagaki, A.; Akita, M. *Dalton Trans.* **2008**, No. 14, 1888–1898.

(76) Ahamed, B. N.; Arunachalam, M.; Ghosh, P. *Inorg. Chem.* **2011**, *50* (11), 4772–4780.

(77) Turner, D. R.; Paterson, M. J.; Steed, J. W. *J. Org. Chem.* **2006**, *71* (4), 1598–1608.

(78) Wong, W. W. H.; Vickers, M. S.; Cowley, A. R.; Paul, R. L.; Beer, P. D. *Org. Biomol. Chem.* **2005**, *3* (23), 4201–4208.

(79) Choi, K.; Hamilton, A. D. *J. Am. Chem. Soc.* **2001**, *123* (10), 2456–2457.

(80) Lee, D. Y.; Singh, N.; Kim, M. J.; Jang, D. O. *Org. Lett.* **2011**, *13* (12), 3024–3027.

(81) Gonzalez, M. del C.; Oton, F.; Espinosa, A.; Tarraga, A.; Molina, P. *Org. Biomol. Chem.* **2015**, *13* (5), 1429–1438.

(82) Chawla, H. M.; Santra, A.; Pant, N.; Kumar, S.; Kumar, N.; Black, D. S. *J. Incl. Phenom. Macrocycl. Chem.* **2011**, *73* (1–4), 55–65.

(83) Turner, D. R.; Paterson, M. J.; Steed, J. W. *Chem. Commun.* **2008**, No. 12, 1395–1397.

(84) Arunachalam, M.; Ghosh, P. *Inorg. Chem.* **2010**, *49* (3), 943–951.

(85) Arunachalam, M.; Ghosh, P. *Chem. Commun.* **2009**, *2* (36), 5389–5391.

(86) Valkenier, H.; Dias, C. M.; Porter Goff, K. L.; Jurček, O.; Puttreddy, R.; Rissanen, A. P.; Davis. *Chem. Commun.* **2015**, *51* (75), 14235–14238.

(87) Immaculada Dinares, C. G. de M.; Neus Mesquida, and E. A. *J. Am. Chem. Soc.* **2009**, *74*, 482–485.

(88) Cameron, B. R.; Loeb, S. J. *Chem. Commun.* **1997**, No. 6, 573–574.

(89) Shaabani, B.; Shaghaghi, Z. *Appl. Organomet. Chem.* **2011**, *25* (4), 317–322.

(90) Boiocchi, M.; Del Boca, L.; Gómez, D. E.; Fabbrizzi, L.; Licchelli, M.; Monzani, E. *J. Am. Chem. Soc.* **2004**, *126* (50), 16507–16514.

(91) Gotor, R.; Costero, A. M.; Gaviña, P.; Gil, S.; Parra, M. *European J. Org. Chem.* **2013**, *2013* (8), 1515–1520.

(92) Chang, K.-C.; Minami, T.; Koutnik, P.; Savechenkov, P. Y.; Liu, Y.; Anzenbacher, P. *J. Am. Chem. Soc.* **2014**, *136* (4), 1520–1525.

(93) Anzenbacher, P.; Try, A. C.; Miyaji, H.; Jursíková, K.; Lynch, V. M.; Marquez, M.; Sessler, J. L. *J. Am. Chem. Soc.* **2000**, *122* (42), 10268–10272.

(94) Umali, A. P.; Anslyn, E. V. *Curr. Opin. Chem. Biol.* **2010**, *14* (6), 685–692.

(95) Yoo, J.; Kim, M.-S.; Hong, S.-J.; Sessler, J. L.; Lee, C.-H. *J. Org. Chem.* **2009**, *74* (3), 1065–1069.

(96) He, X.; Herranz, F.; Cheng, E. C.-C.; Vilar, R.; Yam, V. W.-W. *Chem. Eur. J.* **2010**, *16* (30), 9123–9131.

(97) Pérez, J.; Riera, L. *Chem. Soc. Rev.* **2008**, *37* (12), 2658–2667.

(98) Carreira-Barral, I.; Rodríguez-Blas, T.; Platas-Iglesias, C.; de Blas, A.; Esteban-Gómez, D. *Inorg. Chem.* **2014**, *53* (5), 2554–2568.

(99) Sharma, R. P.; Kumar, S.; Saini, A.; Venugopalan, P.; Rodríguez-Diéguez, a.; Salas, J. M. *J. Mol. Struct.* **2014**, 1071, 11-17.

(100) Maity, D.; Bhaumik, C.; Mondal, D.; Baitalik, S. *Inorg. Chem.* **2013**, *52* (24), 13941–13955.

(101) Saha, D.; Das, S.; Maity, D.; Baitalik, S. *Indian J. Chem.* **2011**, *50*, 1418–1428.

(102) Ramdass, A.; Sathish, V.; Velayudham, M.; Thanasekaran, P.; Lu, K.-L.; Rajagopal, S. *Inorg. Chem. Commun.* **2013**, *35*, 186–191.

(103) Zheng, Y.; Tan, C.; Drummen, G. P. C.; Wang, Q. *Spectrochim. Acta. A. Mol. Biomol. Spectrosc.* **2012**, *96*, 387–394.

(104) Dickson, S. J.; Biagini, S. C. G.; Steed, J. W. *Chem. Commun.* **2007**, *3* (46), 4955.

(105) Dickson, S. J.; Paterson, M. J.; Willans, C. E.; Anderson, K. M.; Steed, J. W. *Chem. Eur. J.* **2008**, *14* (24), 7296–7305.

(106) Lakowicz, J. R. *Principles of Fluorescence Spectroscopy*; Springer US: Boston, MA, 1999.

(107) Kuang, D.; Ito, S.; Wenger, B.; Klein, C.; Moser, J.-E.; Humphry-Baker, R.; Zakeeruddin, S. M.; Grätzel, M. *J. Am. Chem. Soc.* **2006**, *128* (12), 4146–4154.

(108) Goswami, S.; Sen, D.; Das, N. K. *Tetrahedron Lett.* **2010**, *51* (51), 6707–6710.

(109) Pei, L.-M.; Lin, Q.-T.; Chao, H.; Ji, L.-N. *Inorg. Chem. Commun.* **2012**, *22*, 90–92.

(110) Yang, H.-X.; Liu, Y.-J.; Zhao, L.; Wang, K.-Z. *Spectrochim. Acta. A. Mol. Biomol. Spectrosc.* **2010**, *76* (2), 146–149.

(111) Wulfsberg, G. *Inorganic Chemistry*; University Science Books: Sausalito, CA, 2000.

(112) Mishra, A.; Vajpayee, V.; Kim, H.; Lee, M. H.; Jung, H.; Wang, M.; Stang, P. J.; Chi, K.-W. *Dalton Trans.* **2012**, *41* (4), 1195–1201.

(113) Mercer, D. J.; Loeb, S. J. *Chem. Soc. Rev.* **2010**, *39* (10), 3612–3620.

(114) Yao, L.-Y.; Qin, L.; Xie, T.-Z.; Li, Y.-Z.; Yu, S.-Y. *Inorg. Chem.* **2011**, *50* (13), 6055–6062.

(115) Zhou, Y.; Xu, Z.; Yoon, J. *Chem. Soc. Rev.* **2011**, *40* (5), 2222–2235.

(116) Nagarkar, S. S.; Saha, T.; Desai, A. V; Talukdar, P.; Ghosh, S. K. *Sci. Rep.* **2014**, *4*, 7053.

(117) Sharma, H.; Bhardwaj, V. K.; Kaur, N.; Singh, N.; Jang, D. O. *Tetrahedron Lett.* **2013**, *54* (45), 5967–5970.

(118) Saluja, P.; Kaur, N.; Singh, N.; Jang, D. O. *Tetrahedron* **2012**, *68* (41), 8551–8556.

(119) Chung, C. Y. S.; Yam, V. W. W. *Chem. Eur. J.* **2014**, *20* (40), 13016–13027.

(120) Hau, F. K. W.; Lo, H. S.; Yam, V. W. W. *Chem. Eur. J.* **2016**, *22* (11), 3738–3749.

(121) Li, K.; Zou, T.; Chen, Y.; Guan, X.; Che, C. M. *Chem. Eur. J.* **2015**, *21* (20), 7441–7453.

(122) Charbonnière, L. J.; Schurhammer, R.; Mameri, S.; Wipff, G.; Ziessel, R. F. *Inorg. Chem.* **2005**, *44* (20), 7151–7160.

(123) Schäferling, M. *Angew. Chem. Int. Ed. Engl.* **2012**, *51* (15), 3532–3554.

(124) Shinoda, S.; Mizote, A.; Masaki, M. E.; Yoneda, M.; Miyake, H.; Tsukube, H. *Inorg. Chem.* **2011**, *50* (13), 5876–5878.

(125) Butler, S. J.; McMahon, B. K.; Pal, R.; Parker, D.; Walton, J. W. *Chem. Eur. J.* **2013**, *19* (29), 9511–9517.

(126) Walton, J. W.; Bourdolle, A.; Butler, S. J.; Soulie, M.; Delbianco, M.; McMahon, B. K.; Pal, R.; Puschmann, H.; Zwier, J. M.; Lamarque, L.; Maury, O.; Andraud, C.; Parker, D. *Chem. Commun.* **2013**, *49* (16), 1600–1602.

(127) Carter, K. P.; Young, A. M.; Palmer, A. E. *Chem. Rev.* **2014**, *114* (8), 4564–4601.

(128) McConnell, A. J.; Beer, P. D. *Angew. Chemie* **2012**, *51* (21), 5052–5061.

(129) Park, I.-W.; Yoo, J.; Kim, B.; Adhikari, S.; Kim, S. K.; Yeon, Y.; Haynes, C. J. E.; Sutton, J. L.; Tong, C. C.; Lynch, V. M.; Sessler, J. L.; Gale, P. A.; Lee, C.-H. *Chem. Eur. J.*

2012, *18* (9), 2514–2523.

(130) Park, I.-W.; Yoo, J.; Adhikari, S.; Park, J. S.; Sessler, J. L.; Lee, C.-H. *Chem. Eur. J.* **2012**, *18* (47), 15073–15078.

(131) Picot, S. C.; Mullaney, B. R.; Beer, P. D. *Chem. - A Eur. J.* **2012**, *18* (20), 6230–6237.

(132) Alfonso, M.; Tárraga, A.; Molina, P. *Inorg. Chem.* **2013**, *52* (13), 7487–7496.

(133) McConnell, A. J.; Serpell, C. J.; Beer, P. D. *New J. Chem.* **2012**, *36* (1), 102–112.

(134) Chen, Y.; Wang, D.-X.; Huang, Z.-T.; Wang, M.-X. *Chem. Commun.* **2011**, *47* (28), 8112–8114.

(135) Janiak, C. *Dalt. Trans.* **2000**, No. 21, 3885–3896.

(136) Karbarz, M.; Romański, J. *Inorg. Chem.* **2016**, *55* (7), 3616–3623.

(137) Legrand, Y.-M.; Michau, M.; van der Lee, A.; Barboiu, M. *CrystEngComm* **2008**, *10* (5), 490–492.

(138) Le Duc, Y.; Michau, M.; Gilles, A.; Gence, V.; Legrand, Y.-M.; van der Lee, A.; Tingry, S.; Barboiu, M. *Angew. Chemie* **2011**, *123* (48), 11568–11574.

Chapter 2

Coordination chemistry and anion binding profiles of imidazole compounds containing urea derivatives.

2.1 Introduction and Project Aims

The main aim of this research is to investigate the anion binding properties and coordination chemistry of a set of imidazole compounds containing urea derivatives to characterise the ligands' metal coordination and anion binding modes and hence design new imidazole urea-based anion hosts. Imidazoles are a class of heterocyclic compounds that are essential in biological processes and are common functional groups in biological molecules, such as histamine and histidine.[1] Due to their amphoteric nature, imidazole compounds can serve as selective and effective anion, cation or neutral molecule sensors that are capable of interacting with a broad range of drugs and proteins. The acidity of the NH proton of imidazole can also be tuned by varying the electronic properties of the substituents attached to the ring. Also, the presence of a basic nitrogen atom within the ring, which can coordinate to cations, makes imidazole a suitable candidate for the construction of metal-based and ditopic anion receptors.[1] Initial studies on simple urea derivatised imidazole compounds by the Barboiu group[2] has shown the ability of these compounds to form a homomeric association of the urea and imidazole functional groups giving rise to a dipolar proton channel. With this in mind, we have prepared series of imidazole ligands containing urea derivatives which are interesting in the context of cation and anion binding.[3]

2.2 Results and Discussions

2.2.1 Synthesis and crystal structure of imidazole urea ligands

A series of imidazole ligands containing urea derivatives (**2.1**-**2.8**) were readily synthesised in good yield *via* one-pot reaction of histamine with appropriate isocyanates in a continuous nitrogen stream for 18 hours or overnight. The (unoptimised) isolated

yields are also high (80-95%) similar to related pyridine urea analogues.[4] The formation of the imidazole urea ligands with aliphatic chains and *tert*-butyl groups, **2.1**-**2.3** and **2.8** was confirmed by characteristic NH urea signals in the ^{1}H NMR spectrum of the products at 5.88 (N1-H) and 5.79 (N2-H) ppm for all four compounds. The ESI-MS results also show a molecular ion peak ($M+H^{+}$) of 211, 267, 323 and 211 for compounds **2.1**-**2.3** and **2.8**, respectively. On the other hand, for the imidazole urea ligands with aromatic substituents, the urea NH signals were observed in the range of 7.47-6.09 (N1-H) and 7.49-6.82 (N2-H) ppm. The formation of the compounds, **2.4**-**2.7** has also been supported by the ESI-MS results showing molecular ion peaks ($M+H^{+}$) of 245, 276, 288 and 265, respectively. Of all the imidazole urea compounds synthesised, four of them yielded single crystals that are suitable for Single Crystal X-Ray Diffraction (SC-XRD) analysis. Table 2.1 below summarises the crystallographic data for all the crystals obtained and the details of the molecular structure and crystal packing will be discussed further. The synthesis route of imidazole urea derivatives is depicted in Scheme 2.1.

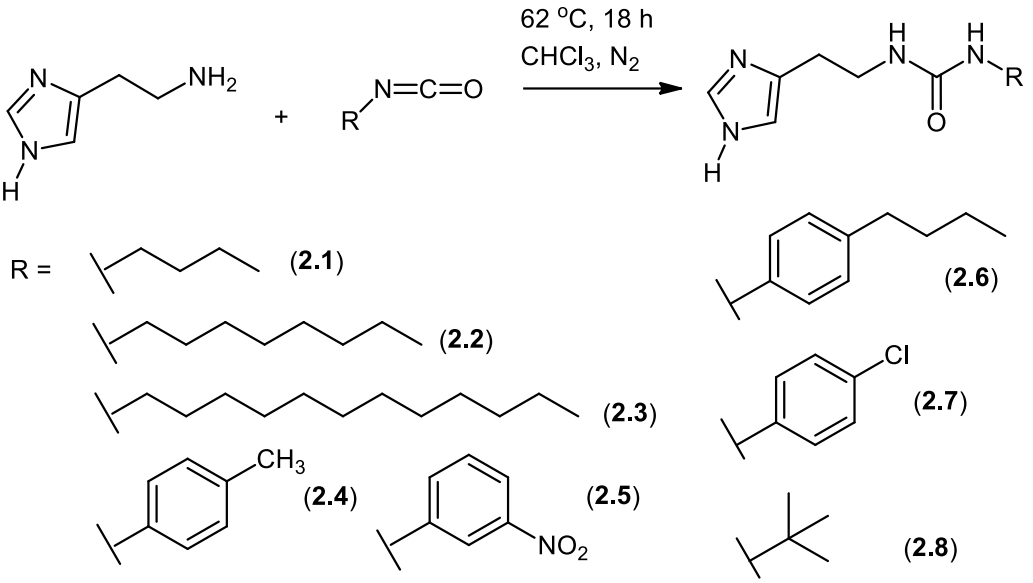

Scheme 2.1 Synthetic pathway of imidazole ligands containing urea derivatives (**2.1-2.8**).

Imidazole-derived compounds as-synthesised can show tautomerism at nitrogen atoms if the two nitrogen atoms present in the five membered is not symmetrically substituted.[5] This means that the hydrogen atom can either be bonded to the N1 or N2 atom and can be interconverted between N(1) and N(2)-type isomer as illustrated in Figure 2.1.

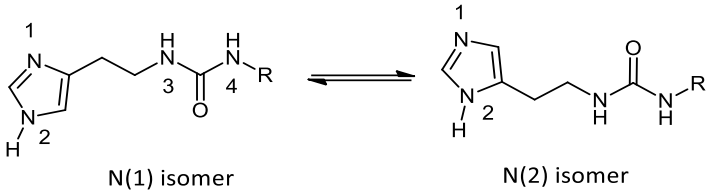

Figure 2.1 Interconversion between N(1) and N(2) type tautomers.

Table 2.1 Crystallographic data for compound **2.1**, **2.4**, **2.6** and **2.7**

	2.1	**2.4**	**2.6**	**2.7**
Formula	$C_{10}H_{18}N_4O$	$C_{13}H_{16}N_4O.CH_3NO_2$	$C_{16}H_{22}N_4O$	$C_{12}H_{13}ClN_4O$
Formula weight	210.28	305.34	286.38	264.71
Space group	$P2_1/c$	$Pca2_1$	$P2_12_12_1$	$P2_1$
***a* / Å**	11.1384(4)	12.3460(3)	8.2251(2)	9.6232(4)
***b* / Å**	5.6178(3)	13.9709(3)	9.7345(2)	4.8410(2)
***c* / Å**	17.6812(5)	9.1894(2)	18.8588(4)	13.9243(5)
A / °	90	90	90	90
β / °	94.171(3)	90	90	109.642(3)
γ / °	90	90	90	90
***V* / Å^3**	1103.44(7)	1585.03(6)	1509.97(6)	610.93(4)
Z	4	4	4	2
***D*$_{calc}$ / g cm^{-3}**	1.266	1.280	1.260	1.439
***R*$_{int}$**	0.0488	0.0578	0.0871	0.0708
***R*$_1$ [*I* ≥ 2σ (*I*)]**	0.0427	0.0476	0.0384	0.0519
***wR*$_2$ [all data]**	0.0896	0.0976	0.0864	0.1128

All of the crystal structures of the synthesised imidazole urea ligands are prone to form N1 type isomers, as this form is less sterically hindered in comparison to the N2 type isomer, particularly in solid state. A single crystal of **2.1** was obtained from slow evaporation of an acetonitrile solution of the compound and characterised by X-ray crystallography. Compound **2.1** crystallises in monoclinic system with space group $P2_1/c$.

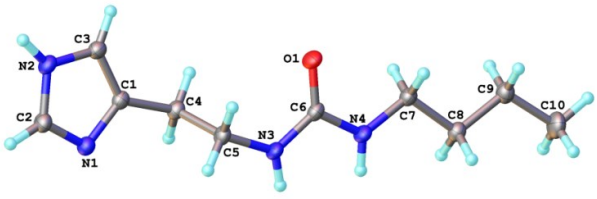

Figure 2.2 Molecular structure of 1 - [2 - (1*H* - imidazol - 4 - yl)ethyl] - 3 - (4 - butyl)urea (**2.1**)

The molecules are not linked together by a typical urea α-tape as observed in most of urea and bis(urea) systems.[6–9] Instead, there are intermolecular hydrogen bonds between imidazole nitrogen, N1 with the hydrogen atoms of the urea group, H3 and H4 with N···H distances of 3.066(16) and 3.274(16) Å, respectively. The crystal is also stabilised by another hydrogen bond between the urea oxygen, O1 with the hydrogen atom of the imidazole group, N2-H with O1···H2 distance of 2.7758(4) Å (Figure 2.3).

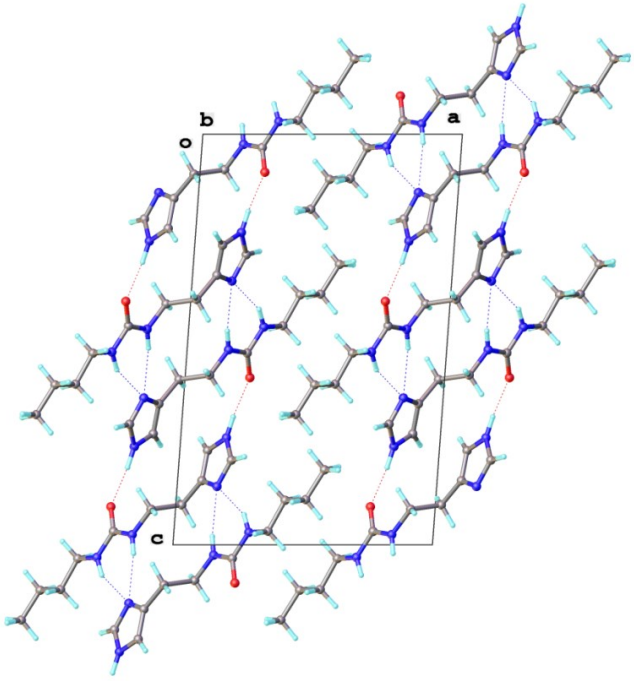

Figure 2.3 Hydrogen bonding patterns in the molecular packing of compound **2.1**.

Single crystals of **2.4** were obtained from the slow evaporation of nitromethane. This compound crystallises as a nitromethane solvate, which is analogous to the previously reported structures of **2.4**[10] and its phenyl analogue[2] which crystallise as acetonitrile solvates. It crystallises in orthorhombic system with a space group *Pca*2_1 different from the previously reported acetonitrile solvate, which crystallised in the monoclinic system (*P*2_1/*n).* However, this structure is isostructural to the acetonitrile solvate reported by the Steed group.

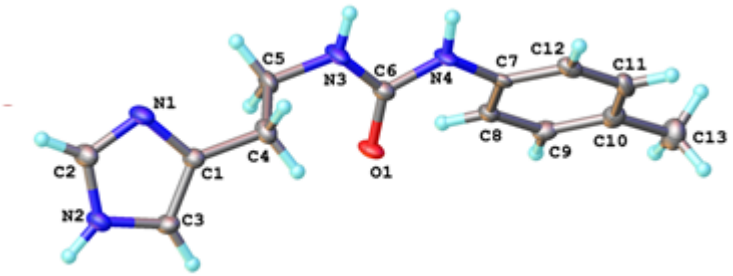

Figure 2.4 Molecular structure of 1 - [2 - (1*H* - imidazol - 4 - yl)ethyl] - 3 - (4 - methylphenyl)urea (**2.4**).

This compound exhibits a typical hydrogen bonded urea α-tape motif[10,11] with short and symmetrical interactions between the oxygen atom, O1 and H3 and H4 based on urea nitrogen atoms with distances of 2.898(2) and 2.838(2) Å, respectively and is consistent with the previously reported structure of acetonitrile solvate.[12] The formation of the urea α-tape network allows the adjacent molecules to aggregate along the tape axis in an alternating fashion. In addition to that, there is also a formation of a second 'zigzag' hydrogen bonded tape between the imidazole nitrogen atoms (Figure 2.5).

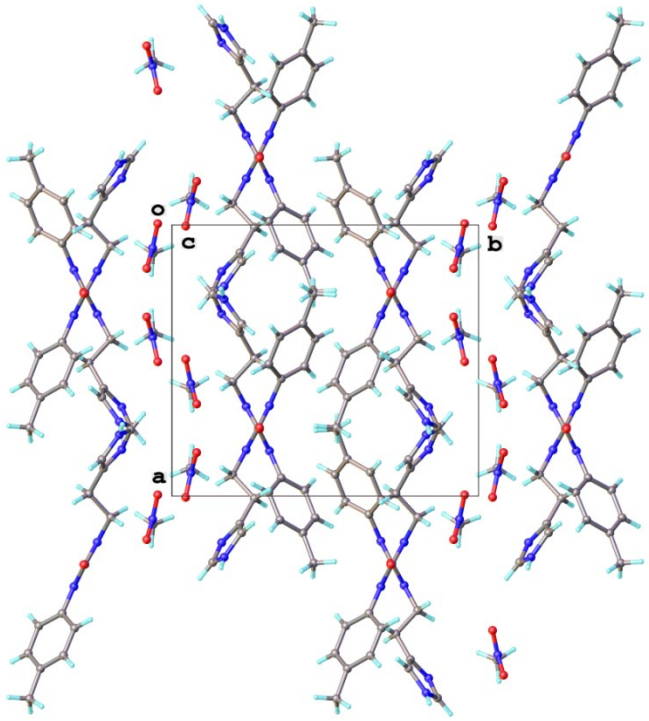

Figure 2.5 Crystal packing of compound **2.4**.

On the other hand, compound **2.6** crystallises from the slow cooling of methanol in the orthorhombic system with space group $P2_12_12_1$. Similarly to compound **2.4**, the structure is characterised by a urea α-tape motif arising from hydrogen bonds between O1 and H1 and H2, with the bond lengths of 2.844(2) and 3.029(2) Å, respectively.

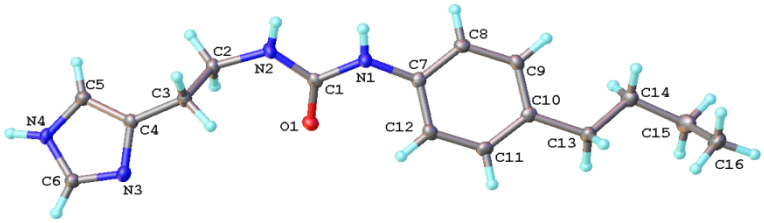

Figure 2.6 Molecular structure of 1-[2-(1*H*-imidazol-4-yl)ethyl]-3-(4-butylphenyl)urea (**2.6**).

In the packing, a similar 'zigzag' hydrogen bonding pattern forms from the interactions between the imidazole nitrogen atoms with a distance of 2.851(2) Å (Figure 2.7).

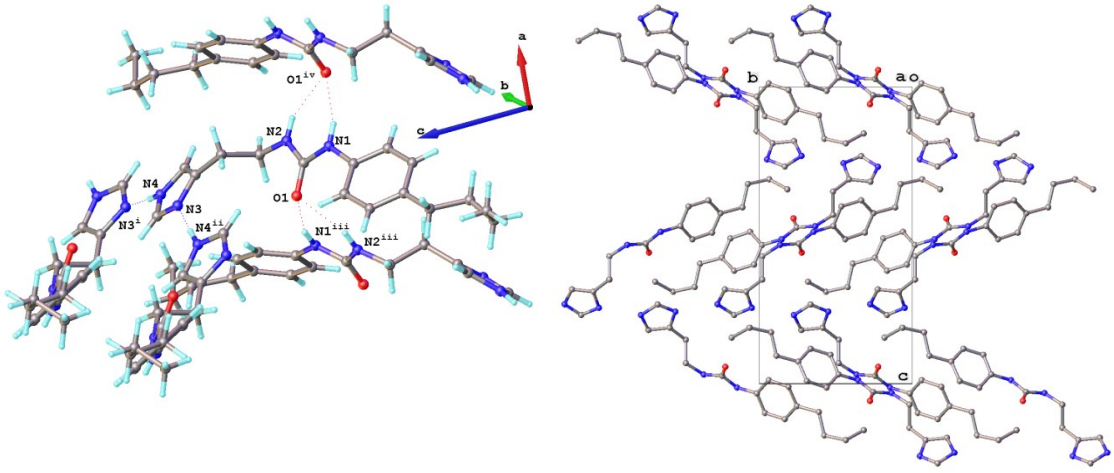

Figure 2.7 Hydrogen bonding patterns in the molecular packing of compound **2.6**.

Colourless single crystals of **2.7** were isolated *via* slow evaporation of methanol and characterised by X-ray crystallography. Compound **2.7** crystallises in the monoclinic system in the chiral space group $P2_1$.

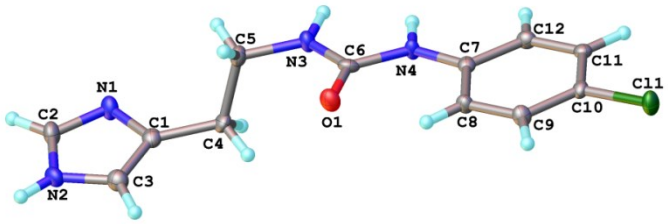

Figure 2.8 Molecular structure of 1 - [2 - (1*H* - imidazol - 4 - yl)ethyl] - 3 - (4 - chlorophenyl)urea (**2.7**).

In contrast to compounds **2.4** and **2.6**, this compound does not exhibit a typical urea α-tape, instead the molecule forms a three-dimensional network that is linked by intermolecular hydrogen bond between imidazole nitrogen, N1 with hydrogen atom of the urea group, H3 and H4 with bond lengths of 3.244(5) and 2.979(4) Å, respectively. There is also an intramolecular hydrogen bond between the oxygen atom, O1 with the hydrogen atom of the aromatic chain, H8 with a distance of 2.873(5) Å, forming a six-membered ring. The presence of electron withdrawing substituent promotes CH…O intramolecular interactions as previously described.[13] In the packing, the molecule is also stabilised by a hydrogen bond between urea oxygen, O1 with hydrogen of an imidazole group, N2 with a distance of 2.765(4) Å (Figure 2.9).

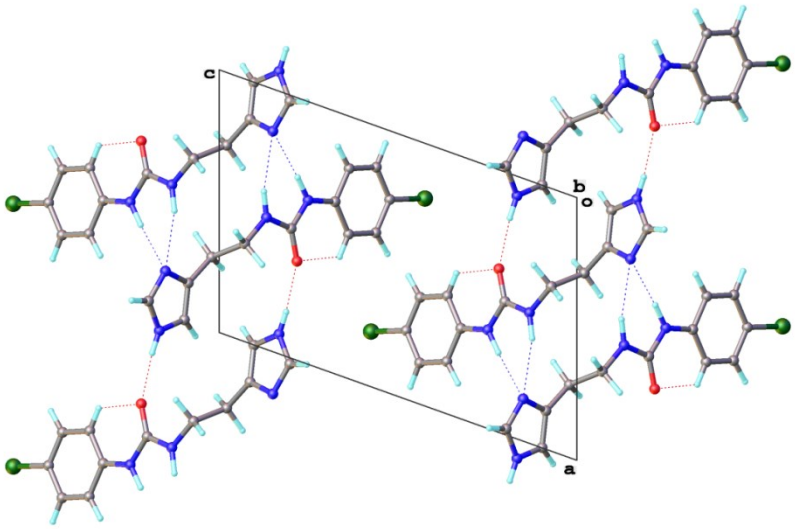

Figure 2.9 Hydrogen bonding patterns in the crystal packing of compound **2.7**.

In conclusion, there are some factors that influence the formation of urea α-tape between the urea moiety. For compound **2.1**, the less steric aliphatic butyl chain inhibit the formation of urea α-tape as the molecules assemble themselves through the formation of a NH···N imidazolyl– urea hydrogen-bonded synthon.[14] However, In the case of imidazole urea with an aromatic chain such as compound **2.4**, the presence of nitromethane solvate promotes the formation of urea α-tape as the oxygen of the nitromethane interacts with the CH imidazole (O2-H2A with a distance of 2.466 Å) thus leaving the urea group free to interact with each other. In addition, the hydrogen bonding patterns in imidazole derivatives containing urea derivatives are also highly influenced by the chain length and substituents of the urea group. From the crystal structure of all the imidazole urea compounds, it can be observed that in some compounds namely **2.4** and **2.6**, the self-complementary hydrogen bond donor and acceptor capacity of the imidazole groups allow the hydrogen bond interaction between the basic imidazole nitrogen with the imidazole N-H proton thus leaving the urea moiety free to form the usual hydrogen bonded α-tape motif. In addition, the presence of electron donating substituents in compound **2.4** and **2.6** decrease the acidity of the urea N-H protons, thus promotes the self-complementary interaction between NH···N of the imidazole groups. On the contrary, the presence of an electron withdrawing substituent in compound **2.7** contributes to the greater acidity of the urea N-H compared to that of imidazole N-H, thus promotes the NH···N interaction between urea N-H and basic imidazole nitrogen and disrupts the α-urea tape formation. This is an interesting finding in which the simultaneous interactions of urea and imidazole H-bonding moieties can be structurally tuned for specific potential application for example in the generation of multiple supramolecular architectures.

2.2.2 Transition metal complexes of imidazole urea ligands

One of the aims of this project is to synthesise a series of metal-based anion receptors from various transition metals. The basic nitrogen atom in imidazole groups makes them suitable as ligands for transition metals. Unlike pyridyl systems, the smaller size of imidazole groups could potentially result in the less steric crowding at the metal centre and hence higher metal:ligand stoichiometry. For example, the complexation reactions

of imidazole urea ligands with transition metal salts namely cobalt(II) and nickel(II) were performed with higher metal to ligand ratio of 1:6. For copper(II) metals, the reaction was performed with metal:ligand ratio of 1:4 based on the common coordination number of copper(II) metals. Different metals salts such as copper(II) chloride dihydrate, copper(II) nitrate hydrate, cobalt(II) chloride hexahydrate, cobalt(II) nitrate hexahydrate, nickel(II) chloride hexahydrate and nickel(II) nitrate hexahydrate have been used for this purpose. For these complexation reactions, 0.003 mmol of ligands **2.1**-**2.4** and **2.6**-**2.8** in 0.2 mL of methanol was reacted with selected transition metals dissolved in water in 2 mL vials.

Most of the reactions showed colour changes after the addition of the ligands to the respective transition metals solution indicating that the complexation reaction has taken place. The solution mixture was then heated in a water bath at about 50 °C for 5 minutes and briefly sonicated to allow dispersion and thorough mixing. The mixture was then left to evaporate at room temperature to obtain transition metal complexes of the imidazole urea ligands. With the exception of ligand **2.3**, all of the complexation reactions gave a coloured solution upon addition of the metal ions. In contrast, the addition of metal ions to ligand **2.3** results in the immediate precipitation of the complexes. The coloured solution of the complexes was left to evaporate to afford pure compounds or single crystals. Precipitates obtained were filtered, isolated and dried in the dessicator. For the synthesis of Co(II) and Ni(II) complexes, the ratio of metal:ligand was decided on the maximum coordination number of six, giving octahedral complexes, while for Copper(II), the metal:ligand ratio is fixed at 1:4 based on the common coordination number of Copper(II) metal although in some cases, Cu(II) might form a five-coordinated complexes due to Jahn-Teller distortion effect as reported previously by our group.[10] These metal:ligand ratio are used in the calculated data of the elemental analysis. Table 2.2 summarises the colour of the complexes formed along with the metal:ligand ratio and the elemental analysis results.

From the elemental analysis data, it is suggested that there are also some complexes that were not fully dried and still contain some amount of water. However, there are two complexes, namely $[Ni(\mathbf{2.6})_6](NO_3)_2$ and $[Co(\mathbf{2.8})_6]SO_4$ which are impure and might contain unreacted starting materials that affect their elemental analysis percentages.

Table 2.2 Physical data of transition metal complexes of imidazole ureas (the calculated values are enclosed in the bracket)

Entry	Complex	Metal: Ligand ratio	Colour	Microelemental analysis		
				C (%)	H (%)	N (%)
1	$[Co(\mathbf{2.1})_6]Cl_2.2H_2O$	1:6	Pink	50.91 (50.48)	8.01 (7.91)	23.13 (23.55)
2	$[Co(\mathbf{2.1})_6](NO_3)_2$	1:6	Pink	49.32 (49.89)	7.78 (7.54)	24.26 (25.21)
3	$[Co(\mathbf{2.1})_6]SO_4.5H_2O$	1:6	Purple	47.69 (47.83)	7.32 (7.89)	21.86 (22.31)
4	$[Cu(\mathbf{2.1})_4]Cl_2.2H_2O$	1:4	Blue	47.84 (47.49)	7.40 (7.57)	21.86 (22.15)
5	$[Cu(\mathbf{2.1})_4](NO_3)_2$	1:4	Blue	46.30 (46.70)	7.07 (7.06)	23.80 (24.51)
6	$[Ni(\mathbf{2.1})_6]Cl_2.2H_2O$	1:6	Light blue	50.26 (50.49)	7.70 (7.91)	22.87 (23.55)
7	$[Ni(\mathbf{2.1})_6](NO_3)_2$	1:6	Light blue	49.20 (49.89)	7.56 (7.54)	24.36 (25.21)
8	$[Co(\mathbf{2.2})_6]Cl_2$	1:6	Purple	58.17 (58.38)	9.08 (9.10)	19.15 (19.45)
9	$[Co(\mathbf{2.2})_6](NO_3)_2$	1:6	Purple	56.26 (56.64)	8.78 (8.83)	20.12 (20.45)
10	$[Co(\mathbf{2.2})_6]SO_4.5H_2O$	1:6	Purple	55.00 (54.73)	8.63 (9.08)	18.10 (18.24)
11	$[Cu(\mathbf{2.2})_4]Cl_2$	1:4	Blue	55.51 (56.05)	8.64 (8.74)	18.34 (18.68)
12	$[Cu(\mathbf{2.2})_4](NO_3)_2$	1:4	Blue	53.94 (53.68)	8.41 (8.37)	19.83 (20.12)
13	$[Ni(\mathbf{2.2})_6]Cl_2$	1:6	Light blue	57.82 (58.39)	9.04 (9.10)	18.95 (19.45)
14	$[Ni(\mathbf{2.2})_6](NO_3)_2$	1:6	Light blue	56.94 (56.65)	8.91 (8.83)	20.32 (20.45)
15	$[Co(\mathbf{2.3})_6]Cl2.2H_2O$	1:6	Purple blue	61.86 (61.61)	9.78 (9.91)	15.74 (16.12)

16	$[Co(\mathbf{2.3})_6](NO_3)_2$	1:6	Purple	61.11 (61.25)	9.56 (9.71)	16.33 (17.20)
17	$[Co(\mathbf{2.3})_6]SO_4.5H_2O$	1:6	Dark purple	59.32 (59.50)	9.50 (9.89)	15.03 (15.42)
18	$[Cu(\mathbf{2.3})_4]Cl_2$	1:4	Blue	60.39 (60.71)	9.66 (9.62)	15.35 (15.73)
19	$[Cu(\mathbf{2.3})_4](NO_3)_2$	1:4	Purple	58.63 (58.83)	9.29 (9.28)	16.59 (17.06)
20	$[Ni(\mathbf{2.3})_6]Cl_2.4H_2O$	1:6	Light green-blue	60.64 (60.71)	9.68 (10.00)	15.38 (15.73)
21	$[Ni(\mathbf{2.3})_6](NO_3)_2$	1:6	Light green-blue	60.50 (61.26)	9.64 (9.71)	16.47 (17.20)
22	$[Co(\mathbf{2.4})_6]Cl_2$	1:6	Green	58.81 (58.71)	6.32 (6.06)	20.07 (21.07)
23	$[Co(\mathbf{2.4})_6](NO_3)_2$	1:6	Pale pink	56.45 (56.82)	5.94 (5.87)	21.48 (22.09)
24	$[Co(\mathbf{2.4})_6]SO_4$	1:6	Pale pink	57.32 (57.80)	5.96 (5.97)	19.81 (20.74)
25	$[Cu(\mathbf{2.4})_4]Cl_2$	1:4	Dark blue	54.37 (56.18)	6.15 (5.80)	18.34 (20.16)
26	$[Cu(\mathbf{2.4})_4](NO_3)_2$	1:4	Dark blue	53.92 (53.62)	5.92 (5.54)	18.28 (21.65)
27	$[Ni(\mathbf{2.4})_6]Cl_2.2H_2O$	1:6	Light blue	57.82 (57.18)	6.41 (6.11)	18.33 (20.78)
28	$[Ni(\mathbf{2.4})_6](NO_3)_2$	1:6	Light blue	56.84 (56.83)	6.19 (6.87)	18.73 (22.09)
29	$[Co(\mathbf{2.6})_6]Cl_2$	1:6	Purple-blue	62.61 (62.39)	7.31 (7.20)	18.48 (18.19)
30	$[Co(\mathbf{2.6})_6](NO_3)_2$	1:6	Purple	60.61 (60.65)	7.10 (7.00)	19.10 (19.16)
31	$[Co(\mathbf{2.6})_6]SO_4.H_2O$	1:6	Purple	60.15 (60.21)	7.06 (6.92)	17.56 (18.32)
32	$[Cu(\mathbf{2.6})_4]Cl_2$	1:4	Blue	59.00 (60.06)	6.96 (6.93)	17.28 (17.51)
33	$[Cu(\mathbf{2.6})_4](NO_3)_2$	1:4	Blue-green	57.58 (57.66)	6.78 (6.65)	18.66 (18.91)

34	$[Ni(\mathbf{2.6})_6]Cl_2.2H_2O$	1:6	Light blue	60.81 (60.46)	7.16 (7.06)	17.78 (18.39)
35	$[Ni(\mathbf{2.6})_6](NO_3)_2$	1:6	Light blue	61.61 (60.66)	7.17 (7.00)	19.04 (19.16)
36	$[Co(\mathbf{2.7})_6]Cl_2$	1:6	Light blue	50.03 (50.33)	4.60 (4.58)	19.21 (19.57)
37	$[Co(\mathbf{2.7})_6](NO_3)_2$	1:6	Light purple	48.59 (48.82)	4.45 (4.44)	20.29 (20.56)
38	$[Co(\mathbf{2.7})_6]SO_4.4H_2O$	1:6	Purple	47.74 (47.64)	4.44 (4.78)	20.29 (18.52)
39	$[Cu(\mathbf{2.7})_4]Cl_2$	1:4	Blue	48.35 (48.31)	4.77 (4.39)	18.45 (18.78)
40	$[Ni(\mathbf{2.7})_4]Cl_2$	1:6	Light blue	49.38 (49.31)	4.81 (4.71)	18.95 (19.17)
41	$[Ni(\mathbf{2.6})_6](NO_3)_2$	1:6	Light blue	48.62 (48.83)	4.56 (4.44)	20.12 (20.56)
42	$[Co(\mathbf{2.8})_6]Cl_2.2H_2O$	1:6	Purple	50.80 (50.48)	7.88 (7.91)	23.47 (23.55)
43	$[Co(\mathbf{2.8})_6](NO_3)_2$	1:6	Pink	49.36 (49.89)	7.69 (7.54)	24.33 (25.21)
44	$[Co(\mathbf{2.8})_6]SO_4$	1:6	Purple	42.39 (50.87)	6.75 (7.68)	19.58 (23.73)
45	$[Cu(\mathbf{2.8})_4]Cl_2.2H_2O$	1:4	Blue	47.29 (47.49)	7.46 (7.57)	21.72 (22.15)
46	$[Cu(\mathbf{2.8})_4](NO_3)_2$	1:4	Blue	46.38 (46.70)	7.25 (7.06)	23.43 (24.51)
47	$[Ni(\mathbf{2.8})_6]Cl_2.4H_2O$	1:6	Light blue	48.92 (49.25)	7.61 (7.99)	22.60 (22.97)
48	$[Ni(\mathbf{2.8})_6](NO_3)_2$	1:6	Light blue	50.00 (49.89)	7.79 (7.54)	24.56 (25.21)

The paramagnetic nature of the transition metals complexes of imidazole urea ligands limits the use of NMR spectroscopy to characterise the complexes. However, FTIR data can provide some valuable information regarding the essential stretching vibration that occurs or changes before and after the complexation reaction. For most of the complexes, the v(NH) stretch is shifted towards higher energy upon complexation with metals in comparison to the respective ligand. This indicates that the hydrogen bonding between the urea moieties and imidazole groups is weakened upon coordination to the metal ion as the coordination inhibits inter-ligand interactions. In most of the cases, the v(C=O) stretch of the complexes are shifted to higher energy possibly due to the formation of NH···anion hydrogen bonding in the complexes instead of NH···O hydrogen bonding in the free ligand. The important FTIR stretching vibrations of the remaining imidazole urea compounds and their complexes are listed in Table 2.3.

Table 2.3 FTIR stretching vibration of free imidazole urea ligands and their transition metal complexes.

Entry	Compounds	Selected FTIR stretching vibrations			
		v (N-H)	*v* (C=O)	*v* (C-H imidazole ring)	*v* (C=N-C=C) imidazole
1	Free ligand **2.1**	3290	1650	1564	1454
2	$[Co(\mathbf{2.1})_6]Cl_2$	3376	1652	1548	1436
3	$[Co(\mathbf{2.1})_6](NO_3)_2$	3366	1656	1546	1435
4	$[Co(\mathbf{2.1})_6]SO_4$	3363	1656	1550	1435
5	$[Cu(\mathbf{2.1})_4]Cl_2$	3363	1650	1550	1435
6	$[Cu(\mathbf{2.1})_4](NO_3)_2$	3368	1646	1550	1435
7	$[Ni(\mathbf{2.1})_6]Cl_2$	3364	1646	1550	1435
8	$[Ni(\mathbf{2.1})_6](NO_3)_2$	3363	1656	1550	1436
9	Free ligand **2.2**	3306	1617	1570	1434
10	$[Co(\mathbf{2.2})_6]Cl_2$	3363	1653	1551	1463
11	$[Co(\mathbf{2.2})_6](NO_3)_2$	3371	1647	1551	1435
12	$[Co(\mathbf{2.2})_6]SO_4$	3363	1648	1551	1435

13	[Cu(**2.2**)$_4$]Cl$_2$	3367	1648	1552	1436
14	[Cu(**2.2**)$_4$](NO$_3$)$_2$	3363	1649	1551	1435
15	[Ni(**2.2**)$_6$]Cl$_2$	3363	1653	1552	1435
16	[Ni(**2.2**)$_6$](NO$_3$)$_2$	3363	1649	1551	1436
17	Free ligand **2.3**	3309	1611	1570	1450
18	[Co(**2.3**)$_6$]Cl$_2$	3308	1616	1575	1459
19	[Co(**2.3**)$_6$](NO$_3$)$_2$	3308	1620	1575	1459
20	[Co(**2.3**)$_6$]SO$_4$	3303	1622	1573	1462
21	[Cu(**2.3**)$_4$]Cl$_2$	3299	1622	1572	1463
22	[Cu(**2.3**)$_4$](NO$_3$)$_2$	3308	1630	1573	1463
23	[Ni(**2.3**)$_6$]Cl$_2$	3308	1635	1564	1467
24	[Ni(**2.3**)$_6$](NO$_3$)$_2$	3328	1636	1567	1466
25	Free ligand **2.4**	3304	1633	1558	1448
26	[Co(**2.4**)$_6$]Cl$_2$	3329	1654	1540	1450
27	[Co(**2.4**)$_6$](NO$_3$)$_2$	3377	1660	1544	1451
28	[Co(**2.4**)$_6$]SO$_4$	3366	1664	1558	1447
29	[Cu(**2.4**)$_4$]Cl$_2$	3371	1654	1547	1436
30	[Cu(**2.4**)$_4$](NO$_3$)$_2$	3363	1651	1545	1435
31	[Ni(**2.4**)$_6$]Cl$_2$	3363	1656	1546	1436
32	[Ni(**2.4**)$_6$](NO$_3$)$_2$	3363	1656	1544	1436
33	Free ligand **2.6**	3359	1632	1554	1408
34	[Co(**2.6**)$_6$]Cl$_2$	3363	1649	1551	1435
35	[Co(**2.6**)$_6$](NO$_3$)$_2$	3328	1634	1553	1410
36	[Co(**2.6**)$_6$]SO$_4$	3328	1634	1553	1410
37	[Cu(**2.6**)$_4$]Cl$_2$	3338	1635	1550	1410
38	[Cu(**2.6**)$_4$](NO$_3$)$_2$	3321	1652	1549	1410
39	[Ni(**2.6**)$_6$]Cl$_2$	3308	1653	1549	1410
40	[Ni(**2.6**)$_6$](NO$_3$)$_2$	3324	1653	1549	1410
41	Free ligand **2.7**	3309	1611	1564	1462

42	$[Co(\mathbf{2.7})_6]Cl_2$	3348	1671	1539	1490
43	$[Co(\mathbf{2.7})_6](NO_3)_2$	3317	1679	1539	1491
44	$[Co(\mathbf{2.7})_6]SO_4$	3297	1679	1544	1491
45	$[Cu(\mathbf{2.7})_4]Cl_2$	3269	1661	1544	1490
46	$[Ni(\mathbf{2.7})_4]Cl_2$	3553	1671	1539	1490
47	Free ligand **2.8**	3348	1648	1559	1447
48	$[Co(\mathbf{2.8})_6]Cl_2$	3297	1640	1555	1450
49	$[Co(\mathbf{2.8})_6](NO_3)_2$	3349	1639	1555	1450
50	$[Co(\mathbf{2.8})_6]SO_4$	3287	1637	1555	1450
51	$[Cu(\mathbf{2.8})_4]Cl_2$	3297	1640	1558	1450
52	$[Cu(\mathbf{2.8})_4](NO_3)_2$	3353	1641	1557	1450
53	$[Ni(\mathbf{2.8})_6]Cl_2$	3328	1641	1556	1450
54	$[Ni(\mathbf{2.8})_6](NO_3)_2$	3327	1640	1558	1450

2.2.2.1 Single crystal X-ray Diffraction (SC-XRD) analysis

Despite the large number of complexes prepared, only three formed crystals suitable for SC-XRD analysis. All of the crystals were obtained from slow evaporation of the methanol:water (10:1) mixture. The elemental analysis and FTIR data of the complexes are consistent with the formula of the isolated crystals. Table 2.4 summarises the crystallographic data for these coordination complexes.

Table 2.4 The crystallographic data of coordination complexes **2.9**-**2.11**.

	2.9	**2.10**	**2.11**
Formula	$[Co(C_{12}H_{13}ClN_4O)_6](NO_3)_2.CH_3OH$	$[Ni(C_{12}H_{13}ClN_4O)_6](NO_3)_2.(CH_3OH)_2$	$[Co(C_{12}H_{13}ClN_4O)_6](Cl)_2$
Formula weight	1803.28	1835.10	1718.11
Space group	$P\overline{1}$	$P\overline{1}$	$R\overline{3}$
***a* / Å**	13.2050(12)	13.2143(9)	15.7778(6)
***b* / Å**	13.2170(12)	13.2247(9)	15.7778(6)
***c* / Å**	13.3182(12)	13.2483(9)	28.7892(11)
α / °	73.249(2)	73.531(3)	90
β / °	74.350(2)	73.859(3)	90
γ / °	73.579(3)	73.568(2)	120
***V* / Å^3**	2089(3)	2079.7(2)	6206.6(4)
Z	1	1	3
D_{calc} / g cm^{-3}	1.433	1.465	1.379
R_{int}	0.0638	0.0769	0.0545
R_1 [$I \geq 2\sigma(I)$]	0.1011	0.0964	0.0691
wR_2 [all data]	0.2544	0.2191	0.1914

A pink-coloured crystal of formula $[Co(C_{12}H_{13}ClN_4O)_6](NO_3)_2.CH_3OH$ (**2.9**) was obtained from the reaction of ligand **2.7** with cobalt(II) nitrate hexahydrate and was characterised using X-ray crystallography. The crystal formed from the slow evaporation of a methanol:water solution containing complex **2.9**. This structure exhibits unidentate coordination of six imidazole moieties to the cobalt centre, arranged in an octahedral geometry, in which two of the ligands are severely disordered. The bond lengths of the cobalt centre to all nitrogen atoms are fairly symmetrical in the range of 2.143(5) to

2.151(5) Å, in contrast with the previously reported copper(II) complex of ligand **2.4** that exhibit a Jahn-Teller distorted octahedral geometry.[10]

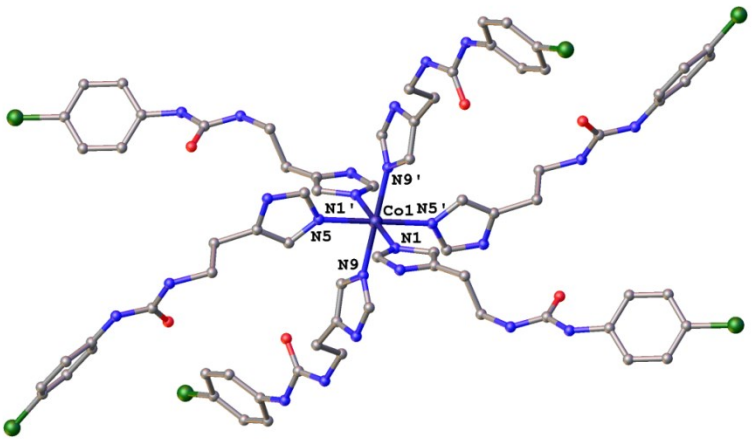

Figure 2.10 Molecular structure of the cobalt(II) complex of ligand **2.7** (**2.9**)**.** (H atoms omitted for clarity).

In the packing, the oxygen atom of the NO_3^- anion, (O5) form hydrogen bond with the urea hydrogen (H8) with a distance of 3.007(9) Å (Figure 2.11). A hydrogen bond between the urea oxygen atom and the hydrogen atom of the imidazole group that is observed in the structure of ligand **2.7** is also retained. Selected bond lengths and angles of complex **2.9** are listed in Table 2.5.

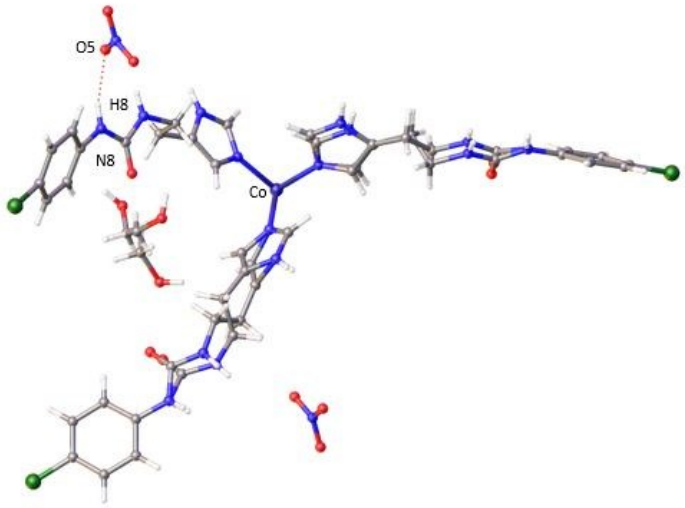

Figure 2.11 Hydrogen bonding interaction (O5···H8) in one asymmetric unit of the cobalt(II) complex of ligand **2.7** (**2.9**)

Table 2.5 Selected bond lengths and bond angles for complex **2.9**.

Bond		Bond lengths (Å)	
Co1-N1		2.151(5)	
Co1-N5		2.149(5)	
Co-N9		2.143(5)	
Hydrogen Bonds	Bond lengths (Å)	Hydrogen Bonds	Bond lengths (Å)
N2A-H2A-O3A[1]	2.847(12)	N7 H7 O5[3]	3.032(9)
N2B-H2B-O3A[1]	2.601(19)	N8 H8 O5[3]	3.007(9)
N2B-H2B-O3B[1]	2.91(2)	N8 H8 O6[3]	3.065(9)
N3A-H3A-O6[1]	2.978(10)	N10 H10 O2[3]	2.852(9)
N4-H4B-O4[1]	2.968(9)	N11A H11A O4[4]	3.059(10)
N4-H4B-O6[1]	3.124(9)	N11B H11B O4[4]	3.181(17)
N6-H6-O1A[2]	2.829(10)	N12 H12A O4[4]	2.983(8)
N6-H6-O1B[2]	3.135(17)	N12 H12A O5[4]	3.110(8)
[1]-1+X,+Y,+Z; [2]+X,+Y,1+Z; [3]2-X,1-Y,1-Z; [4]3-X,1-Y,-Z			
Bond	Bond angles (º)	Bond	Bond angles (º)
N1-Co1-N1[1]	180.0	N9-Co1-N1[1]	88.84(18)
N5-Co1-N1	90.79(19)	N9[1]-Co1-N1	88.84(18)
N5-Co1-N1[1]	89.29(19)	N9[1]-Co1-N5[1]	89.32(19)
N5[1]-Co1-N1[1]	90.71(19)	N9-Co1-N5[1]	90.69(19)
N5[1]-Co1-N1	89.29(19)	N9-Co1-N5	89.31(19)
N5-Co1-N5[1]	180.00(1)	N9[1]-Co1-N5	90.68(19)
N9-Co1-N1	91.16(18)	N9-Co1-N9[1]	180.0
N9[1]-Co1-N1[1]	91.16(18)		

The reaction of ligand **2.7** with nickel(II) nitrate hexahydrate gave a crystal of $[Ni(C_{12}H_{13}ClN_4O)_6]$ $(NO_3)_2.(CH_3OH)_2$ (**2.10**) isostructural with **2.9**. Complex **2.10** show the same coordination mode as **2.9**. The Ni-N bond lengths are symmetrical in the range of 2.097(5) to 2.104(5) Å, but somewhat shorter than the Co-N distances in **2.9** consistent with the smaller ionic radius of Ni(II).

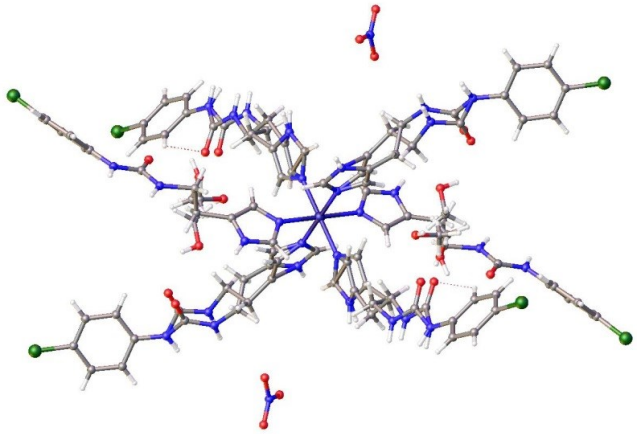

Figure 2.12 Molecular structure of the nickel(II) complex of ligand **2.7** (**2.10**).

A hydrogen bond between the counter ion, NO_3^- with the urea moiety of the ligand is observed in a similar manner to compound **2.9**. The hydrogen bond between the urea oxygen and a hydrogen atom of the imidazole group that is observed in the structure of ligand **2.7** is also retained in this complex. Selected bond lengths and angles of complex **2.10** are listed in Table 2.6.

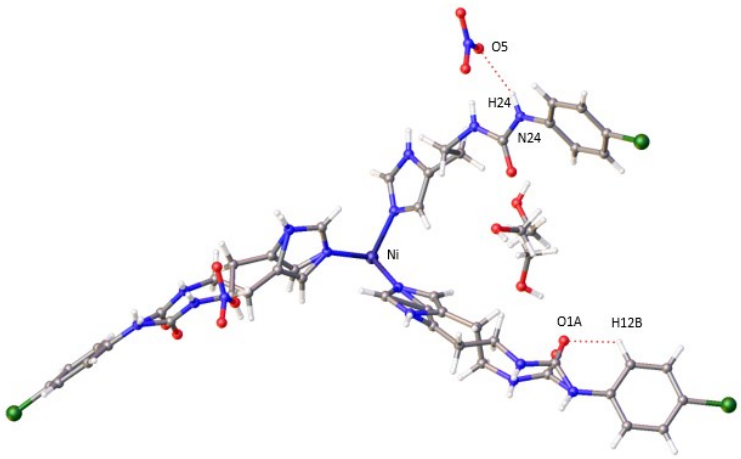

Figure 2.13 Hydrogen bonding interaction (O5···H24) in one asymmetric unit of the nickel(II) complex of ligand **2.7** (**2.10**)

Table 2.6 Selected bond lengths and bond angles for complex **2.10**.

Bond		Bond lengths (Å)	
Ni1-N1		2.104(5)	
Ni1-N11		2.100(5)	
Ni1-N21		2.097(5)	
Hydrogen Bonds	Bond lengths (Å)	Hydrogen Bonds	Bond lengths (Å)
N2-H2A-O3[1]	2.879(8)	N13A-H13A-O6[4]	3.155(19)
N3-H3-O4[2]	3.020(9)	N14-H14-O6[4]	3.023(8)
N3A-H3A-O4[2]	3.235(19)	N14-H14A-O4[4]	3.067(8)
N4-H4B-O4[2]	3.064(8)	N22-H22-O2[5]	2.811(9)
N4-H4B-O5[2]	3.029(8)	N22-H22-O2A[5]	3.175(17)
N12-H12-O1[3]	2.805(9)	N23-H23-O5[5]	3.064(8)
N12-H12-O1A[3]	3.183(16)	N24-H24-O5[5]	3.023(8)
N13-H13-O6[4]	3.020(9)	N24-H24-O2[5]	3.086(8)
[1]1-X,1-Y,1-Z; [2]+X,+Y,-1+Z; [3]+X,+Y,1+Z; [4]1-X,2-Y,2-Z; [5]+X,-1+Y,+Z			
Bond	Bond angles (**º**)	Bond	Bond angles (**º**)
N1-Ni1-N1[1]	179.999(1)	N21[1]-Ni1-N1	91.04(19)
N1-Ni1-N11	90.73(19)	N21[1]-Ni1-N1[1]	88.95(19)
N1[1]-Ni1-N11	89.27(19)	N21[1]-Ni1-N11[1]	90.62(18)
N11[1]-Ni1-N1	89.27(19)	N21-Ni1-N11	90.61(18)
N11[1]-Ni1-N1[1]	90.73(19)	N21-Ni1-N11[1]	89.39(18)
N11[1]-Ni1-N11[1]	180.0	N21[1]-Ni1-N11[1]	89.38(18)
N21-Ni1-N1	88.95(19)	N21[1]-Ni1-N21	179.999(1)
N21-Ni1-N1[1]	91.05(19)		

Compound **2.11**, $[Co(C_{12}H_{13}ClN_4O)_6](Cl)_2$ is formed from the reaction between ligand **2.7** with cobalt(II) chloride hexahydrate. It crystallises from slow evaporation of methanol and adopts the trigonal system with space group $R\bar{3}$ Similar to compound **2.9** and **2.10**, the cobalt centre is bonded to six monodentate imidazole urea ligand, **2.7** and arranged in an octahedral geometry. There is still hydrogen bonding between the urea oxygen atom and the hydrogen atom of an imidazole group, consistent with the hydrogen bonding motif that is seen in compound **2.7**, **2.9** and **2.10**.

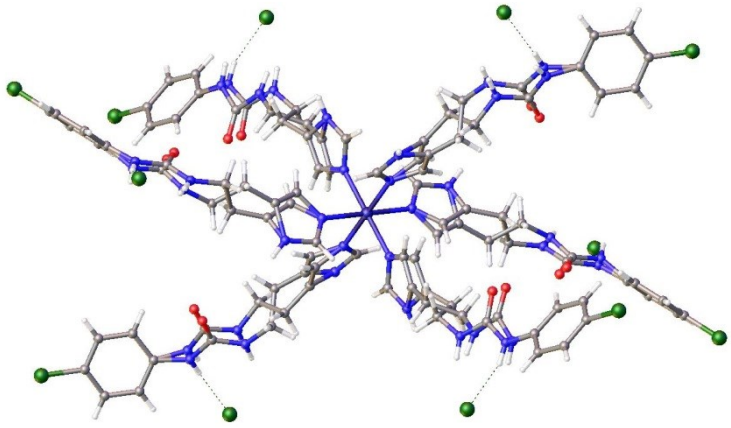

Figure 2.14 Molecular structure of cobalt(II) complex of ligand **2.7** (**2.11**) showing the ligand disorder.

In the packing, the molecules are arranged in three-dimensional network forming a helical structure with chloride anion encapsulated in the binding pocket. The chloride ion forms hydrogen bonds with the hydrogen of the urea moiety, N4-H4-Cl2 and N4A-H4AC-Cl2, with N…Cl distances of 3.062(5) and 3.297(9), respectively. Selected bond lengths and angles of complex **2.11** are listed in Table 2.7.

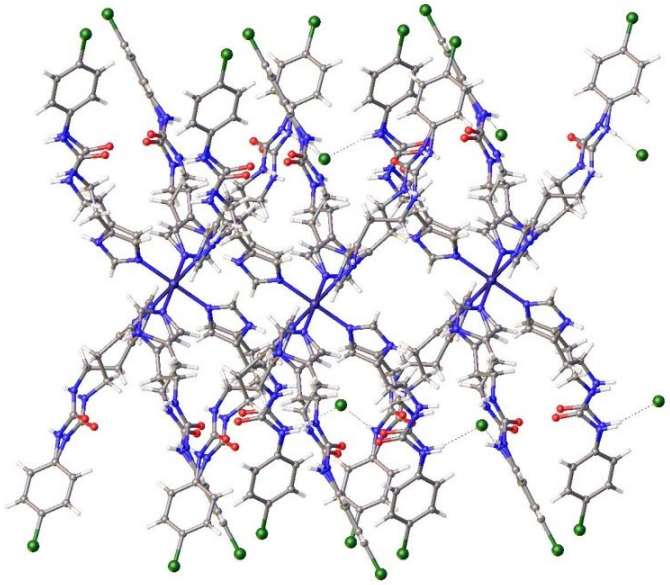

Figure 2.15 Crystal packing diagram of cobalt(II) complex of ligand **2.7** (**2.11**)

Table 2.7 Selected bond lengths and bond angles for complex **2.11**.

Bond		Bond lengths (Å)	
Co1-N1		2.164(2)	
Hydrogen Bonds	Bond lengths (Å)	Hydrogen Bonds	Bond lengths (Å)
N2-H2-O1[1]	2.802(5)	N4-H4-Cl2	3.062(5)
N2-H2-O1A[1]	3.050(9)	N4A-H4AC-Cl2	3.297(9)
[1]2/3-Y+X,1/3+X,1/3-Z			
Bond	Bond angles (**º**)	Bond	Bond angles (**º**)
N1[1]-Co1-N1[2]	89.20(9)	N1[2]-Co1-N1[3]	180.0
N1[3]-Co1-N1[4]	90.79(9)	N1[2]-Co1-N1	90.80(9)
N1[1]-Co1-N1[4]	89.20(9)	N1[5]-Co1-N1[3]	89.20(9)
N1[5]-Co1-N1[4]	180.0	N1[2]-Co1-N1[5]	90.80(9)
N1[5]-Co1-N1	89.20(9)	N1[1]-Co1-N1	180.0
N1[3]-Co1-N1	89.20(9)	N1[2]-Co1-N1[4]	89.20(9)
N1[1]-Co1-N1[3]	90.80(9)	N1[4]-Co1-N1	90.80(9)
N1[1]-Co1-N1[5]	90.80(9)		

2.2.3 Solution state anion binding studies of imidazole ureas with halides.

The solution state binding properties of compounds **2.1** and **2.2** were investigated using ^{1}H NMR spectroscopic titrations in CD_3CN solvent with some anionic guests. This study was performed as a control experiment for comparison with the preorganised anion receptors discussed in the following chapters. The binding isotherms are shown in Figure 2.17. During the titration, important signals namely CH1 and CH2 protons of imidazole as well as NH3 and NH4 protons of urea (Figure 2.16) were followed to investigate the anion binding behaviour of the respective compounds.

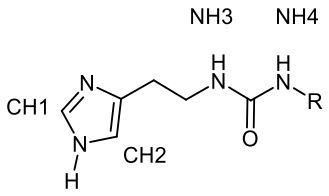

Figure 2.16 Important protons followed during the anion binding titration experiments.

Significant chemical shift changes in the resonances assigned to the urea protons (NH3 and NH4) were observed, with very small shifts for the other CH protons of the imidazole unit. In all cases, the addition of chloride, bromide and iodide anions causes the resonances of the urea protons to be shifted further downfield indicating binding to the anions. After the addition of 6 equivalent of anions, chloride was found to give rise to the largest chemical shift change for compound **2.1** (Δ 1.43 ppm) and **2.2** (Δ 1.32 ppm), followed by bromide, (Δ 0.88 ppm) and (Δ 0.93 ppm), respectively. Iodide ion showed the least chemical shift change than chloride and bromide ions, consistent with its larger size and its smaller charge to radius ratio. On the other hand, the addition of 0.2 equivalent of fluoride ion (as TBA salt) to the acetonitrile-d_3 solution of compound **2.1** results in the broadening of the NH3 urea resonance and a downfield change in the chemical shift of the NH resonances. After two equivalents, the signal had disappeared completely indicating the deprotonation of the urea NH protons. This result is in agreement with previous work data [15–17] as fluoride is highly basic.

a)

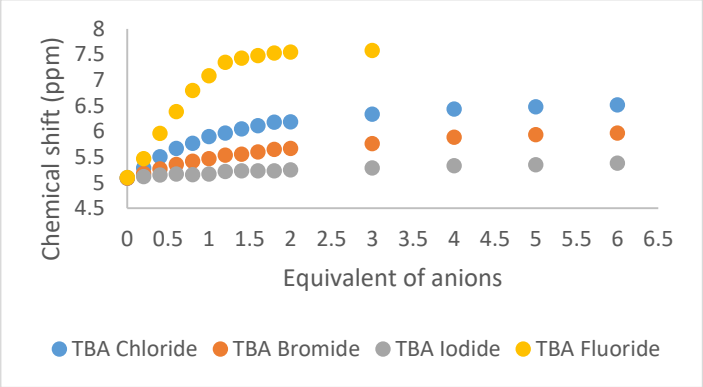

b)

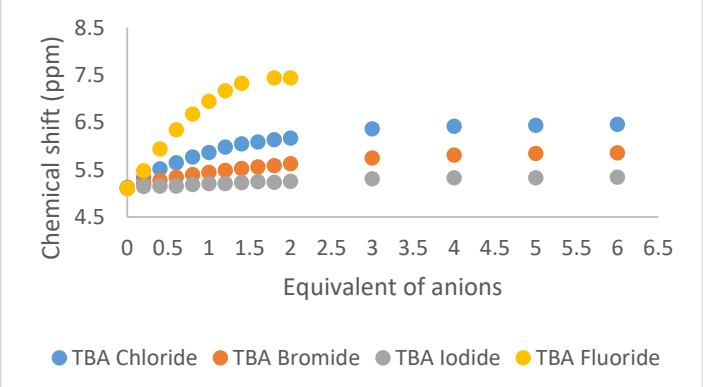

Figure 2.17 Binding isotherms for the urea proton (H3) of a) compound **2.1** and b) compound **2.2** with various anions in CD_3CN.

Job plot analysis of the ^{1}H NMR titrations carried out in acetonitrile-d_3 revealed a maximum at a 50% mole fraction, consistent with the proposed 1:1 binding stoichiometry; this proved to be true for all three anions (TBACl, TBABr and TBAI) for which an appreciable binding interaction was noted (Figure 2.18).

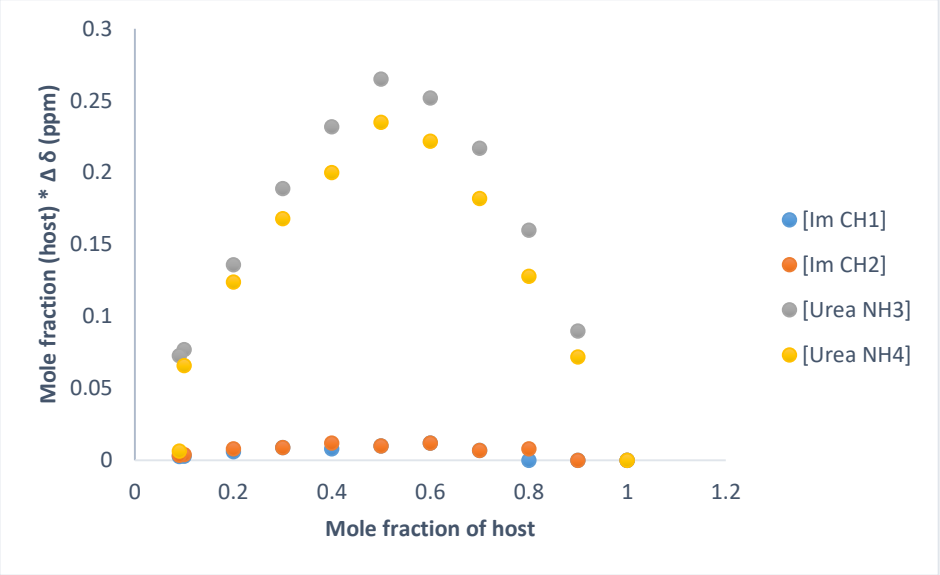

Figure 2.18 Job plot of binding by **2.1** with tetrabutylammonium chloride in acetonitrile-d_3 showing 1:1 host to guest ratio. The maximum amount of shift is shown by the NH protons of the urea groups.

In two cases, the binding constants, K_1 (Table 2.8) were determined by ^{1}H NMR spectroscopic titration using an online tool, Bindfit.[18,19] However, in the case of the titration of compound **2.1** and **2.2** with TBA iodide, the binding constant could not be refined due to the poor fit to the experimental data.

Table **2.8** Binding constants determined by ^{1}H NMR spectroscopic titrations for compounds **2.1** and **2.2** in CD_3CN. All anions used are TBA salts. *a* = Binding constant of compound **2.3** in $CDCl_3$ could not be refined due to poor fit to the experimental data.

	Stoichiometry	**Compounds**	
Anion	**H:G**	**2.1**	**2.2**
Chloride	1:1	177±2%	116±2%
Bromide	1:1	63.44±1%	25±1%
Iodide	1:1	*a*	*a*

In contrast, the solution state binding properties of compound **2.3** were performed using ^{1}H NMR spectroscopic titrations in a less polar solvent, $CDCl_3$ with fluoride, chloride, bromide and iodide ions. The binding isotherms are shown in Figure 2.19. Significant chemical shift changes in the resonances assigned to the urea protons (NH3 and NH4) were observed, with very small shifts for the CH protons of the imidazole group. Addition of chloride, bromide and iodide, moved the chemical shifts of the urea protons further downfield indicating a hydrogen-bonding interaction involving the halide anions with the urea N-H groups. For compound **2.3**, the binding constant could not be calculated accurately and refined due to the poor fit of the experimental data which results in high percentage of error. Thus, the anion-binding behaviour of this compound are discussed based on the changes in the chemical shift of the urea protons.

Titration of compound **2.3** with chloride ion results in the largest shift of urea protons (Δ 1.13 ppm), followed by bromide, (Δ 0.75 ppm). A similar result was found as iodide ion is bound more weakly to the urea NH than both of the anions afore-mentioned (Δ 0.73 ppm), consistent with its larger size and its smaller charge to radius ratio. On the other hand, the addition of 0.2 equivalent of fluoride ion (as TBA salt) to the chloroform-d_3 solution of compound **2.3** results in the downfield shift of NH3 urea resonance from 5.32 to 5.54 pm with significant broadening of the peak. After 0.8 equivalents, the NH3 and NH4 urea signals have totally disappeared indicating the deprotonation of the urea protons. This result is consistent with data published elsewhere[15–17] as fluoride ion is highly basic and would be able the deprotonate urea protons. From the binding isotherms of compound **2.1**, **2.2** and **2.3**, it is shown that the chemical shifts changes do not differ significantly in the less polar solvent chloroform.

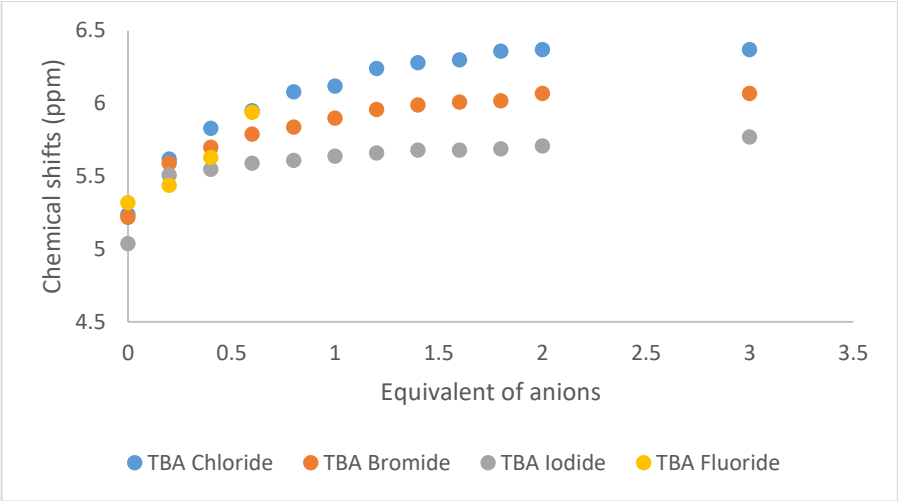

Figure 2.19 Binding isotherms for the urea proton (NH3) of compound **2.3** with various anions in $CDCl_3$.

The chemical shift change for all imidazole urea derivatives with aliphatic chain after the addition of 3 equivalent of NBu_4X is summarised in Table 2.9.

Table 2.9 The chemical shift change (Δδ) in ppm of the CH1 and CH2 protons of the imidazole ring and NH3 and NH4 protons of the urea group after the addition of 3 equivalent of NBu_4X at room temperature.

Compounds	Solvent	Protons	Cl^-	Br^-	I^-
2.1	CD_3CN	CH1	0.05	0.03	0.01
		CH2	0.06	0.02	0
		NH3	1.25	0.67	0.17
		NH4	1.07	0.64	0.16
2.2	CD_3CN	CH1	0.06	0.03	0.01
		CH2	0.07	0.02	0.01
		NH3	1.3	0.63	0.16
		NH4	1.17	0.62	0.18
2.3	$CDCl_3$	CH1	0.09	0.06	0.03
		CH2	0.09	0.06	0.05
		NH3	1.27	0.92	0.73
		NH4	1.24	1.05	0.85

Solution state anion binding studies were also performed on the imidazole urea compounds with aromatic substituents, namely compounds **2.6** and **2.7**. The titration experiments for both of the compounds were carried out in a more competitive solvent, DMSO-d_6 as both of the compounds were not very soluble in acetonitrile-d_3. In contrast to compound **2.1**-**2.3**, compound **2.6** and **2.7** are showing more complex speciation accompanied by slow guest complexation kinetics or conformational change on the ^{1}H NMR spectroscopic timescale, as evidenced by significant broadening and splitting of several peaks at room temperature. As a result, binding constants could not be reliably determined.

In detail, for compound **2.6** and **2.7**, changes in the chemical shifts were observed for four different protons, namely the CH proton neighbouring the nitrogen atom in the imidazole ring (CH1 and CH2) and the protons of the urea group (NH3 and NH4). Both of the compounds appear to have more complex speciation in comparison with compounds **2.1**–**2.3**, as evidenced by significant broadening and splitting of several peaks at room temperature.

The addition of 0.2 equivalent of fluoride anion (as TBA salt) has resulted in the splitting of all the above-mentioned proton signals. For example, the CH1 signal of compound **2.6** at 8.42 ppm has split into two peaks at 8.42 and 8.54 ppm. The same trend was also observed for a CH2 signal from 7.55 ppm to 7.55 and 7.52 ppm, as well as the splitting of the urea signals, NH3 from 6.89 ppm to 6.89 and 6.79 ppm and for NH4 from 6.08 to 6.08 and 6.25 ppm. Adding more equivalent of fluoride moved the split signal of CH1 further downfield until it disappears after 0.6 equivalent of fluoride added. For the CH2 proton of the imidazole, the split signal at 7.52 moved further upfield and later merged with the signals of the aromatic CH protons.

The signal of NH3 urea proton also moved further upfield when fluoride ion was added. For NH4 proton, the addition of 0.2 equivalent of fluoride ion also causes the signal to split and eventually disappear after subsequent addition of the fluoride ion (Figure 2.20). The anion binding stoichiometry has not been determined due to the splitting patterns of the proton resonances.

Titration of compound **2.7** with fluoride ion (as TBA salt) (Figure 2.21) also resulted in the same binding pattern as compound **2.6**, splitting and disappearance of all the signals

due to the deprotonation of all the designated protons. A possible explanation for the splitting of the signals is the presence of two different isomers of compound **2.6** and **2.7**, in which one of the isomers does not bond to the anions, while the other responds well to the anions added. As imidazole compounds can show tautomerism, this would explain the presence of two different isomers.

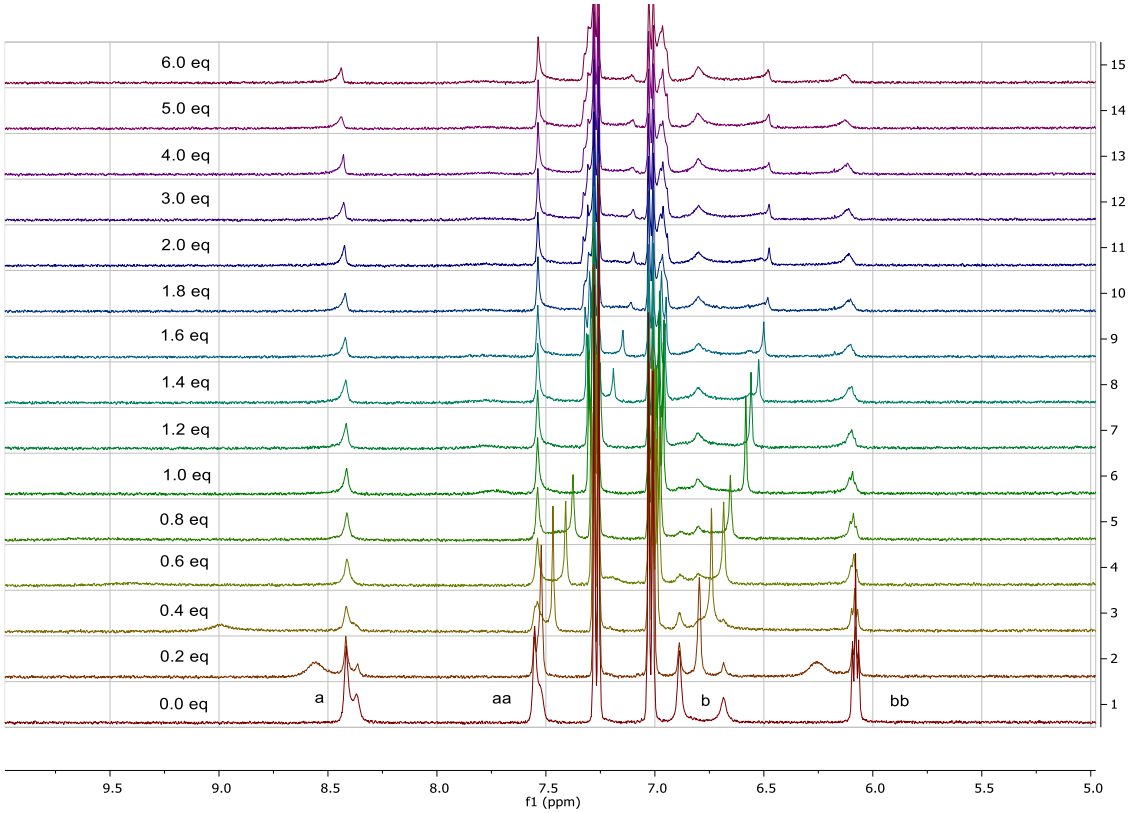

Figure 2.20 Stack plot showing the ^{1}H NMR spectrum of compound **2.6** in DMSO-d_6 in the presence of fluoride ion as tetrabutylammonium salt.

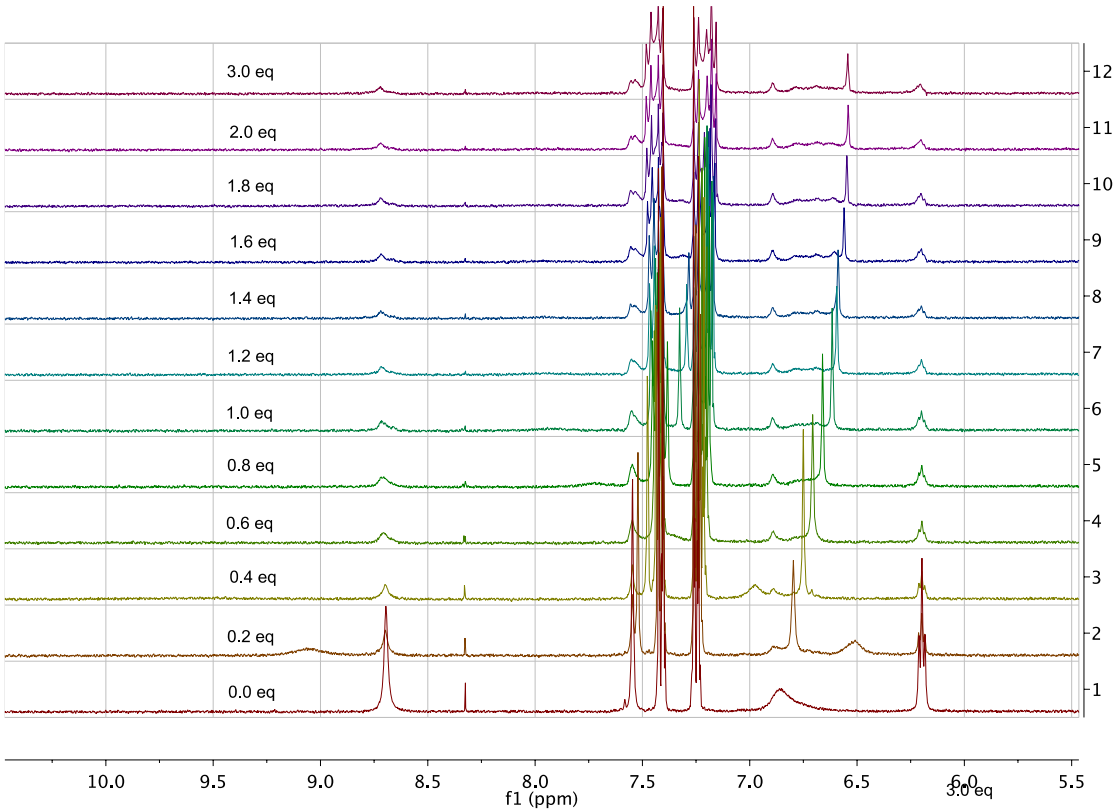

Figure 2.21 Stack plot showing the ^{1}H NMR spectrum of compound **2.7** in DMSO-d_6 in the presence of fluoride ion as tetrabutylammonium salt.

Titration of compound **2.6** and **2.7** with the chloride ion also show the splitting trend of the peak, however, in contrast with fluoride ion, only two protons interact with the chloride anion, the CH1 proton of the imidazole ring and the NH4 urea proton (Figure 2.22 and 2.23). The addition of up to 2 equivalent of chloride caused the splitting of the CH1 signal into two peaks; until it remains unchanged after more than 2 equivalent chloride ion added.

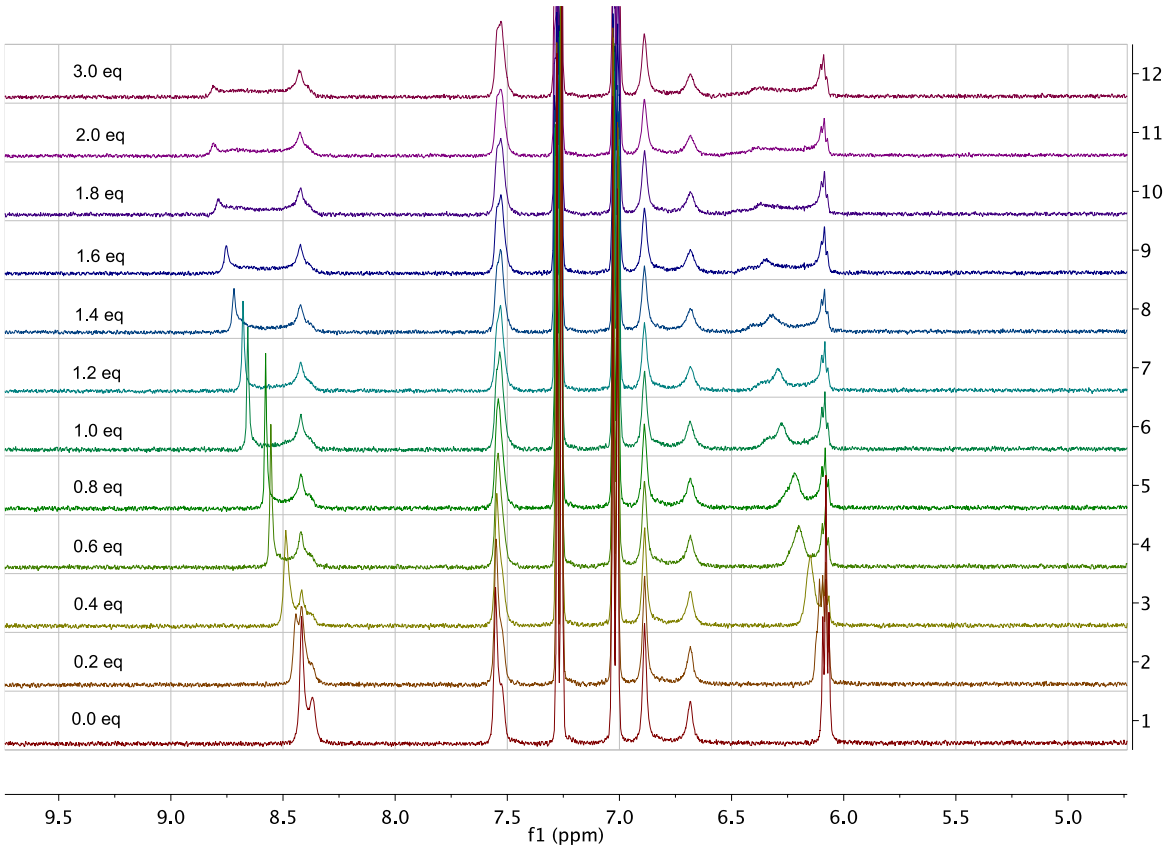

Figure 2.22 Stack plot showing the ^{1}H NMR spectrum of compound **2.6** in DMSO-d_6 in the presence of chloride ion as tetrabutylammonium salt.

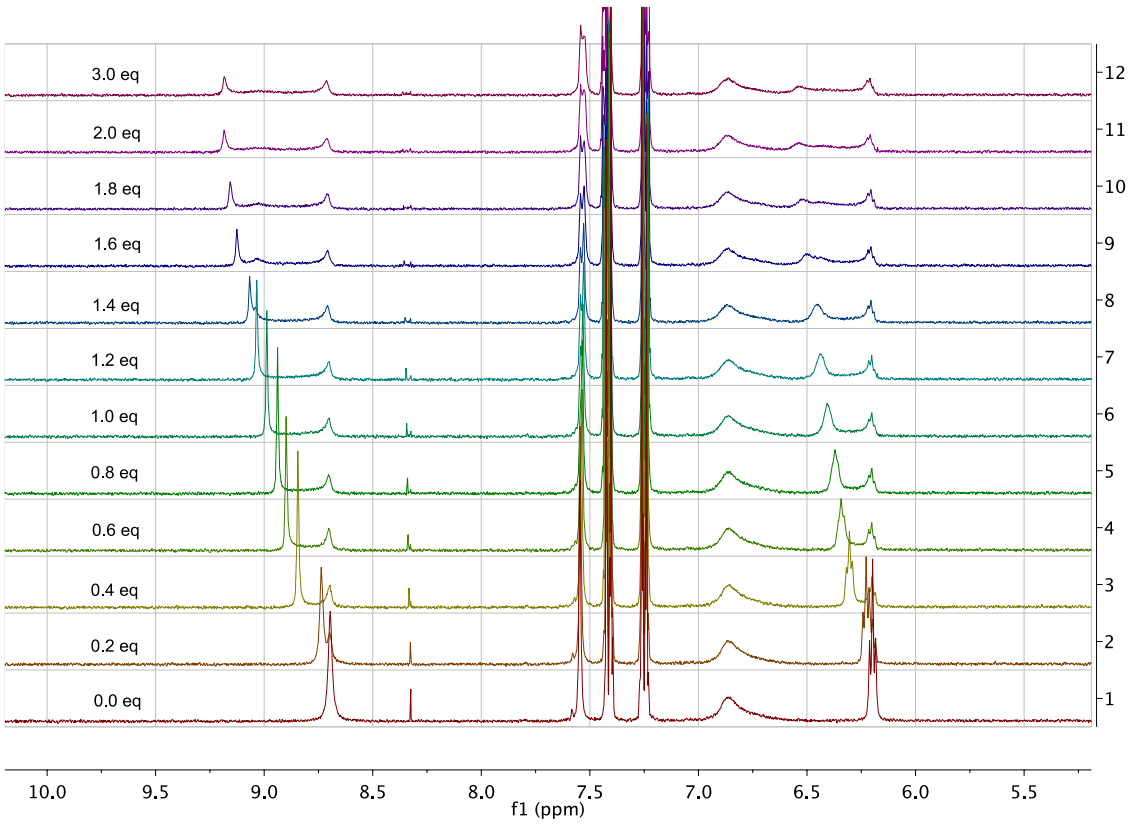

Figure 2.23 Stack plot showing the ^{1}H NMR spectrum of compound **2.7** in DMSO-d_6 in the presence of chloride ion as tetrabutylammonium salt.

On the contrary, although titration of compound **2.6** and **2.7** with bromide ion does show similar observation with chloride ion titration, the changes in the chemical shifts were less pronounced in comparison with the chloride ion (Figure 2.24 and 2.25). This observation has been anticipated as bromide ion has a larger size and smaller charge to radius ratio compare to chloride ion.

On the other hand, the addition of iodide ion to the solution of compound **2.6** and **2.7** does not result in any significant changes to the chemical shifts of the designated protons except a less pronounced broadening of the CH1 of the imidazole ring (Figure 2.26 and 2.27).

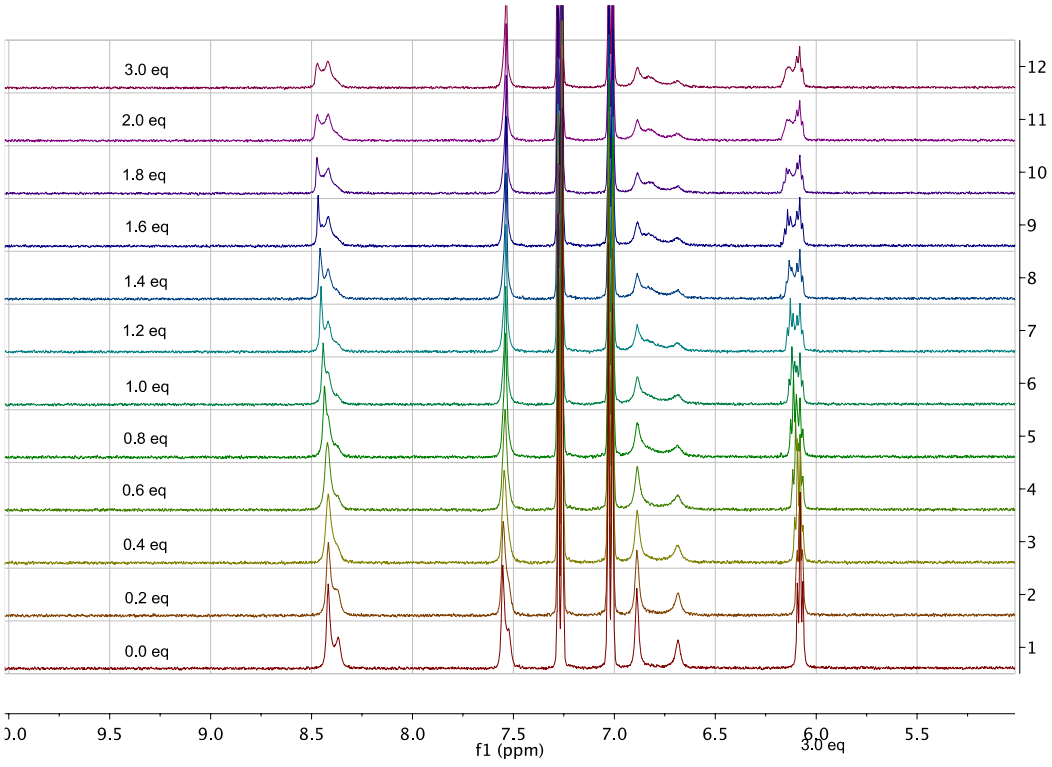

Figure 2.24 Stack plot showing the ^{1}H NMR spectrum of compound **2.6** in DMSO-d_6 in the presence of bromide ion as tetrabutylammonium salt.

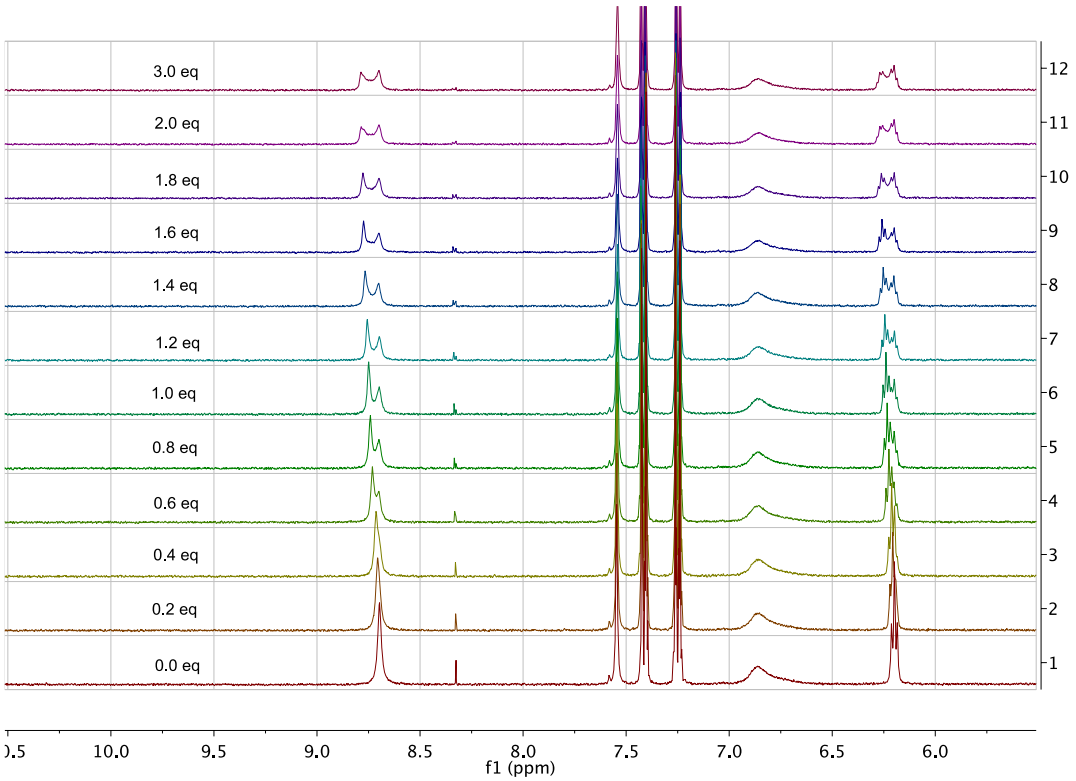

Figure 2.25 Stack plot showing the ^{1}H NMR spectrum of compound **2.7** in DMSO-d_6 in the presence of bromide ion as tetrabutylammonium salt.

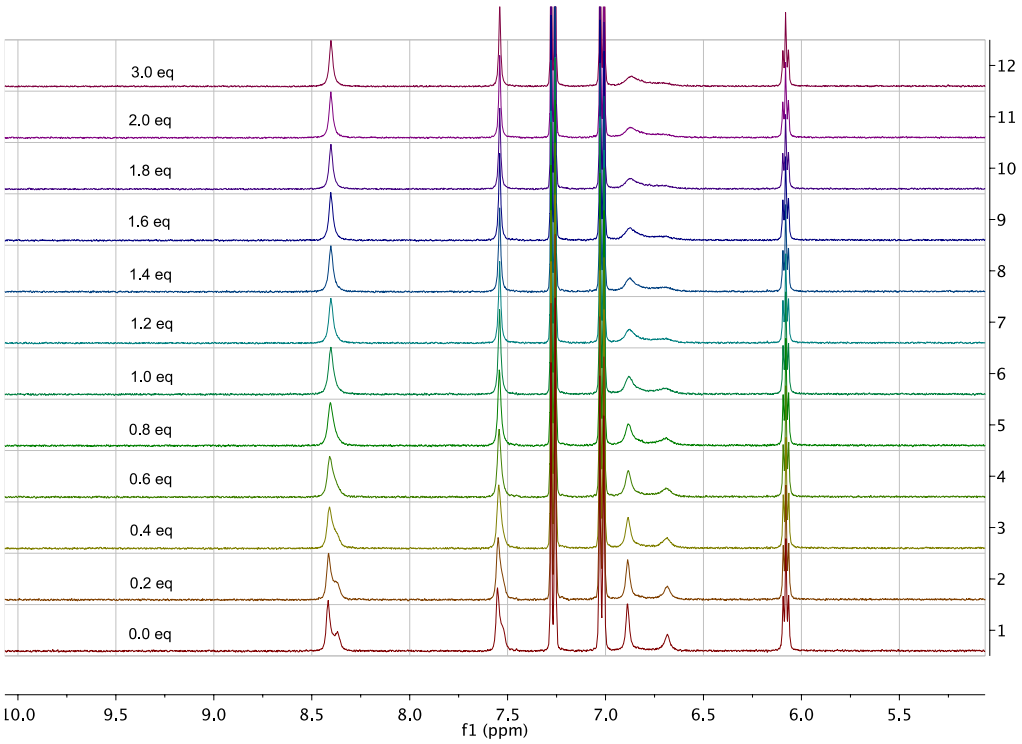

Figure 2.26 Stack plot showing the ^{1}H NMR spectrum of compound **2.6** in DMSO-d_6 in the presence of iodide ion as tetrabutylammonium salt.

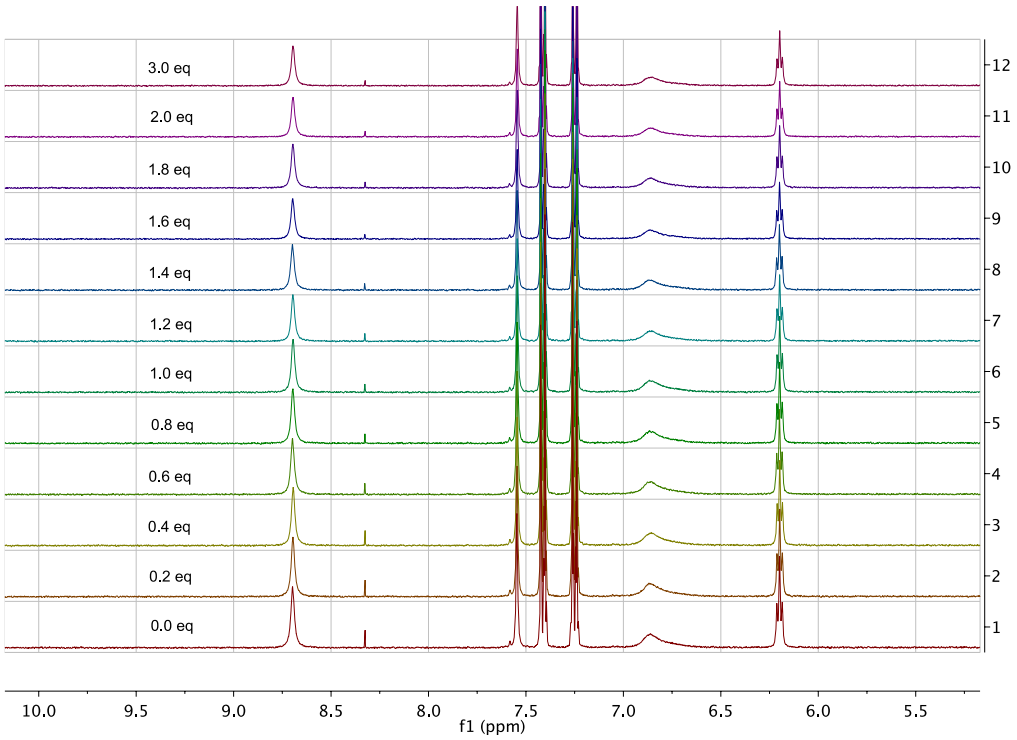

Figure 2.27 Stack plot showing the ^{1}H NMR spectrum of compound **2.7** in DMSO-d_6 in the presence of iodide ion as tetrabutylammonium salt.

Table 2.9 The chemical shift change (Δδ) in ppm of the CH1 and CH2 protons of the imidazole ring and NH3 and NH4 protons of the urea group after the addition of 3 equivalent of NBu_4X at room temperature.

Compounds	Solvent	Protons	Cl^-	Br^-	I^-
2.6	DMSO-d_6	CH1	0.39 and 0	0.04 and 0	0
		CH2	0	0	0
		NH3	0	0	0
		NH4	0.18 and 0	0.05 and 0	0
2.7	DMSO-d_6	CH1	0.48 and 0	0.09 and 0	0
		CH2	0	0	0
		NH3	0	0	0
		NH4	0.32 and 0	0.06 and 0	0

The designated protons in all of the compounds, **2.1**, **2.2**, **2.3**, **2.6** and **2.7**, are shifted downfield or upfield and becomes broad after the addition of fluoride anion and disappears completely much before the complete addition of TBAF, possibly due to the hydrogen bonding interaction with the fluoride ions followed by deprotonation.[20–23] For other halide ions namely chloride, bromide and iodide ions, the ^{1}H NMR titration experiment shows that the anions formed a hydrogen bonding only with N-H group of urea ions in the case of compound **2.1**-**2.3**. Conversely, in compound **2.6** and **2.7**, the

anions are connected to the imidazole urea compounds through hydrogen bonding interactions with CH1 (imidazole ring) and NH3 protons.

2.3 Summary

We have synthesised a series of imidazole compounds containing urea derivatives that comprise of an imidazole group, which serves as the cation binding sites and urea groups that show hydrogen bonding interaction with anions. The imidazole urea compounds bind to transition metals namely Cu(II), Co(II) and Ni(II) in unidentate fashion. It is also possible that the anion binding behaviour of the molecules revealed through ^{1}H NMR titration experiments with halide anions was caused by the urea conformation along with the imidazole tautomerism. Moreover, the broadening and splitting of the designated chemical shifts upon the addition of the halide anions into the solution of compound **2.6** and **2.7** indicates the presence of isomers for imidazole urea with aromatic substituents, while there are no isomers found for imidazole ureas with aliphatic chains. These findings have led this project to the design of anion receptors based on organic frameworks and transition metals, which is discussed in detail in the following chapters.

2.4 Experimental

All solvents used in the synthesis and purification were of analytical reagent grade. Anhydrous solvents were prepared on an SPS solvent purification system. Commercial reagents were used as supplied, without further purification.

2.4.1 Instrumentation and Analytical Measurements

All NMR spectra were obtained from a Bruker Avance 400 at a frequency of 400 MHz for ^{1}H and 100 MHz for ^{13}C, while ^{1}H, ^{13}C, ^{1}H-^{1}H COSY, ^{1}H-^{13}C HSQC and ^{1}H-^{13}C HMBC spectra were obtained from a Varian INOVA 500 spectrometer at a frequency of 500 MHz for ^{1}H and 125 MHz for ^{13}C. All chemical shifts are reported in parts per million (δ) relative to tetramethylsilane as an internal reference. Electrospray ionisation (ESI) mass spectrometry was recorded on a TQD mass spectrometer instrument. Fourier transforms infrared spectra were recorded with a Perkin-Elmer Spectrum 100 FT-IR spectrometer in which for each spectrum, 64 scans were conducted over a spectral range of 4000 to 600 cm^{-1} with a resolution of 4 cm^{-1}. Elemental analysis was performed using an Exeter Analytical CE-400 Elemental Analyser. The single crystal diffraction data for all compounds were collected at 120 K on an Agilent XCalibur diffractometer (Sapphire-3 CCD detector, graphite monochromator, λMoKα radiation λ = 0.71073 Å) equipped with Cryostream (Oxford Cryosystems) open flow nitrogen cryostat. Structures were solved and refined using the SHELX programs[24] operating within the Olex2 interface[25], or solved using Superflip.[26]

2.4.2 Synthesis of imidazole ligands

Synthesis of 1 - [2 - (1*H* - imidazol - 4 - yl)ethyl] - 3 - (4 - butyl)urea (**2.1**)

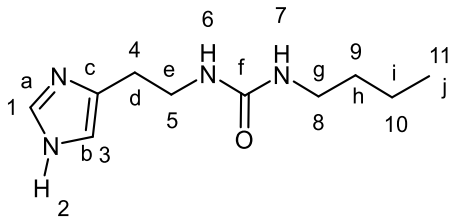

2.1

The synthesis of this compound was performed according to the published procedures described by Barboiu group.[2] At 40 °C, histamine (1.10 g, 9.9 mmol) was dissolved in anhydrous chloroform (120 ml). Subsequently, a solution of n-butyl isocyanate (0.98 g, 9.9 mmol) in anhydrous chloroform (10 ml) was slowly added *via* the dropping funnel over the course of 2 hours, before refluxing for a further 18 hours. The resulting white precipitate was filtered under reduced pressure, washed with chloroform (3 x 50 ml) and dried under vacuum for three hours to yield the pure product as a white powder (1.56 g, 7.42 mmol, 75%). **^{1}H NMR:** δ_H (400 MHz; DMSO-d_6; Me_4Si) 11.84 (1 H, br s, *H2*), 7.52 (1 H, d, *J* 1.1, *H1*), 6.76 (1 H, s, *H3*), 5.88 (1 H, t, *J* 5.6, *H6*), 5.79 (1 H, t, *J* 5.6, *H7*), 3.21 (2 H, m, *H5*), 2.97 (2 H, m, *H8*), 2.57 (2 H, t, *J* 7.1 *H4*), 1.30 (2 H, m, *H9*), 1.25 (2 H, m, *H10*) , 0.85 (3 H, t, *J* 8.0, *H11*). **^{13}C {^{1}H} NMR:** δ_C {^{1}H} (101 MHz; DMSO) 158.46 (*Cf*), 135.01 (*Ca*), 39.96 (*Cc*), 39.35 (*Cb*), 32.62 (*Ce* and *Cg*), 28.27 (*Cd*), 20.00 (*Ch* and *Ci*), 14.18 (*Cj*). **FTIR:** ν_{max}/cm^{-1} 3084 (NH), 1647 (CO), 1562 and 1502 (imid. ring), m/z (ESI-MS) 211 $[M+H]^+$ 210 $[M]^+$, 443 $[2M+Na]^+$. Elem. Anal. Calc. (%) ($C_{10}H_{18}N_4O$) C, 57.12; H, 8.63; N, 26.64 %; Found: C, 56.76; H, 8.54; N, 26.52 %

Synthesis of 1 - [2 - (1*H* - imidazol - 4 - yl)ethyl] - 3 - (4 - octyl)urea (**2.2**)

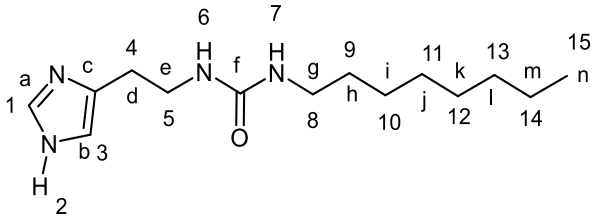

2.2

At 40 °C, histamine (1.10 g, 9.9 mmol) was dissolved in anhydrous chloroform (120 ml). Subsequently, a solution of n-butyl isocyanate (0.98 g, 9.9 mmol) in anhydrous chloroform (10 ml) was slowly added *via* the dropping funnel over the course of 2 hours, before

refluxing for a further 18 hours. The resulting white precipitate was filtered under reduced pressure, washed with chloroform (3 x 50 ml) and dried under vacuum for three hours to yield the pure product as a white powder (2.25 g, 8.42 mmol, 85%). **^{1}H NMR:** δ_H (400 MHz; DMSO-d_6; Me_4Si) 11.83 (1 H, br s, *H2*), 8.33 (1 H, s, *H1*), 7.53 (1 H, s, *H3*), 5.88 (1 H, t, *J* 5.6, *H6*), 5.79 (1 H, t, *J* 5.6, *H7*), 3.21 (2 H, dt, *H5*), 2.95 (2 H, q, *H8*), 2.58 (2 H, t, *J* 7.1 *H4*), 1.24 (12 H, m, *H9-H14*), 0.86 (3 H, t, *J* 8.0, *H15*). **^{13}C {^{1}H} NMR:** δ_C {^{1}H} (101 MHz; DMSO) 158.45 (*Cf*), 134.99 (*Ca*), 39.80 (*Cc*), 39.69 (*Cd*), 31.72 (C*g*), 30.49 (C*h*), 29.25 (C*i*), 29.18 (C*j*), 28.17 (*Ck*), 26.89 (C*l*), 22.56 (C*m*), 14.42 (C*n*). **FTIR:** ν_{max}/cm^{-1} 3306 (NH), 1617 (CO), 1570 (imid. ring). m/z (ESI-MS) 267 $[M+H]^+$. Elem. Anal. Calc. (%) ($C_{14}H_{26}N_4O$): C, 63.12; H, 9.84; N, 21.03 %; Found: C, 61.89; H, 9.64; N, 20.70 %

Synthesis of 1 - [2 - (1*H* - imidazol - 4 - yl)ethyl] - 3 - (4 - dodecyl)urea (**2.3**)

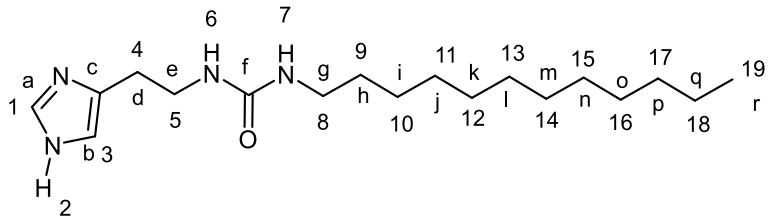

2.3

At 40 °C, histamine (1.10 g, 9.9 mmol) was dissolved in anhydrous chloroform (120 ml). Subsequently, a solution of n-butyl isocyanate (0.98 g, 9.9 mmol) in anhydrous chloroform (10 ml) was slowly added *via* the dropping funnel over the course of 2 hours, before refluxing for a further 18 hours. The resulting white precipitate was filtered under reduced pressure, washed with chloroform (3 x 50 ml) and dried under vacuum for three hours to yield the pure product as a white powder (2.55 g, 7.92 mmol, 80%). **^{1}H NMR:** δ_H (400 MHz; DMSO-d_6; Me_4Si) 7.58 (1 H, s, *H1*), 6.79 (1 H, s, *H3*), 5.88 (1 H, t, *J* 5.6, *H6*), 5.79 (1 H, t, *J* 5.6, *H7*), 3.21 (2 H, dt, *H5*), 2.95 (2 H, q, *H8*), 2.58 (2 H, t, *J* 7.1 *H4*), 1.24 (20 H, m, *H9-H18*), 0.86 (3 H, t, *J* 8.0, *H19*). **^{13}C {^{1}H} NMR:** δ_C {^{1}H} (101 MHz; DMSO) 158.45 (*Cf*), 134.99 (*Ca*), 117.60 (C*b*), 39.78 (*Cd*), 31.76 (*Ce*), 30.47 (C*g*), 29.52 (C*h-l*), 29.32 (C*m*), 29.18 (C*n*), 28.19 (*Co*), 26.86 (C*p*), 22.56 (C*q*), 14.40 (C*r*). **FTIR:** ν_{max}/cm^{-1} 3309 (NH), 1611 (CO), 1570 (imid. ring). m/z (ESI-MS) 323.9 $[M+H]^+$. Elem. Anal. Calc. (%) ($C_{18}H_{34}N_4O$): C, 67.04; H, 10.63; N, 17.37 %; Found: C, 66.62; H, 10.45; N, 17.24 %

Synthesis of 1 - [2 - (1*H* - imidazol - 4 - yl)ethyl] - 3 - (4 - methylphenyl)urea (**2.4)**

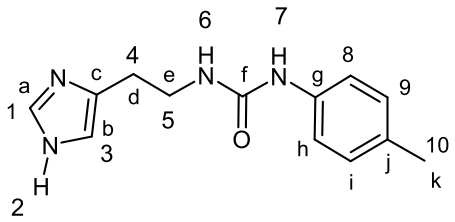

2.4

At 40 °C, histamine (1.10 g, 9.9 mmol) was dissolved in anhydrous chloroform (120 ml). Subsequently, a solution of *p*-tolyl isocyanate (1.32 g, 9.9 mmol) in anhydrous chloroform (10 ml) was slowly added *via* the dropping funnel over the course of 2 hours. The solution mixture was then heated to reflux for further 18 hours. The resulting white precipitate was filtered under reduced pressure, washed with chloroform (3 x 50 ml) and dried under vacuum for three hours to yield the pure product as a white powder (2.22 g, 9.1 mmol, 92%).

^{1}H NMR: δ_H (400 MHz; DMSO-d_6; Me_4Si) 10.15 (1 H, br s, *H2*), 8.41 (1 H, s, *H1*), 7.55 (1 H, d, *J* 1.1, *H3*), 7.26 (2 H, m, *H8*), 7.01 (2 H, m, *H9*), 6.82 (1 H, br s, *H7*), 6.09 (1 H, t, *J* 5.7, *H6*), 3.34 (2 H, dt, *H5*), 2.66 (2 H, t, *J* 6.9, *H4*), 2.21 (3 H, s, *H10*). **^{13}C {^{1}H} NMR:** δ_C {^{1}H} (101 MHz; DMSO) 155.67 (*Cf*), 147.29 (*Cc*), 141.06 (*Ca*), 138.49 (*Cb*), 135.14 (*Ce*), 130.04 (*Cg*), 129.46 (*Ch*), 121.48 (*Cj*), 118.11 (*Ci*), 28.05 (*Cd*), 20.75 (*Ck*). **FTIR:** ν_{max}/cm^{-1} 3307 and 3107 (NH), 1553 (CO), 1597 (Ph C-C), 1511 (imid. ring). m/z (ESI-MS) 245 $[M+H]^+$ 244 $[M]^+$, 489 $[2M+H]^+$. Elem. Anal. Calc. (%) ($C_{13}H_{16}N_4O$): C, 63.91; H, 6.60; N, 22.93 %; Found: C, 63.5; H, 6.54; N, 22.93 %.

Synthesis of 1 - [2 - (1*H* - imidazol - 4 - yl)ethyl] - 3 - (3 - nitrophenyl)urea (**2.5**)

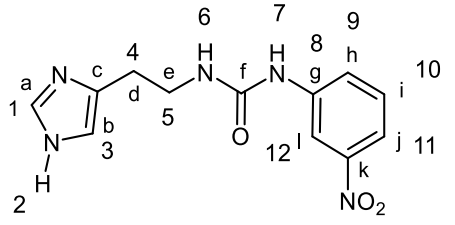

2.5

At 40 °C, histamine (1.10 g, 9.9 mmol) was dissolved in anhydrous chloroform (120 ml). Subsequently, a solution of *p*-tolyl isocyanate (1.32 g, 9.9 mmol) in anhydrous chloroform (10 ml) was slowly added *via* the dropping funnel over the course of 2 hours. The solution mixture was then heated to reflux for further 18 hours. The resulting white precipitate was

filtered under reduced pressure, washed with chloroform (3 x 50 ml) and dried under vacuum for three hours to yield the pure product as a yellow powder (2.63 g, 9.6 mmol, 97%). **^{1}H NMR:** δ_H (400 MHz; DMSO-d_6; Me_4Si) 11.85 (1 H, br s, *H2*), 9.17 (1 H, s, *H11*), 8.53 (1 H, s, *H2*), 7.73 (1 H, m, *H8*), 7.64 (1 H, m, *H10*), 7.57 (1 H, d, *J 1.1*, *H9*), 7.51 (1 H, s, *H3*), 7.49 (1 H, s, *H7*), 7.47 (1 H, s, *H6*), 3.37 (2 H, q, *H4*), 2.69 (2 H, t, *J* 6.9, *H5*). **^{13}C {^{1}H} NMR:** δ_C {^{1}H} (101 MHz; DMSO) 155.31 (*Cf*), 148.57 (*Cc*), 142.39 (*Ca*), 135.19(*Cg* & *Ck*), 130.31 (*Ce*), 123.98 (*Ch*), 115.80 (*Ci*), 111.86 (1 C, *Cj*),.68 (1 C, *Cd*), 27.83 (1 C, *Ce*). m/z (ESI-MS) 276 $[M+H]^+$. **FTIR:** ν_{max}/cm^{-1} 3307 (NH), 1597 (CO), 1533 (imid. ring). Elem. Anal. Calc. (%) ($C_{12}H_{13}N_5O_3$): C, 52.36; H, 4.76; N, 25.44 %; Found: C, 51.51; H, 4.67; N, 25.00 %

Synthesis of 1 - [2 - (1*H* - imidazol - 4 - yl)ethyl] - 3 - (4 - butylphenyl)urea (**2.6**)

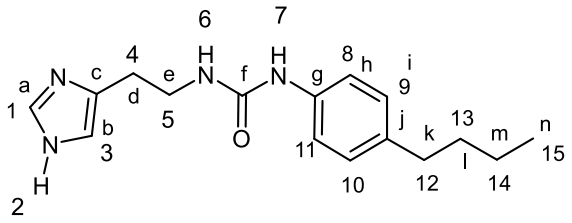

2.6

At 40 °C, histamine (1.10 g, 9.9 mmol) was dissolved in anhydrous chloroform (120 ml). Subsequently, a solution of *p*-tolyl isocyanate (1.32 g, 9.9 mmol) in anhydrous chloroform (10 ml) was slowly added *via* the dropping funnel over the course of 2 hours. The solution mixture was then heated to reflux for further 18 hours. The resulting white precipitate was filtered under reduced pressure, washed with chloroform (3 x 50 ml) and dried under vacuum for three hours to yield the pure product as a white powder (2.65 g, 9.2 mmol, 93%). **^{1}H NMR:** δ_H (400 MHz; DMSO-d_6; Me_4Si) 11.84 (1 H, br s, *H2*), 8.43 (1 H, s, *H1*), 7.55 (1 H, d, *J* 1.1, *H3*), 7.27 (2 H, m, *H8* & *H11*), 7.02 (2 H, m, *H9* & *H10*), 6.82 (1 H, br s, *H7*), 6.11 (1 H, t, *J* 5.7, *H6*), 3.34 (2 H, dt, *H5*), 2.66 (2 H, t, *J* 6.9, *H4*), 2.48 (2 H, d, *J* 1.1, *H12*), 1.50 (2 H, m, *H13*), 1.28 (2 H, m, *H14*), 0.88 (3 H, t, *H15*). **^{13}C {^{1}H} NMR:** δ_C {^{1}H} (101 MHz; DMSO) 155.68 (*Cf*), 138.68 (*Cc, Cg* & *Cj*), 135.15 (*Ca*), 128.79 (*Ch*), 118.12 (*Cb* & *Ci*), 39.57 (*Cd*), 34.59 (*Ce*), 33.79 (C*k*), 22.15 (C*l* & C*m*), 14.26 (C*n*). **FTIR:** ν_{max}/cm^{-1} 3359 (NH), 1632 (CO), 1554 (imid. ring). m/z (ESI-MS) 288 $[M+H]^+$. Elem. Anal. Calc. (%) ($C_{16}H_{22}N_4O$): C, 67.11; H, 7.74; N, 19.56 %; Found: C, 66.16; H, 7.64; N, 19.53 %

Synthesis of 1 - [2 - (1*H* - imidazol - 4 - yl)ethyl] - 3 - (4 - chlorophenyl)urea (**2.7**)

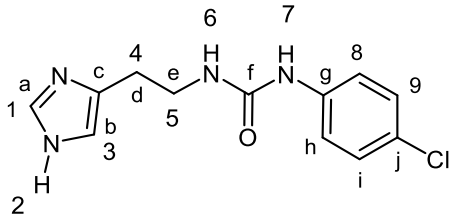

2.7

At 40 °C, histamine (1.10 g, 9.9 mmol) was dissolved in anhydrous chloroform (120 ml). Subsequently, a solution of *p*-tolyl isocyanate (1.32 g, 9.9 mmol) in anhydrous chloroform (10 ml) was slowly added *via* the dropping funnel over the course of 2 hours. The solution mixture was then heated to reflux for further 18 hours. The resulting white precipitate was filtered under reduced pressure, washed with chloroform (3 x 50 ml) and dried under vacuum for three hours to yield the pure product as a white powder (2.61 g, 9.1 mmol, 92%). **^{1}H NMR:** δ_H (400 MHz; DMSO-d_6; Me_4Si) 11.84 (1 H, br s, *H2*), 8.73 (1 H, s, *H1*), 7.56 (1 H, d, *J* 1.1, *H3*), 7.42 (2 H, dd, *H8*), 7.25 (2 H, dd, *H9*), 6.83 (1 H, br s, *H7*), 6.23 (1 H, t, *J* 5.7, *H6*), 3.34 (2 H, dt, *H5*), 2.66 (2 H, t, *J* 6.9, *H4*). **^{13}C {^{1}H} NMR:** δ_C {^{1}H} (101 MHz; DMSO) 155.43 (*Cf*), 140.08 (*Cc* & C*j*), 135.16 (C*a* & *Cb*), 128.89 (*Ci*), 124.78 (*Cg*), 119.45 (*Ch*), 39.59 (C*d* & C*e*). **FTIR:** ν_{max}/cm^{-1} 3309 (NH), 1611 (CO), 1564 (imid. ring). m/z (LC ESI-MS) 265 $[M+H]^+$. Elem. Anal. Calc. (%) ($C_{12}H_{13}ClN_4O$): C, 54.45; H, 4.95; N, 21.17 %; Found: C, 53.95; H, 4.89; N, 20.77 %

Synthesis of 1 - [2 - (1*H* - imidazol - 4 - yl)ethyl] - 3 - (tert-butyl)urea (**2.8**)

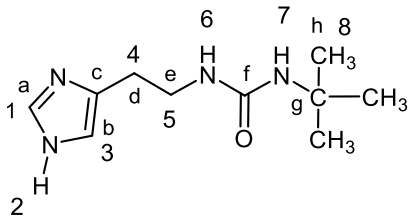

2.8

At 40 °C, histamine (1.10 g, 9.9 mmol) was dissolved in anhydrous chloroform (120 ml). Subsequently, a solution of *tert*-butyl isocyanate (1.96 g, 9.9 mmol) in anhydrous chloroform (10 ml) was slowly added *via* the dropping funnel over the course of 2 hours. The solution mixture was then heated to reflux for further 18 hours. The resulting white precipitate was filtered under reduced pressure, washed with chloroform (3 x 50 ml) and

dried under vacuum for three hours to yield the pure product as a white powder (1.79 g, 8.5 mmol, 86%). **^{1}H NMR:** δ_H (400 MHz; DMSO-d_6; Me_4Si) 11.82 (1 H, br s, *H2*), 7.49 (1 H, s, *H1*), 6.73 (1 H, s, *H3*), 5.66 (1 H, br s, *H6*), 5.61 (1 H, t, *J* 5.6, *H7*), 3.16 (2 H, q, *H5*), 2.54 (2 H, t, *J* 7.1, *H4*), 1.18 (9 H, s, *H8*). **^{13}C {^{1}H} NMR:** δ_C {^{1}H} (101 MHz; DMSO) 157.78 (*Cf*), 134.97 (*Ca & Cb*), 49.36 (*Cg*), 40.08 (*Cd & Ce*), 29.76 (*Ch)*. **FTIR:** ν_{max}/cm^{-1} 3348 (NH), 1648 (CO), 1559 (imid. ring)**.** m/z (ESI-MS) 212.3 $[M+2H]^{2+}$. Elem. Anal. Calc. (%) $C_{10}H_{18}N_4O$: C, 57.12; H, 8.63; N, 26.64%; Found: C, 57.08; H, 8.59; N, 26.59%

2.4.3 Crystallographic Data:

Single crystal crystallographic analysis were performed on a Bruker Photon D8 Venture diffractometer (ImuS microsource, λMoKα, λ = 0.71073 Å) equipped with a Cryostream (Oxford Cryosystems) open-flow nitrogen cryostat, at 120 K. The data collection and refinement was kindly carried out by Dr Dmitry S. Yufit.

Crystals of compound **2.1** were grown in nitromethane by slow evaporation of the solvent.

Crystal data for **2.1**, $C_{10}H_{18}N_4O$, M = 210.28, colourless plate, 0.02 x 0.02 x 0.2 mm^3, monoclinic, space group $P2_1/c$, a = 11.1384(4), b = 5.6178(3), c = 17.6812(5) Å, α = 90.00, β = 94.171(3), γ = 90.00°, V = 1103.44(7) Å^3, Z = 4, D_c = 1.266 g/cm^3, F_{000} = 456, MoKα radiation, λ = 0.71073 Å, T = 120(2)K, $2\vartheta_{max}$ = 56.0º, 12467 reflections collected, 2672 unique (R_{int} = 0.0488). Final *GooF* = 1.027, *R1* = 0.0427, *wR2* = 0.0896, *R* indices based on 2672 reflections with I >2σ (I) (refinement on F^2), 208 parameters, 0 restraints. Lp and absorption corrections applied, μ = 0.086 mm^{-1}.

Crystals of compound **2.4** were grown from nitromethane by slow evaporation of the solvent.

Crystal data for **2.4**, $C_{13}H_{16}N_4O.CH_3NO_2$, M = 305.34, colourless plate, 0.02 x 0.02 x 0.2 mm^3, orthorhombic, space group $Pca2_1$, a = 12.3460(3), b = 13.9709(3), c = 9.1894(2)Å, α = 90.00, β = 90.00, γ = 90.00°, V = 1585.03(6) Å^3, Z = 4, D_c = 1.280 g/cm^3, F_{000} = 648, MoKα radiation, λ = 0.71073 Å, T = 120(2)K, $2\vartheta_{max}$ = 55.98º, 21748 reflections collected,

3835 unique (R_{int} = 0.0578). Final *GooF* = 1.028, *R1* = 0.0476, *wR2* = 0.0976, *R* indices based on 3835 reflections with I >2σ (I) (refinement on F^2), 201 parameters, 1 restraints. Lp and absorption corrections applied, μ = 0.093mm^{-1}.

Crystals of compound **2.6** were grown from methanol by slow evaporation of the solvent.

Crystal data for **2.6**, $C_{16}H_{22}N_4O$, *M* = 286.38, colourless block, 0.02 x 0.02 x 0.2 mm^3, orthorhombic, space group $P2_12_12_1$, *a* = 8.2251(2), *b* = 9.7345(2), *c* = 18.8588(4) Å α = 90.00, β = 90.00, γ = 90.00°, *V* = 1509.97(6) Å^3, *Z* = 4, D_c = 1.260 g/cm^3, F_{000} = 616, MoKα radiation, λ = 0.71073 Å, *T* = 120(2)K, $2\vartheta_{max}$ = 56.0º, 29162 reflections collected, 2085 unique (R_{int} = 0.0871). Final *GooF* = 1.036, *R1* = 0.0384, *wR2* = 0.0864, *R* indices based on 2085 reflections with I >2σ (I) (refinement on F^2), 203 parameters, 0 restraints. Lp and absorption corrections applied, μ = 0.082 mm^{-1}.

Crystals of compound **2.7** were grown from methanol by slow evaporation of the solvent.

Crystal data for **2.7**, $C_{12}H_{13}ClN_4O$, *M* = 264.71, colourless block, 0.02 x 0.02 x 0.2 mm^3, monoclinic, space group $P2_1$, *a* = 9.6232(4), *b* = 4.8410(2), *c* = 13.9243(5) Å, α = 90.00, β = 109.642(3), γ = 90.00°, *V* = 610.93(4) Å^3, *Z* = 2, D_c = 1.439 g/cm^3, F_{000} = 276, MoKα radiation, λ = 0.71073 Å, *T* = 120(2)K, $2\vartheta_{max}$ = 144.9º, 6974 reflections collected, 2231 unique (R_{int} = 0.0708). Final *GooF* = 1.058, *R1* = 0.0519, *wR2* = 0.1128, *R* indices based on 2231 reflections with I >2σ (I) (refinement on F^2), 215 parameters, 1 restraints. Lp and absorption corrections applied, μ = 2.725 mm^{-1}.

Crystals of compound **2.9** were grown in methanol by slow evaporation of the solvent.

Crystal data for **2.9**, $C_{72}H_{78}Cl_6CoN_{24}O_6 \cdot 2NO_3 \cdot CH_3OH$, *M* = 1803.28, pale pink plate, 0.22 x 0.18 x 0.14 mm^3, triclinic, space group $P\overline{1}$, *a* = 13.2050(12), *b* = 13.2170(12), *c* = 13.3182(12) Å, α = 73.249(2), β = 74.350(2), γ = 73.579(3)°, *V* = 2089.7(3) Å^3, *Z* = 1, D_c = 1.433 g/cm^3, F_{000} = 935, MoKα radiation, λ = 0.71073 Å, *T* = 120(2)K, $2\vartheta_{max}$ = 53.0º, 35618 reflections collected, 8658 unique (R_{int} = 0.0638). Final *GooF* = 1.029, *R1* = 0.1001, *wR2*

= 0.2544, *R* indices based on 8658 reflections with I >2σ (I) (refinement on F^2), 525 parameters, 5 restraints. Lp and absorption corrections applied, μ = 0.474 mm^{-1}.

Crystals of compound **2.10** were grown in methanol by slow evaporation of the solvent.

Crystal data for **2.10**, $C_{72}H_{78}Cl_6NiN_{24}O_6.2NO_3.2CH_3OH$, *M* = 1835.10, pale green plate, 0.26 x 0.11 x 0.11 mm^3, triclinic, space group $P\overline{1}$, *a* = 13.2143(9), *b* = 13.2247(9), *c* = 13.2483(9) Å, α = 73.531(3), β = 73.859(3), γ = 73.568(2)°, *V* = 2079.7(2) $Å^3$, *Z* = 1, D_c = 1.465 g/cm^3, F_{000} = 954, MoKα radiation, λ = 0.71073 Å, *T* = 120 K, $2\vartheta_{max}$ = 54.0º, 28147 reflections collected, 9012 unique (R_{int} = 0.0769). Final *GooF* = 1.037, *R1* = 0.0964, *wR2* = 0.2191, *R* indices based on 9012 reflections with I >2σ (I) (refinement on F^2), 542 parameters, 67 restraints. Lp and absorption corrections applied, μ = 0.505 mm^{-1}.

Crystals of compound **2.11** were grown in methanol by slow evaporation of the solvent.

Crystal data for **2.11**, $C_{72}H_{78}Cl_6CoN_{24}O_6.2Cl$, *M* = 1718.11, pale pink plate, 0.42 x 0.33 x 0.21 mm^3, trigonal, space group $R\overline{3}$, *a* = 15.7778(6), *b* = 15.7778(6), *c* = 28.7892(11) Å, α = 90, β = 90, γ = 120, *V* = 6206.6(4) $Å^3$, *Z* = 3, D_c = 1.379 g/cm^3, F_{000} = 2667, MoKα radiation, λ = 0.71073 Å, *T* = 270K, $2\vartheta_{max}$ = 55.0º, 48744 reflections collected, 3179 unique (R_{int} = 0.0545). Final *GooF* = 1.095, *R1* = 0.0691, *wR2* = 0.1914, *R* indices based on 3179 reflections with I >2σ (I) (refinement on F^2), 160 parameters, 10 restraints. Lp and absorption corrections applied, μ = 0.531 mm^{-1}.

2.5 References

(1) Molina, P.; Tárraga, A.; Otón, F. *Org. Biomol. Chem.* **2012**, *10* (9), 1711–1724.

(2) Legrand, Y.-M.; Michau, M.; van der Lee, A.; Barboiu, M. *CrystEngComm* **2008**, *10* (5), 490–492.

(3) Leduc, Y.; Michau, M.; Gilles, A.; Gence, V.; Legrand, Y. M.; Vanderlee, A.; Tingry, S.; Barboiu, M. *Angew. Chemie - Int. Ed.* **2011**, *50*, 11366–11372.

(4) Hoque, M. N.; Manna, U.; Das, G. *Polyhedron* **2016**, *119*, 307–316.

(5) Kurzepa, M.; Dobrowolski, J. C.; Mazurek, A. P. *J. Mol. Struct.* **2001**, *565–566*, 107–113.

(6) Yamanaka, M. *J. Incl. Phenom. Macrocycl. Chem.* **2013**, *77*, 33–48.

(7) Piepenbrock, M.-O. M.; Clarke, N.; Steed, J. W. *Soft Matter* **2011**, *7* (6), 2412.

(8) Steed, J. W. *Chem. Soc. Rev.* **2010**, *39* (10), 3686–3699.

(9) Lloyd, G. O.; Piepenbrock, M.-O. M.; Foster, J. A.; Clarke, N.; Steed, J. W. *Soft Matter* **2011**, *8* (1), 204–216.

(10) James, S. J.; Perrin, A.; Jones, C. D.; Yufit, D. S.; Steed, J. W. *Chem. Commun.* **2014**, *50* (85), 12851–12854.

(11) Dawn, A.; Andrew, K. S.; Yufit, D. S.; Hong, Y.; Reddy, J. P.; Jones, C. D.; Aguilar, J. A.; Steed, J. W. *Cryst. Growth Des.* **2015**, *15*, 4591–4599.

(12) James, S. J.; Perrin, A.; Jones, C. D.; Yufit, D. S.; Steed, J. W. *Chem. Commun.* **2014**, *50* (85), 12851–12854.

(13) Chandran, S. K.; Nath, N. K.; Cherukuvada, S.; Nangia, A. *J. Mol. Struct.* **2010**, *968* (1–3), 99–107.

(14) Kennedy, S. R.; Jones, C. D.; Yufit, D. S.; Nicholson, C. E.; Cooper, S. J.; Steed, J. W. *CrystEngComm* **2018**, *20* (10), 1390–1398.

(15) Kundu, T.; Chowdhury, A. D.; De, D.; Mobin, S. M.; Puranik, V. G.; Datta, A.; Lahiri, G. K. *Dalton Trans.* **2012**, *41* (15), 4484–4496.

(16) Kumari, N.; Jha, S.; Bhattacharya, S. *J. Org. Chem.* **2011**, *76* (20), 8215–8222.

(17) Cametti, M.; Rissanen, K. *Chem. Commun.* **2009**, No. 20, 2809–2829.

(18) No Title http://supramolecular.org.

(19) Thordarson, P. *Chem. Soc. Rev.* **2011**, *40*, 1305–1323.

(20) Goswami, S.; Chakrabarty, R. *Eur. J. Chem.* **2011**, *2* (3), 410–415.

(21) Bhosale, S. V.; Kalyankar, M. B.; Langford, S. *J. Org. Lett.* **2009**, *11*, 5418–5421.

(22) Mashraqui, S. H.; Betkar, R.; Chandiraramani, M.; Quinonero, D.; Frontera, A.

Tetrahedron Lett. **2010**, *51*, 596–599.

(23) Camiolo, S.; Gale, P. A.; Hursthouse, M. B.; Light, M. E. *Org. Biomol. Chem.* **2003**, *1*, 741–744.

(24) Sheldrick, G. . *Acta Crystallogr. Sect. A* **2008**, *64*, 112.

(25) Dolomanov, O. V.; Bourhis, L. J.; Gildea, R. J.; Howard, J. A. K.; Puschmann, H. *J. Appl. Cryst* **2009**, *42*, 339.

(26) Palatinus, L.; Chapuis, G. *J. Appl. Crystallogr.* **2007**, *40*, 786.

Chapter 3

Gelation studies of silver(I) complexes of imidazole derived urea compounds

3.1 Background and Project Aims

3.1.1 Introduction to supramolecular gels: Definition, formation and characterisation.

Gels have been used widely in a number of products, such as hair gel, lubricants, adhesives, soaps, cosmetics and medical implants.[1] These gels are constructed through the immobilisation of a liquid component by an entangled network that arises from cross-linking of the polymers. The widespread applications of gels are mainly due to their unique properties in that they are 'solid-like' and hence can support their own weight while exhibiting 'liquid-like' behaviour that allows them to be moulded, printed and injected as required.[2]

By IUPAC[3] definition, a gel can be defined as "a colloidal network that is expanded throughout its whole volume by a fluid". Gels can be formed from different types of solvent, such as water, organic solvents and ionic liquid and are termed as hydrogel,[4] organogel[5] and ionogel[6] accordingly.

Cross-linking bonds in covalent polymeric gels are generally very stable and not reversible which can limit the reusability and versatility of the gel. As a result there is growing interest in gels formed from 'low molecular weight gelators' (LMWGs).[7] This type of gelator is made up of small molecules that self-assemble through non-covalent interactions such as hydrogen bonds, π-π stacking, van der Waals, charge-transfer and coordination interactions and solvophobic effects. The ease of disrupting the weak non-covalent interactions gives LMWGs many advantages over traditional polymeric gels such as thermoreversibility, stimuli response[8–10] and self-healing.[11,12] On account of the dynamic nature of the noncovalent interaction, a broader range of potential application in areas such as catalysis,[13] soft electronics, drug delivery and as crystal growth media[14] can be explored.

To form LMWGs, the gelator molecules are often briefly heated in particular solvents or a mixture of solvents until all the solids are completely dissolved and form a clear solution. During the cooling process, the gelator molecules undergo supramolecular assembly to form three-dimensional nano- or microstructures that immobilise the solvents thus giving rise to a stable gel.[15] The first step to identify the formation of a gel is usually done by the popular inversion test, in which a gel is said to form if it can withstand its own weight and does not fall under gravity. However, the limitation of this test is it is highly dependent on container size and composition.[16] Furthermore, in the identification of weak and partial gels, this method might give false results particularly if applied to viscous liquids, suspensions and strongly adhered solids.

The formation of supramolecular gels is driven by the noncovalent interactions that connect the gelator molecules. However, the dynamic nature of these interactions has imparted difficulties in the characterisation of the supramolecular gels. There are various methods and techniques that can be employed to characterise supramolecular gels such as spectroscopic, X-ray, microscopic, thermal analysis, rheology as well as computational methods.[17] Combination of all these techniques provide an insight on the self-assembled fibrillar networks (SAFINs) at molecular and bulk levels.

For supramolecular gels, rheology provides useful information on the structures of the assemblies (their size or cross-linking density), about their dynamics, and even about their self-assembly mechanisms. Rheology[18] is a study of deformation and flow of matter under the influence of an applied stress. In a typical rheology experiment, the gel sample is placed in between two plates where a given oscillatory stress is applied onto one of the plates. This applied stress then induced movement of the other plate, which is translated to an in and out-of-phase component. The two important parameters measured in a typical rheology experiment is G', elastic storage modulus and G", elastic loss modulus. G' represents the elastic or solid-like properties of a gel, while G" represents the viscous or liquid-like properties of a gel. These parameters can be measured as a function of the applied oscillation strain, stress or frequency.[19]

In typical rheology experiment, the value of G' is kept invariant with frequency up to a yield stress and a sample is identified as a gel when the value of G' exceed G" value at least an order of magnitude.[20] A yield stress point is a point where gel state is changed

to sol state; a state where the solid will start to flow. Above the yield stress point, the decreasing value of G' indicates the breakage of the network of the gel. The structure of a gel can be modelled mathematically from the behaviour, concentration dependence and magnitude of the moduli (G' and G").[21]

X-ray diffraction is also a very useful approach, at least indirectly, to characterise the supramolecular gel. For instance, single crystal X-ray diffraction can be performed to get information on the packing of the supramolecular networks particularly the nonconvalent interactions such as hydrogen bond, π-π stacking, CH···π interaction and halogen bond that drive the formation of supramolecular gel, although the technique is limited by questions over the relevance of single crystal studies to the gel state. Another scattering technique, small-angle neutron scattering (SANS) can also be performed to investigate the structure of various substances at a mesoscopic scale ranging from 1 to 1000 nm. In other words, this experiment provides the information about the structure on the nanoscale involved in the networks of a supramolecular gel. Small angle X-ray scattering (SAXS) and wide angle X-ray scattering (WAXS) are also useful to characterise the shape, size and distribution of the supramolecular gel fibres. These two techniques are similar to each other, except the diffraction maxima are observed at different angles. In SAXS, scattering intensity is measured at scattering angles (2θ) close to 0°, while in WAXS, the scattering angles is larger. From the key parameters obtained, the packing mode in the structure can be derived.[22–24]

However, in cases where a single crystal structure cannot be obtained, computational approaches can be used to simulate molecular and atomic behaviour based on the fundamental description of atomic and molecular orbitals. The simulation can be done using different methods such as *ab initio* quantum mechanics, molecular mechanics or combination of both (semiempirical methods). The modelling is crucial to investigate the interaction between the gelators, which can aid in the understanding of the gelation mechanism.[25–28] Using high-level energy minimisation and molecular dynamic calculations, possible modes of aggregation in gel network can be identified.

3.1.2 Urea-based gelators

Hydrogen bonding is a versatile and directional interaction that is commonly utilized in the synthesis of self-assembled supramolecular structures.[29–31] There are quite a number of reports on organo- and hydrogelators that contain the urea functionality and it is the hydrogen bonding interactions between urea groups that give rise to gelation behaviour.[32–34] Each urea moiety can potentially form two strong and directional hydrogen bonds. Although supramolecular gel formation is normally associated with bisurea compounds, there are a few examples in which mono(urea) compounds are also able to form supramolecular gels. Recently, an L-histidine-derived mono(urea), **3.1** has been reported to form a stable gel in nitromethane with a concentration between 0.5 and 2.0% (w/v) and partial gels in ethyl acetate as low as 0.3% (w/v).[35] The morphology of the xerogel obtained from the nitromethane gel comprises of long entangled ribbon-like fibres that exhibit a helical twist and are homochiral consistent with the use of non-racemic L-histidine derivatives. Addition of cobalt(II) chloride to the gelator molecules at a very low metal:gelator molar ratio (1:0.05) in acetonitrile does not disrupt the gel formation, however when the ratio of metal gelator was increased (1:0.2), only a partial gel was formed. It is, therefore, suggested that the complexation of the metal to the N atom of the imidazole unit has interrupted the imidazole NH···N interactions that are also implicated in gel formation. In addition, the counter anions present also are likely to form hydrogen bonds to the urea group, further disrupting gelation.

a)

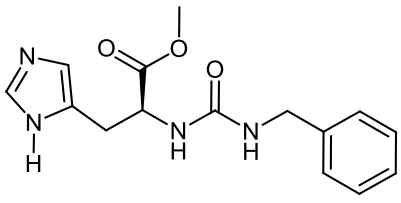

3.1

b)

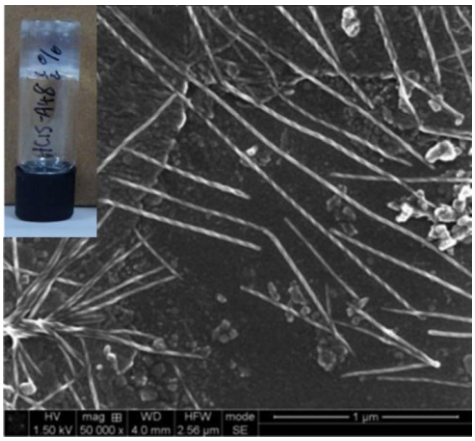

Figure 3.1 a) Molecular structure of gelator **3.1** b) SEM images of xerogels of compound **3.1** obtained from gels of nitromethane (0.5% w/v) (reproduced with permission from reference 34)

In another example, a series of mono(urea)-based gelators (**3.2**-**3.4**), linked into dimers by a supramolecular hydrogen bond motif instead of by a covalent bond has been reported to form gels in 1,2,4-trichlorobenzene, 1,2-dibromoethane, 1,2-dichlorobenzene and 1,3-dichlorobenzene.[36] These monoureas were synthesised from the facile reaction between 5-aminosalicylic acid with appropriate isocyanate. The crystal structure of gelator **3.2** exhibits a head to head carboxylic dimer arrangement through strong intramolecular OH···H hydrogen bond that allows them to behave as a pseudobis(urea) (Figure 3.2). The formation of the dimer is also supported by ES^+ mass spectrum of **3.2**. The authors suggested that the gelation behaviour of these gelators are driven by the urea α-tape motif, similar to gelation behaviour of bis(urea) compounds.

a)

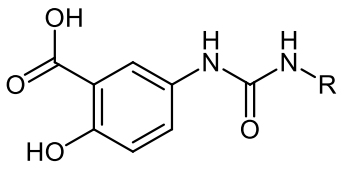

3.2, R = *n*Bu
3.3, R = *n*Pr
3.4, R = Et

b)

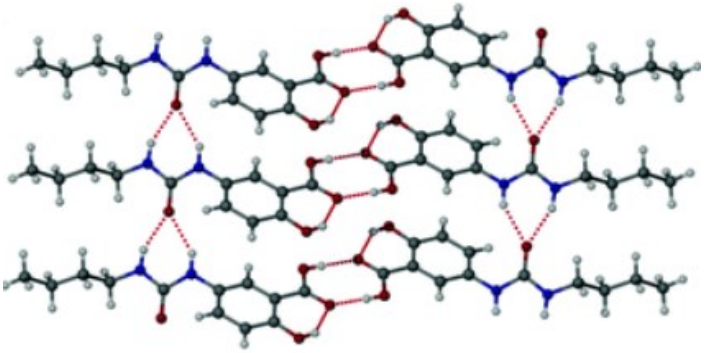

Figure 3.2 a) Molecular structure of gelators **3.2**-**3.4** b) short NH···O interactions in the gelator **3.2**. Selected hydrogen bonding distances (Å) for compound **3.2**, O···O 2.629(6); N···O 2.797(7), 2.816(7) (reproduced with permission from reference 35).

Bis(urea) compounds are known to form supramolecular gels in various organic solvents due to the formation of the urea α-tape network. Recently, supramolecular gels have been applied as pharmaceutical growth media in which the crystallisation of important drugs in the gel phase could control the polymorphism and crystal habit. Kumari and co-workers have designed a series of bis(urea) gelators, type A and type B gelators containing long chain alkyl (**3.5**-**3.8**) and perfluoroalkyl substituents (**3.9**-**3.10**), respectively.[37] The fluorinated analogues could be potentially used as crystal growth media for some fluorinated drugs such as lansoprazole and fluoxetine. Type A gelators gelled cyclohexanone, 1-butanol, toluene and xylene while type B gelators gelled more

polar solvents namely DMSO, DMF and cyclopentanone at lower concentration, in the range of 0.2 to 10% wt giving a transparent gel that is suitable to be used as crystal growth media.

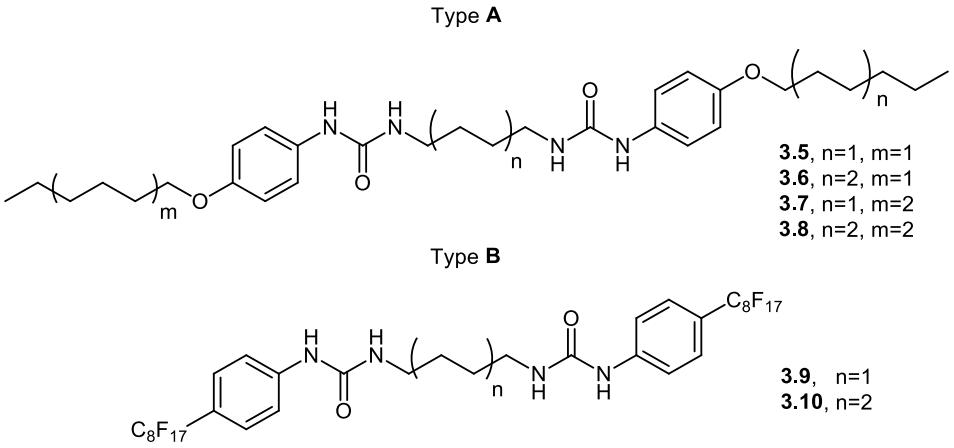

Gelator **3.10** also formed a gel in perfluorodecalin at 10% wt to give opaque and thermoreversible gel. SEM micrographs of type B gelators shows that these gels are composed of more amorphous, less linear and cylindrical fibres ranging from 50 to 130 nm in diameter in contrast to type A gels, which are more crystalline with ribbon-like fibres of diameter ranging from 0.9 to 5µm (Figure 3.3). The xerogel fibres also exhibit high aspect ratio that contributes to the highly entangled fibrous networks. To probe the supramolecular structure of the gel, small angle neutron scattering (SANS) analysis has been performed. The SANS results demonstrated that for type B gelators, the gel structure is retained up to its T_{gel} of the material (80 °C) but fully collapse to spherical aggregates after exceeding the T_{gel}. SANS data also revealed that the elastic properties of the fluorinated gels are not affected by the metastable nature when the gel was initially formed.

a) b)

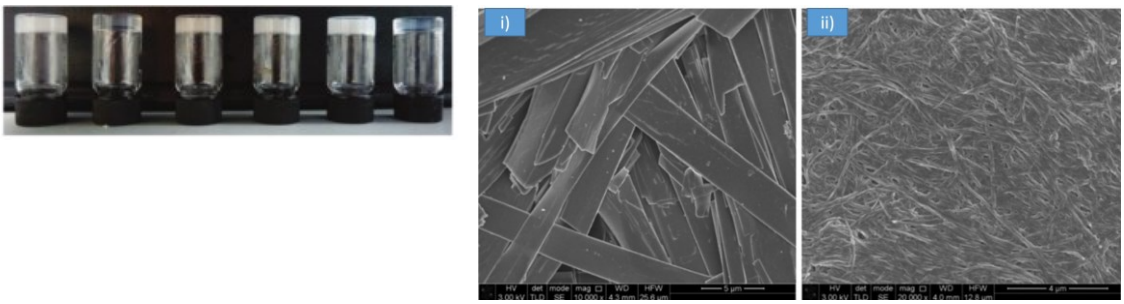

Figure 3.3 a) Gels in DMSO at the minimum gel concentration (mcg): from left to right **3.8** (3 wt%), **3.10** (0.5 wt%), **3.6** (7 wt%), **3.7** (2.5 wt%), **3.5** (3 wt%) and **3.9** (0.2 wt%). The fluorinated gels have a markedly more transparent appearance. b) SEM micrographs of ethanol xerogels (i) large, flat ribbons of compound **3.8** typical of compound of type A, (ii) narrow cylindrical fibres of **3.10** typical of compounds of type B (reproduced with permission from reference 36).

Wezenberg and co-workers has described a new set of photoresponsive bis(urea) LMWGs based on an overcrowded alkene switch.[38] Under UV irradiation, *trans* bisureas **3.11**-**3.13** can be transformed into *cis* isomers as illustrated in Figure 3.4a. Supergelator **3.12** with a hexyl chain can form a gel in aromatic hydrocarbons at very low concentration of 0.4 mg/mL and upon UV irradiation (312 nm) the gel collapses to sol form. The process is reversible by irradiating the solution under UV light of 365 nm for 15 minutes. From the X-ray structures of gelator **3.12** (Figure 3.4b), it was observed that the *trans* form allows intermolecular hydrogen bonding interaction that is necessary for gel formation, whereas in the *cis* form, this interaction is interrupted and thus results in gel dissolution. These photoresponsive gels are potentially useful in applications such as self-healing and drug delivery.

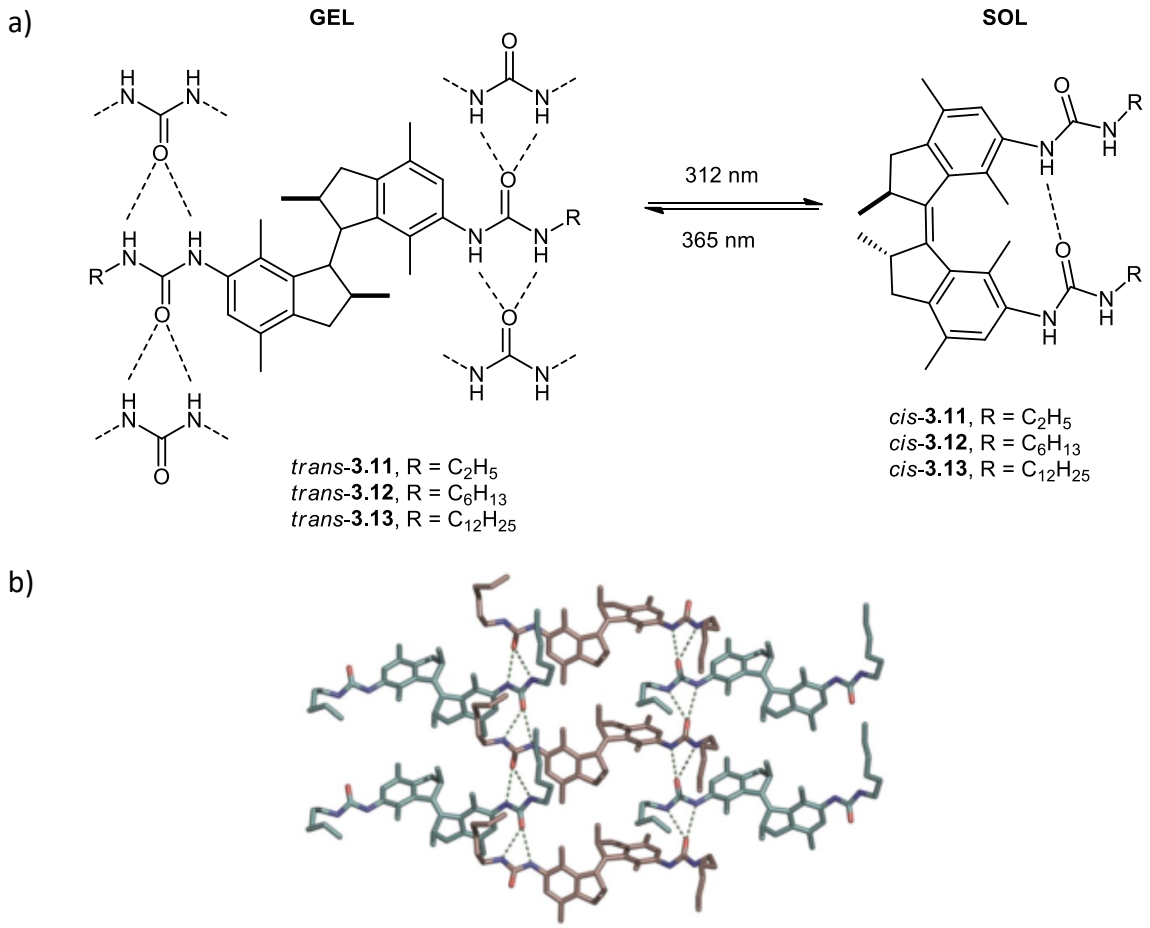

Figure 3.4 a) Photoisomerization behaviour and predicted urea hydrogen bonding pattern of *trans* and *cis* bis-urea LMWGs **3.11**-**3.13** b) crystal packing showing the intermolecular hydrogen bond arrays. The (R,R)-enantiomer is shown in blue, the (S,S)-enantiomer in pink. Hydrogen atoms have been omitted in the packing for clarity. Selected hydrogen bond distances (˚A): N···O: 3.053(2), 2.996(2), 2.940(2), 2.936(2) (reproduced with permission from reference 37).

Sensing of organophosphorus (OP) based nerve agents, DMPP and GD using tris(urea) gels, **3.14** has been reported recently by Hiscock and co-workers.[33] The sensing process is functioned via the suppression of the sol-gel phase change in toluene. Upon the addition of 0.1 mL (100 equivalents of the gelator) of DMPP, the gel was not formed at all, clearly showing a clear ON-OFF response in the absence versus presence of DMMP. Interestingly, the addition of another stimulant, GD, trigger the gel-sol phase change at a much lower concentration of 0.01 mL than DMMP, possibly due to the higher degree of polarity that strengthen the hydrogen bonding interactions. Both of the nerve agents contain phosphonate ion that binds to the urea groups resulting in inhibition of gel formation.

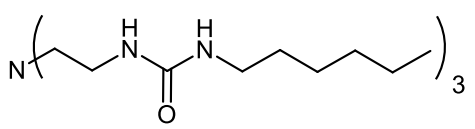

3.14

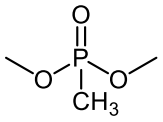

DMMP

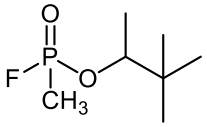

Soman (GD)

3.1.3 Metal-containing gels

In recent years, there has been increasing interest in metal-containing low molecular weight gelators (LMWGs). Incorporation of the metal centres into gelators allows the design of materials that possess unique properties such as magnetism, colour, catalytic activity and redox behavior.[39] In addition, the network structure in metallogels is cross-linked by metal-ligand interactions, which can be tuned easily by changing the transition metal ions. There are two ways of preparing metallogels; first, the metal complexes of organic gelators are pre-formed before being tested for gelation with a variety of solvents. Alternatively, a coordination-induced in situ gelation approach can be adopted.[15,40–42] To form metallogels, gelators having metal binding sites such as pyridine, bipyridine, terpyridines and carboxylates are used as the core of the metallogelators.[43–45] One example is the use of pyridine-pyrazole based gelator **3.15** that gels in the presence of silver salts in water.[46] The three- dimensional network interconnected by the ligand and the silver ions provides an excellent platform for the growth of silver nanoparticles. As the nanoparticles exclusively attach onto the gel fibres, they play a significant role in strengthening and stabilising the gel network. These silver nanoparticles have shown excellent catalytic activity in the reduction of 4-nitrophenol and methylene blue with the presence of sodium borohydride.

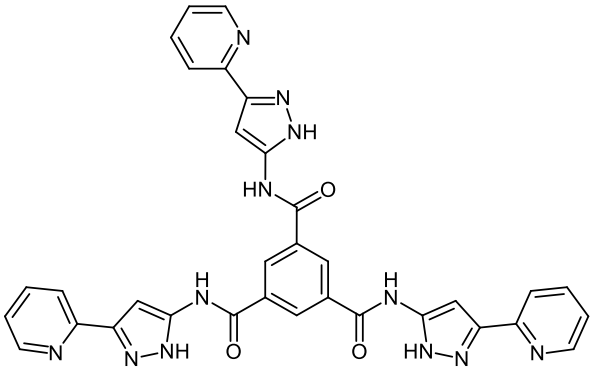

3.15

Another series of bipyridine ligands, **3.16** to **3.18** that gel silver salts in DMSO:H_2O has been reported by Tatikonda and co-workers.[47] Of all the three ligands, only **3.17** and **3.18** gel silver nitrate.

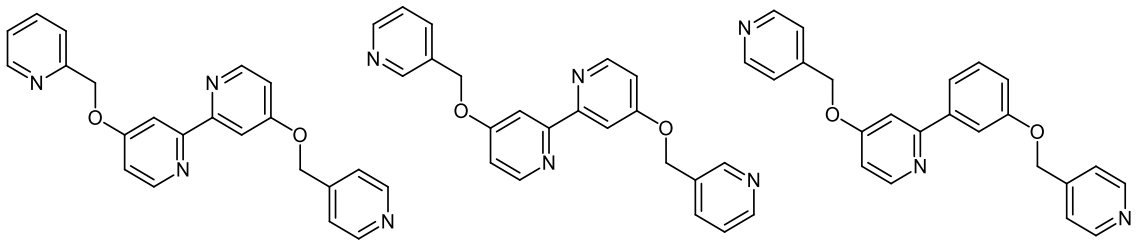

3.16 **3.17** **3.18**

From SEM micrographs, it has been shown that silver nitrate complex of **3.17** gels form fine and film-like fibres in contrast to silver nitrate complex of **3.18** that forms thicker nanofibrillar networks (Figure 3.5). When silver salts with different counter ions namely PF_6^-, BF_4^-, ClO_4^-, OAc^- and $CF_3SO_3^-$ were used, only ligand **3.17** formed stable metallogel, while ligand **3.18** formed less stable gels that collapsed after few hours at room temperature.

a) b)

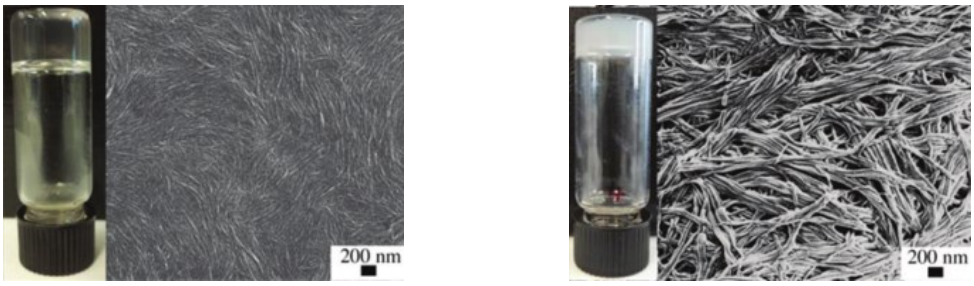

Figure 3.5 SEM micrograph of a) [**3.17**·$AgNO_3$] gel in DMSO: H_2O (8:2) b) [**3.18**·$AgNO_3$] gel in DMSO: H_2O (8:2) (reproduced with permission from reference 46).

Apart from normal heating and ultrasonication, metallogels can also be formed under solvothermal conditions exemplified by the work of Knichal and co-workers in 2015.[48] They reported a metallogel that formed from the reaction of 5-allenyl-1,3-benzenedicarboxylic acid, **3.19** and lead(II) acetate trihydrate. This metallogel only formed when the reaction mixture was heated to 100 °C for 72 hours with critical gelation concentration of 1%. The SEM micrographs of the gel show two most prominent

morphological features of the gel, the rod-like fibres of 40 nm in diameter and a large agglomeration of worm-like morphology of varying diameter ranging from 40-160 nm.

a) b) c)

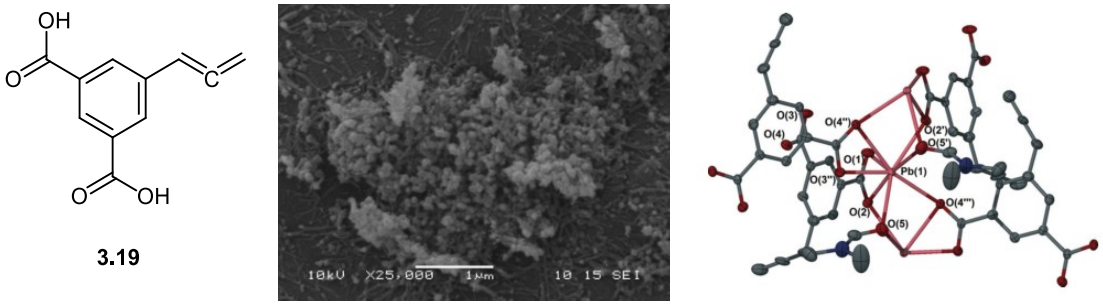

Figure 3.6 a) Molecular structure of ligand **3.19** b) SEM micrograph of [**3.19**(PbOAc)] gel c) Coordination environment about the Pb(II) atom in **3.19**. Thermal ellipsoids are shown with 50% probability (reproduced with permission from reference 48).

Recently, Wang and co-workers have prepared a ligand that comprises two metal coordination sites, the carboxyl part of tryptophan and the pyridyl segment, **3.20**.[49] This compound does not gel on its own but formed a pink and opaque metallohydrogel immediately after the addition of Co^{2+} ions (as chloride, nitrate and acetate salts) at pH 7.0 to 8.0 without any heating or ultrasonication step. The metallohydrogel formed was robust, thermoreversible and able to show a rapid thixotropic response. SEM micrographs of the metallohydrogels show uniform nanofibrils with widths between 25 and 40 mm and several micrometers in length. The metal ligand ion coordination interaction also contributes to the entangled fibrous morphology of the gels. As suggested by the authors, this metallohydrogel could be potentially applied in the chiral recognition field, as it does not gel when a racemic mixture is used.

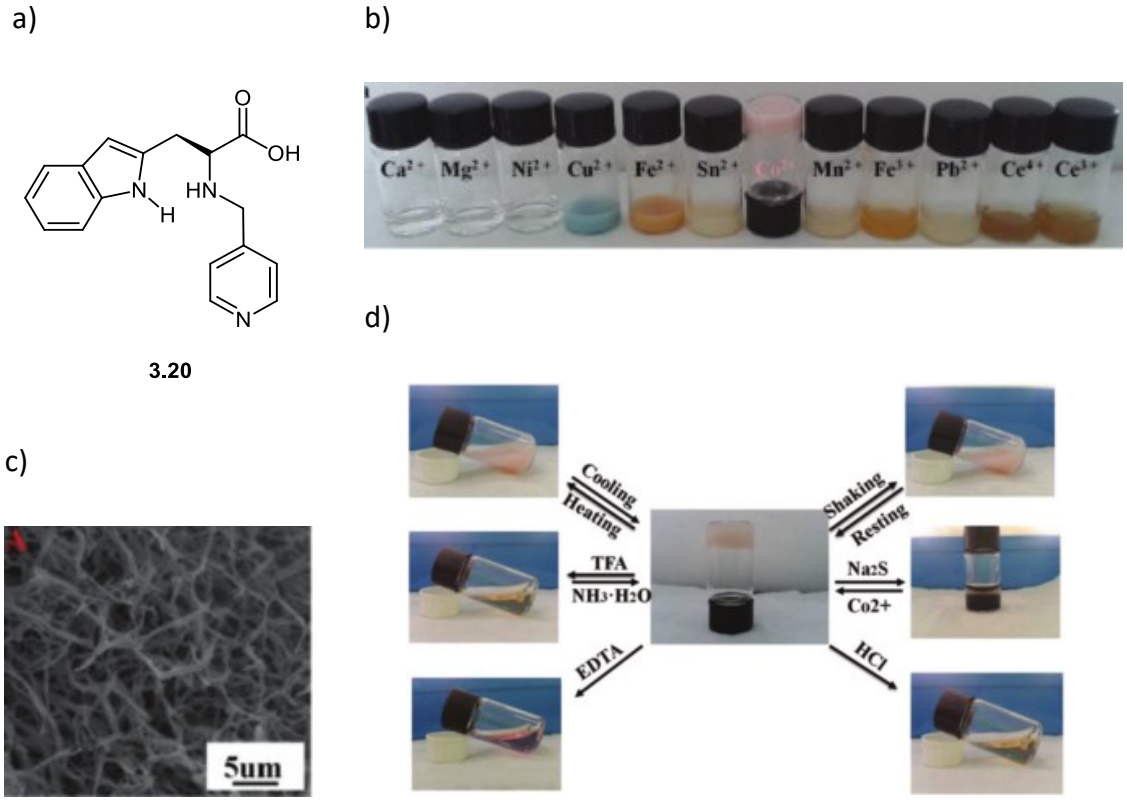

Figure 3.7 a) Molecular structure of **3.20** having tryptophan and pyridyl unit b) Gelation test screening of **3.20** with various transition metals c) SEM micrograph of **3.20**–Co metallohydrogel d) Gel–sol transitions of the **3.20**–Co metallohydrogel triggered by various stimuli (thermal, mechanical, pH, and chemical reaction) (reproduced with permission from reference 49).

Although most of reported works on metallogels employ one type of metal ion in their system, there are also some studies that incorporate two different metals as the structural part of their metallogelators.[50,51] Using compound **3.21**, that contains an o-hydroxynaphthaldehyde unit, Sun *et al*. investigated the role of various cations and anions in the formation of metallogels.[52] In DMSO solution of compound **3.21**, the addition of metal ions such as Fe^{3+}, Ag^{+}, Hg^{2+}, Cu^{2+}, Zn^{2+}, Ni^{2+}, Fe^{2+} and Al^{3+} as perchlorate salts did not induce the formation of a gel. However, upon the addition of sodium acetate to the DMSO solution of compound **3.21** results in instant gelation as shown in Figure 3b. The authors suggested that the anions plays a critical role in the gelation.

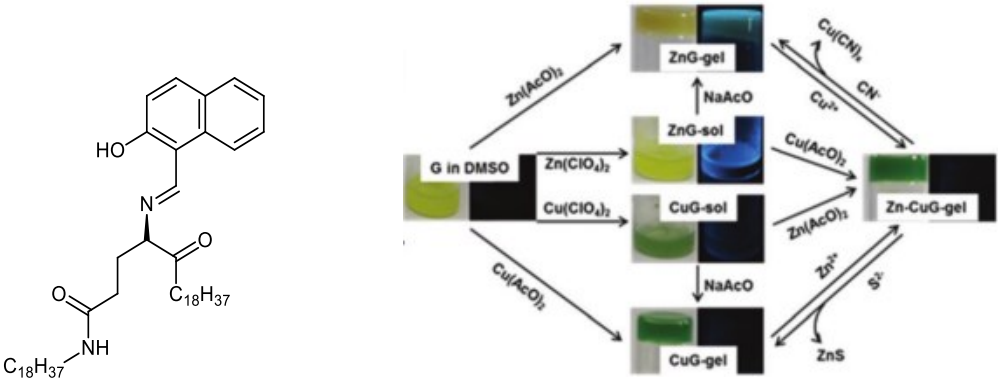

Figure 3.8 (a) Molecular structure of **3.21** and (b) photographs of G (**3.21**) (1%, in DMSO), metallogels Zn(**3.21**), Cu(**3.21**) and Zn-Cu(**3.21**) (1%, in DMSO, for Zn(**3.21**), **3.21**:Zn^{2+} = 1:1; for Cu(**3.21**), **3.21**:Cu^{2+} = 1:1; for Zn-Cu(**3.21**), **3.21**:Cu^{2+} :Zn^{2+} = 1 : 1 : 1) treated with different ions (G in the photograph is referred to **3.21**) (reproduced with permission from reference 52).

Different anions were compared and they reported that gels were only formed in the presence of these anions, SO_4^{2-}, HPO_4^{2-}, AcO^-, F^-, Cl^-, NO_3^-, HSO_4^- and NO_2^-, and remains as a solution with Br^-, I^-, SO_3^{2-}, HSO_3^-, S^{2-} and CN^- in agreement with the Hofmeister series (Figure 3.9). The Zn-Cu(**3.21**) complex can also act as a Cu^{2+} and CN^- controlled "OFF-ON-OFF" fluorescence switch due to the quenching of the fluorescence of Zn(**3.21**) complex upon the addition of Cu^{2+} ion.

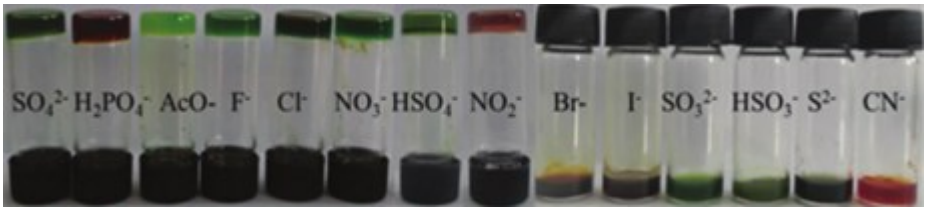

Figure 3.9 Photographs of solutions and gels from **3.21** (10 mg mL^{-1}) and $Cu(ClO_4)_2$ in DMSO in the presence of various anions. (**3.21**: anion:copper perchlorate = 1:1:1) (reproduced with permission from reference 52).

3.1.3 Project Aims

Previous reports have shown that the addition of a pyridyl group to the urea derivatives as a metal binding site can result in 'switch on' gelation because metal complexation removes competing urea-pyridyl hydrogen bonding interactions.[53] Silver(I) ions are known to bind nitrogen-containing ligands forming complexes with a linear geometry. The linear geometry of the silver(I) complexes would allow the self-assembly of the complexes to form extended one-dimensional linear polymeric structures for gel formation in appropriate solvents. With these in mind, we are interested in using imidazole urea compounds as discussed in Chapter 2 to produce metal-switched supramolecular gels based on the self-assembly of the urea functional group.[54] To date, there has been little published work on the use of a silver(I) to link two urea-based ligands to give a gel-forming bis(urea) motif by metal complexation, with the exception of one earlier report of a silver(I) coordinated mono urea based gel system.[55]

3.2 Results and discussion

3.2.1 Gel studies and morphology of the gel

The gelation test of ligands **2.1**, **2.2**, **2.3**, **2.4**, **2.5**, **2.6** and **2.7** were carried out in 14 organic solvents. About 10 mg of the ligands (2% w/v) were added into 2 mL vials containing organic solvents and were heated gently to dissolve the ligands. Then, the solution was sonicated. The solutions were allowed to cooled down to room temperature and the state was observed. At room temperature, all of the ligands are soluble in polar solvents such as methanol, ethanol, propanol and dimethyl sulphoxide. In solvents such as acetonitrile, THF, mixture of THF and water and nitomethane, all the ligands dissolved when the solution was heated briefly. However, none of the ligand formed gels in any of the solvents tested. The screening of the ligands in various solvents is summarised in Table 3.1.

Table 3.1 Gelation studies performed on ligands **2.1**, **2.2**, **2.3**, **2.4**, **2.5**, **2.6** and **2.7** (2% w/v) in common organic solvents.

Solvents	Ligands						
	2.1	**2.2**	**2.3**	**2.4**	**2.5**	**2.6**	**2.7**
Acetone	I	I	I	I	I	I	I
Acetonitrile	P	P	P	P	P	P	P
THF:H_2O (8:2)	P	P	P	P	P	P	P
THF:H_2O (7:3)	P	P	P	P	P	P	P
THF	P	P	P	P	P	P	P
Diethyl ether	I	I	I	I	I	I	I
Nitromethane	P	P	P	P	P	P	P
Hexane	I	I	I	I	I	I	I
Chloroform	I	I	I	I	I	I	I
Dichloromethane	I	I	I	I	I	I	I
Methanol	S	S	S	S	S	S	S
Ethanol	S	S	S	S	S	S	S
Propanol	S	S	S	S	S	S	S
DMSO	S	S	S	S	S	S	S

*P = precipitate, I = insoluble, S = solution,

In addition, the gelation screening of all the ligands was also performed in the presence of four different silver salts, namely i) silver tetrafluoroborate, silver perchlorate, silver hexafluorophosphate and silver nitrate in selected organic solvents, in which the ligands can be dissolved such as acetonitrile, THF:water (8:2), THF:water (7:3), THF, nitromethane, methanol, ethanol, propanol and DMSO. Samples were heated and sonicated briefly to ensure thorough mixing. Immediately after the heating and sonication process, the samples were cooled down to room temperature and the state of the samples are observed. The samples were kept in dark to protect them from light.

Interestingly, ligand **2.3**, which does not form any gels by itself is found to gel THF/water mixtures (7:3) with the addition of 0.5 to 1.0 equivalents of silver tetrafluoroborate, silver perchlorate and silver hexafluorophosphate. Other than this solution mixture, ligand **2.3** also formed gels in THF, THF:water (8:2), DMSO and acetonitrile (2% w/v). In every case, aggregates formed upon the addition of the silver salts (tetrafluoroborate, perchlorate and hexafluorophosphate) to the solution of ligand **2.3** and within a few hours after brief sonication, slightly opaque gels at the concentration of 2% (w/v) were formed that did not flow under tube inversion. In contrast, the addition of silver nitrate to ligand **2.3** results in the formation of a white precipitate instead of a gel (Figure 4.1). The gel formed was kept in the dark to avoid the formation of metallic silver particles. The gelation experiments on every ligand with different types of aqueous silver salts are tabulated in Table 3.2.

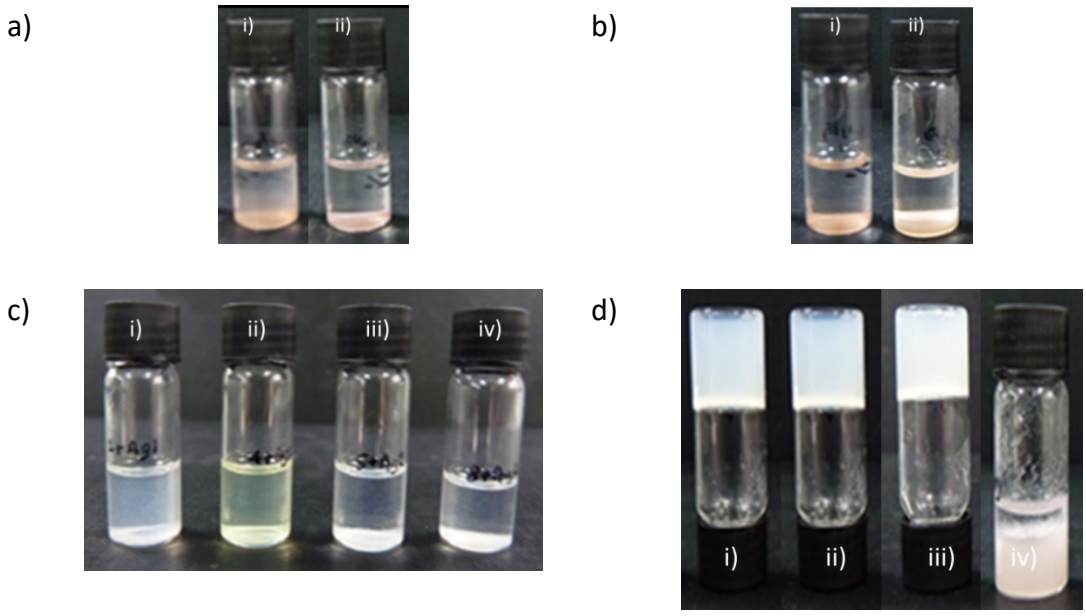

Figure 3.10 a) Precipitate from addition of i) $AgBF_4$ and ii) $AgNO_3$ to ligand **2.1** b) Precipitate from addition of i) $AgBF_4$ and ii) $AgNO_3$ to ligand **2.2** c) Precipitate from addition of $AgBF_4$ to ligand i) **2.4** ii) **2.5** iii) **2.6** iv) **2.7** d) Gel from addition of i) $AgBF_4$, ii) $AgPF_6$, iii) $AgClO_4$ to ligand **2.3** and precipitate from addition of d) $AgNO_3$ to ligand **2.3**.

Table 3.2 Gelation screening of all ligands (**2.1**-**2.7**) in the presence of i) silver tetrafluoroborate, ii) silver hexafluorophosphate, iii) silver perchlorate and iv) silver nitrate in selected organic solvents.

Solvents	Ligands																											
	2.1				**2.2**				**2.3**				**2.4**				**2.5**				**2.6**				**2.7**			
	i	ii	iii	iv	i	ii	iii	iv	i	ii	iii	iv	i	ii	iii	iv	i	ii	iii	iv	i	ii	iii	iv	i	ii	iii	iv
Acetonitrile	P	P	P	P	P	P	P	P	P	P	P	P	P	P	P	P	P	P	P	P	P	P	P	P	P	P	P	P
THF:H_2O (8:2)	P	P	P	P	P	P	P	P	G	G	G	P	P	P	P	P	P	P	P	P	P	P	P	P	P	P	P	P
THF:H_2O (7:3)	P	P	P	P	P	P	P	P	G	G	G	P	P	P	P	P	P	P	P	P	P	P	P	P	P	P	P	P
THF	P	P	P	P	P	P	P	P	G	G	G	P	P	P	P	P	P	P	P	P	P	P	P	P	P	P	P	P
Nitromethane	P	P	P	P	P	P	P	P	P	P	P	P	P	P	P	P	P	P	P	P	P	P	P	P	P	P	P	P
Methanol	P	P	P	P	P	P	P	P	P	P	P	P	P	P	P	P	P	P	P	P	P	P	P	P	P	P	P	P
Ethanol	P	P	P	P	P	P	P	P	P	P	P	P	P	P	P	P	P	P	P	P	P	P	P	P	P	P	P	P
Propanol	P	P	P	P	P	P	P	P	P	P	P	P	P	P	P	P	P	P	P	P	P	P	P	P	P	P	P	P
DMSO	P	P	P	P	P	P	P	P	G	G	G	P	P	P	P	P	P	P	P	P	P	P	P	P	P	P	P	P

** P = precipitate, S = solution, G = gel, i = silver tetrafluoroborate, ii = silver hexafluorophosphate, iii = silver perchlorate, iv = silver nitrate

These results indicate that the formation of the metallogels strongly depends on the types of counter anions of the silver salts. In comparison with tetrafluoroborate, perchlorate and hexafluorophosphate anions, which are weakly coordinating anions, nitrate anions are able to act as hydrogen bond acceptors with the NH group of the urea moiety which directly disrupt the formation of α-urea tape that is responsible for the gel formation as often observed in bis(urea)s systems.[54]

It is suggested that the dodecyl chains of ligand **2.3** also facilitate the formation of the fibrous networks due to the strong Van der Waals interactions[56] between them and solvophobic effects that allow them to form one directional alignment of gelator molecules.[55] In addition, it was also observed that ligand **2.3** forms a stable gel at 2:1 (ligand: metal) and 1:1 ratio with silver tetrafluoroborate, while at 1:2 ratio, a metastable gel is formed (Figure 3.2). Subsequent addition of silver tetrafluoroborate results in the formation of precipitate instead of a gel. Nevertheless, due to the poor solubility of the ligand-silver aggregates in the solvent mixture, the silver metallogels were not thermoreversible upon heating although they appear to be robust and homogeneous.[13,57]

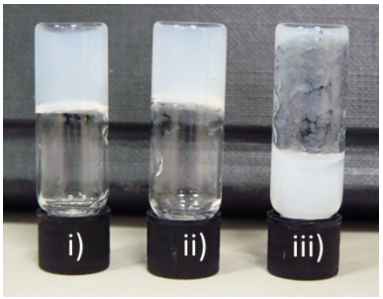

Figure 3.11 Gels of ligand **2.3** with a) 0.5 equivalent b) 1.0 equivalent c) 2.0 equivalent of AgBF4 in THF:H_2O 7:3 (v/v).

To seek insight on the arrangement of the gelator molecules which contributes to the gelation, gelation tests have also been performed on ligand **2.3** with copper(II) tetrafluoroborate, which will form complexes of square planar, square pyramidal or Jahn-Teller distorted octahedral geometry, in contrast with the linear geometry of the silver complexes. After the addition of copper(II) tetrafluoroborate to the ligand **2.3** solution in THF: H_2O (7:3), the colour of the solution changed from colourless to blue, indicating a reaction between the ligands and the metal ion. The mixture was then

heated and briefly sonicated to ensure thorough mixing and maximum interaction between the ligand and the metal salt. After a while, a blue precipitate formed in the solution and no gel was observed (Figure 3.3). This could be likely due to the 4-6 coordinate nature of the copper(II) ion that does not result in a geometry that allows the formation of α-urea tape hydrogen bonding motif that is responsible for the formation of the fibrous network in a gel. This result is also in agreement with the theory that in order to obtain fibrous aggregates for gels, linear or planar coordination of metal ions in the complex is necessary.[58] This result is comparable to the previous report on the imidazole urea hydrogel in which the presence of copper(II) nitrate significantly reduces its yield point.[59]

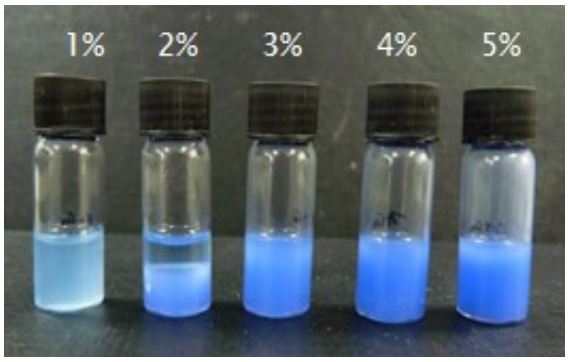

Figure 3.12 Precipitates formed upon addition of 0.25 equivalent copper(II) tetrafluoroborate to the solution of ligand **2.3** in THF: H_2O (7:3) (v/v).

To provide insights into the morphology of silver(I) metallogel of ligand **2.3**, a xerogel was prepared from slow evaporation of the gel samples and then coated with Platinum prior to the examination by scanning electron microscope (SEM). At 2 wt. %, the dried xerogel features elongated fibres forming an entangled fibrillar network along with a slightly twisted fibril (Figure 3.4a). By increasing the concentration of the sample up to 3 wt. %, helical left and right-handed fibres are observed (Figure 3.4b). Helical fibres are commonly observed in xerogels derived from ribbon-like fibres of chiral, racemic and achiral gelators as exemplified in previous work.[35,59]

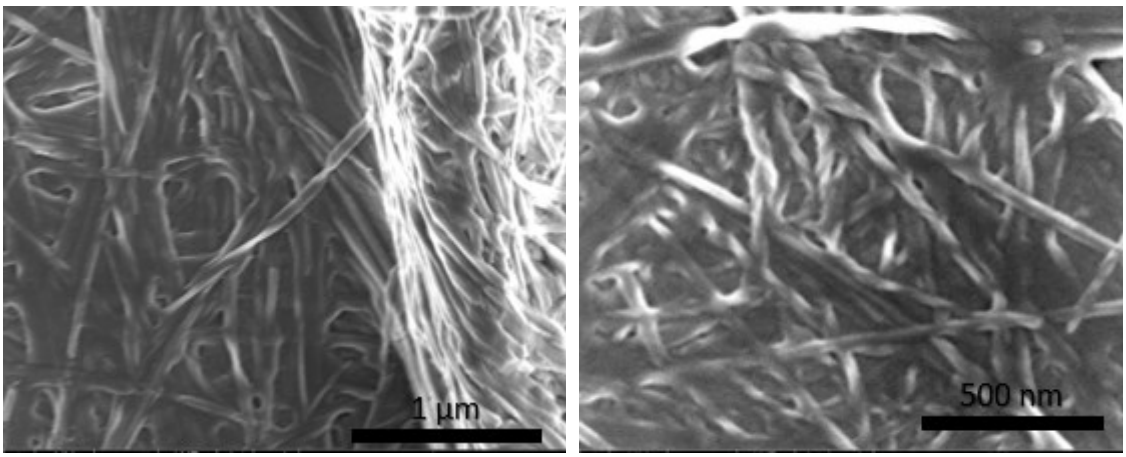

Figure 3.13 SEM micrographs of a dried a) 2 wt. % xerogel b) 3 wt. %. Both gels were prepared thermally with sonication.

3.2.2 Rheological properties of the metallogel

The rheological properties of silver(I) metallogel of ligand **2.3** confirm that the material shows the characteristics of a true gel. A stress sweep at 2 wt. % (w/v) shows that at low stresses, storage modulus *G*' is, at least, one order of magnitude greater than loss modulus *G*", typically observed for gel-like materials (Figure 4.5).[42] To elucidate the mechanical properties in terms of gel morphology, the values of initial modulus *G*° of the initial plateau and the values of the stress at which the gel breaks (yield point) are used. From the stress sweep rheometry data, the yield stress reaches a pronounced maximum at 0.5 equivalent of silver tetrafluoroborate. On addition of excess silver salts in the case of 1.0 and 2.0 equivalent of silver tetrafluoroborate, the yield point drops dramatically from 211 to 119 Pa and 112 Pa, respectively (Figure 4.6). The significant decrease in the yield point is possibly due to the increase in the number of anions that competes in the hydrogen bonding of the ureas.[57]

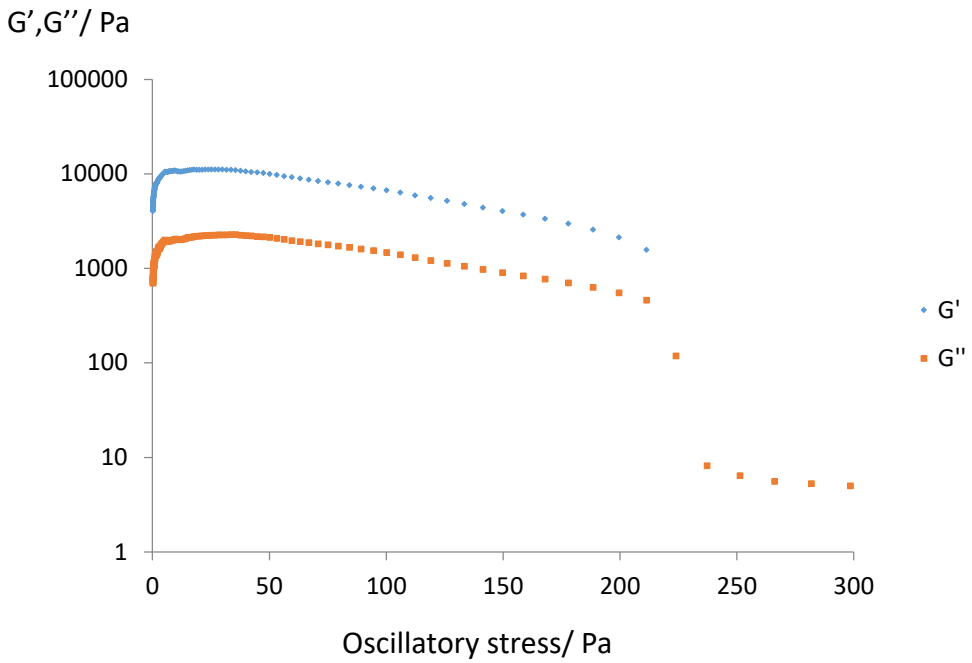

Figure 3.14 Stress sweep rheometry data for a 2 wt. % silver metallogel of compound **2.3** with 0.5 equivalent of silver tetrafluoroborate.

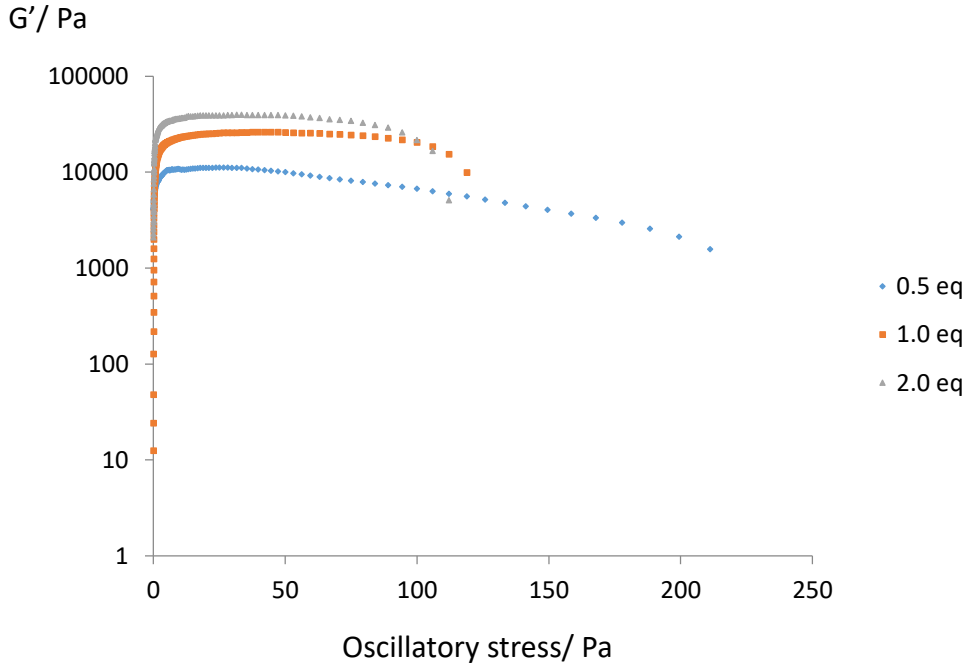

Figure 3.15 Stress sweep rheometry data for a 2 wt. % silver metallogel of compound **2.3** with 0.5, 1 and 2 equivalents of silver tetrafluoroborate.

As proved by rheometry data, 2:1 ratio is the optimum ratio for gelation, consistent with the 2-coordinate nature of Ag(I) and monodentate nature of ligand **2.3.** We, therefore, propose a linear binding between two imidazole urea ligands of type **2.3** with one silver ion to form one-dimensional sheet that was linked by conventional urea α-tape

hydrogen bonding motif, which is typically seen in bis(urea)s systems (Scheme 3.1).[60,61] The rheometry data is also comparable to the previous report on the silver(I) metallogel of pyridyl urea.[57] The binding stoichiometry of the ligand and silver ion can also be examined through a Job plot, however due to the formation of a gel in DMSO solvent, the experiment could not be carried out.

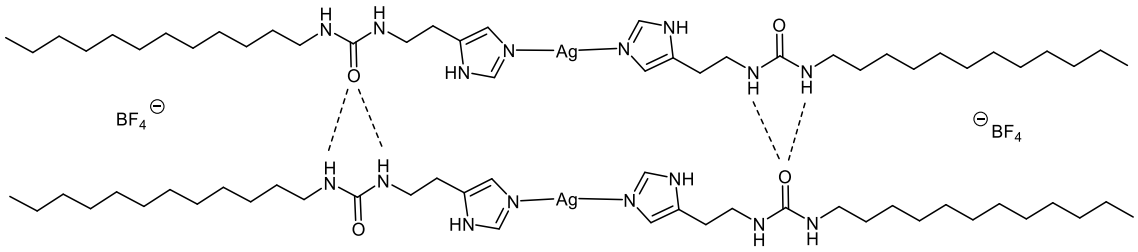

Scheme 3.1 Proposed binding mode of ligand **2.3** to silver ion linked by conventional urea tape hydrogen bonding motif.

On the other hand, the strength of gel is also influenced by the counter anions of the silver salts. The metallogel of silver tetrafluoroborate forms stronger gels compared to that of silver hexafluorophosphate and silver perchlorate; almost four times the yield stress (Figure 3.16).

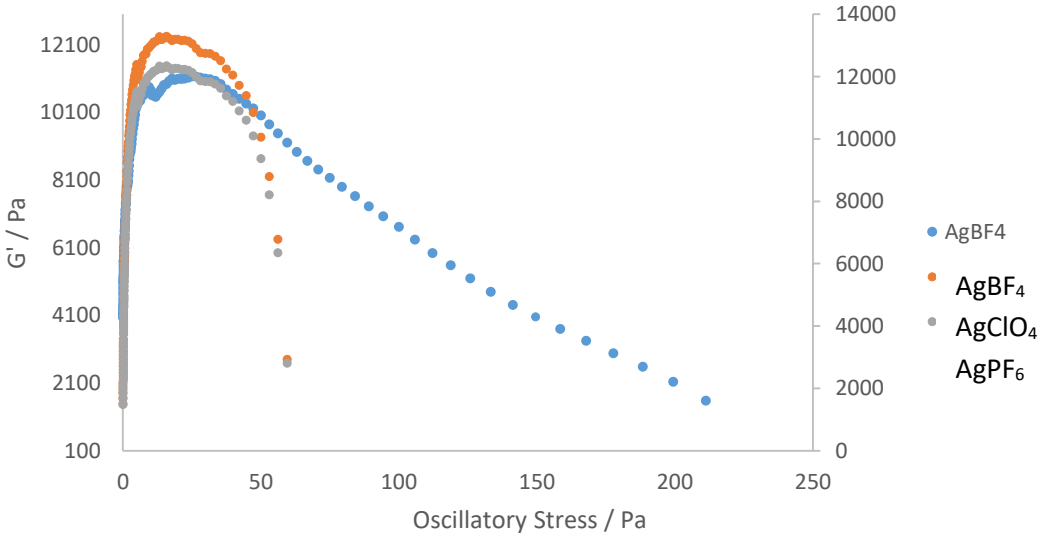

Figure 3.16 Stress sweep rheometry data for a 2 wt. % silver metallogel of compound **2.3** hexafluorophosphate ($AgPF_6$) and silver tetrafluoroborate ($AgBF_4$).

3.2.3 Stability of the gel and formation of silver nanoparticle

The most stable metallogel of ligand **2.3** formed from silver tetrafluoroborate, which proved to be stable at least over a period of weeks when stored in the dark. However, on an open bench, a brown colouration due to the formation of silver nanoparticles by photoreduction is observed when the gels are exposed to sunlight. It was anticipated that irradiating the metallogel under UV light at 365 nm would enhance the formation of silver nanoparticles.[13,57] It is found that gels with 0.5 equivalent of silver tetrafluoroborate show colour changes from colourless to brown after being irradiated under UV light and a more intense brown colouration is observed as the irradiation time was increased from 1 hour to 24 hours (Figure 3.17). At regular intervals, a sample of the gel (0.15 mg, 100 mM) was dissolved in 2 ml DMSO and the UV/Vis spectrum of the solution was recorded. A typical surface plasmon of spherical silver nanoparticle characterised by a band that develops at around 430 nm was observed after about 3 hours (Figure 3.18).[13,57]

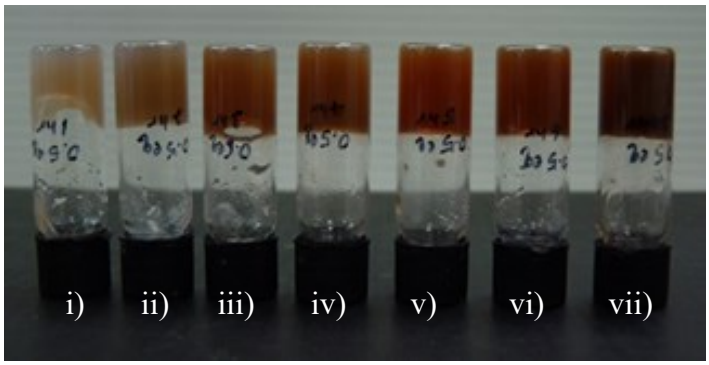

Figure 3.17 Gels of ligand **2.3** with 0.5 equivalent of $AgBF_4$ in THF : H_2O 7 : 3 (v/v) after i) 1 h, ii) 2 h, iii) 3 h, iv) 4 h, v) 5 h, vi) 6 h and vii) 24 h under UV 365 nm.

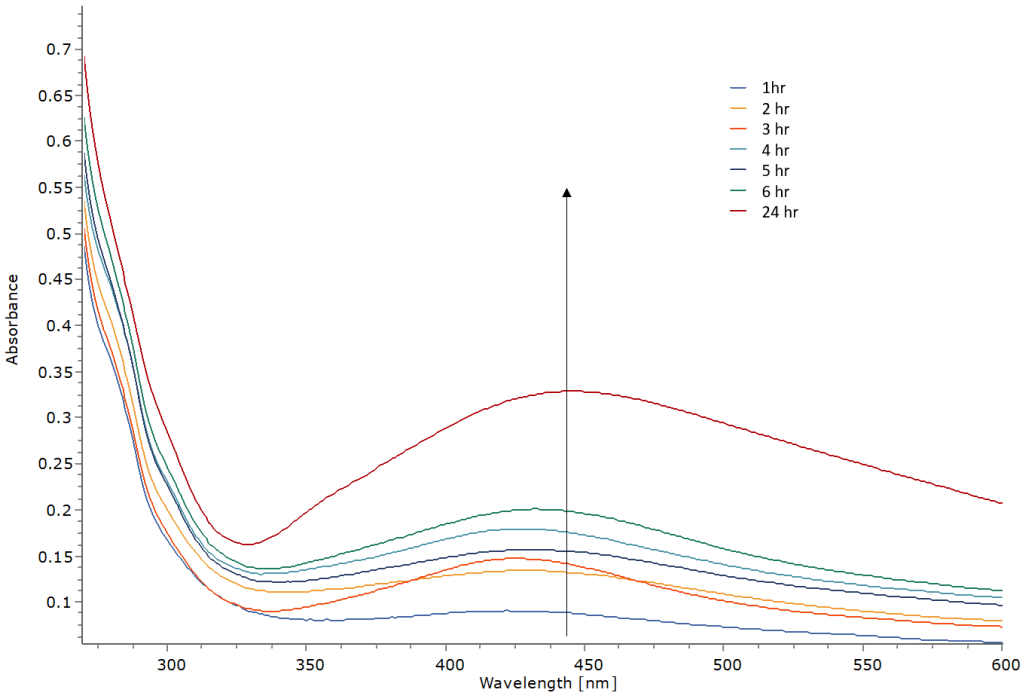

Figure 3.18 UV/vis spectrum of gels of ligand **2.3** with 0.5 equivalent of $AgBF_4$ in THF:H_2O (7:3) (v/v) after 1 h, 2 h, 3 h, 4 h, 5 h, 6 h and 24 h.

In contrast, metallogels of ligand **2.3** with 1 and 2 equivalents of silver tetrafluoroborate form a grey-coloured gel and grey precipitate, respectively after UV light irradiation (Figure 3.19a). These colour changes indicated the formation of bulk silver[57] due to the excess silver ions that are present in the solution. Apart from that, in the case of gel with 1 equivalent of silver tetrafluoroborate, the formation of bulk silver has significantly weakened the gel (Figure 3.19b).

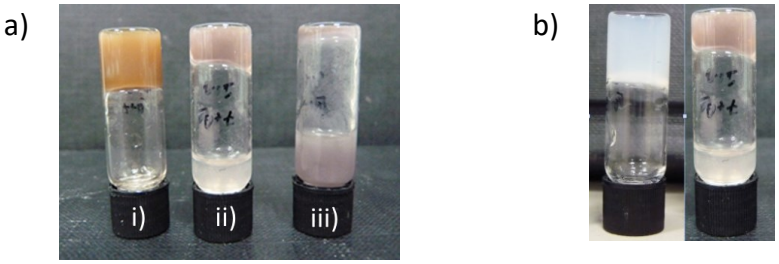

Figure 3.19 a) Metallogels of ligand **2.3** with i) 0.5 equivalent ii) 1.0 equivalent iii) 2.0 equivalent of $AgBF_4$ in THF:H_2O (7:3) (v/v) after 24 h under UV light 365 nm b)Weakening of the gel with 1 equivalent of silver tetrafluoroborate after 24 h under UV light 365 nm (left: fresh gel, right: gel after 24 hours).

The presence of the silver nanoparticles was further confirmed by Transmission Electron Microscopy (TEM) after being irradiated under UV light for 24 hours in the solvent mixtures of THF:water (7:3). A drop of the gel solution was applied to a copper grid, dried under vacuum and mounted on JEOL 2100F FEG TEM instrument at 200 kV operating voltage.

For the silver metallogel of **2.3** with 0.5 equivalent of $AgBF_4$, there was a small amount of nanoparticles formed, exclusively distributed in the gel fibre (Figure 3.20), which possibly contributes to the strength of the gel. In this sample, only small amount of nanoparticles formed as most of the silver ions coordinate to ligand **2.3**. Irradiation under UV light also collapsed the fibrous nature of the gel and results in the leaching of some of the nanoparticles into the solution. However, when 2 equivalents of $AgBF_4$ were used, more spherical-shaped silver nanoparticle were observed (Figure 3.21)

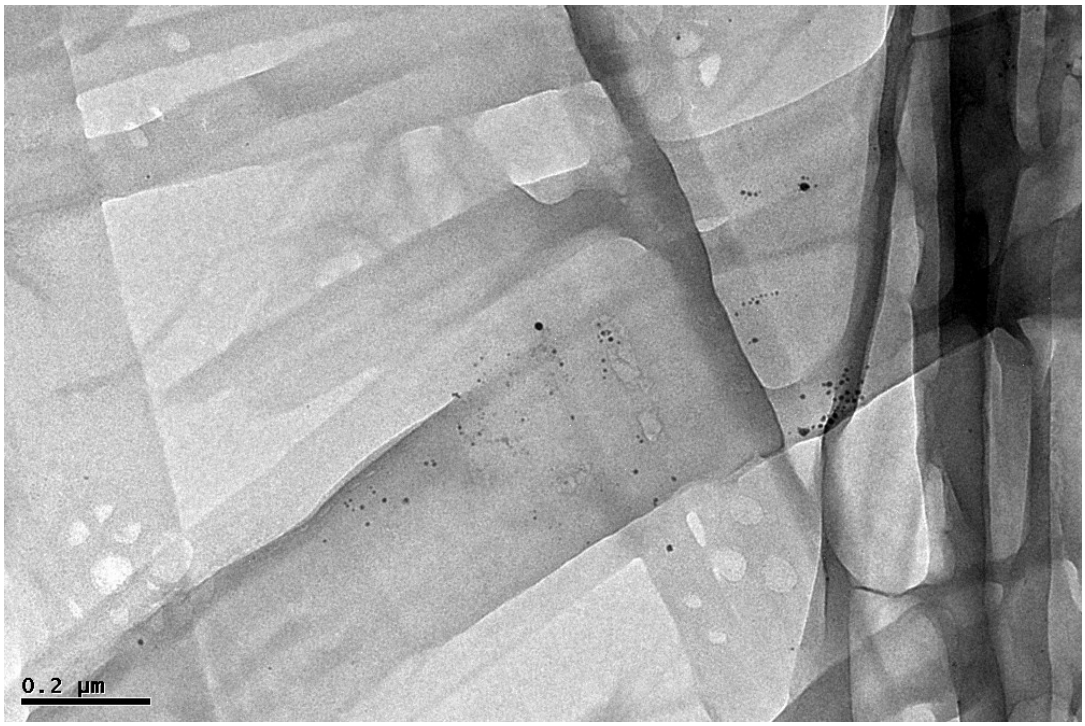

Figure 3.20 TEM images of the metallogel of **2.3** with 0.5 equivalent of $AgBF_4$.

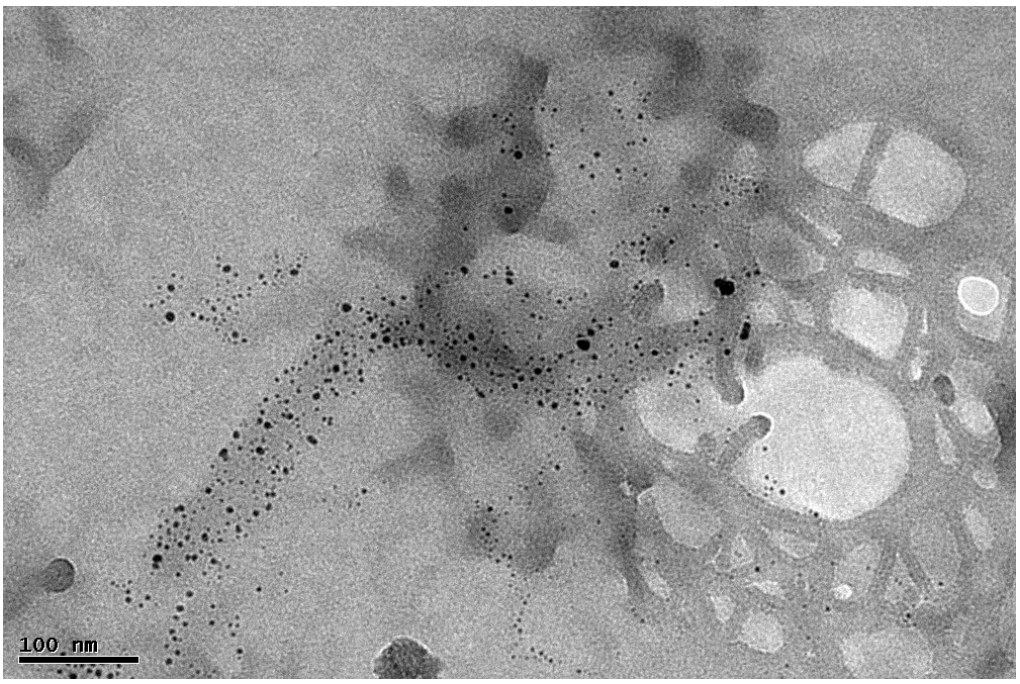

Figure 3.21 TEM images of the metallogel of **2.3** with 2 equivalents of $AgBF_4$.

On the other hand, the use of 3 equivalents of $AgBF_4$ not only promotes the growth of larger particles with a diameter in the range of 278 to 411 nm, but also promotes the growth of silver nanorods with a uniform diameter of 88 nm and a length varying from 200 to 264 nm (Figure 3.22) although the size of the observed particles may not represent the bulk materials. The bigger size particle results from the agglomeration of the spherical nanoparticles.

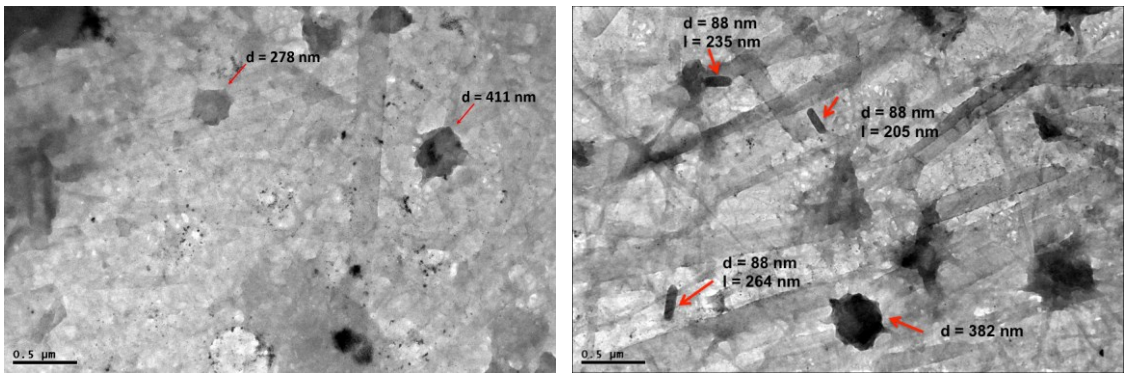

Figure 3.22 TEM images of the metallogel of **2.3** with 3 equivalents of $AgBF_4$.

An energy dispersive X-ray (EDX) spectrum of the metallogel confirmed the presence of silver metal in all the metallogel samples (Figure 3.23). These findings are consistent with the previous report in which the silver ion serves as the gelling agent and as the nanoparticle growth substrate.[13]

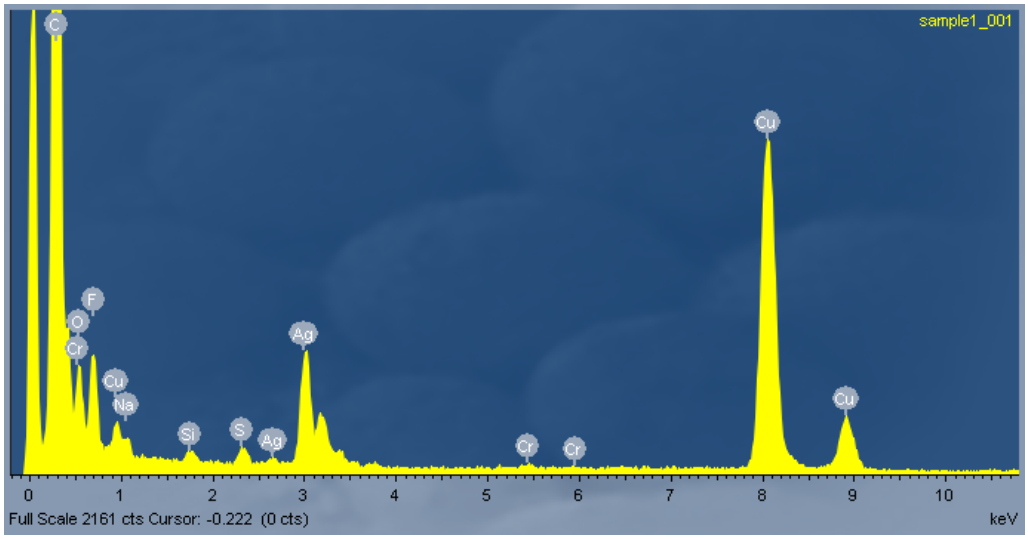

Figure 3.23 An EDX spectrum of metallogel of **2.3** with 0.5 equivalent of $AgBF_4$.

3.2.4 Anion addition studies

Several reports have shown that the structural properties of supramolecular gels are tuneable by the interactions between anion stimuli and the gelator molecule.[14,54,62] Urea is a common hydrogen bond donor group that can interact with anions and has found application in a variety anion sensors.[63–65] Anions are able to form hydrogen bonds with the NH group of urea (Figure 3.24 a), which directly causes the disruption of the urea tape, responsible for the formation of a fibrous network (Figure 3.24 b).[40,62]

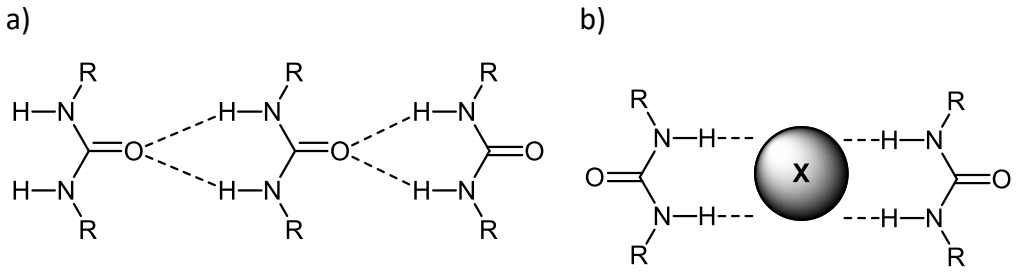

Figure 3.24 a) urea tape hydrogen bonding motif which gives rise to long fibres b) hydrogen bonding motif adopted by ureas in the presence of anions resulting in breakdown of gel fibres.

Addition of more than one equivalent of chloride ions disrupts the silver(I) gel of ligand **2.3** and transformed it into sols with white precipitates (Figure 3.25). When anions such as chloride, bromide and nitrate ion were added to the gel, the anion reacts with the silver metal to form AgCl, AgBr and $AgNO_3$ that precipitates and disrupts the gel network that is driven by the urea tape and argentophilic interactions.[66] The addition of fluoride ion also results in the formation of a precipitate in the gel, possibly AgF. Conversely, the addition of 10 equivalents of benzoate and lactate does not compromise the integrity of the gel probably due to the larger size that limits them from penetrating the gel network.

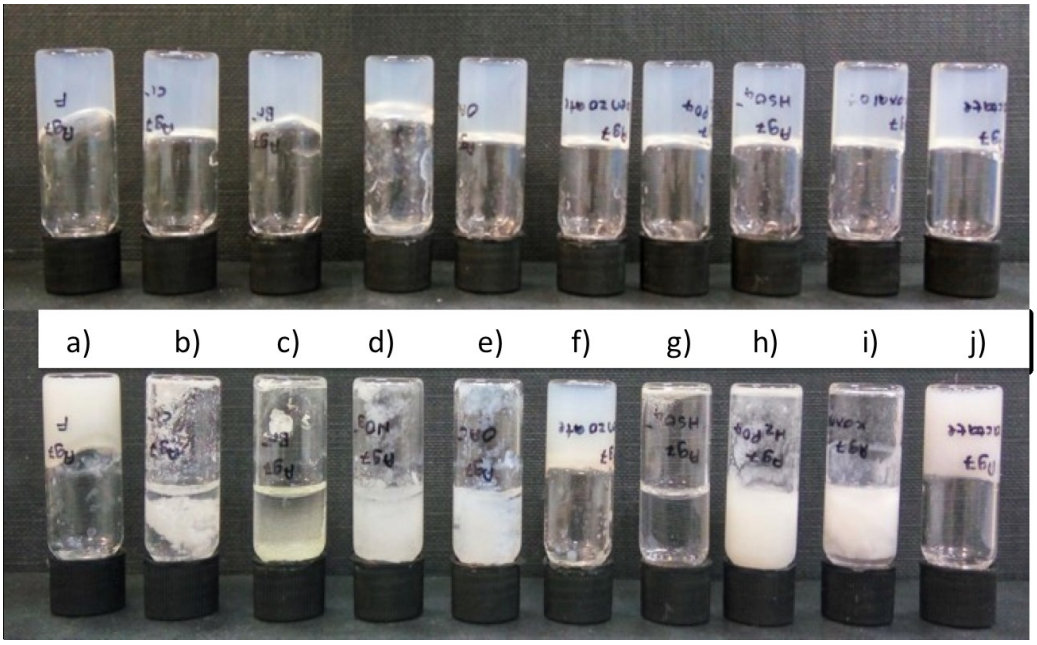

Figure 3.25 Top: Silver(I) gels of **2.3** before the addition of 10 equivalents of anions as tetrabutylammonium salts Bottom: Silver(I) gels of **2.3** after the addition of 10 equivalents of a) F^- b) Cl^- c) Br^- d) NO_3^- e) acetate f) benzoate g) HSO_4^- h) $H_2PO_4^-$ i) oxalate j) lactate in THF:H_2O (7:3) (v/v).

3.3 Summary

To conclude, silver(I) metallogels have been obtained by the combination of silver ion and an organic component bearing imidazole head group containing urea derivatives. Both the coordination structure of the complex and the symmetrical hydrogen bonding between complexes as well as the van der Waals interaction of the hydrophobic alkyl chains are thought to be responsible for the gelation.

3.4 Experimental

All solvents used in the synthesis and purification were of analytical reagent grade. Anhydrous solvents were prepared on an SPS solvent purification system. Commercial reagents were used as supplied, without further purification.

3.4.1 Synthesis

The synthesis procedure for all the ligands used in this chapter has been detailed in the experimental section of Chapter 2.

3.4.2 Gel Preparation and Rheology

Oscillatory rheometry measurements were performed at 0.1-1000 Pa using a TA Instruments AR 2000 on a rough Peltier plate with a 25 mm rough plate geometry and 2.5 mm gap. Samples were prepared by dissolving 40 mg of compound **2.3** in a mixture of THF: H_2O 7:3 (v/v) (2 mL). A stock solution of $AgBF_4$,$AgClO_4$, $AgPF_6$ and $AgNO_3$ in 0.5 mL water was prepared so that 100 µL represents 1 equivalent of the silver salt with respect to the ligand. The silver solution was injected into the ligand solution and was thoroughly mixed by brief sonication in sealed 7 cm^3 vials. The solution mixtures then were poured into a 25 mm cylindrical glass mould on the Peltier plate and the gels were allowed to form and equilibrate 45 minutes prior to analysis. The materials were left to cool down at 10 °C using the rheometer inbuilt temperature control to minimize the evaporation of the material throughout the formation and analysis. Stress sweep experiments were performed with a constant frequency of 1 Hz.

3.4.3 Instrumentation and Analytical Measurements

SEM samples were prepared on silicon wafers, dried in the dark for 3 days prior to imaging, and coated with 2 nm of platinum using a Cressington 328 Ultra High Resolution EM Coating System. Using an FEI Helios NanoLab DualBeam microscope, the images were obtained in immersion mode, with beam settings of 1.5 kV and 0.17 nA.

TEM and EDX experiments were performed on a JEOL 2100F FEG TEM instruments at 200 kV operating voltage on samples dissolved in DMSO and applied to a copper grid. During the analysis, the temperature was maintained at -65 ^{o}C by cryo-cooling with liquid nitrogen, and monitored using a Gatan 900 SmartSet controller. UV/vis spectra were recorded on a Perkin Elmer UV Lambda 25 spectrometer in DMSO. Gels irradiation was performed using a 6 W hand held UV lamp at 365 nm.

3.5 References

(1) Osada, Y.; Kajiwara, K. *Gels Handbook: Applications*; Academic Press, 2001.

(2) Nishinari, K. *Prog. Colloid Polym. Sci.* **2009**, *136*, 87–94.

(3) Alemán, J.; Chadwick, A. V.; He, J.; Hess, M.; Horie, K.; Jones, G.; Kratochvíl, P.; Meisel, I.; Mita, I.; Moad, G.; Penczek, S.; Stepto, R. F. T. *Pure Appl. Chem* **2007**, *79*, 1801–1827.

(4) Estroff, L. A.; Hamilton, A. D. *Chem. Rev.* **2004**, *104*, 1201–1217.

(5) Terech, P.; Weiss, R. G. *Chem. Rev.* **1997**, *97*, 3133–3159.

(6) Le Bideau, J.; Viau, L.; Voux, A. *Chem. Soc. Rev.* **2011**, *40*, 907–925.

(7) Steed, J. W. *Chem. Commun.* **2011**, *47*, 1379–1383.

(8) Díaz Díaz, D.; Kühbeck, D.; Koopmans, R. J. *Chem. Soc. Rev.* **2011**, *40* (1), 427–448.

(9) Kawano, S. I.; Fujita, N.; Shinkai, S. *J. Am. Chem. Soc.* **2004**, *126* (28), 8592–8593.

(10) Ganta, S.; Chand, D. K. *Dalton Trans.* **2015**, *44*, 15181–15188.

(11) Yu, X.; Chen, L.; Zhang, M.; Yi, T. *Chem. Soc. Rev.* **2014**, *43* (15), 5346.

(12) Yan, L.; Li, G.; Ye, Z.; Tian, F.; Zhang, S. *Chem. Commun.* **2014**, *50* (94), 14839–14842.

(13) Lee, J. H. Y. H. Y.; Kang, S.; Lee, J. H. Y. H. Y.; Jung, J. H. *Soft Matter* **2012**, *8*, 6557–6563.

(14) Foster, J. A.; Piepenbrock, M.-O. M.; Lloyd, G. O.; Clarke, N.; Howard, J. A. K.; Steed, J. W. *Nat. Chem.* **2010**, *2* (12), 1037–1043.

(15) Tam, A. Y.-Y.; Yam, V. W.-W. *Chem. Soc. Rev.* **2013**, *42* (4), 1540.

(16) Raghavan, S. R.; Cipriano, B. H. *Molecular Gels*; Springer, 2006.

(17) Yu, G., Yan, X., Han, C., Huang, F. *Chem. Soc. Rev.* **2013**, *42*, 6697–6722.

(18) Mezger, T. G. *The Rheology Handbook*, 2nd Editio.; Wiiliam Andrew Publishing: Norwich N. Y., 2006.

(19) Piepenbrock, Marc-Oliver M.; Lloyd, Gareth O.; Clarke, Nigel; Steed, J. W. *Chem. Rev.* **2010**, *110*, 1960.

(20) Zhang, M.; Xu, D.; Yan, X.; Chen, J.; Dong, S.; Zheng, B.; Huang, F. *Angew. Chemie Int. Ed.* **2012**, *51*, 7011.

(21) Stanley, C. E.; Clarke, N.; Anderson, K. M.; Elder, J. A.; Lenthall, J. T.; Steed, J. W. *Chem. Commun.* **2006**, *1* (30), 3199–3201.

(22) Sutton, M. *C. R. Phys.* **2008**, *9*, 657.

(23) Hirst, A. R.; Smith, D. K.; Feiters, M. C.; Geurts, H. P. M. *Chem. Eur. J.* **2004**, *10*, 5901.

(24) Dreiss, C. A.; Cosgrove, T.; Newby, F. N.; Sabadini, E. *Langmuir* **2004**, *20*, 9124.

(25) Sheehan, R.; Cragg, P. J. *No Title*; Wiley-VCH, 2012.

(26) Saez, J. A.; Escuder, B.; Miravet, J. F. *Chem. Commun.* **2010**, *46*, 7996.

(27) Dou, C.; Wang, C.; Zhang, H.; Gao, H.; Wang, Y. *Chem. Eur. J.* **2010**, *16*, 10744.

(28) Das, A.; Molla, M. R.; Maity, B.; Koley, D.; Ghosh, S. *Chem. Eur. J.* **2012**, *18*, 9849.

(29) Zhong, J.-L.; Jia, X.-J.; Liu, H.-J.; Luo, X.-Z.; Hong, S.-G.; Zhang, N.; Huang, J.-B. *Soft Matter* **2015**, *12* (1), 191–199.

(30) Qi, Z.; Malo De Molina, P.; Jiang, W.; Wang, Q.; Nowosinski, K.; Schulz, A.; Gradzielski, M.; Schalley, C. A. *Chem. Sci.* **2012**, *3* (6), 2073–2082.

(31) Yamanaka, M. *J. Incl. Phenom. Macrocycl. Chem.* **2013**, *77*, 33–48.

(32) Yamanaka, M. *Chem. Rec.* **2016**, *16* (2), 768–782.

(33) Hiscock, J. R.; Piana, F.; Sambrook, M. R.; Wells, N. J.; Clark, A. J.; Vincent, J. C.; Busschaert, N.; Brown, R. C. D.; Gale, P. A. *Chem. Commun.* **2013**, *49*, 9119–9121.

(34) Sengupta, S.; Mondal, R. *RSC Adv.* **2016**, *6* (17), 14009–14015.

(35) Coubrough, H. M.; Jones, C. D.; Yufit, D. S.; Steed, J. W. *Supramol. Chem.* **2018**, *30*, 384–394.

(36) Hooper, A. E.; Kennedy, S. R.; Jones, C. D.; Steed, J. W. *Chem. Commun.* **2015**, *52*, 198–201.

(37) Kumari, H.; Armitage, S. E.; Kline, S. R.; Damodaran, K. K.; Kennedy, S. R.; Atwood, J. L.; Steed, J. W. *Soft Matter* **2015**, *11* (43), 8471–8478.

(38) Wezenberg, S. J.; Croisetu, C. M.; Stuart, M. C. A.; Feringa, B. L. *Chem. Sci.* **2016**, *7*, 4341–4346.

(39) Wang, Z.; Wille, U.; Juaristi, E. *Encyclopedia of Physical Organic Chemistry*; John Wiley & Sons, Inc., 2017.

(40) Piepenbrock, M. O. M.; Clarke, N.; Steed, J. W. *Langmuir* **2009**, *25* (15), 8451–8456.

(41) Mercer, D. J.; Loeb, S. J. *Chem. Soc. Rev.* **2010**, *39* (10), 3612–3620.

(42) Piepenbrock, M. O. M.; Lloyd, G. O.; Clarke, N.; Steed, J. W. *Chem. Rev.* **2010**, *110* (4), 1960–2004.

(43) Adarsh, N. N., Dastidar, P. *Cryst. Growth Des.* **2011**, *11*, 328–336.

(44) Sambri, L., Cucinotta, F., Paoli, G. D., Stagni, S., Cola, L. D. *New J. Chem.* **2010**, *34*, 2093–2096.

(45) Song, S., Song, A., Feng, L., Wei, G., Dong, S., Hao, J. *Appl. Mater. Interfaces* **2014**, *6*, 18319–18328.

(46) Online, V. A.; Sengupta, S.; Goswami, A.; Mondal, R. *New. J. Chem* **2014**, *38*, 2470–2479.

(47) R. Tatikonda, Nonappa, K. Bertula, S. Hietala, K. R. and M. H. *Dalton Trans.* **2017**, *46*, 2793–2802.

(48) Knichal, J. V; Gee, W. J.; Burrows, A. D.; Raithby, P. R.; Wilson, C. C. *CrystEngComm* **2015**, *17* (42), 8139–8145.

(49) Wang, xiaojuan; He, T.; Yang, L.; Wu, H.; Zhang, R.; Zhang, Z.; Shen, R.; Xiang, J.; Zhang, Y.; Wei, C.-W. *Nanoscale* **2016**, *8*, 6479–6483.

(50) Yang, L.; Luo, L.; Zhang, S.; Su, X.; Lan, J.; Chen, C.-T.; You, J. *Chem. Commun.* **2010**, *46*, 3938–3940.

(51) Zhang, J.; Su, C. Y. *Coord. Chem. Rev.* **2013**, *257* (7–8), 1373–1408.

(52) Sun, J.; Liu, Y.; Jin, L.; Chen, T.; Yin, B. *Chem. Commun.* **2016**, *52* (4), 768–771.

(53) Byrne, P.; Lloyd, G. O.; Applegarth, L.; Anderson, K. M.; Clarke, N.; Steed, J. W. *New J. Chem.* **2010**, *34*, 2261–2274.

(54) Steed, J. W. *Chem. Soc. Rev.* **2010**, *39* (10), 3686–3699.

(55) Arai, S.; Imazu, K.; Kusuda, S.; Yoshihama, I.; Tonegawa, M.; Nishimura, Y.; Kitahara, K.; Oishi, S.; Takemura, T. *Chem. Lett.* **2006**, *35* (6), 634–635.

(56) Dawn, A.; Andrew, K. S.; Yufit, D. S.; Hong, Y.; Reddy, J. P.; Jones, C. D.; Aguilar, J. a.; Steed, J. W. *Cryst. Growth Des.* **2015**, *15*, 4591–4599.

(57) Piepenbrock, M.-O. M.; Clarke, N.; Steed, J. W. *Soft Matter* **2011**, *7* (6), 2412.

(58) Liu, Q.; Wang, Y.; Li, W.; Wu, L. *Langmuir* **2007**, *23* (15), 8217–8223.

(59) James, S. J.; Perrin, A.; Jones, C. D.; Yufit, D. S.; Steed, J. W. *Chem. Commun.* **2014**, *50* (85), 12851–12854.

(60) Byrne, P.; Turner, D.; Lloyd, G. *Cryst. Growth Des.* **2008**, *2* (8), 1–10.

(61) Chandran, S. K.; Nath, N. K.; Cherukuvada, S.; Nangia, A. *J. Mol. Struct.* **2010**, *968* (1–3), 99–107.

(62) Piepenbrock, M.-O. M.; Clarke, N.; Foster, J. A; Steed, J. W. *Chem. Commun.* **2011**, *47* (7), 2095–2097.

(63) Chudzinski, M. G.; McClary, C. A.; Taylor, M. S. *J. Am. Chem. Soc.* **2011**, *133* (27), 10559–10567.

(64) Babu, J. N.; Bhalla, V.; Kumar, M.; Puri, R. K.; Mahajan, R. K. *New J. Chem.* **2008**,

33, 675–681.

(65) Li, A.-F.; Wang, J.-H.; Wang, F.; Jiang, Y.-B. *Chem. Soc. Rev.* **2010**, *39* (10), 3729–3745.

(66) Casuso, P.; Carrasco, P.; Loinaz, I.; Cabañero, G.; Grande, H. J.; Odriozola, I. *Soft Matter* **2011**, *7* (7), 3627.

Chapter 4

Anion binding by pre-organised imidazole urea derivatives of triethylbenzene and a mesitylcalixarene

4.1 Background and Project Aims

The binding and sensing of biologically important anions such as citrate,[1] phosphate,[2,3] lactate[4–6] and chloride[7–9] as well as pollutant ions namely fluoride,[10,11] cyanide,[12–14] sulphate[15,16] and nitrate[17–19] is particularly topical. A typical anion sensor usually comprises an anion binding moiety such as urea,[16,20,21] thiourea,[16,22,23] amide or sulfonamide coupled to a signalling group such as a fluorophore that can transduce binding into a measurable signal. In order to achieve effective sensing of anions, there is an urge to design a more flexible receptor that can respond to a range of analytes to varying degree. The previous work of our research group[24] has explored the *induced fit*[25] concept, in which flexible receptors can bind to the analytes and result in conformational change that can generate a measurable output signal.[25,26]

The mechanism of this *induced fit* concept is that only analytes that induce an appropriate conformational change will result in signal generation even though they may not be the strongest bound by the receptor. The Steed group has applied this concept to the sensing of anions using the flexible triethylbenzene and mesitylcalixarene scaffolds.[25,27] These two versatile platforms can be used to construct and design small and flexible anion and cation receptors. In this chapter, triethylbenzene- and mesitylcalixarene-based anion hosts are synthesised and the binding affinity towards anions are compared to that of ligands **2.2**, **2.3** and **2.4** discussed in Chapter 2. The binding affinities of these hosts are also compared to previously reported anion hosts.

4.2 Results and Discussion

4.2.1 Synthesis and characterisation of trialkylbenzene-based anion hosts

Ligands **2.2** - **2.4** were prepared and characterised as discussed in Chapter 2. Hosts **4.1** and **4.2** were synthesised by reacting imidazole urea arms **2.2** and **2.3** with 1,3,5-tri(bromomethyl)-2,4,6-triethylbenzene. Reactions were carried out in dry tetrahydrofuran (THF), continuously stirred and heated to reflux for 24-48 hours. In order for this reaction to occur, the presence of a base is necessary to deprotonate the imidazole N-H, hence ligands **2.2** and **2.3** were used in slight excess acting as a base as well as being a reactant (Scheme 4.1). For both of the reactions, within four to six hours, light yellow precipitates began to form in the reaction flask. During the first attempt, the reaction between ligand **2.2** with the tripodal core was performed for 24 hours. After 24 hours, the brown sticky oil of host **4.1** was isolated by removing the solvent by decanting as the oil sticks to the bottom of the flask. The solvent was removed while the solution was still warm to remove most of the unreacted starting material. The brown oil was then evaporated to dryness to give a brown solid. Upon exposure to air and moisture, the brown solid became sticky again, presumably due to absorption of atmospheric moisture.

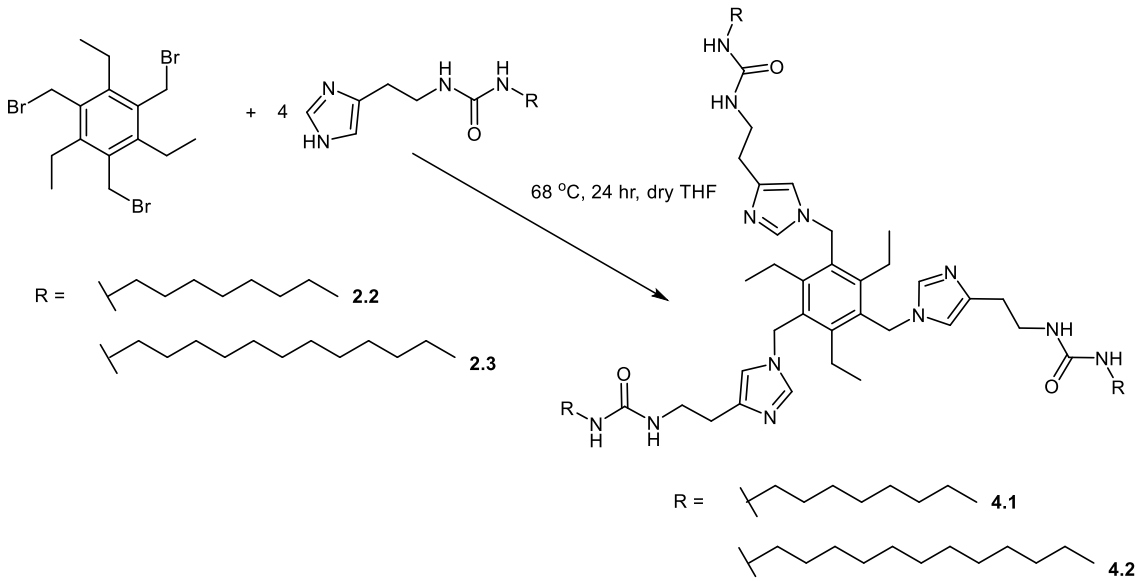

Scheme 4.1 Synthesis route of compound **4.1** and **4.2** using excess ligand as the base (Note: The structure of compound **4.1** and **4.2** drawn in this figure represents 1,3 isomer).

Even after 24 hours of reaction, the yield of the product was quite low, with unoptimised yield of approximately 25%. This could be due to the use of only a slight excess of ligand that was not enough to deprotonate the NH proton of all of the imidazole ligands to allow the reaction to take place. Nevertheless, the formation of host **4.1** has been confirmed by ESI-MS, ^{1}H and ^{13}C NMR spectroscopy. From the ESI-MS spectrum of host **4.1**, there are peaks that correspond to the mass of the molecular ion, particularly 1019.6 for $[M+Na]^{+}$, 499.3 for $[(M/2)+2H^{+}]^{2+}$ and 333.4 for $[(M/3)+3H^{+}]^{3+}$. In the ^{1}H NMR spectrum, the formation of host **4.1** is indicated by the appearance of a CH_2 signal that connects the tripodal core with the imidazole urea ligands at 5.35 ppm.

Due to the low yield of host **4.1**, the reaction to form host **4.2** was performed for a longer time, up to 48 hours with a higher excess of ligand **2.3** (for example 1 mole of triethylbenzenetribromide was reacted with 6 moles of ligand **2.3**). After 48 hours, a yellow sticky solid was isolated from the reaction mixture. This material was evaporated to dryness using rotary evaporator giving yellow solid that upon exposure to air begin to turn sticky again. Although the reaction time was prolonged to 48 hours, the yield of host **4.2** was still low at 45% unoptimised yield. With the use of a higher excess of the ligand, the yield can be improved somewhat, but the removal of the excess ligand now becomes a challenge. Nevertheless, the formation of host **4.2** has been confirmed by ESI-MS showing molecular ion mass peak of 1185.5 for $[M+Na]^{+}$, 583.6 for $[(M/2)+2H^{+}]^{2+}$ and 389.6 for $[(M/3)+3H^{+}]^{3+}$. The ^{1}H NMR spectrum of host **4.2** also confirmed the presence of CH_2 signal that connects the tripodal core with the imidazole urea ligands at 5.19 ppm. Although the targeted product has been successfully synthesised, this method is not optimal due to the need to use excess ligand and difficulty in the separation and removal of the residual reactants since the reactants and products show similar solubility in a range of solvents such as alcohols.

Multiple recrystallisations using different types of solvents have been performed to purify compound **4.1** and **4.2** as tabulated in Table 4.1. To perform the crystallisation

experiments, about 50 mg of host **4.1** and **4.2** were weighed into a 2 cm^3 glass vials and the vials were filled with an appropriate amount of solvent around 1-1.5 cm^3 depending on the solubility. All samples were heated and sonicated until everything had dissolved. The vials were loosely sealed with lid resting on top of the vial to allow slow evaporation of the solvent. The samples were checked every couple of days until either crystal formed or non-crystalline solids formed, or a sticky oil which did not change over the course of a few weeks. Unfortunately, the crystallisation experiments only give either impure solids or impure sticky solid in which the impurities can still be seen in ^1H NMR spectra of both hosts **4.1** and **4.2**. Host **4.1** obtained after recrystallisation was also washed with hot acetonitrile and the solution decanted. Washing with hot acetonitrile caused the formation of a brown viscous liquid that was then dried in the oven at 60 ^oC for two days.

Table 4.1 Crystallisation experiments of host **4.1** and host **4.2**
(Note: P = precipitate, I = Insoluble).

	Hosts	
Solvents	**4.1**	**4.2**
Acetonitrile	P	P
Nitromethane	P	P
1-propanol	P	P
Tetrahydrofuran	I	I
Ethyl acetate	I	I
Acetone	I	I
Acetonitrile: Methanol (few drops)	P	P
Nitromethane: Methanol (few drops)	P	P
Acetonitrile: Ethanol (few drops)	P	P
Nitromethane: Ethanol (few drops)	P	P
Ethyl acetate: Ethanol (few drops)	P	P
Ether diffusion into methanol solution	P	P

*P = Precipitate, I = Insoluble

On the other hand, attempts to purify host **4.2** were performed using different techniques such as membrane dialysis and column chromatography. Membrane dialysis technique was not the best solution as it decomposes the product after overnight stirring in methanol. Column chromatography was also employed to separate the residual reactants from the product using silica gel as the stationary phase and a mixture of ethyl acetate: *iso*-propyl alcohol: water (4:2:1) with 0.1% NH_4OH as the eluent. The addition of 0.1% of NH_4OH is necessary to deactivate the

silica gel, otherwise, host **4.2** will decompose on the column. Regardless of the high polarity of the eluent system being used, the residual reactants still cannot be separated from the product as the signal of the residual reactants can still be observed in the ^{1}H NMR spectra of the product. The use of a higher amount of excess ligand also results in the higher percentage of impurities retained in the mixture (Figure 4.1).

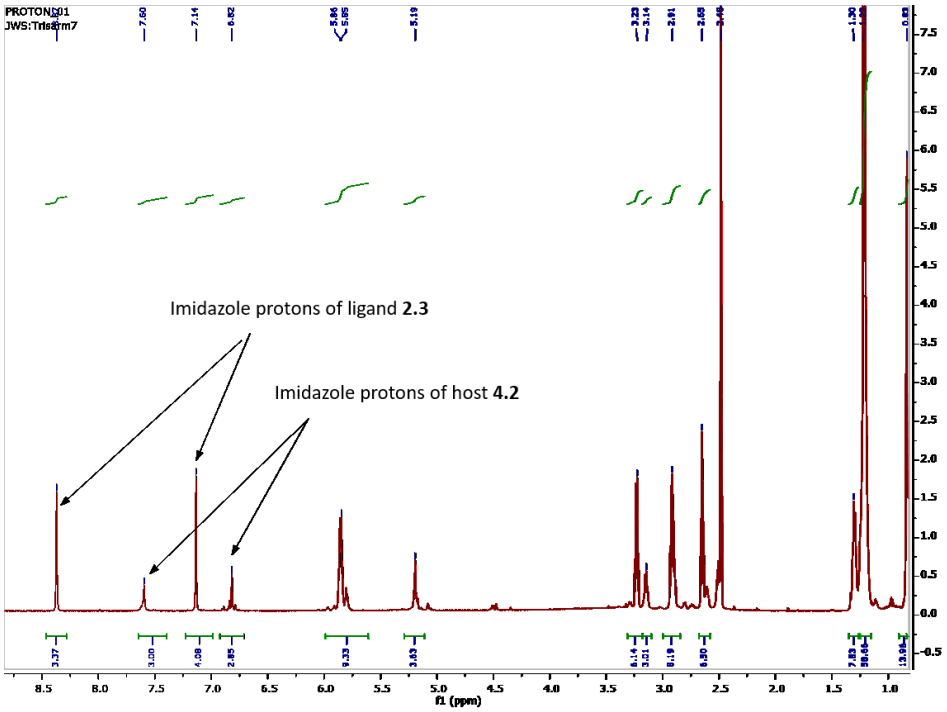

Figure 4.1 ^{1}H NMR spectrum of compound **4.2**.

For host **4.2**, a ^{1}H DOSY NMR (Diffusion Ordered Spectroscopy) experiment was performed to distinguish the signals of the excess reactants and product. The ^{1}H DOSY NMR spectrum of **4.2** indicates the presence of two compounds proved by two distinct layers with the diffusion coefficient of 1.0 x 10^{-10} m^2s^{-1} and 1.8 x 10^{-10} m^2s^{-1}, corresponding to the residual reactants and product, respectively (Figure 4.1 and 4.2). ^{1}H DOSY NMR is a very useful technique that is predominantly used for investigating aggregation behaviour in solution. The principle of the technique is based on the diffusion coefficient parameter that is highly sensitive towards changes in the molecular or aggregate size and the number of individual molecules, which constitutes an aggregate. The molecular mass of the aggregate can then be estimated using the Stokes-Einstein equation.[28] From the DOSY spectrum, the molecular mass calculated from the diffusion coefficient suggest the presence of ligand **2.3** and compound **4.2**

both in dimeric form, hence the molecular mass calculated is compared to that of theoretical molecular mass of the dimers. The estimated molecular weight of both compounds is summarised in Table 4.2.

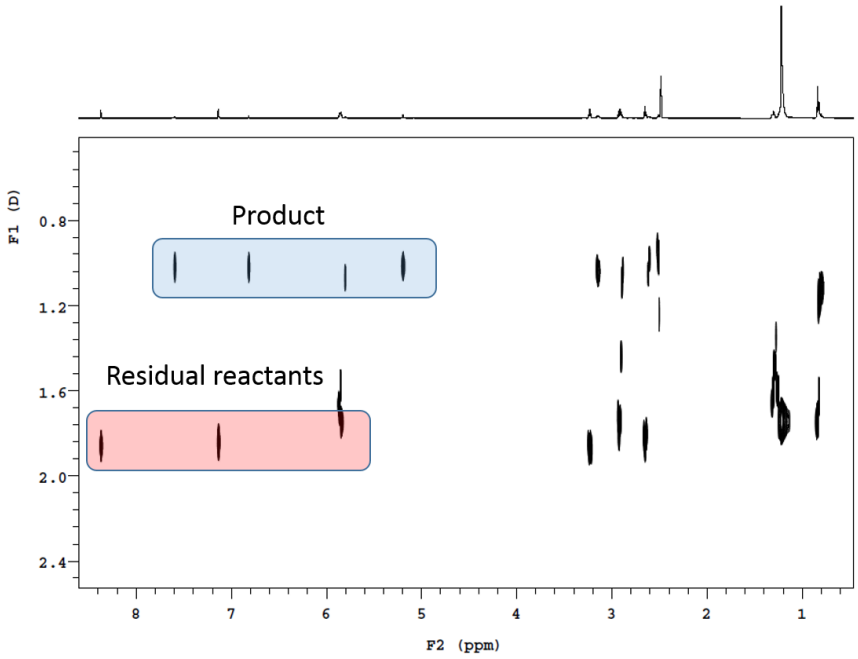

Figure 4.2 ^{1}H DOSY NMR of compound **4.2**.

Table 4.2 Estimated molecular mass (g/mol) of both mixtures found in the DMSO-d_6 solution of compound **4.2**.

Entry	Diffusion Coefficient, D_{obs} (m^2s^{-1})	Estimated molecular mass of the dimer (g/mol)	Calculated molecular mass of the dimer (g/mol)	Difference (%)
Host **4.2**	1.0 x 10^{-10}	2985.8	2331.6	±28.06
Ligand **2.3**	1.8 x 10^{-10}	760.7	645	±17.94

From the estimated molecular mass in Table 4.2, it can also be observed that the residual reactants and products are prone to form dimers in the solution as the estimated molecular mass are closer to the calculated molecular mass for both of the dimers. The compound with lower molecular weight tends to diffuse more quickly in solution, in this case, the residual reactants, in comparison with the product that is heavier, having a molecular mass of at least three times of the residual reactants. From

this data, the peaks can be separated and assigned unambiguously, and it can be seen that the higher intensity peak of imidazole proton belongs to the residual reactants, while the lower intensity peak belongs to the product.

Due to the difficulty in the purification step, compound **4.2** was used in its impure form for qualitative anion binding studies, which is discussed in the following subsection. Due to the lower yield and the challenge in the purification of products when excess ligands were used as a base in the synthesis, a different type of inorganic base was introduced for the reaction between the triethylbenzene core with ligand **2.4**. All of the synthesis attempts were monitored using LC ESI-MS in methanol for quick characterisation of the product obtained. The first attempt that was carried out in the presence of strong bases such as potassium hydroxide and sodium hydroxide, did not yield the desired product, most likely due to the insolubility of the base in organic solvent. Another alternative such as potassium carbonate also was unsuccessful in synthesising the desired compounds.

To overcome the solubility problem of the inorganic base, a phase transfer catalyst, tetrabutylammonium bromide, was also added to the reaction mixture along with potassium carbonate. However, the ESI-MS spectrum does not show any molecular ion mass that corresponds to the desired product. The use of triethylamine as a base also was not successful although triethylamine readily dissolved in the solution mixture.

The reaction of 1,3,5-tri(bromomethyl)-2,4,6-triethylbenzene with ligand **2.4** also has been performed in the presence of cesium carbonate. After 48 hours, the product was isolated and dried. The ESI-MS analysis data of the product did not show the presence of a peak that corresponds to the product. The ^{1}H NMR spectrum, however, shows resonances that can be assigned to the desired product which are different from the chemical shifts of the resonances observed for both of the reactants suggesting that the desired product might have formed (Figure 4.3 and 4.4). The ^{1}H NMR spectrum of compound **4.3** shows a downfield shift compared to the free ligand of both CH protons of the imidazole rings, *ca* Δδ 0.37 ppm and *ca* Δδ 0.51 ppm whereas the urea NH protons of NH3 and NH4 both shifted more upfield upon the formation of the product, *ca* Δδ 0.17 and *ca* Δδ 0.56 ppm, respectively. However, due to the impurity of the product obtained, the integration could not be determined accurately.

Table 4.3 summarises the inorganic bases used in the synthesis and the approximate percentage of the conversion to the targeted product. All reactions were performed in tetrahydrofuran and some were repeated in acetonitrile solvent. The reasons behind the use these two solvents in the synthesis of the host is because the products formed from this reaction will not dissolve in both of the solvents but the reactants used are soluble in this solvent at reflux temperature, hence the solution can be removed after the reaction leaving majority of the products in the reaction flask.

Table 4.3 Summary of the inorganic bases and solvents used in the synthesis of triethylbenzene-based anion host, **4.3**.

Entry	Inorganic base	Solvents used	Unoptimised Percentage of conversion (%)
1	Slight excess of imidazole urea ligands	THF and MeCN	20 - 25
2	Sodium hydroxide (NaOH)	THF and MeCN	0
3	Potassium hydroxide (KOH)	THF and MeCN	0
4	Potassium carbonate (K_2CO_3)	THF and MeCN	0
5	Potassium carbonate (K_2CO_3) with tetrabutylammonium bromide as phase transfer catalyst	THF	0
6	Triethylamine	THF	0
7	Caesium carbonate (Cs_2CO_3)	THF	41

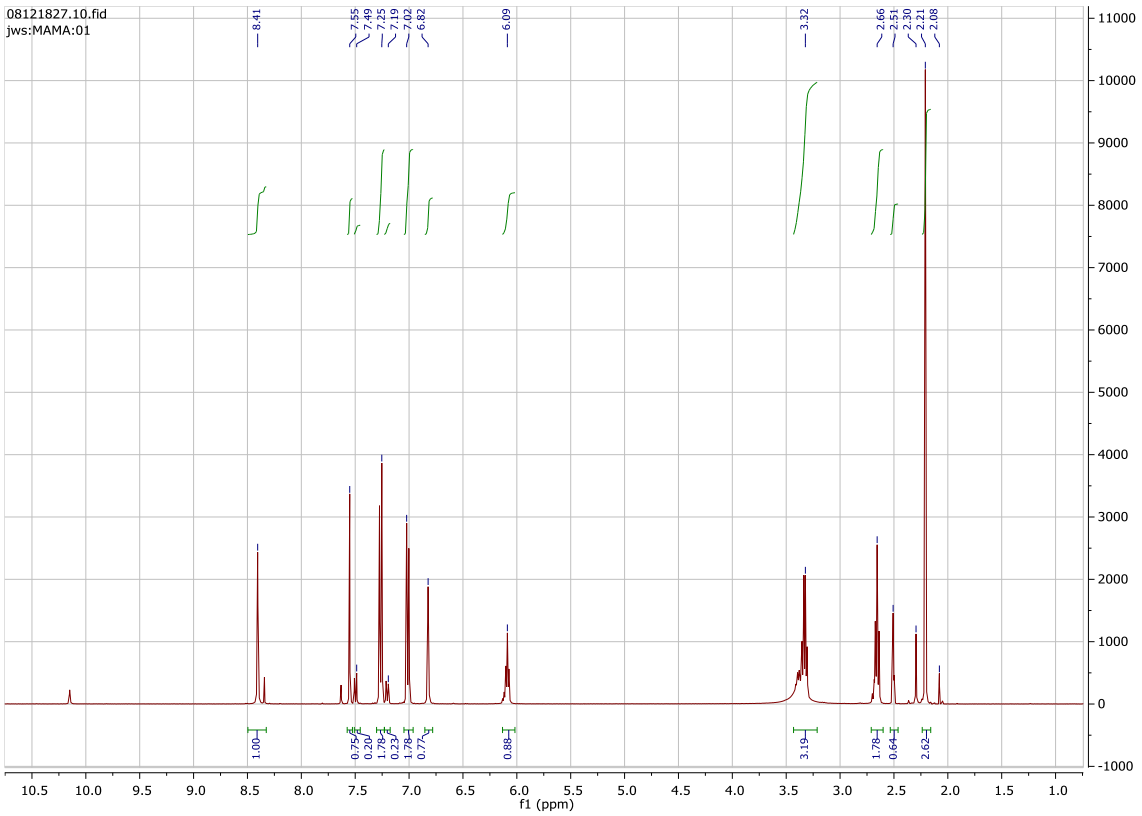

Figure 4.3 ^{1}H NMR spectrum of ligand **2.4.**

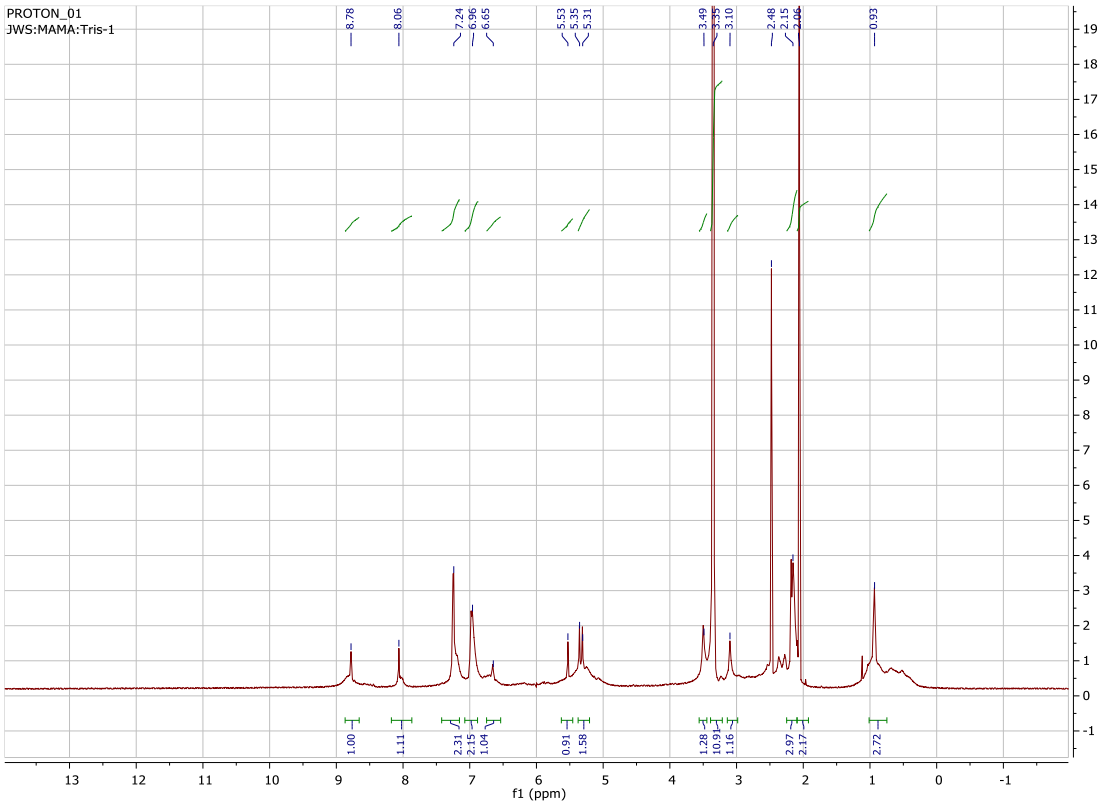

Figure 4.4 ^{1}H NMR spectrum of trisurea **4.3** obtained from the reaction of 1,3,5-tribromo-2,4,6-triethylbenzene with compound **2.4** in the presence of Cs_2CO_3.

4.2.2 Anion binding studies of host 4.2 and 4.3

The ^{1}H NMR spectrum of host **4.2** shows that, for 1 mole of host **4.2**, there are 3 moles of the reactant, ligand **2.3**. Therefore, in the anion binding study, the concentration of the guest added is based on the concentration of one mole of host **4.2** and three moles of ligand **2.3**. The anion binding properties of fluoride, chloride, and acetate by host **4.2** was studied by means of ^{1}H NMR spectroscopic titrations in dimethylsulfoxide-d_6. Although host **4.2** is fairly soluble in chloroform, the proton signals are broad and hard to follow, possibly due to the aggregation of the host in chloroform making the solvent not suitable for the titration experiment. Also, due to the free ligand impurities, it is not possible to calculate the binding constant for all the hosts. Hence, only qualitative results will be discussed in this subsection. The first titration experiment was performed between host **4.2** with fluoride ion (as the NBu_4^+ salt). Only the proton signals from the products (H1, H2 and urea N-H, H3 and H4) are followed in this titration (Figure 4.5).

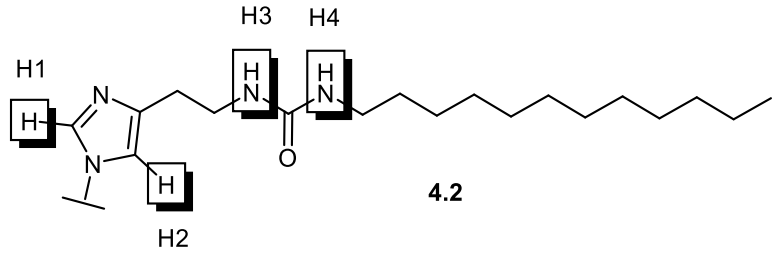

Figure 4.5 Proton signals (H1, H2, H3 and H4) that are followed for the anion binding experiments (Note: structure represent one of the binding arm of host **4.2**).

Addition of 0.5 to 1.0 equivalent of fluoride ion does not perturb the chemical shift of all four protons. However, upon the addition of 2.0 equivalent of fluoride ion, the H1 peak corresponding to the imidazole proton became broad and shifted further upfield. Similarly, addition of 2.0 equivalent of fluoride also caused the broadening of the H2 signal, attributed to another imidazole proton and the peak also shifted further upfield (Figure 4.6). The urea protons are not significantly affected by the fluoride ion but upon addition of 2.0 equivalent of fluoride ion, the urea proton peaks, H3 and H4 starts to broaden and split forming two different signals after 5.0 equivalent of fluoride ions is added. Addition of 2.0 equivalent of fluoride ion also caused significant colour

changes to the solution from yellow to pink (Figure 4.8), indicating the deprotonation of imidazole proton H1 and H2 by the basic fluoride ion.

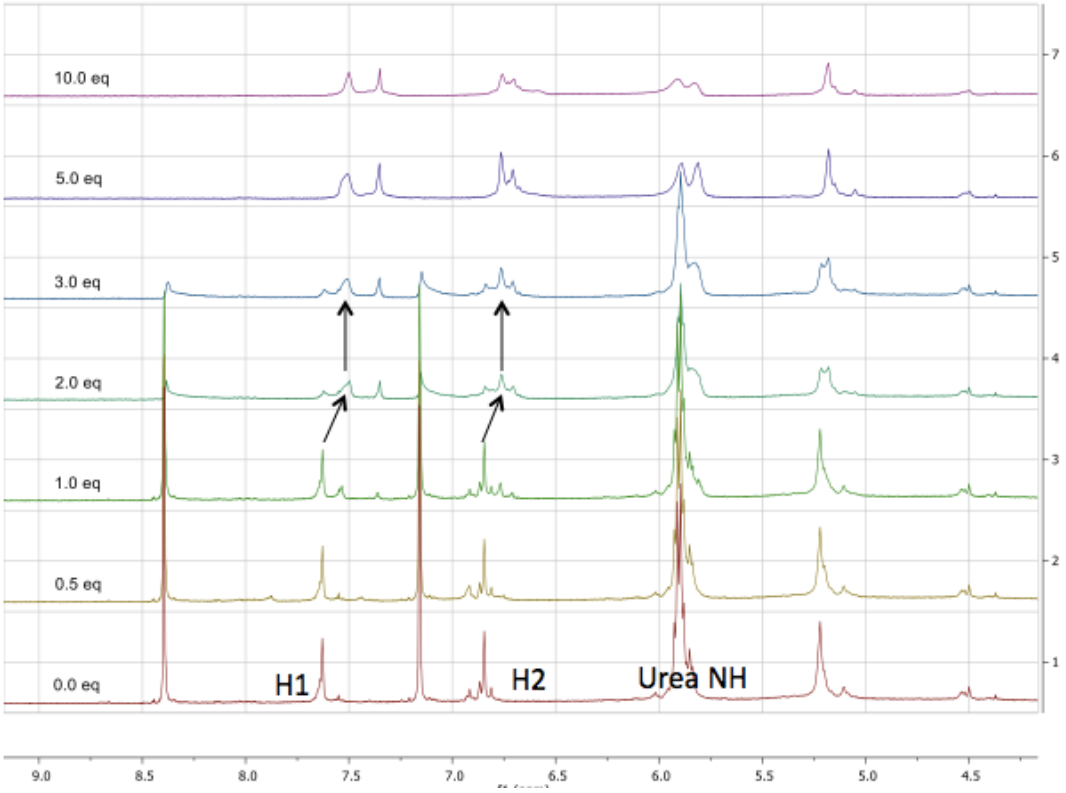

Figure 4.6 Stack plot showing the ^{1}H NMR spectrum of compound **4.2** in DMSO-d_6 in the presence of fluoride ion as tetrabutylammonium salt.

The second titration experiment was performed between host **4.2** with acetate ion (as NBu_4^+ salt). Similar to the titration with fluoride ions, only the proton signals from the products (H1, H2 and urea N-H, H3 and H4) are followed in this titration. Addition of 0.5 to 1.0 equivalent of acetate ion also does not perturb the chemical shift of all three protons. Likewise, upon the addition of 2.0 equivalent of acetate ion, both the H1 and H2 signals shifted upfield (Figure 4.7). The urea protons are not significantly affected by the acetate ion, only showing an insignificant broadening of the peak upon the addition of 2.0 equivalent of acetate ions. Addition of 2.0 equivalent of acetate ion also induced the colour changes of the solution from yellow to pink (Figure 4.8).

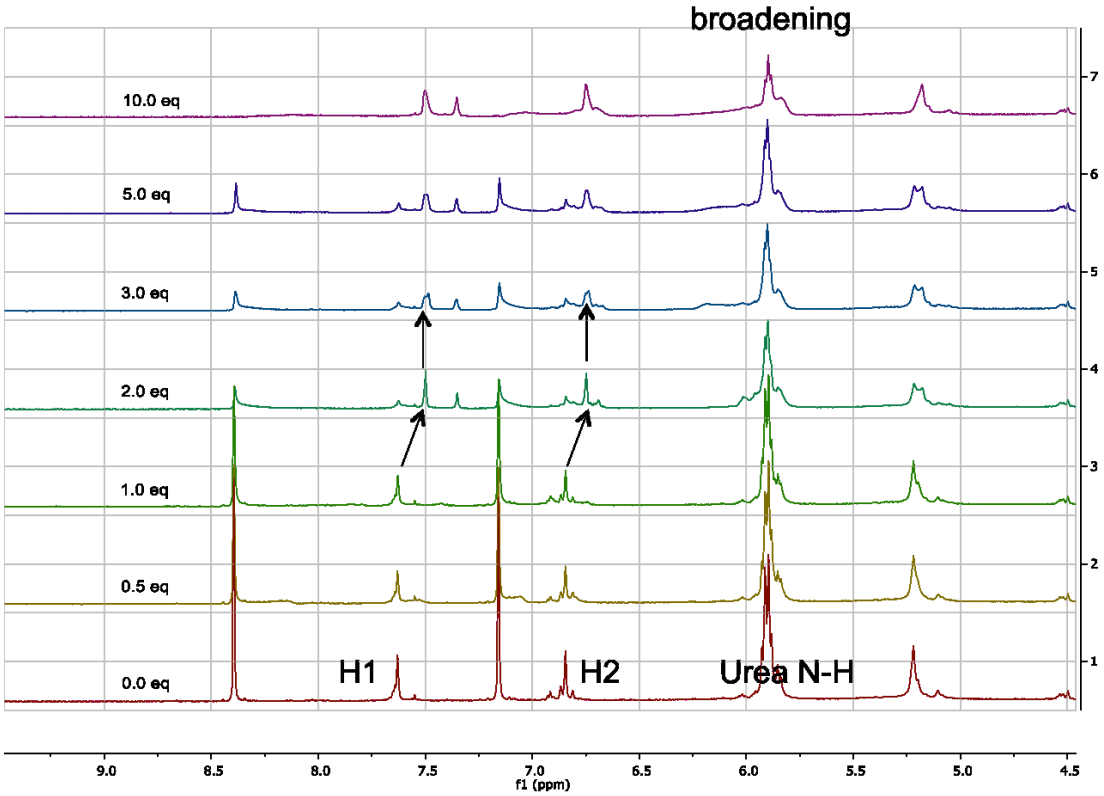

Figure 4.7 Stack plot showing the ^{1}H NMR spectrum of compound **4.** in DMSO-d_6 in the presence of acetate ion as tetrabutylammonium salt.

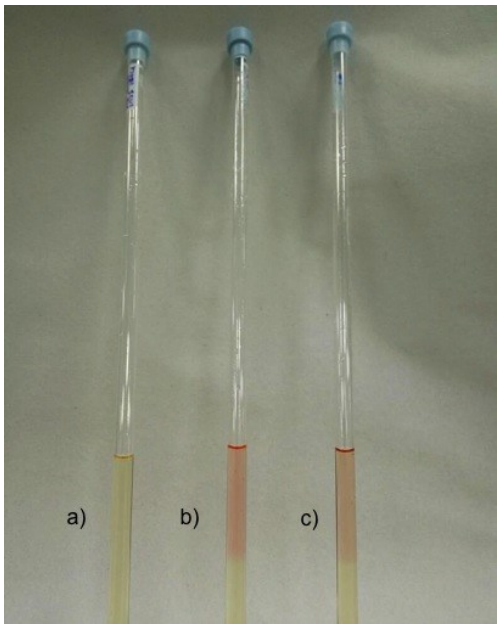

Figure 4.8 Colour changes upon addition of 2.0 equivalent of a) tetrabutylammonium chloride b) tetrabutylammonium fluoride hydrate c) tetrabutylammonium acetate (photographs taken before solution mixing).

The chloride binding properties of host **4.2** was also examined in DMSO-d_6. Suprisingly, host **4.2** does not interact with chloride in this medium. Addition of chloride ion does not result in any changes on the chemical shift changes for any of the proton signals examined except an insignificant broadening of the urea NH signal after the addition of 2 equivalent of chloride (Figure 4.9). This result is in contrast with the chloride binding experiment on the free arm **2.3** that has been discussed in detail in Chapter 2. The addition of chloride to the solution of free **2.3** results in the downfield shift of the urea protons with chemical shift changes of $\Delta\delta$ 1.24 ppm. The addition of the chloride ion also does not result in any colour change of the solution and the yellow colour is retained. Although the titration experiment of **2.3** were done in a less competitive solvent, $CDCl_3$ and results in large chemical shift changes, the competitiveness of the solvent is not the only factor that determines the binding affinity of a compound to anions. Turner *et al.* reported similar titration experiment using a tripodal pyridinyl urea analogues having an *n*-octyl chain and this system binds chloride well with a binding constant of 7079 M^{-1}.[29] While we do not have a definite explanation for this effect it could be rationalized by the competitiveness of the DMSO solvent and possibly self-association.

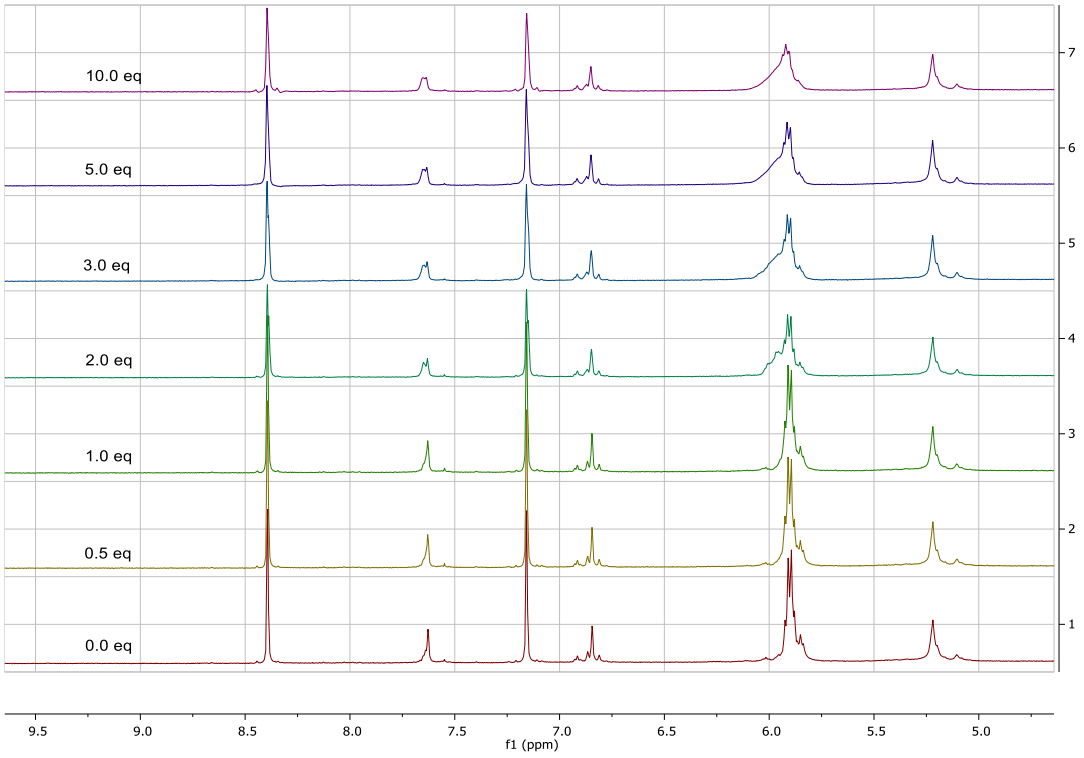

Figure 4.9 Stack plot showing the ^{1}H NMR spectrum of compound **4.2** in DMSO-d_6 in the presence of chloride ion as tetrabutylammonium salt.

For host **4.3**, the anion binding titration experiment was performed on chloride, fluoride and acetate as the tetrabutylammonium salts in DMSO-d_6. Upon the addition of these three anions, there are no changes observed in the chemical shifts of the designated protons; H1 and H2 protons of imidazole and urea NH (Figure 4.10 - 4.12).

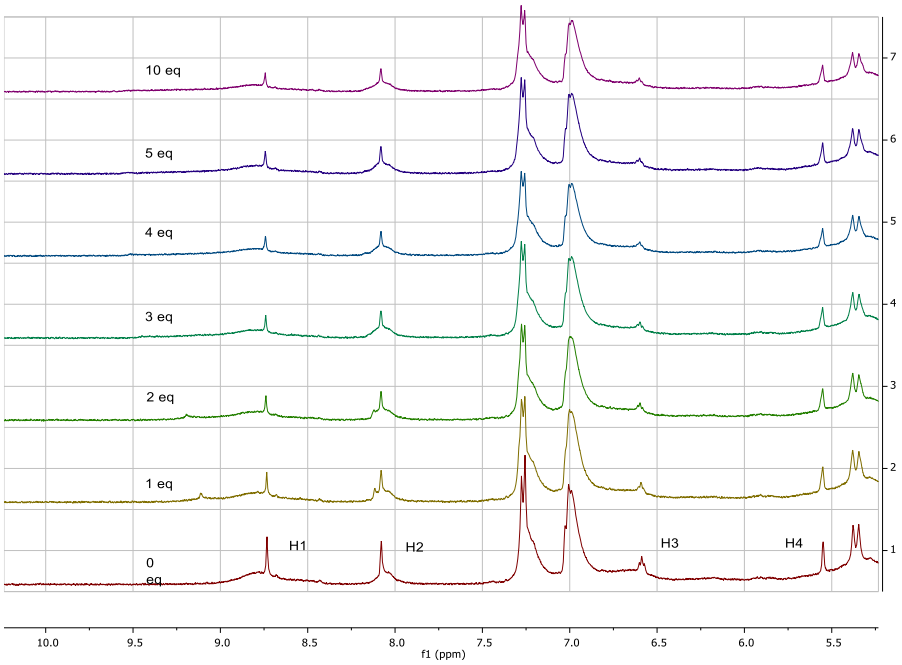

Figure 4.10 Stack plot showing the ^{1}H NMR spectrum of compound **4.3** in DMSO-d_6 in the presence of chloride ion as tetrabutylammonium salt.

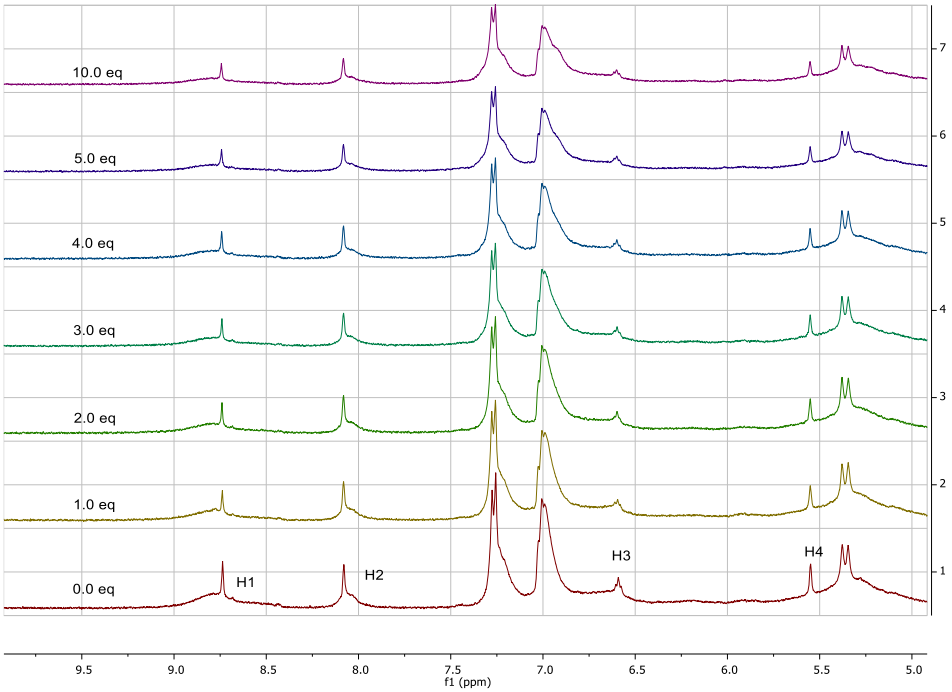

Figure 4.11 Stack plot showing the ^{1}H NMR spectrum of compound **4.3** in DMSO-d_6 in the presence of fluoride ion as tetrabutylammonium salt.

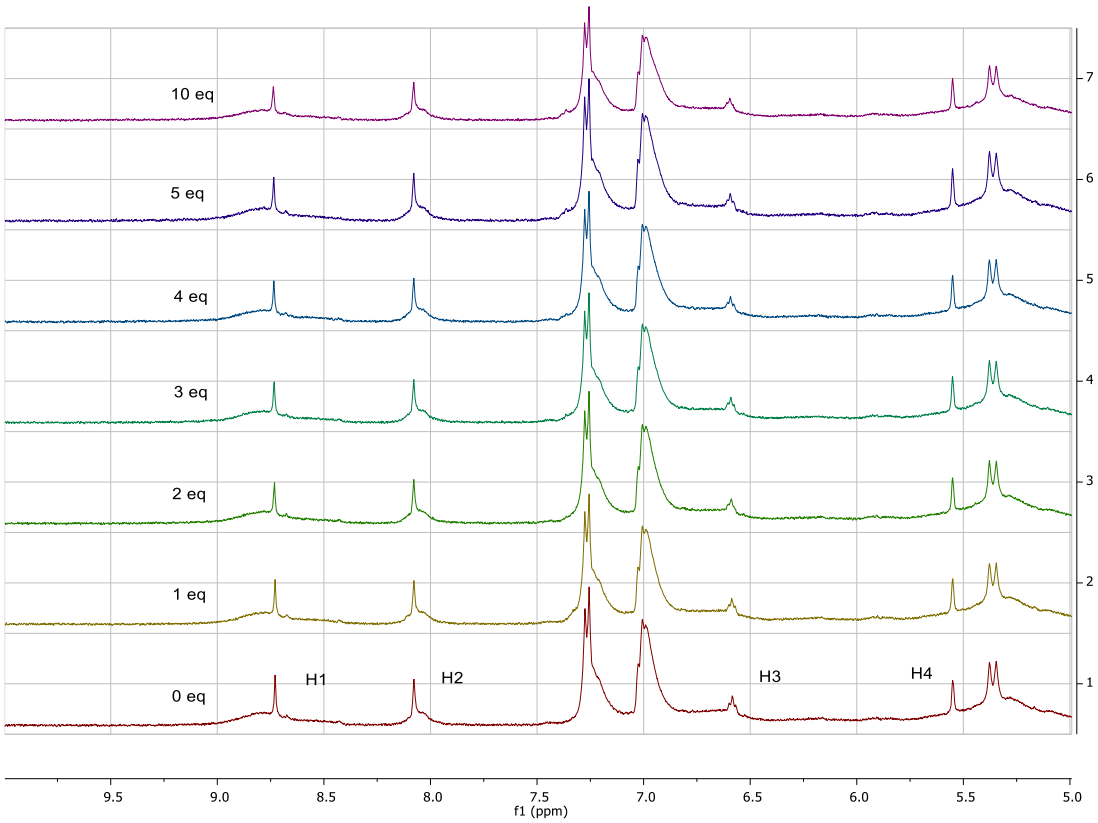

Figure 4.12 Stack plot showing the ^{1}H NMR spectrum of compound **4.3** in DMSO-d_6 in the presence acetate ion as tetrabutylammonium salt.

From the titration data, there could be a few possible reasons why the imidazole CH, H1 and H2 as well as urea NH3 and NH4 of compound **4.3** are not affected by the addition of Cl^-, F^- and OAc^- ions. One of the plausible reason might be that compound **4.3**, may form a carbonate complex, in which the carbonate ion from cesium carbonate hydrogen bonds with the urea moieties of compound **4.3**. The presence of the carbon signal of a carbonate can be seen in the ^{13}C NMR spectrum of compound **4.3** at 206.9 ppm. Similar hydrogen bonds between urea NH and carbonate ion have been reported previously,[30] in which the carbonate ion was encapsulated tightly in a cavity of tripodal hexaurea receptor by strong 12 NH···O bonds ($d_{NH\cdots O}$ = 2.703(3) – 2.989(3) Å) from 12 NH groups of urea units (Figure 4.13). The use of competitive solvent DMSO for the titration also could contribute to the low binding affinity of the host towards Cl^-, F^- and OAc^- ions.

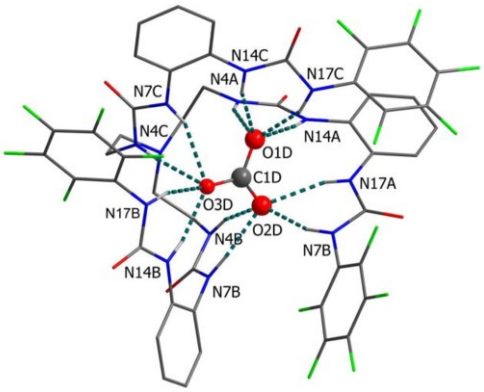

Figure 4.13 Single-crystal X-ray structure of the carbonate complex of tripodal hexaurea receptor (countercations and hydrogen atoms on carbons are omitted for clarity). Reproduced with permission from reference 31.

Another reason that could contribute to the non-interaction between compound **4.3** with all of the aforementioned anions is compound **4.3** might self-assemble and form a dimer that is interconnected by hydrogen bonds between the urea NH with the carbonyl group that subsequently leads to the formation of a molecular capsule or belt as reported previously by Shimazu and Yamanaka (Figure 4.14).[31]

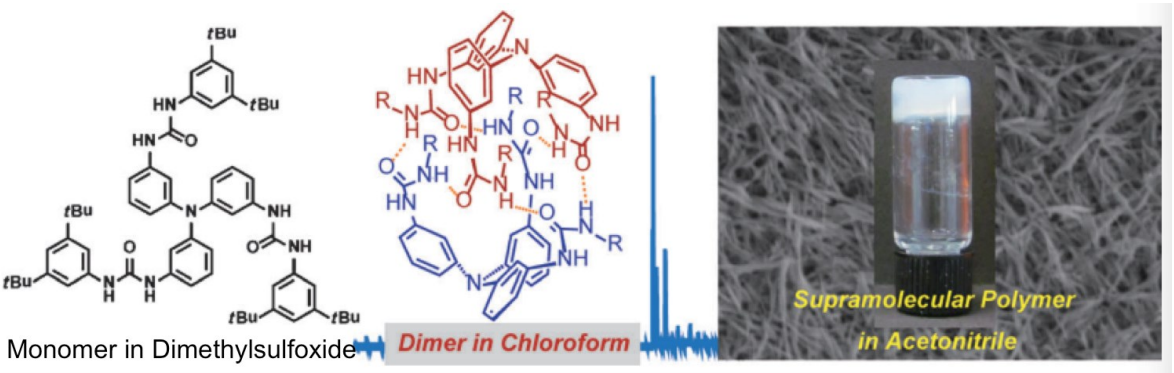

Figure 4.14 Formation of a discrete dimer of C3-Symmetric tris-urea in less polar solvent, chloroform through self-assembly, whereas in the more polar acetonitrile and acetone a supramolecular gel was obtained. Reproduced with permission from reference 32.

4.2.3 Synthesis and characterisation of mesitylcalixarene-based compounds

Flexible receptors using a mesitylcalixarene core have also been synthesised. Firstly, the precursor, mesityl calix[4]arene (**4.4**) was prepared in good yield by self-condensation of α^2-chloro isodurene in the presence of $SnCl_4$ as the catalyst. Next, bromomethylation of **4.4** to afford tetrakis-*p*-bromomethylated mesityl calix[4]arene (**4.5**) scaffold was achieved in a single step using a simplified version of the literature procedure[32,33] as depicted in Scheme 4.2.

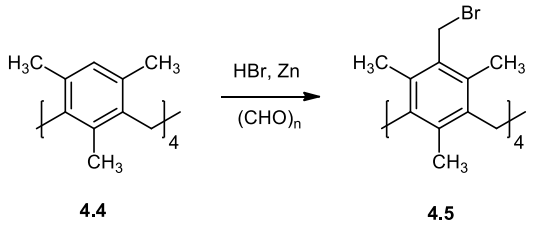

Scheme 4.2 Bromomethylation of mesityl calix[4]arene.

In order to synthesise the ditopic anion receptor compounds, the scaffold, **4.5** was reacted with a slight excess of imidazole urea ligands with butyl chain (**2.1**) by adapting the procedure described by Willans and co-workers[32] with some modification on the reaction temperature and solvent used (Scheme 4.3).

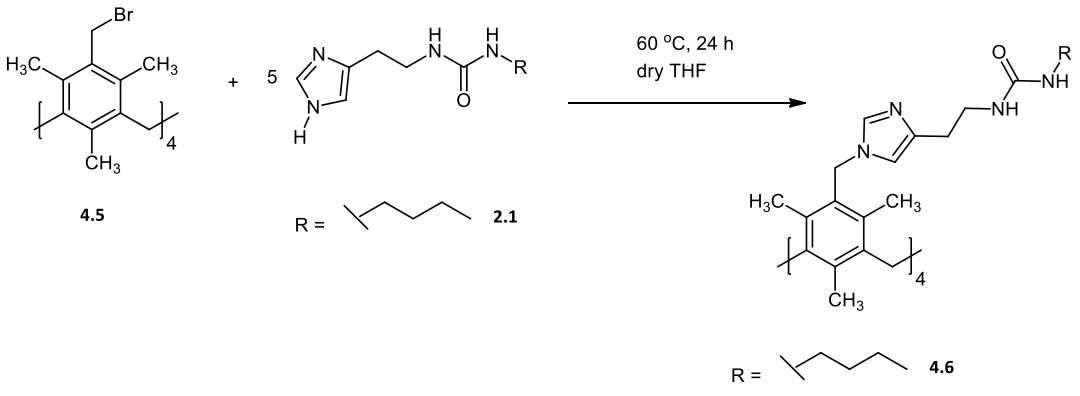

Scheme 4.3 Synthesis route of compound **4.6** using excess ligand as the base.

ESI-MS confirmed the formation of compound **4.6**, from molecular ion peaks of 473.47 that corresponds to $((M/3)+3H^+)^{3+}$. The reaction was monitored using ESI-MS and even

after 24 hours of reaction, the conversion of the reactants to the product was very low, <20%. This low conversion could be due to the use of only a slight excess of ligands that was not enough to deprotonate the NH proton of imidazole to allow the reaction to take place. This method is problematic due to the need of using a very large excess of ligands to afford higher yield, which is not cost effective. In addition, the product, **4.6** was only soluble in polar solvents such as methanol, DMSO and DMF. Attempts to purify the compound have been performed by recrystallisation from nitromethane, acetonitrile and a range of solvents, but a pure compound still could not be obtained. Attempts to purify the compound using membrane dialysis were also were unsuccessful due to decomposition after overnight stirring in the dialysis membrane. Therefore, another compound **4.7** with a longer alkyl chain, was synthesised in order to improve the solubility of the product and for this purpose, instead of using excess ligands, another base, caesium carbonate was introduced to aid in the deprotonation of the NH group of the imidazole (Scheme 4.4). However, due to the insolubility of the caesium carbonate in the organic solvent, the reaction time was prolonged to 48 hours with constant stirring at 60 ^{o}C.

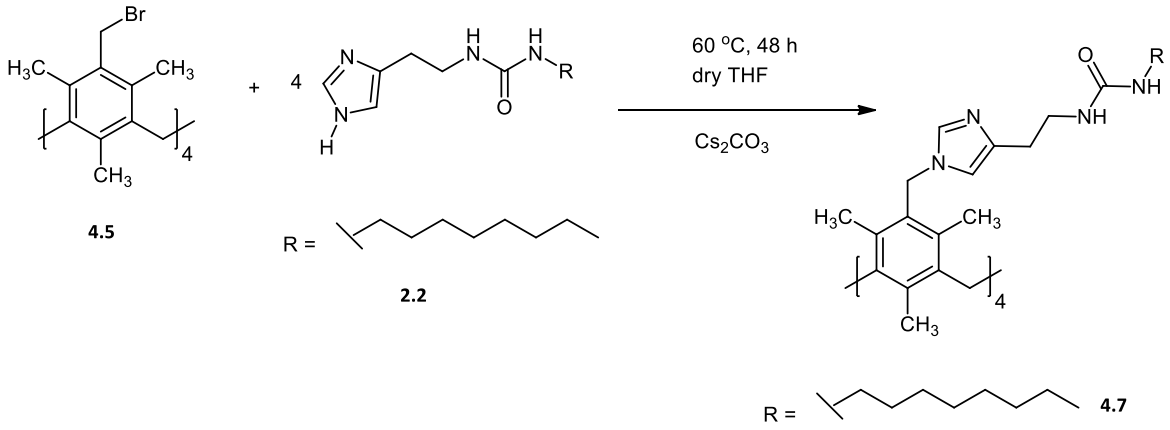

Scheme 4.4 Synthesis route of compound **4.7** using caesium carbonate as base.

A beige-coloured precipitate formed after the reaction at reasonable yield (52 %), but unfortunately, the product obtained cannot be characterised by solution NMR spectroscopy due to the insolubility of the product in most organic solvents including DMSO and DMF. A solid state NMR experiment was carried out to attempt to identify the target compound, but unfortunately the CH_2 signal that connects the tripodal core

with ligand **2.2** was not observed thus we cannot confirm the formation of compound **4.7**. In order to improve the solubility of compound **4.7**, an attempt to modify the structure was performed by reacting compound **4.7** with excess methyl iodide to give the methylated imidazolium derivative. Methyl iodide was added to a methanol solution containing compound **4.7** at 0 ^{o}C, and then solution was stirred and heated to 40 °C for 2 hours to afford compound **4.8** (Scheme 4.5). After compound **4.8** was isolated, a metathesis reaction with potassium hexafluorophosphate (KPF_6) was carried out to exchange the iodide ion with less coordinating hexafluorophosphate ion to obtain compound **4.9** (Scheme 4.5).

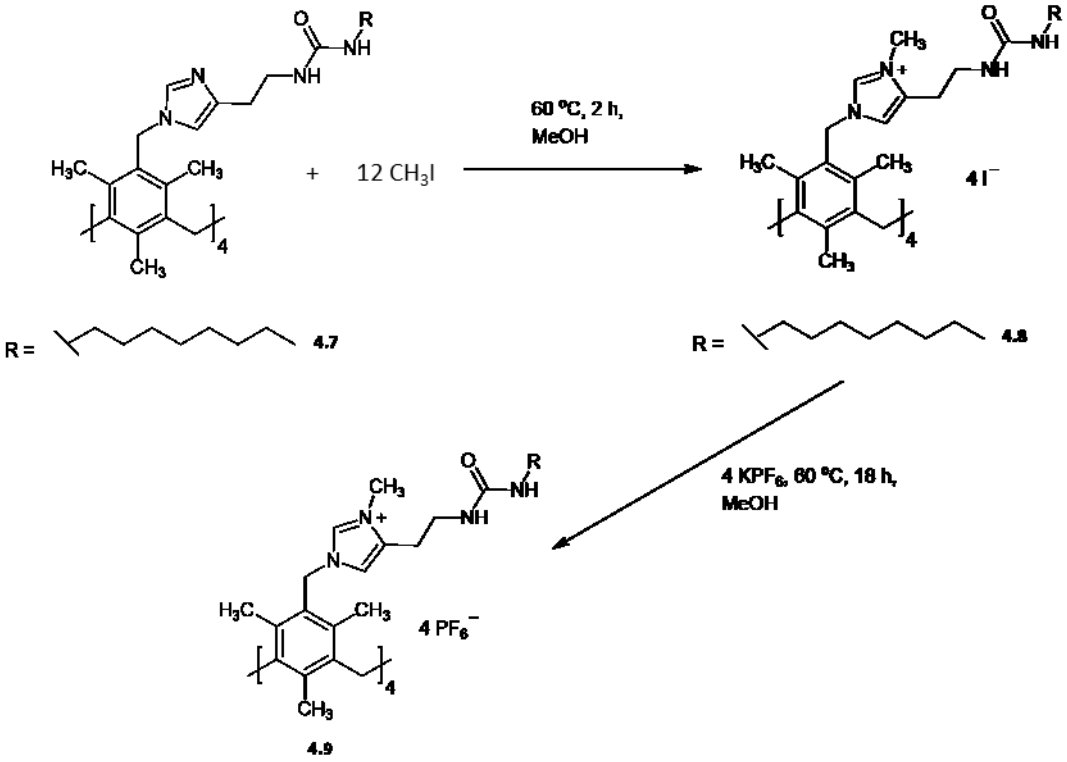

Scheme 4.5 Reaction of compound **4.7** with excess CH_3I and subsequent metathesis reaction with KPF_6 in methanol.

Although the final product, **4.9**, shows better solubility in DMSO and DMF, it remains insoluble in less polar solvents such as acetone and acetonitrile. However, ESI-MS analysis does not prove the formation of this compound as there are no molecular ion peaks that correspond to compound **4.9**. The ^{1}H NMR spectrum of compound **4.9** also show a mixture of broad signals that makes the characterisation difficult. Hence, it is

concluded that the attempt to modify the structure of compound **4.7** was unsuccessful and further work on these series was not carried out.

4.2.4 Anion binding studies of host 4.6

Host **4.6** is only soluble in polar solvents such as alcohols, DMF and DMSO, therefore for host **4.6**, anion binding titration experiments were performed with fluoride, nitrate, chloride and acetate ion as tetrabutylammonium salts in dimethylsulfoxide. From the ^{1}H NMR titration spectra of host **4.6** with chloride, it is observed that there were no significant changes on the chemical shift of Imidazole protons, H1 and H2 as well as urea protons, H3 and H4 (Figure 4.15 and 4.16). The possible explanation might be due to the competitiveness of DMSO solvent.

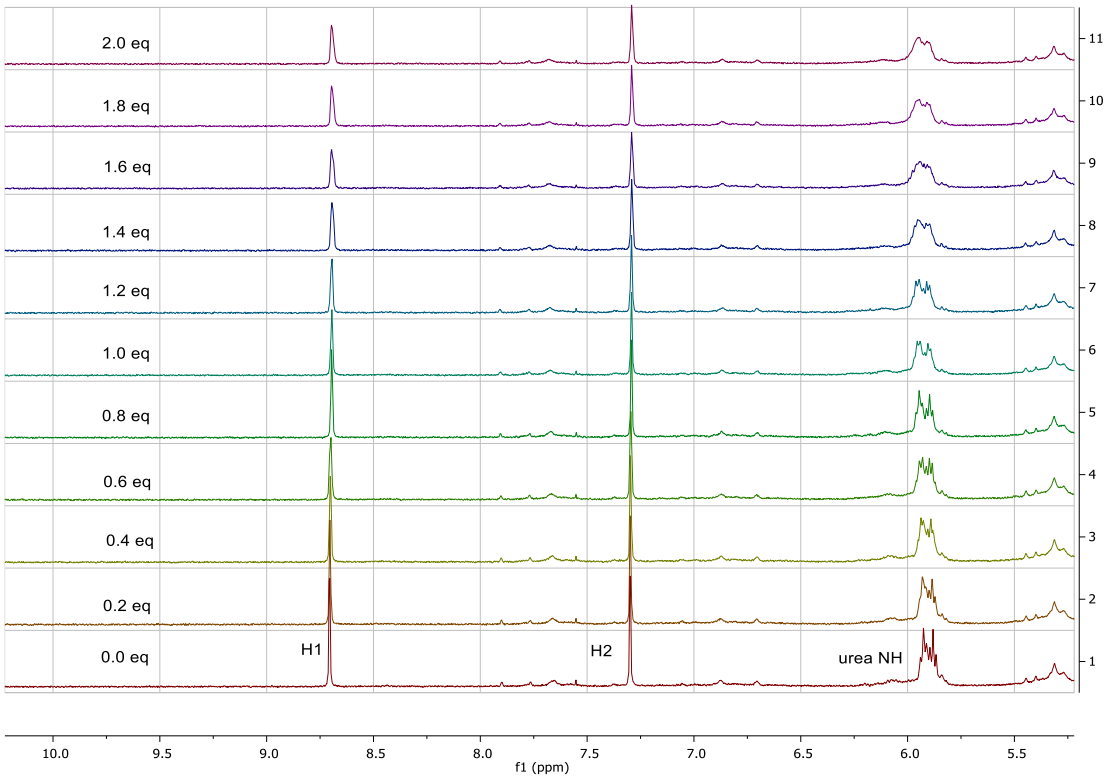

Figure 4.15 Stack plot showing the ^{1}H NMR spectrum of compound **4.6** in DMSO-d_6 in the presence of chloride ion as tetrabutylammonium salt.

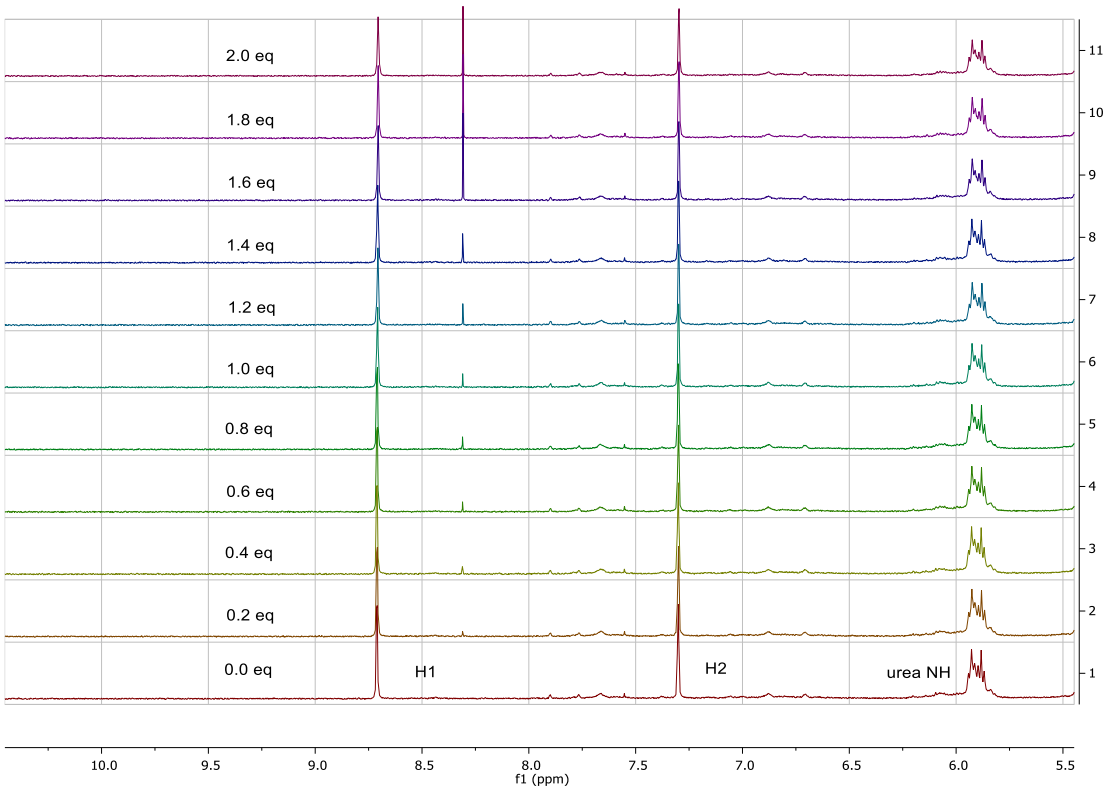

Figure 4.16 Stack plot showing the ^{1}H NMR spectrum of compound **4.6** in DMSO-d_6 in the presence of nitrate ion as tetrabutylammonium salt.

In contrast, the addition of 0.2 equivalent of acetate ion (as NBu_4^+ salt) results in the splitting of H1 and H2 signal at almost the same ratio (Figure 4.17), possibly due to the interaction of acetate with only one out of the two binding pockets.

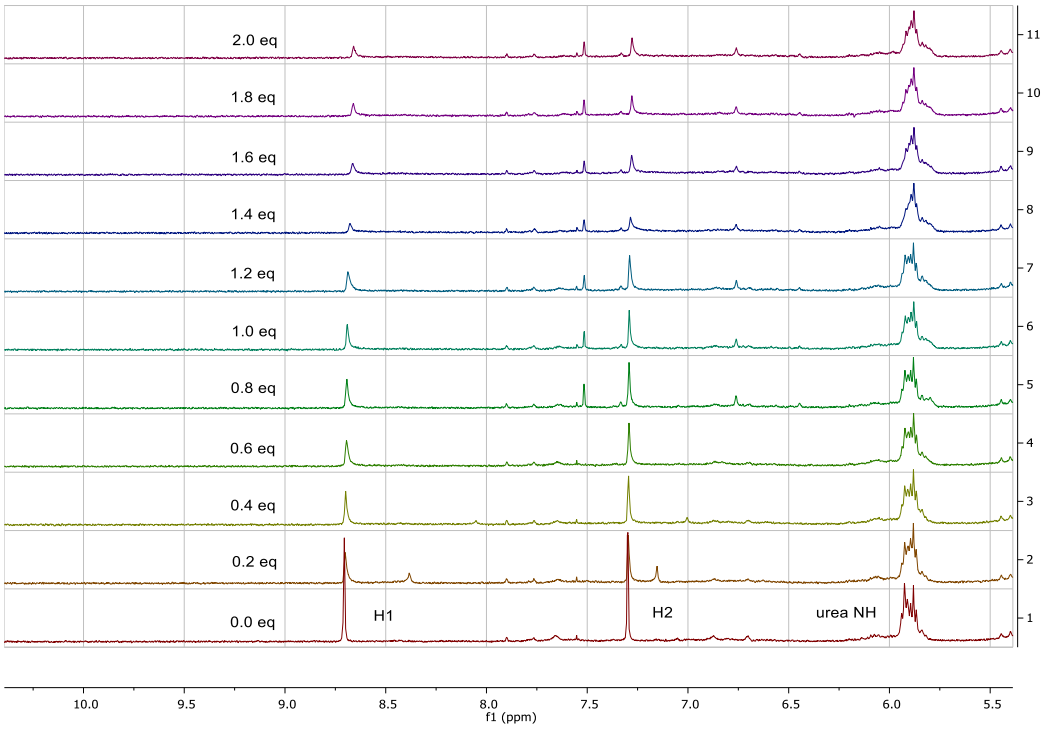

Figure 4.17 Stack plot showing the ^{1}H NMR spectrum of compound **4.6** in DMSO-d_6 in the presence of acetate ion as tetrabutylammonium salt.

From the X-ray crystal structure of ligand **2.1** discussed in Chapter 2, it is shown that the imidazole nitrogen can form self-complementary hydrogen bonding with NH of the other imidazole. There is a possibility that the presence of imidazole moiety in this compound might result in the formation of an array of self-complementary hydrogen bonds that is strong enough and resistant to anion binding. In order to probe the role of self-complementarity in host **4.6**, titration of host **4.6** with zinc(II) nitrate, zinc(II) chloride and zinc(II) acetate was undertaken. The presence of zinc ions will disrupt the NH···N hydrogen bond and leave the imidazole protons free to interact with the anion guest. The first titration was performed using zinc(II) nitrate in dimethylsulfoxide. The addition of 0.6 equivalent of zinc(II) nitrate results in small changes in the chemical shift of imidazole protons, H1 ($\Delta\delta$ 0.14 ppm) and H2 ($\Delta\delta$ 0.06 ppm). The downfield shift of H1 signal is due to the hydrogen bonding interaction with the oxygen atom of the nitrate ion, decreasing the electron density around the H1 proton (Figure 4.18).[34]

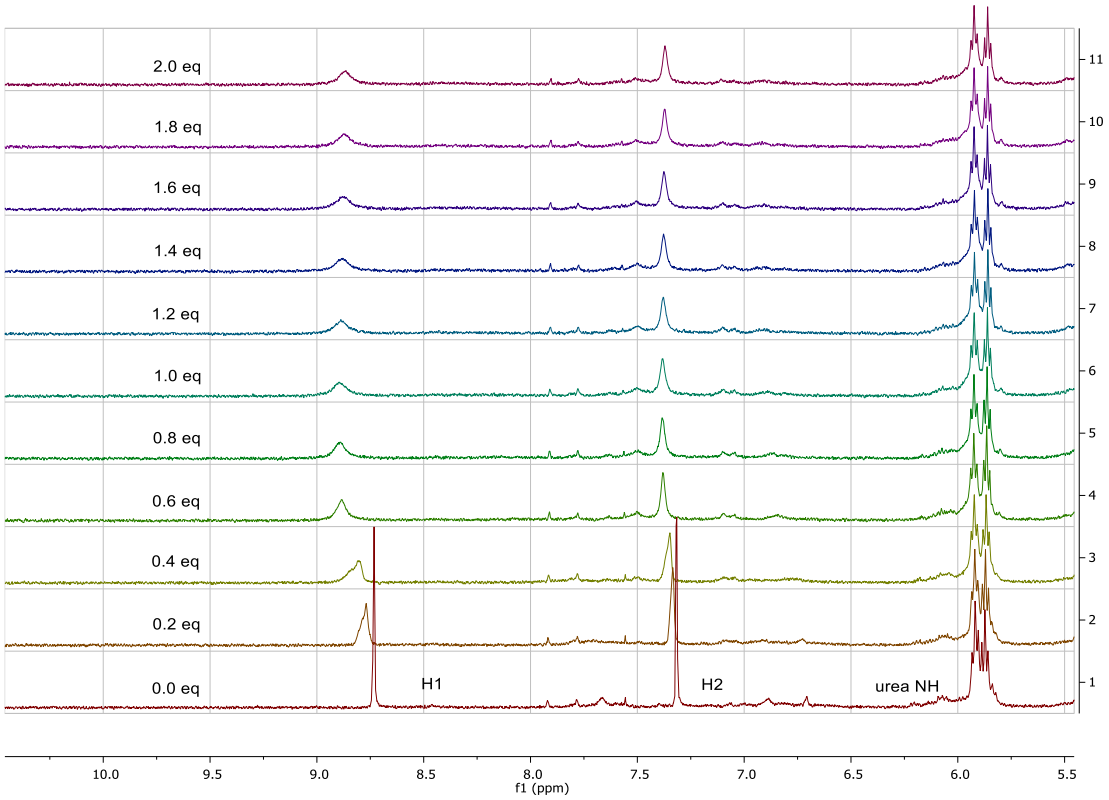

Figure 4.18 Stack plot showing the ^{1}H NMR spectrum of compound **4.6** in DMSO-d_6 in the presence of increasing equivalents of zinc(II) nitrate.

On the other hand, the titration experiment of host **4.6** with zinc(II) chloride and zinc(II) acetate was performed in a less competitive solvent, DMF-d_7. From the ^{1}H NMR spectrum (Figure 4.19), the addition of up to 1.0 equivalent of zinc(II) chloride results in the downfield shift of imidazole proton H1 and H2 from 8.98 and 7.61 ppm to 9.31 and 7.76 ppm, respectively. This result is in contrast to the titration experiment of host **4.6** with tetrabutylammonium chloride. The pronounced changes in the chemical shifts suggest that the zinc might coordinate to the imidazole nitrogen atom and the counter chloride ion of the zinc salt is forming hydrogen bonding with the H1 proton of the imidazole.

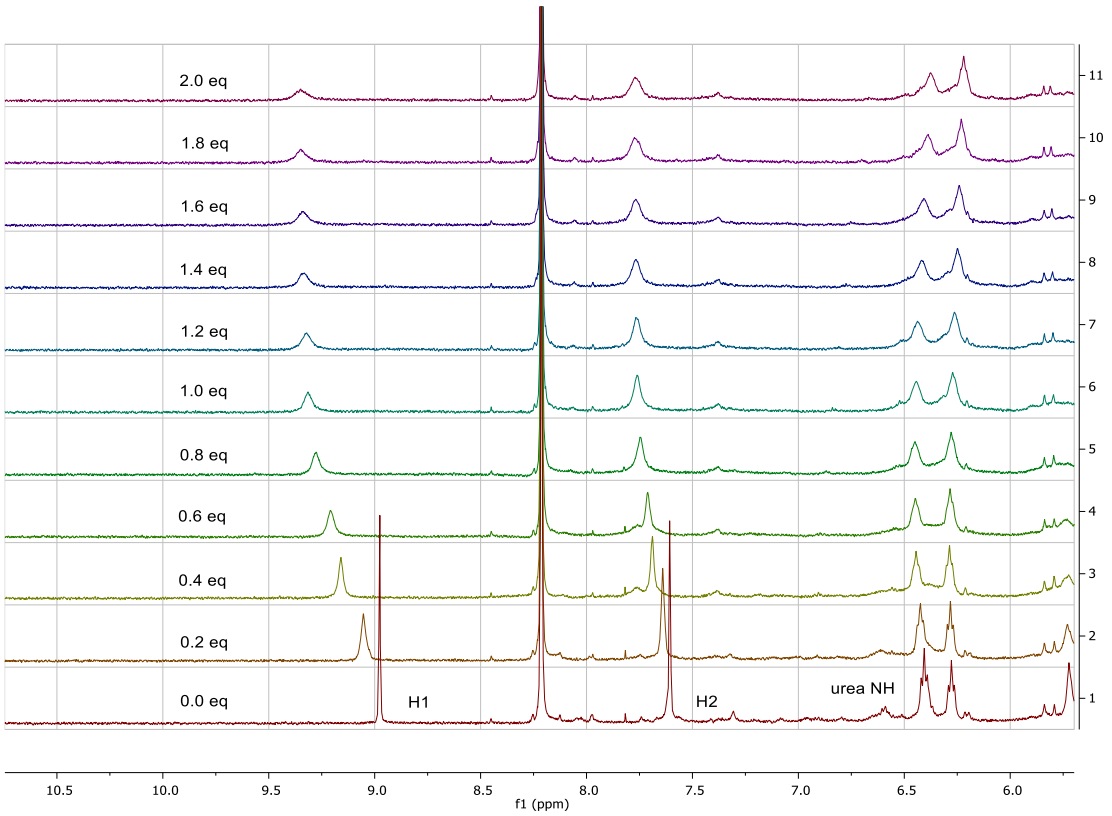

Figure 4.19 Stack plot showing the ^{1}H NMR spectrum of compound **4.6** in DMF-d_7 in the presence of zinc(II) chloride

Titration of host **4.6** with zinc(II) acetate has also been performed in DMF-d_7. This titration experiment shows a more complex binding pattern in comparison to the titration with zinc(II) nitrate and zinc(II) chloride (Figure 4.20). The addition of 0.2 equivalent of zinc(II) acetate results in the upfield shift of the imidazole proton H1 and H2 as well as urea NH, H3 and H4. Subsequent addition of 0.8 equivalent of zinc(II) acetate results in the disappearance of H1 and H3 signals. On the other hand, addition of 0.8 equivalent of zinc(II) acetate cause the broadening of H2 signal that eventually emerges as a sharp peak after the addition of more than 1.0 equivalent of zinc(II) acetate. It is suggested that the disappearance of the H1 and H3 proton signals may be due to deprotonation or slow kinetics of anion exchange on the NMR timescale.[11] The titration data with zinc(II) acetate is atypical and clearly indicative of more than one binding process.

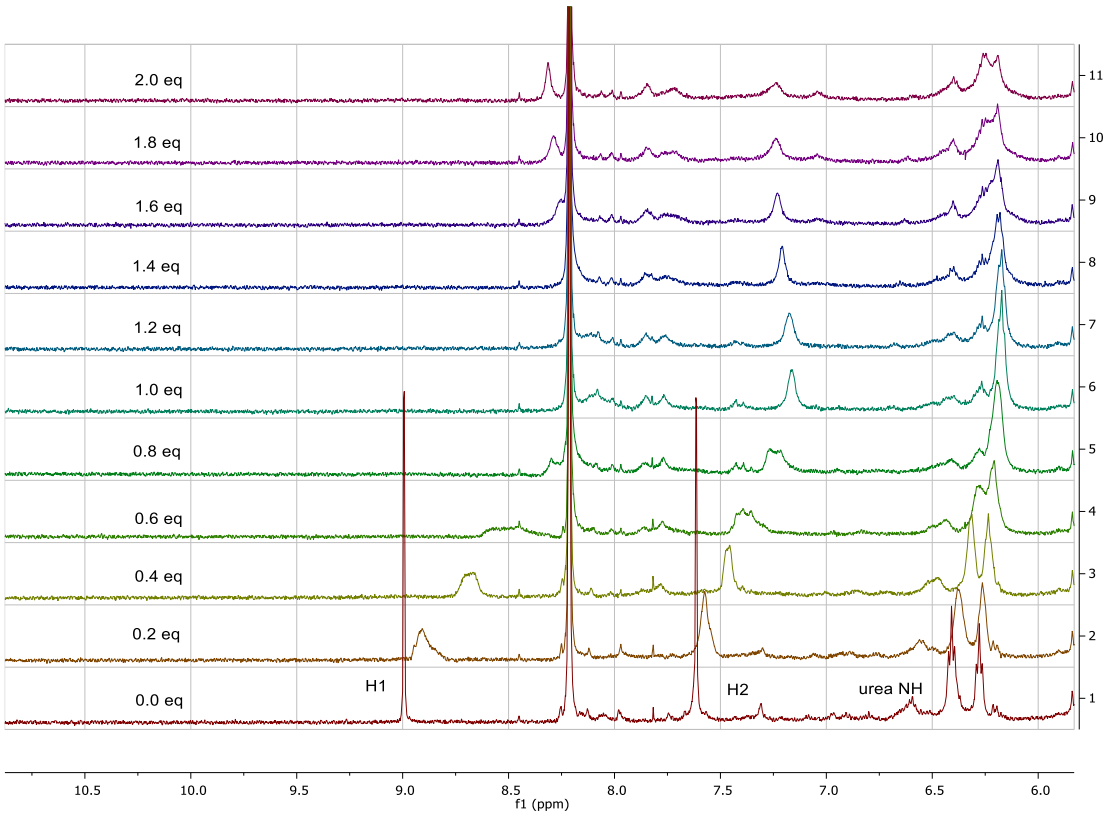

Figure 4.20 Stack plot showing the ^{1}H NMR spectrum of compound **4.6** in DMF-d_7 in the presence of zinc(II) acetate.

4.3 Summary

A series of tripodal hosts, **4.1** – **4.3** have been synthesised from the reaction of tribromotriethylbenzene with respective imidazole urea ligands, **2.2**, **2.3** and **2.4**. ^{1}H NMR titration experiment of host **4.2** with fluoride, chloride and acetate ion (as NBu_4^+ salt) has been performed. The addition of fluoride and acetate induced colour changes of the solution from yellow to pink, suggesting the deprotonation of imidazole protons, H1 and H2 by these strong basic anions. These findings are in contrast to the anion titration experiment performed on the free ligand **2.3** in chloroform in which upon the addition of the anions, the signals that are perturbed are urea N-H, H3 and H4. The addition of chloride ion to the solution of host **4.2** in DMSO does not impart any effect on the chemical shifts of all the designated proton signals, H1, H2 as well as urea N-H. Similar results were obtained in the titration experiment of host **4.3** on tetrabutylammonium chloride and tetrabutylammonium acetate. These findings suggest that this system might not be a suitable system for anion sensing, at least not

in a competitive solvent. It is envisaged that the presence of imidazole moiety, which can form a hydrogen-bonded network might inhibit the interaction of anions with the urea group. However, without more structural information, it is not possible to accurately assign the mechanism of this interaction. A mesitylcalixarene-based host **4.6**, has also been synthesised and its interaction with chloride, acetate and nitrate ions has been investigated. The ^{1}H NMR titration experiment was carried out using two different conditions; the first condition is the titration experiment is performed using tetrabutylammonium salts of chloride, acetate and nitrate whereas, in the second condition, the tetrabutylammonium salts were replaced with zinc(II) chloride, zinc(II) acetate and zinc(II) nitrate. It is found that, without the presence of zinc metal, no interaction was observed between the designated protons with the anions. However, when zinc(II) salts were used, there are some changes in the chemical shift of imidazole and urea protons. The plausible explanation for this result could be due to the coordination of zinc to the imidazole nitrogen atom, hence disrupting the hydrogen-bonding network form by the imidazole moiety.

4.4 Experimental

All solvents used in the synthesis and purification were of analytical reagent grade. Anhydrous solvents were prepared on an SPS solvent purification system. Commercial reagents were used as supplied, without further purification.

4.4.1 General Procedure for ^{1}H NMR spectroscopic experiments

^{1}H-NMR spectroscopic titration experiments were carried out using Varian Mercury 400 spectrometer running at 400 MHz, at room temperature. All chemical shifts are reported in ppm. A specific concentration of host was made up in a single NMR tube in the desired deuterated solvent (0.5 mL). The anions, as their tetrabutylammonium salts, were made up to 1 mL, 5 times the concentration of the host, with the desired deuterated solvent. 10 µL aliquots of the guest were added to the NMR tube and the spectra were recorded after each addition.

4.4.2 Instrumentation

All NMR spectra were obtained from a Bruker Avance 400 at a frequency of 400 MHz for ^{1}H and 100 MHz for ^{13}C, while ^{1}H-^{1}H COSY, ^{1}H-^{13}C HSQC and ^{1}H-^{13}C HMBC spectra were obtained from a Varian INOVA 500 spectrometer at a frequency of 500 MHz for ^{1}H and 125 MHz for ^{13}C. All chemical shifts are reported in parts per million (δ) relative to tetramethylsilane as an internal reference. Electrospray ionisation (ESI) mass spectrometry was recorded on a TQD mass spectrometer instrument. Fourier transform infrared spectra were recorded with a Perkin Elmer Spectrum 100 FT-IR spectrometer in which for each spectrum, 64 scans were conducted over a spectral range of 4000 to 600 cm^{-1} with a resolution of 4 cm^{-1}. Elemental analysis was performed using an Exeter Analytical CE-400 Elemental Analyser.

4.4.3 Synthesis of compounds

4.4.3.1 Synthesis of compound **4.1**

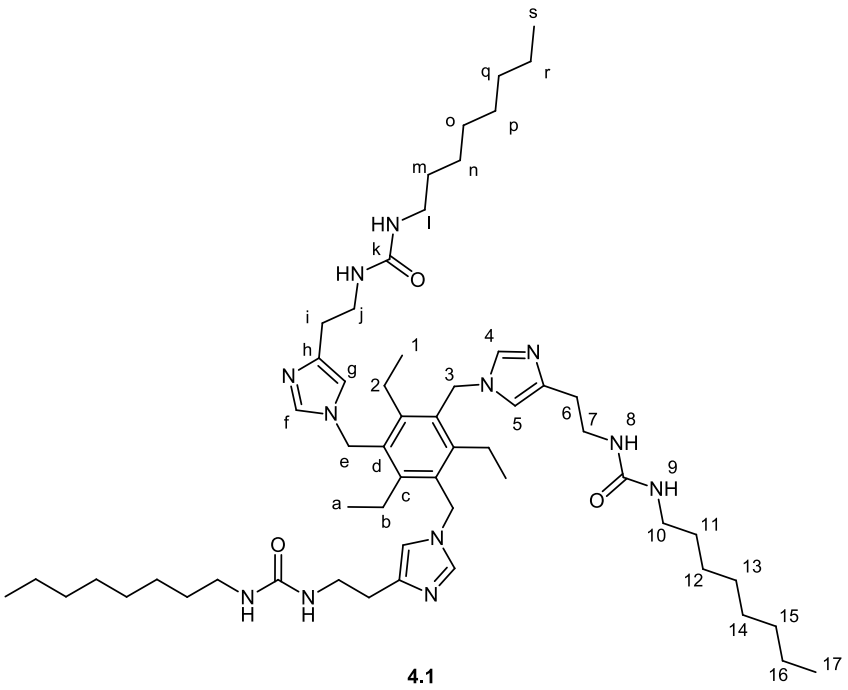

4.1

1,3,5-tribromo-2,4,6-triethylbenzene (0.66 g, 1 mmol) and 1-[2-(1*H*-imidazol-4-yl)ethyl]-3-(octyl)urea, **2.2** (1.0655 g, 4 mmol) were added to a flask and dissolved in dry tetrahydrofuran (50 mL). The solution was stirred and heated to reflux at 60 °C for 24 hours resulting in a brown sticky oil. The solvent was removed while it is still warm and the sticky oil was evaporated to dryness. Unoptimised yield = 0.28 g, 0.24 mmol, 25 %.**^{1}H NMR:** δ_H (400 MHz; $CDCl_3$; Me_4Si) 8.94 (3 H, s, *H4*), 7.38 (3 H, s, *H5*), 6.00 (3 H, t, *J* 5.6, *H8*), 5.92 (3 H, t, *J* 5.6, *H9*), 5.35 (6 H, s, *H3*), 3.26 (6 H, m, *H6*), 3.21 (6 H, q, *H7*), 2.70 (6 H, t, *J* 7.1 *H10*), 2.47 (6 H, t, *J* 5.6, *H2*), 1.20 (36 H, m, *H11-H16*), 0.81 (18 H, t, *J* 8.0, *H1 & H17*). **^{13}C NMR:** δ_C {^{1}H} (101 MHz; $CDCl_3$) 158.44 (*Ck*), 147.01 (*Cf*), 135.28 (*Cg*), 134.11 (*Ch*), 131.83 (*Cd*), 116.46 (*Cc*), 47.26 (*Ce*), 39.80 (*Cj*), 31.68 (*Ci*), 30.39 (C*b*), 29.12 (C*l*), 26.85 (C*m*), 26.05 (C*o*), 23.47 (*Cp*), 22.52 (C*q*), 22.56 (C*r*), 15.58 (Ca), 14.42 (C*s*). **FTIR:** ν_{max}/cm^{-1} 3102 (N-H), 1611 (C=O), 1560 (C=C imidazole ring), 1483 (C=N-C=C imidazole). m/z (ESI-MS) 499 $[M+2H^+]^{2+}$ and 1019 $[M+NH_4^+]^+$. Due to the impurity of the sample, elemental analysis did not give usable information.

4.4.3.2 Synthesis of compound **4.2**

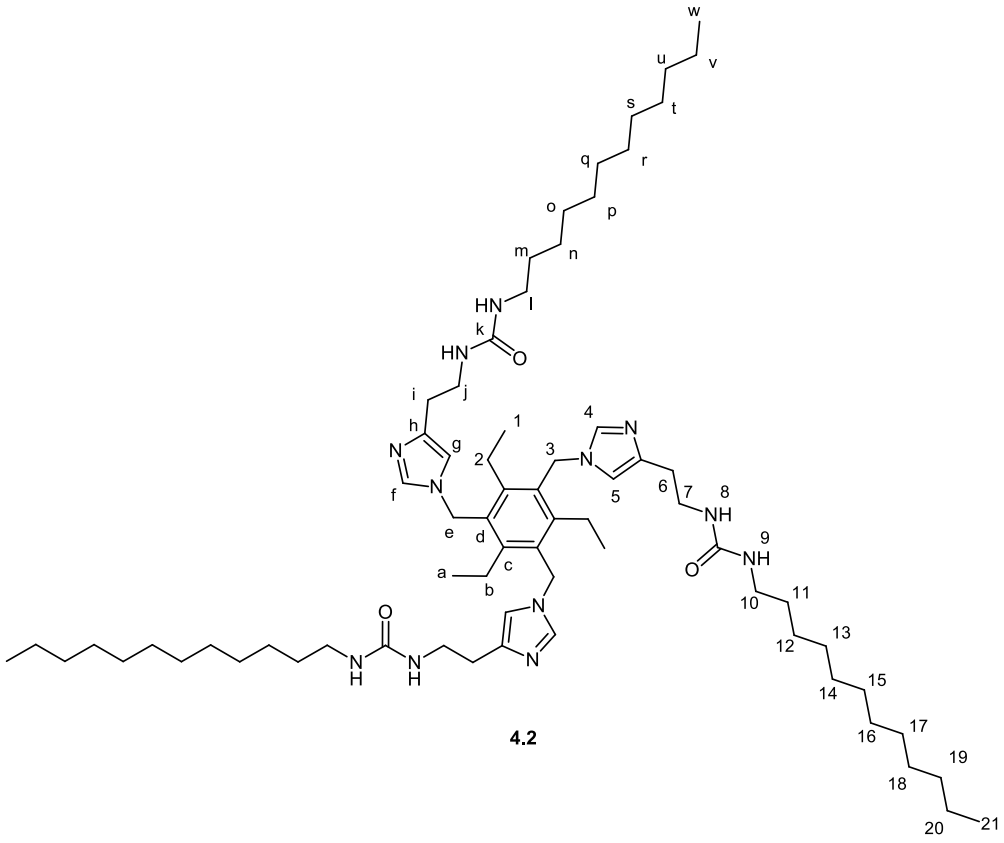

4.2

1,3,5-tribromo-2,4,6-triethylbenzene (0.66 g, 1 mmol) and 1-[2-(1*H*-imidazol-4-yl)ethyl]-3-(dodecyl)urea, **2.3** (1.935 g, 6 mmol) were added to a flask and dissolved in dry tetrahydrofuran (50 mL). The solution was stirred and heated to reflux at 60 °C for 48 hours resulting in a yellow sticky oil. The solvent was removed while it is still warm and the sticky yellow oil was evaporated to dryness. Unoptimised yield = 0.52 g, 0.45 mmol, 45 %.

^{1}H NMR: δ_H (400 MHz; $CDCl_3$; Me_4Si) 7.60 (3 H, s, *H4*), 6.82 (3 H, s, *H5*), 5.86 (3 H, t, *J* 5.6, *H8*), 5.85 (3 H, t, *J* 5.6, *H9*), 5.19 (6 H, s, *H3*), 3.23 (6 H, m, *H6*), 3.14 (6 H, q, *H7*), 2.91 (6 H, t, *J* 7.1 *H10*), 2.65 (6 H, t, *J* 5.6, *H2*), 1.22 (36 H, m, *H11-H20*), 0.83 (18 H, t, *J* 8.0, *H1 & H21*).

^{13}C NMR: δ_C {^{1}H} (101 MHz; $CDCl_3$) 158.41 (*Ck*), 146.82 (*Cf*), 136.08 (*Cg*), 134.46 (*Ch*), 133.02 (*Cd*), 116.87 (*Cc*), 45.20 (*Ce*), 39.01 (*Cj*), 31.74 (*Ci*), 30.43 (C*b*), 29.50 (C*l*), 29.46 – 22.52 (C*m-Cv*), 15.55 (Ca), 14.38 (C*w*). **FTIR:** ν_{max}/cm^{-1} 3104 (N-H), 1670 (C=O), 1600 (C=C imidazole ring), 1448 (C=N-C=C imidazole). m/z (ESI-MS) 583 $[M+2H^+]^{2+}$ and 1187

[M+Na$^+$]$^+$. Due to the impurity of the sample, elemental analysis did not give usable information.

4.4.3.3 Synthesis of compound **4.3**

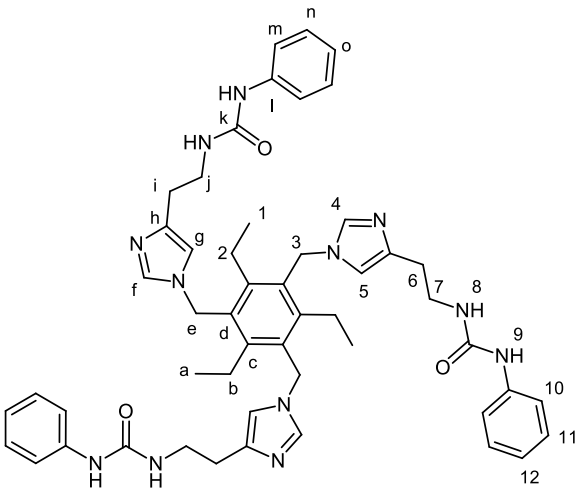

4.3

1-[2-(1*H*-imidazol-4-yl)ethyl]-3-(*p*-tolyl)urea, **2.4** (1.935 g, 3 mmol) and cesium carbonate (0.977 g, 3 mmol) were mixed and stirred for 2 hours at 40**°**C in dry tetrahydrofuran (50 mL). Then, a THF solution of 1,3,5-tribromo-2,4,6-triethylbenzene (0.66 g, 1 mmol) were added to the reaction mixture. The solution was stirred and heated to reflux at 60 °C for 48 hours resulting in a white solid. After 48 hours reaction, the solvent was removed and the white precipitate was washed with water (20ml x 3) and acetone (20ml x 3) to remove excess caesium carbonate. The white precipitate was then dried in the desiccator. Unoptimised yield = 0.38 g, 0.41 mmol, 41 %.

^{1}H NMR: δ_H (400 MHz; DMSO-d_6; Me_4Si) 8.78 (3 H, s, *H4*), 8.06 (3 H, d, *J* 1.1, *H5*), 7.25 (6 H, m, *H10*), 6.96 (6 H, m, *H11*), 6.66 (3 H, d, *J* 1.1, *H9*), 5.53 (3 H, t, *J* 5.7, *H8*), 5.36 (6 H, s, *H3*), 3.09 (6 H, s, *H6*), 2.48 (6 H, s, *H7*), 2.06 (6 H, s, *H2*), 0.94 (18 H, t, *J* 5.7, *H1 & H12*).

^{13}C NMR: δ_C {^{1}H} (101 MHz; DMSO) 156.03 (*Ck*), 138.24 (*Cf*), 130.28 (*Cd, Ch and Cc*), 129.37 (*Cl*), 118.08 (*Cm*), 37.37 (*Ce*), 31.13 (*Ci*), 25.17 (*Cj*), 20.71 (*Cb*), 15.96 (*Cn & Ca*). **FTIR:** ν_{max}/cm^{-1} 3120 (N-H), 1610 (C=O), 1570 (C=C imidazole ring), 1458 (C=N-C=C imidazole). Due to the impurity of the sample, elemental analysis did not give usable information.

4.4.3.4 Synthesis of Mesityl calix[4]arene **4.4**

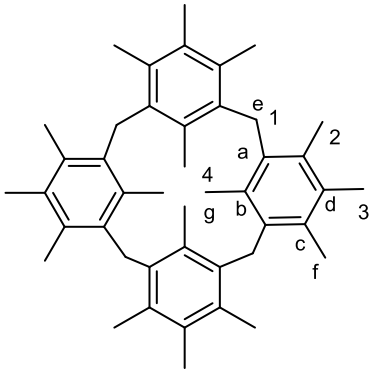

4.4

Under a constant stream of N_2, $SnCl_4$ (0.7 mL, 2.69 mmol) was added to a solution of α-chloroisodurene (5.0g, 39 mmol) in dry CH_2Cl_2 (50 mL). The mixture was stirred and heated under reflux at 62 °C for 2h, resulting in a colour change from colourless to red and subsequent formation of white precipitate. The solution mixture was then hydrolysed and extracted with two portions of CH_2Cl_2 (25mL each). Both layers were separated using separatory funnel and the white precipitate obtained was filtered and dried under vacuum. The pure product was recrystallised from CH_2Cl_2 and ethyl acetate. Yield = 4.67 g, 31.9 mmol, 82 %. **^{1}H NMR:** δ_H (400 MHz; $CDCl_3$; Me_4Si) 6.84 (4 H, s, *H4*), 3.93 (8 H, s, *H1*), 2.38 (24 H, s, *H2*), 1.23 (12 H, s, *H3*) **^{13}C NMR:** δ_C {^{1}H} (101 MHz; $CDCl_3$) 137.63 (*Cc*), 135.91 (*Cd*), 133.24 (*Ca*), 130.33 (*Cb*), 31.93 (*Ce*), 21.43 (*Cf*), 17.96 (*Cg*). **FTIR:** ν_{max}/cm^{-1} 2967 (CH aromatic ring), 1471 (C=C aromatic ring), m/z (ESI-MS) 551.35 $[M+Na]^+$. Elem. Anal. Calc. (%) ($C_{40}H_{48}$) C, 90.89; H, 9.10; Found (%): C, 90.08, H, 9.01%.

4.4.3.5 Synthesis of Tetrakis-*p*-bromomethylated mesityl calix[4]arene **4.5**

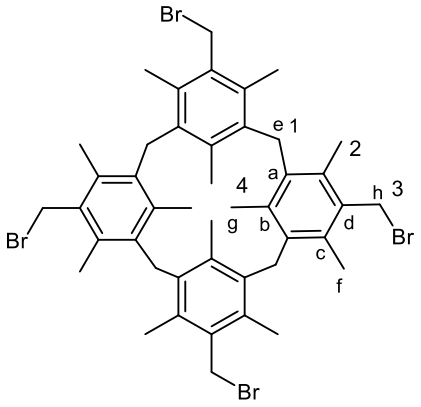

4.5

A mixture of 0.5 molar equivalent (to calixarene) of zinc and HBr (33% in acetic acid) (2mL) was stirred and heated in glacial acetic acid (20 mL) until the zinc was fully dissolved. To this solution mixture, mesityl calix[4]arene (**4.4**) (0.53g, 1.00 mmol), paraformaldehyde (1.5 g, 51.7 mmol), and HBr (33% in acetic acid) (10 mL) was added slowly and heated to reflux for 48 h at 90 ºC. White precipitate formed was filtered and washed thoroughly with water (25 mL), diethyl ether (25 mL) and again with water (25 mL) then dried under vacuum. Yield = 0.76 g, 0.85 mmol, 85 %.**^{1}H NMR:** δ_H (400 MHz; $CDCl_3$; Me_4Si) 4.66 (8 H, s, *H3*), 4.04 (8 H, s, *H1*), 2.47 (24 H, s, *H2*), 1.11 (12 H, s, *H4*) **^{13}C NMR:** δ_C {^{1}H} (101 MHz; $CDCl_3$) δ_C {^{1}H} (101 MHz; $CDCl_3$) 138.06 (8 C, *Cc*), 136.61 (4 C, *Cd*), 133.25 (8 C, *Ca*), 131.88 (4 C, *Cb*), 32.94 (4 C, *Ce*), 20.65 (4 C, *Ch*), 18.73 (4 C, *Cg*), 16.70 (4 C, *Cf*). **FTIR:** ν_{max}/cm^{-1} 2938 (CH aromatic ring), 1448 (C=C aromatic ring). m/z (ESI-MS) 923.3 $[M+Na]^+$. Elem. Anal. Calc. (%) ($C_{44}H_{52}Br_4$) C, 58.69; H, 5.82; Found (%): C, 57.9, H, 5.83%.

4.4.3.6 Synthesis of compound **4.6**

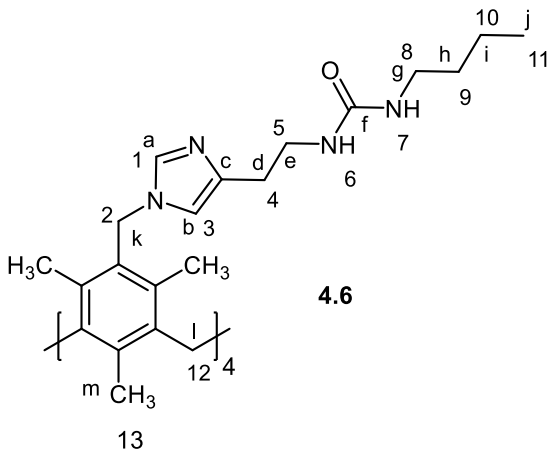

Compound **4.5** (0.50 g, 0.55 mmol) and 1-[2-(1*H*-imidazol-4-yl)ethyl]-3-(butyl)urea, **2.1** (0.53 g, 2.55 mmol) were added to a flask and dissolved in dry tetrahydrofuran (50 mL). The solution was stirred and heated to reflux at 60 °C for 24 hours resulting in a yellow sticky precipitate. The precipitate was filtered, washed with tetrahydrofuran (3 x 25 mL) and and dried under vacuum to give the imidazole tetrapod. Unoptimised yield = 1.92 g, 1.35 mmol, 61%.

^{1}H NMR: 8.88 (4 H, s, *H1*), 7.38 (4 H, s, *H3*), 5.97 (4 H, t, *J* 5.9, *H6*), 5.90 (4 H, t, *J* 5.7, *H7*), 3.60 (8 H, m, *H2*), 3.29 (8 H, dt, *H5*), 2.96 (8 H, dt, *H8*), 2.73 (8 H, t, *J* 6.8, *H4*), 2.33 (24 H, s, *H12*), 1.76 (8 H, m, *H13)***,** 1.32 (8 H, m, *H9*), 1.25 (8 H, m, *H10*), 0.84 (12 H, t, *J* 7.1, *H11)* **^{13}C NMR:** δ_C {^{1}H} (101 MHz; DMSO-d_6) 163.85 (4 C, *Cf*), 136.98 (4 C, *Ca*), 120.96 (4 C, *Ck*), 72.48 (4 C, *Cc*), 43.31 (4 C, *Cd*), 37.16 (8 C, *Ce* and *Cg*), 31.10 (4 C, *Cl*), 30.30 (4 C, *Cj*), 24.75 (8 C, *Ch* and *Ci*), 18.69 (4 C, *Cm*) **FTIR:** ν_{max}/cm^{-1} 3302 and 2956 (NH), 1632 (CO), 1555 (imid. ring). m/z (ESI-MS) 1439.9 $[M+Na]^+$, 731.7 $[(M/2)+2Na^+]^{2+}$, 473.6 $[(M/3)+3H^+]^{3+}$. Due to the impurity of the sample, elemental analysis did not give usable information.

4.5 References

(1) Gonzalez, M. del C.; Oton, F.; Espinosa, A.; Tarraga, A.; Molina, P. *Org. Biomol. Chem.* **2015**, *13* (5), 1429–1438.

(2) Nadella, S.; Sahoo, J.; Subramanian, P. S.; Sahu, A.; Mishra, S.; Albrecht, M. *Chem. Eur. J.* **2014**, *20* (20), 6047–6053.

(3) Korostynska, O.; Mason, a.; Al-Shamma'a, a. *Int. J. Smart Sens. Intell. Syst.* **2012**, *5* (1), 149–176.

(4) Barnard, A.; Dickson, S. J.; Paterson, M. J.; Todd, A. M.; Steed, J. W. *Org. Biomol. Chem.* **2009**, *7* (8), 1554–1561.

(5) Hirschhaeuser, F.; Sattler, U. G. A.; Mueller-Klieser, W. *Cancer Res.* **2011**, *71* (22), 6921–6925.

(6) Butler, S. J.; McMahon, B. K.; Pal, R.; Parker, D.; Walton, J. W. *Chem. Eur. J.* **2013**, *19* (29), 9511–9517.

(7) Vickers, M. S.; Martindale, K. S.; Beer, P. D. *J. Mater. Chem.* **2005**, *15*, 2784.

(8) Babu, J. N.; Bhalla, V.; Kumar, M.; Puri, R. K.; Mahajan, R. K. *New J. Chem.* **2008**, *33*, 675–681.

(9) Li, X.; Shen, B.; Yao, X.-Q.; Yang, D. *J. Am. Chem. Soc.* **2007**, *129* (23), 7264–7265.

(10) Zheng, Y.; Wang, Q.; Tan, C. *Luminescence* **2012**, *27* (4), 302–306.

(11) Kundu, T.; Chowdhury, A. D.; De, D.; Mobin, S. M.; Puranik, V. G.; Datta, A.; Lahiri, G. K. *Dalton Trans.* **2012**, *41* (15), 4484–4496.

(12) Li, J.-B.; Hu, J.-H.; Chen, J.-J.; Qi, J. *Spectrochim. Acta. A. Mol. Biomol. Spectrosc.* **2014**, *133C*, 773–777.

(13) Kumari, N.; Jha, S.; Bhattacharya, S. *J. Org. Chem.* **2011**, *76* (20), 8215–8222.

(14) Hong, S.-J.; Lee, C.-H. *Tetrahedron Lett.* **2012**, *53* (25), 3119–3122.

(15) Langton, M. J.; Beer, P. D. *Chem. Eur. J.* **2012**, *18* (45), 14406–14412.

(16) Ravikumar, I.; Ghosh, P. *Chem. Soc. Rev.* **2012**, *41* (8), 3077–3098.

(17) Langton, M. J.; Duckworth, L. C.; Beer, P. D. *Chem. Commun.* **2013**, *49*, 8608–8610.

(18) Gartia, M. R.; Braunschweig, B.; Chang, T.-W.; Moinzadeh, P.; Minsker, B. S.; Agha, G.; Wieckowski, A.; Keefer, L. L.; Liu, G. L. *J. Environ. Monit.* **2012**, *14* (1), 3068–3075.

(19) Capitán-Vallvey, L. F.; Arroyo-Guerrero, E.; Fernández-Ramos, M. D.; Santoyo-Gonzalez, F. *Anal. Chem.* **2005**, *77* (14), 4459–4466.

(20) Ali, H. D. P.; Kruger, P. E.; Gunnlaugsson, T. *New J. Chem.* **2008**, *32* (7), 1153.

(21) Gogoi, A.; Das, G. *Cryst. Growth Des.* **2012**, *12* (8), 4012–4021.

(22) Soriano, M. L.; Lenthall, J. T.; Anderson, K. M.; Smith, S. J.; Steed, J. W. *Chem. Eur. J.* **2010**, *16* (35), 10818–10831.

(23) Karbarz, M.; Romański, J. *Inorg. Chem.* **2016**, *55* (7), 3616–3623.

(24) Swinburne, A. N.; Paterson, M. J.; Fischer, K. H.; Dickson, J.; Wallace, E. V. B.; Belcher, W. J.; Beeby, A.; Steed, J. W. *Chem. Eur. J.* **2010**, *16*, 1480–1492.

(25) Filby, M. H.; Dickson, S. J.; Zaccheroni, N.; Prodi, L.; Bonacchi, S.; Montalti, M.; Paterson, M. J.; Humphries, T. D.; Chiorboli, C.; Steed, J. W. *J. Am. Chem. Soc.* **2008**, *130* (12), 4105–4113.

(26) Sawada, T.; Hisada, H.; Fujita, M. *J. Am. Chem. Soc.* **2014**, *136* (12), 4449–4451.

(27) Willans, C. E.; Anderson, K. M.; Junk, P. C.; Barbour, L. J.; Steed, J. W. *Chem Commun.* **2007**, *35*, 3634–3636.

(28) Evans, R.; Deng, Z.; Rogerson, A. K.; McLachlan, A. S.; Richards, J. J.; Nilsson, M.; Morris, G. A. *Angew. Chemie - Int. Ed.* **2013**, *52* (11), 3199–3202.

(29) Turner, D. R.; Paterson, M. J.; Steed, J. W. *J. Org. Chem.* **2006**, *71* (4), 1598–1608.

(30) Pramanik, A.; Khansari, M. E.; Powell, D. R.; Fronczek, F. R.; Hossain, M. A. *Org. Lett.* **2014**, *16* (2), 366–369.

(31) Shimazu, H.; Yamanaka, M. *Asian J. Org. Chem.* **2014**, *3* (8), 847–850.

(32) Willans, C. E.; Anderson, K. M.; Potts, L. C.; Steed, J. W. *Org. Biomol. Chem.* **2009**, *7* (13), 2756–2760.

(33) Bullough, E. K.; Kilner, C. A.; Little, M. A.; Willans, C. E. *Org. Biomol. Chem.* **2012**, *10* (14), 2824–2829.

(34) Routasalo, T.; Helaja, J.; Kavakka, J.; Koskinen, A. M. P. *European J. Org. Chem.* **2008**, No. 18, 3190–3199.

Chapter 5

Ruthenium-based tripodal anion hosts

5.1 Background and Project Aims

In recent years, there has been an increasing interest in the use of transition metal ions as sensing and structural elements in the design of supramolecular hosts for anions.[1–5] The main reason is due to the diversity of their geometries, redox activities, photophysical activities and their ability to act as Lewis acids.[6] Metal-based receptors can offer a combination of electrostatic attraction coordination and hydrogen bonds to interact with guest molecules or ions. Hydrogen bond donor unit such as O-H and N-H group are often incorporated into the metal-based receptors to permit the sensing of the anions. The presence of metal as a core unit can enhance hydrogen bond donor ability owing to its electron withdrawing characteristics, hence increase the strength of host-guest interaction.[7]

The use of capping ligands has been extensively studied in the design of bipodal and tripodal anion sensors incorporating a metal scaffold. For instance, anion receptors having an (arene)ruthenium(II) core, **1.80** reported by Mishra and co-workers, also comprises a bis-pyridine amide ligand as a hydrogen-bonding unit.[8] This ruthenium-based metallabowl shows high selectivity and sensitivity for carboxylates such as oxalate, tartrate and citrate in methanol with binding constants of 4 x 10^4 M^{-1}, 5 x 10^4 M^{-1} and 5.5 x 10^4 M^{-1}, respectively. In other work, Dickson and co-workers have prepared semilabile (arene)ruthenium(II) piano stool type complexes (**1.62a** - **1.62c**), consisting of pyridine amine as the anion recognition unit.[9] These coordination compounds are able to coordinate to selected anions and can potentially be explored as fluorescent anion sensors. However, the use of aromatic *p*-cymene group as the capping ligand can lead to the formation of $[ML_2X]^+$ dipodal complex instead of forming fully tri-substituted $[ML_3]^{2+}$ as desired and the ruthenium arene bond can be subject to solvolysis.

Hence, the limitation of *p*-cymene group has directed further research work on the use of another capping ligand, for instance, 1,4,7-trithiacyclononane ([9]ane-S_3) which was

used extensively in this study. This capping ligand is a better choice than *p*-cymene as it can retain the octahedral nature of the Ru(II) core, with 90° angle between the ligands, which has been demonstrated by Todd and co-workers in their work.[10] The ruthenium(II) complexes reported, **5.1**-**5.5** function as supramolecular receptors for anions via three tripodally arranged 3-aminopyridine ligands. Of all the receptors synthesised, receptor **5.5** shows the highest affinity for anions as **5.5** contains a urea moiety that can form two hydrogen bonds with anions. Overall, all the tripodal receptors show a better affinity towards anions in comparison with metal complex with single pyridyl ligand **5.6**,[11] a reflection of the multiple binding groups and positive charge.

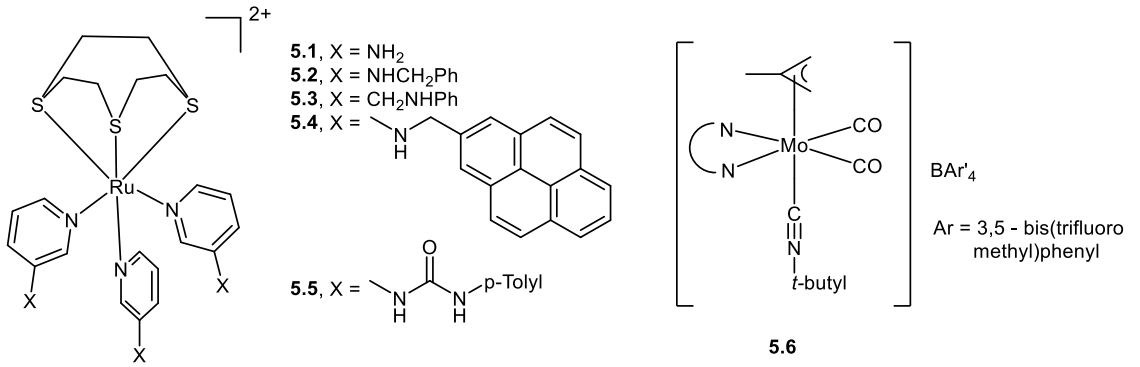

5.6

The use of this ([9]ane-S_3)Ru(II) core to allow the synthesis of tripodal receptors of well-defined geometry has been proved successful in previous work.[10,12,13] Hence, our aim is to synthesise tripodal receptors incorporating ([9]ane-S_3)Ru(II) as the core unit and imidazole urea as the anion binding functionality, investigate their interaction with various anions and compare their anion binding interaction with the free ligands (as discussed in Chapter 2) and previously reported tripodal receptors.

5.2 Results and discussion

5.2.1 Synthesis of the ruthenium complexes of imidazole urea

The [9]ane-S_3-capped ruthenium precursor was successfully synthesised by reacting $[RuCl_2(DMSO)_4]$ with the thioether ring, in which the former was obtained from the reaction between $RuCl_3$ and DMSO as described in the literature.[10] Metathesis of the counter anions from chloride to hexafluorophosphate or triflate was achieved through the addition of silver salts (e.g $AgPF_6$ or $AgCF_3SO_3$) and subsequent removal of the precipitated AgCl, and was carried out prior the addition of the receptor ligands **2.1**, **2.3** and **2.4** (Scheme 5.1).

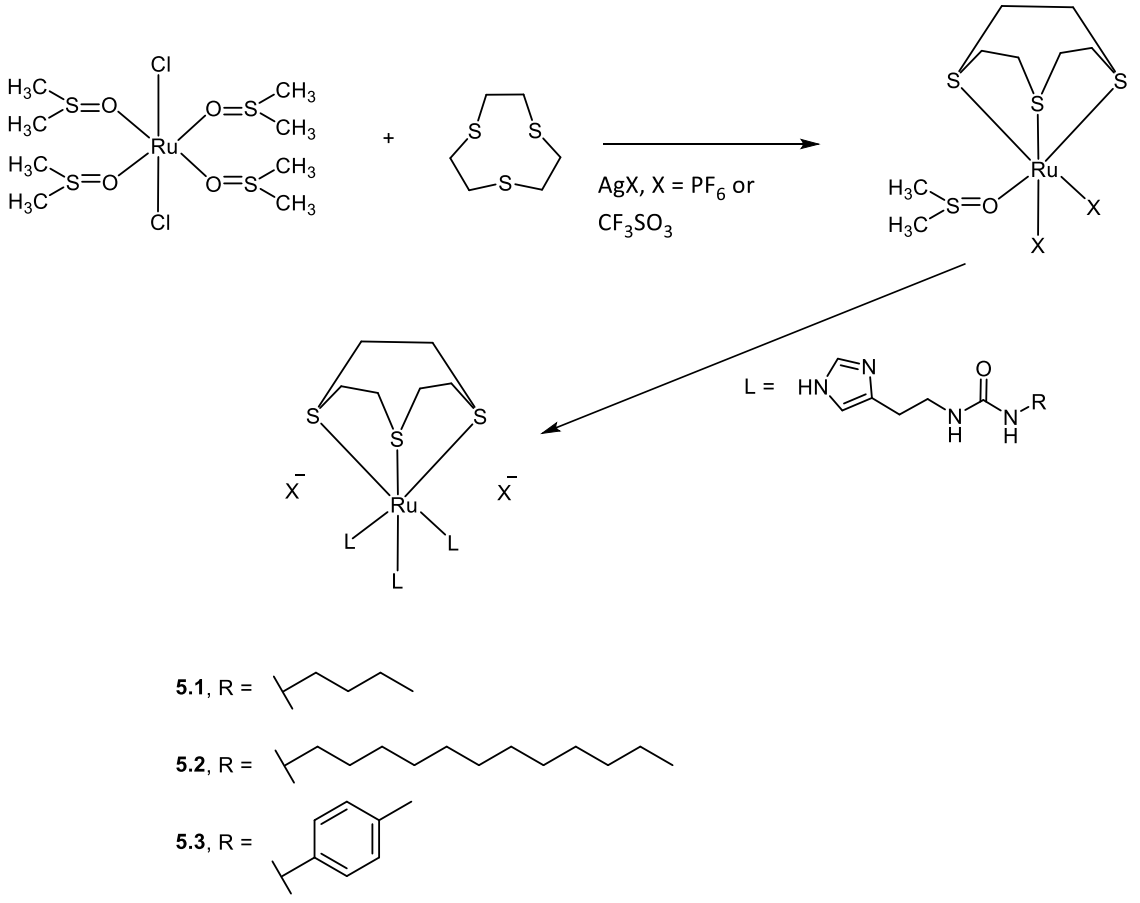

Scheme 5.1 Synthesis route of ruthenium(II) complexes of imidazole urea.

The first attempt to synthesise these Ru(II) complexes was carried out by the addition of ligand **2.1** to the solution of the precursor under continuous nitrogen stream with the metal core to ligand ratio of 1:3. The solution mixture was then constantly stirred and heated under reflux in ethanol:water (4:1) for 18 hours. However, the attempt was not

successful as the resulting complex was not fully (triply) substituted by the imidazole urea ligands as proven by ^{1}H NMR spectroscopy. The second attempt to synthesise complex **5.1** was made by extending the reaction time to 6 days with other conditions such as metal to ligand ratio and reaction temperature remaining the same. Complex **5.1** was obtained as a brown viscous oil after multiple recrystallisations with different solvents. ESI-MS analysis of complex **5.1** shows a molecular ion peak of 456.6 m/z due to the loss of two moles of hexafluorophosphate ions, $[(M\text{-}2PF_6)]^{2+}$. The formation of complex **5.1** has also been confirmed by High Resolution Mass Spectrometry in which the data obtained is in agreement with the expected positive ion mass of complex **5.1**, $[(M\text{-}2PF_6)+ H^+]^{+2}$ (Figure 5.1).

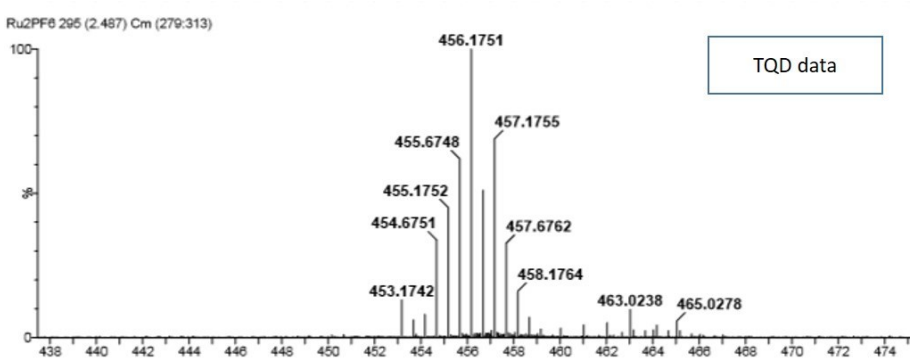

Figure 5.1 High Resolution Mass Spectrometry data for complex **5.1**.

The brown viscous oil was then subjected to Preparative HPLC to obtain the pure triply substituted ruthenium(II) complex. The ^{1}H NMR spectrum of complex **5.1** obtained after HPLC shows a mixture of doubly and triply substituted ruthenium(II) complex. Even after the longer reaction time and purification steps, the pure, fully tri-substituted complex was not successfully obtained. Complex **5.1** dissolves in polar solvents such as alcohols, DMSO and DMF but not soluble in less polar solvents such as acetonitrile and acetone. Therefore, to address the solubility problem of this receptor, we introduced a urea unit with a longer chain, in the form of ligand **2.3**. The synthesis of complex **5.2** using ligand **2.3**, was carried out in the same manner as complex **5.1**, except that ligand **2.3** is used in slight excess, with metal to ligand ratio of 1:4 to ensure the complete substitution by ligand **2.3**. The use of the slight excess of the ligands has directed the reaction in producing only tri-substituted complex as proved by ^{1}H NMR spectroscopy. However, as excess ligands were introduced, the product formed, complex **5.2** was not easily

separated from the excess ligands as both the products and the reactants show similar solubility. Nevertheless, complex **5.2** was purified through column chromatography using alumina as the stationary phase and gradient eluent system starting from diethyl ether: methanol (9:1) up to 100% methanol to afford light yellow solid with an unoptimised yield of 62%. Despite the introduction of ligand **2.3** with a longer chain, the solubility of complex **5.2** was similar to complex **5.1**; insoluble in less polar solvents such as acetonitrile and acetone but soluble in highly polar solvents such as alcohols, DMSO and DMF. The formation of complex **5.2** has been confirmed by two characteristic mass peaks of 625.5 correspond to $[(M\text{-}2PF_6) + H^+]^{+3}$. The formation of compound **5.2** has also been confirmed using High Resolution Mass Spectrometry as in Figure 5.2.

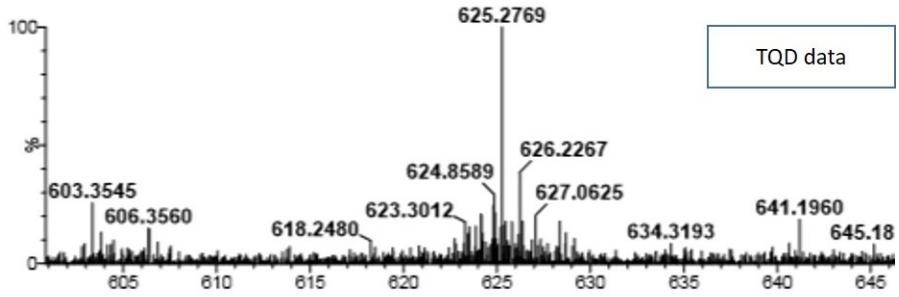

Figure 5.2 High Resolution Mass Spectrometry data for complex **5.2**.

Another ruthenium(II) complex (**5.3**) with aromatic substituents, using ligand **2.4** has also been prepared. This complex was synthesised for the purpose of comparison with complex **5.2** in terms of the anion binding properties. The synthesis of complex **5.3** was carried out using the same procedure as in the synthesis of complex **5.2**, except that complex **5.3** bears triflate ions as counter ions. Complex **5.3** was obtained as a brown solid with an unoptimised yield of 68%. Complex **5.3** has been purified from fractional crystallisation from acetonitrile and nitromethane. Similarly, complex **5.3** shows a characteristic mass peak of 507.15 m/z which corresponds to the loss of two moles of triflate ions, $[(M\text{-}2CF_3SO_3)]^{2+}$. The formation of complex **5.3** has also been confirmed by High Resolution Mass Spectrometry in which the data obtained is in agreement with the expected positive ion mass of complex **5.3**, $[(M\text{-}2\ CF_3SO_3) + H^+]^{+2}$ (Figure 5.3).

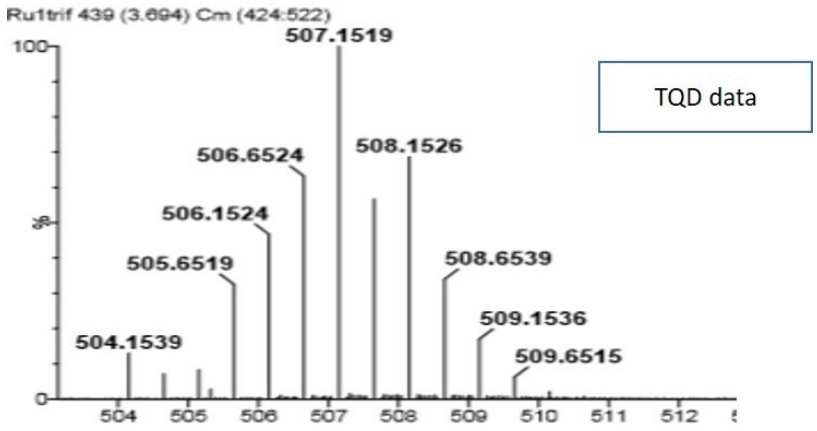

Figure 5.3 High Resolution Mass Spectrometry data for complex **5.3**.

The complexes **5.1** – **5.3** show many similarities in the ^{1}H NMR spectra to that of the ligands **2.1**, **2.3** and **2.4**, respectively. Coordination of the imidazole urea ligand **2.3** and **2.4** to the ruthenium center causes an upfield shift of proton H1 (Δδ 0.26 ppm for complex **5.2** and Δδ 0.15 ppm for complex **5.3**) and H3 (Δδ 0.35 ppm for complex **5.2** and Δ 0.15 ppm for complex **5.3**) of the imidazole region in both complexes, compared to the free uncoordinated ligand. However, in complex **5.1**, the shift in the resonance of proton H1 and H3 cannot be determined accurately due to the presence of impurities in the sample. Additionally, the ^{13}C NMR spectra of complexes **5.1** and **5.2** show a general downfield shift for the imidazole carbon indicating coordination occurs via the nitrogen atom of the imidazole moiety. The shift in the signals of the designated protons and carbon possibly indicating that the face-capping ligand has an impact on the spectroscopic properties of the complexes.

On the other hand, the chemical shifts for the [9]aneS_3 ligand in all complexes observed between δ = 2.55 and 2.71 ppm are in agreement with previous work.[10] However, it is difficult to determine whether there are multiple sets of peaks for the thioether group as the peaks for the [9]aneS_3 macrocyclic ring of all the complexes are of second order which overlapping with each other resulting in lower value of *J*-coupling.

In addition, the FTIR data of all the complexes also provides some valuable information on the changes after the complexation reaction. For instance, the hydrogen bonding in the ligands and complexes can be compared by observing the v(NH) stretch. For all the complexes, the v(NH) stretch is shifted towards higher energy upon complexation with ruthenium(II) in comparison to the respective ligand. This indicates that the hydrogen bonding between the urea moieties and imidazole groups is weakened upon coordination to the ruthenium(II) as the coordination inhibits inter-ligand interactions. Table 5.1 shows some of the important stretching vibrations observed for free ligands, **2.1**, **2.3** and **2.4** in comparison to their respective ruthenium(II) complexes.

Table 5.1 Selected FTIR stretching vibrations of free imidazole urea ligands (**2.1**, **2.3** and **2.4**) in comparison to their ruthenium(II) complexes.

Entry	Compounds	Selected FTIR stretching vibrations			
		v (N-H)	*v* (C=O)	*v* (C-H imidazole ring)	*v* (C=N-C=C) imidazole
1	Free ligand **2.1**	3290	1650	1564	1454
2	Complex **5.1**	3376	1644	1568	1464
3	Free ligand **2.3**	3309	1611	1570	1450
4	Complex **5.2**	3332	1621	1573	1462
5	Free ligand **2.4**	3304	1633	1558	1448
6	Complex **5.3**	3337	1637	1559	1451

For all complexes **5.1** – **5.3**, purification was problematic due to the similar solubilities of the complexes and the unbound ligand. While complex **5.1** has been purified using preparative HPLC, complex **5.2** was only purified through column chromatography using alumina as the stationary phase and gradient eluent system starting from diethyl ether: methanol (9:1) up to 100% methanol. On the other hand, complex **5.3** has been purified by fractional crystallisation from acetonitrile and nitromethane. However, traces of impurities can still be found by elemental analysis and NMR spectroscopy even after

column chromatography and multiple recrystallisations have been carried out. None of the complexes is soluble in less polar solvent such as acetone and acetonitrile although, in the case of complex **5.3**, a dodecyl chain has been introduced to enhance the solubility in less polar solvent. Due to the insolubility of the complexes in acetonitrile, the anion binding studies have been carried out in a more competitive solvent, DMSO-d_6.

5.2.2 Anion binding properties of the ruthenium(II) complexes of imidazole urea

In order to assess the anion-binding properties of this family of metal-based receptors (**5.2** and **5.3**), binding studies were conducted using ^{1}H-NMR spectroscopic titration experiments in a more competitive solvent, DMSO-d_6 due to the insolubility of these two complexes in a less competitive solvent, acetonitrile. An anion binding study was not performed on complex **5.1** as it occurs as a viscous solid and contains a mixture of at least two different compounds, that cannot be separated even with the use of preparative HPLC. However, for complex **5.2** and **5.3**, the presence of impurities in both of the complexes deters the accurate determination of the binding constant.

For complex **5.2**, the addition of up to 1.5 equivalent of chloride ion (as NBu_4^+ salts) to the complex solution did not result in any significant changes to the chemical shifts of the H1 and H2 protons of the imidazole group and the urea protons NH3 and NH4. Only after the addition of 2 equivalent of chloride ion, the urea protons peaks start to broadening (Figure 5.4) possibly due to the rapid exchange upon addition of anions caused by rotation of the urea group about the C-N bond. This is also due to the use of a more competitive solvent, DMSO-d_6 that competes in the hydrogen bonding formation of the anions to the hosts. In comparison, as detailed in the previous Chapter 2, it has been shown that the free ligand **2.3** forms a hydrogen bond upon titration with chloride ion in chloroform solvent although the binding constant was not accurately determined due to the large error.

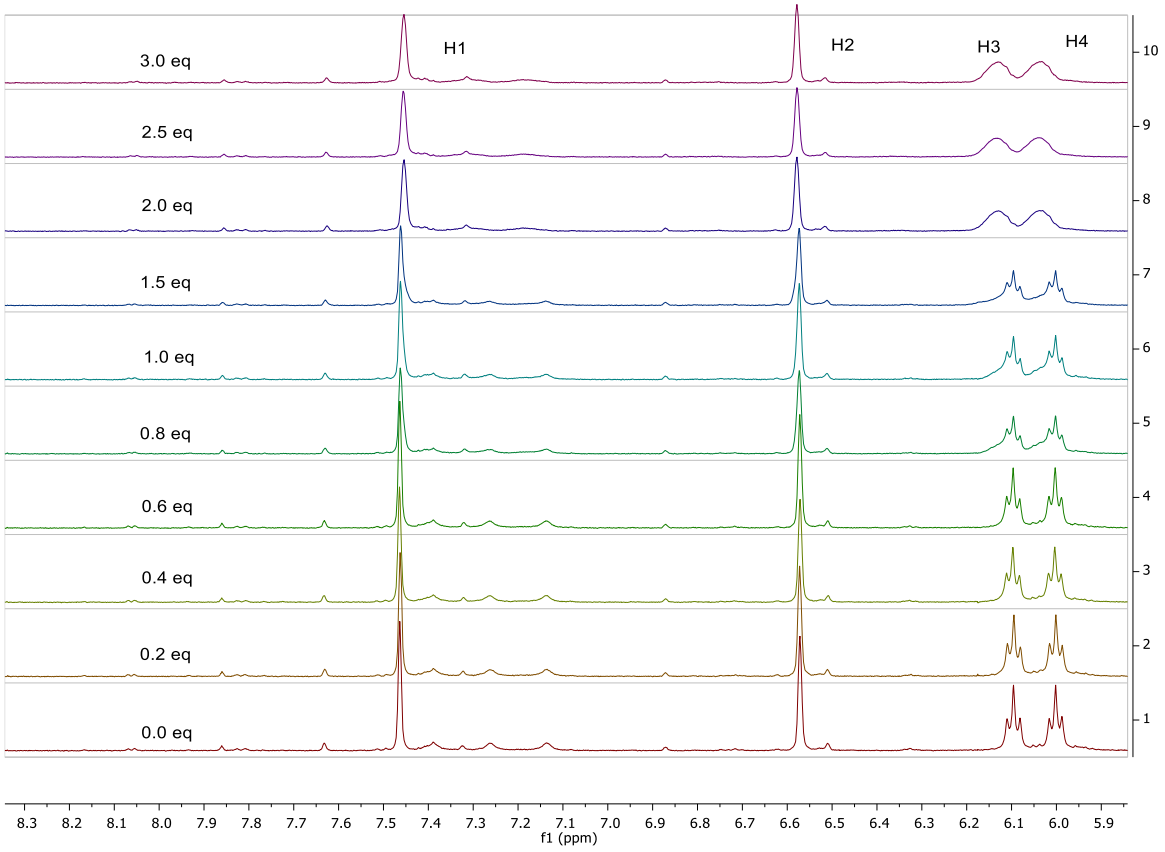

Figure 5.4 Stack plot showing the ^{1}H NMR spectrum of complex **5.2** in DMSO-d_6 in the presence of chloride ion as tetrabutylammonium salt.

On the other hand, there was also a large degree of peak broadening observed for H1, H2 and urea protons, H3 and H4 in the presence of fluoride ion (as NBu_4^+ salt) which indicates that host **5.2** showed possible acid-base interactions with the highly basic fluoride anion (Figure 5.5). To further confirm the acid-base interaction pattern of host **5.2**, a control experiment was performed in which complex **5.2** was titrated with sodium hydroxide solution as illustrated in Figure 5.6. The addition of sodium hydroxide results in severe broadening and subsequent disappearances of the imidazole protons, H1 and H2 as well as resonances assigned to the urea protons, NH3 and NH4. In this case, the disappearance of the resonances could possibly be due to the precipitation of the complex from the solution and also the dissociation of H^+ from the urea. Since the titration of complex **5.2** with the fluoride ions and sodium hydroxide show the same pattern, it can be concluded that complex **5.2** underwent acid-base interaction with fluoride ions.

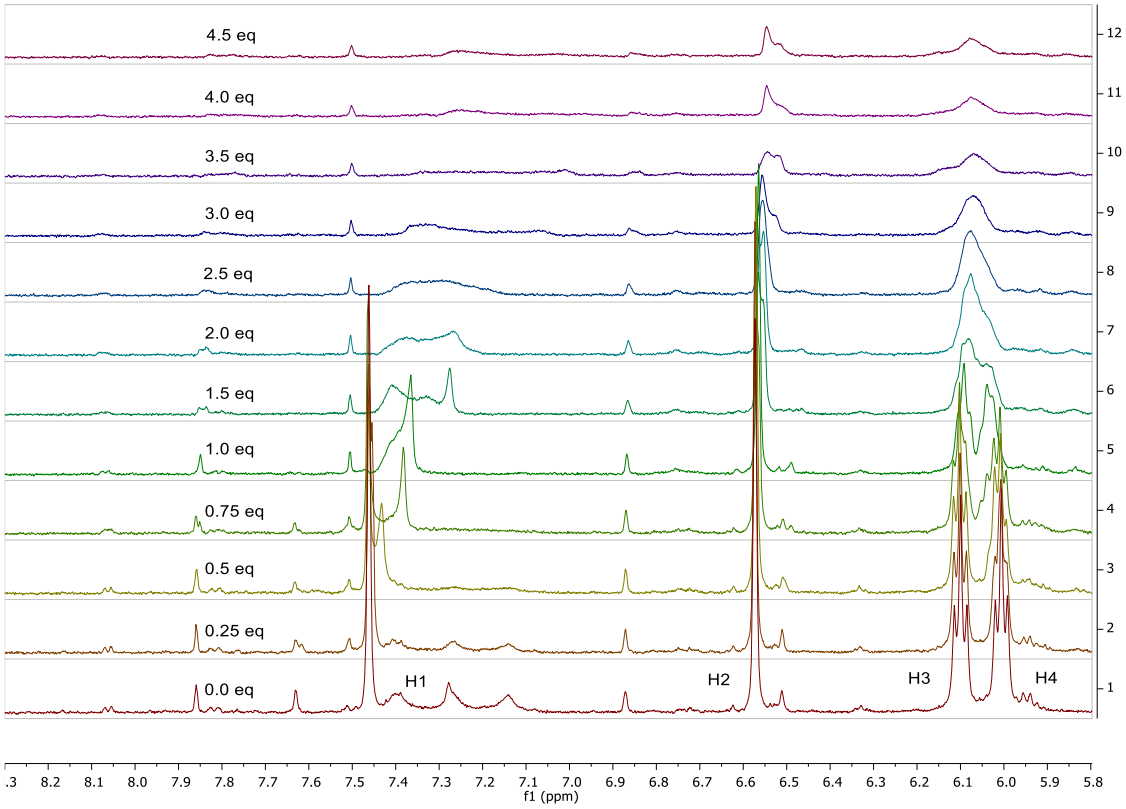

Figure 5.5 Stack plot showing the ^{1}H NMR spectrum of compound **5.2** in DMSO-d_6 in the presence of fluoride ion as tetrabutylammonium salt.

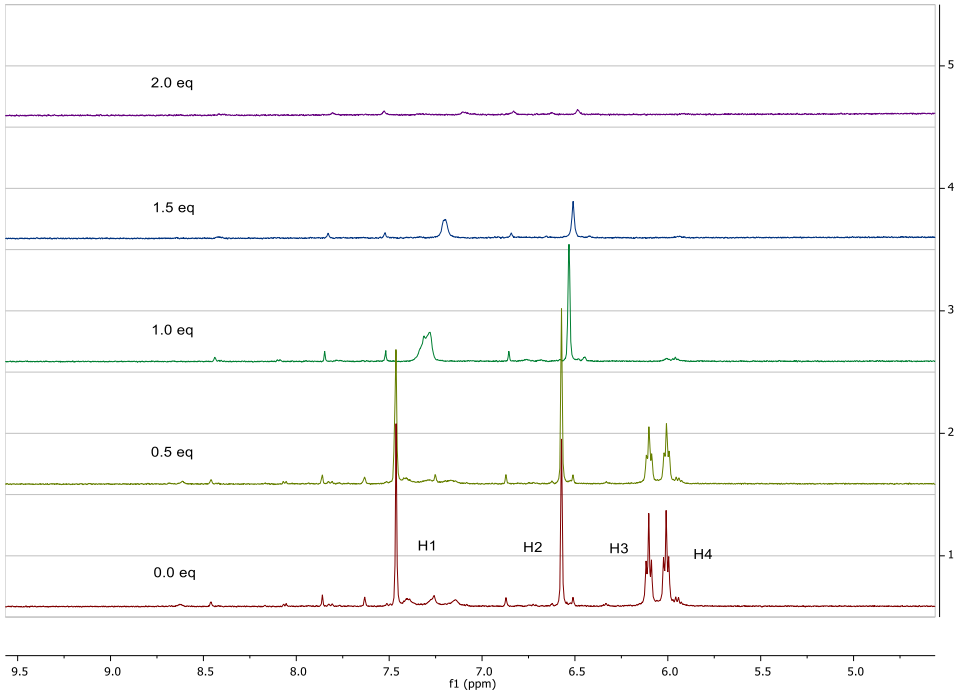

Figure 5.6 Stack plot showing the ^{1}H NMR spectrum of compound **5.2** in DMSO-d_6 in the presence of NaOH.

Similarly, titration of complex **5.2** with acetate ion (as NBu_4^+ salt) shows a similar pattern with fluoride and hydroxide ions although the deprotonation started to be observed upon addition of 3 equivalent of acetate ion. The addition of 1 equivalent of acetate ion to the solution of complex **5.2** results in the splitting of the peaks of H1, H2, NH3 and NH4 signals (Figure 5.7 and 5.8). Further addition of up to 1.5 equivalent of acetate ion to the complex solution results in the presence of two different species at the same ratio as illustrated in Figure 5.9. This result is similar to the anion binding titration experiment of ligand **2.4** in DMSO-d_6, in which the addition of basic anions like fluoride cause the splitting of the signals giving two different species in the solution. The species that respond to the acetate ion shows similar interaction pattern with free ligand **2.3** in DMSO-d_6 as shown in Figure 5.10. Upon the addition of the acetate ion, the urea proton signal H3 and H4 started to move downfield and at some point merge and disappear. The disappearances of the H3 and H4 signal is caused by acid-base interaction between the NH group and acetate ions.

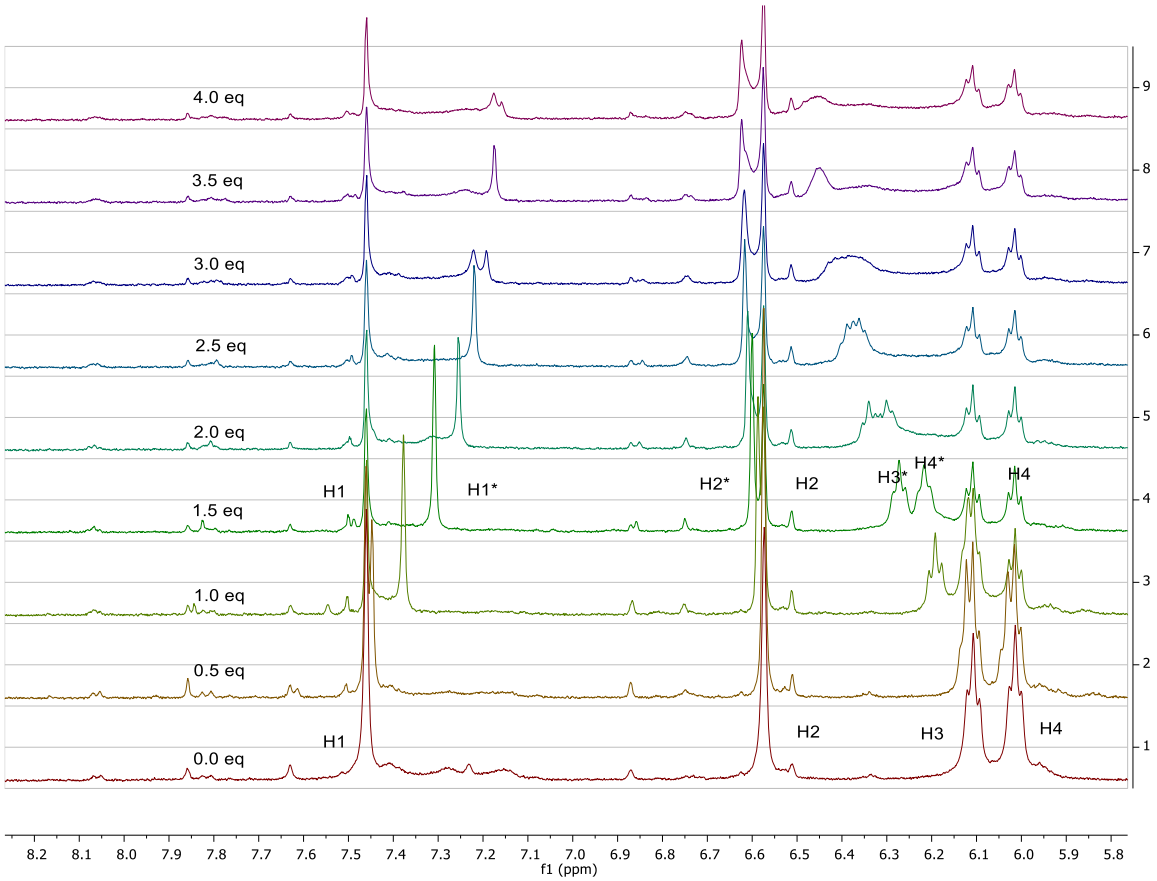

Figure 5.7 Stack plot showing the ^{1}H NMR spectrum of compound **5.2** in DMSO-d_6 in the presence of acetate ion as tetrabutylammonium salt.

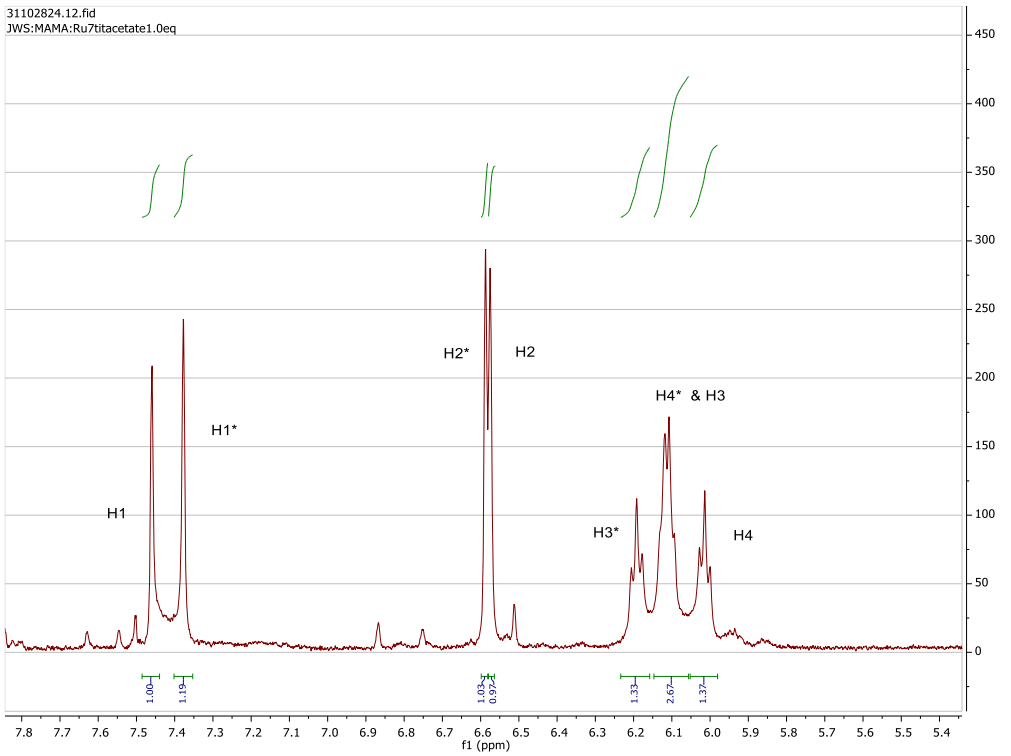

Figure 5.8 The ^{1}H NMR spectrum of compound **5.2** in DMSO-d_6 in the presence of 1 equivalent of acetate ion as tetrabutylammonium salt.

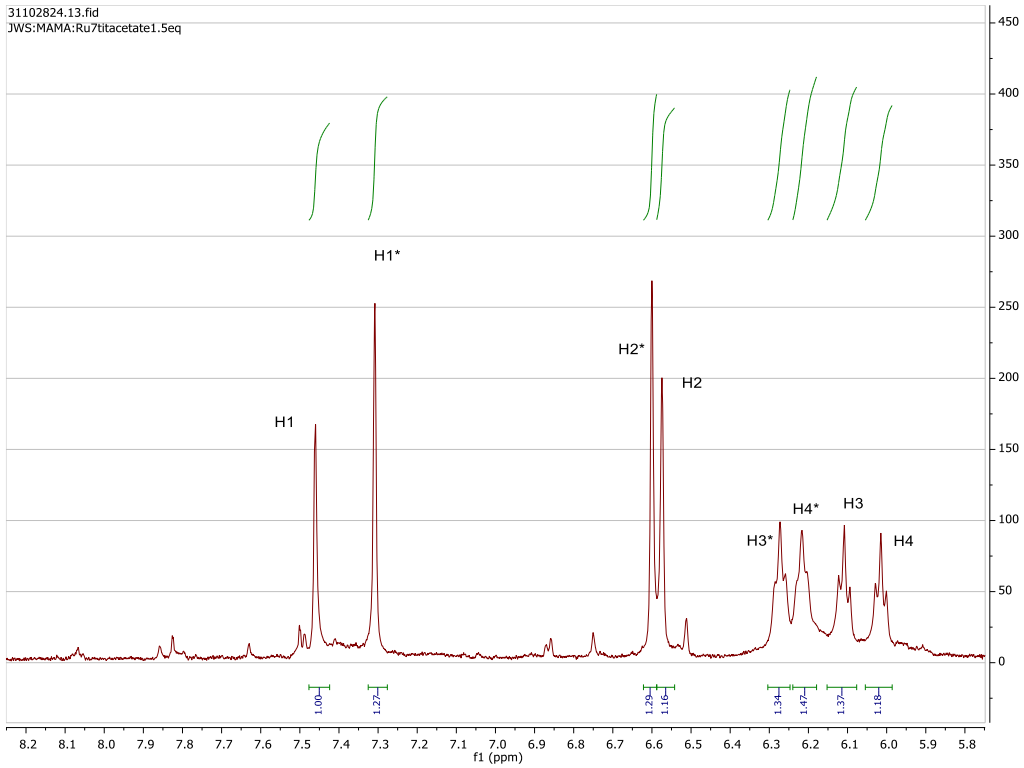

Figure 5.9 The ^{1}H NMR spectrum of compound **5.2** in DMSO-d_6 in the presence of 1.5 equivalent of acetate ion as tetrabutylammonium salt.

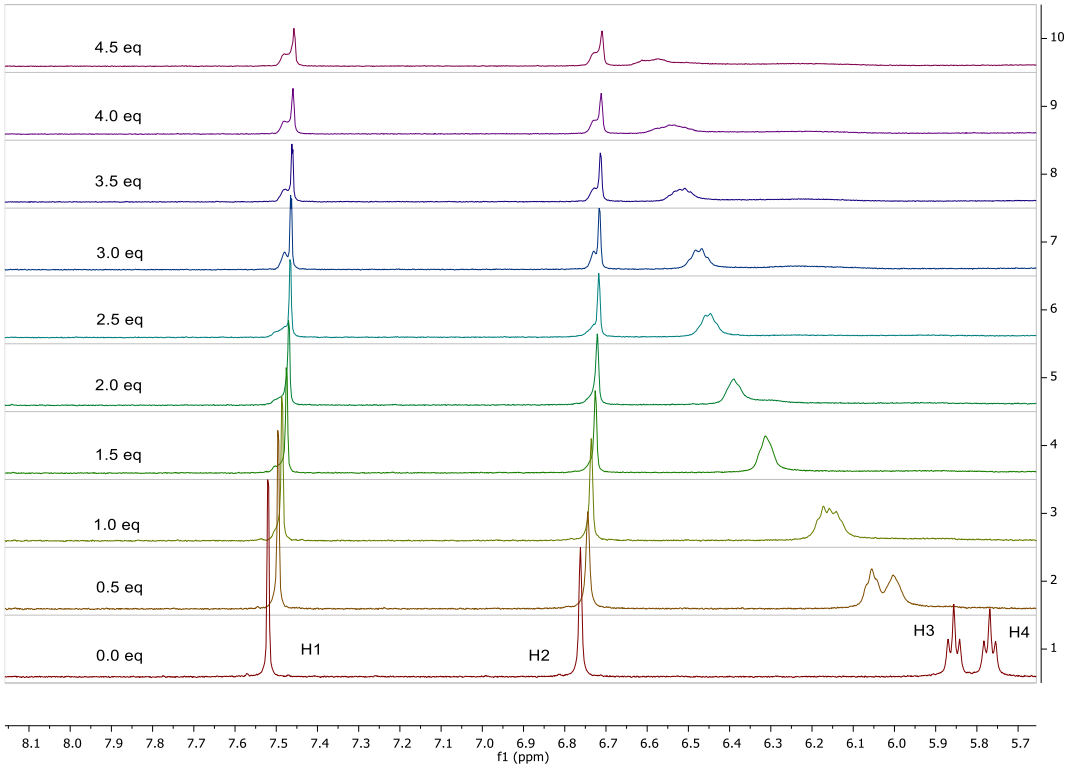

Figure 5.10 Stack plot showing the ^{1}H NMR spectrum of compound **2.3** in DMSO-d_6 in the presence of acetate ion as tetrabutylammonium salt.

A similar observation was found in the titration experiment of complex **5.2** with benzoate ion. Likewise, benzoate ion is basic in nature and could lead to the possible acid-base interaction with complex **5.2** as shown in Figure 5.11. On the other hand, the addition of hydrogen sulphate ion did not perturb any of the proton signals, H1-H4 of complex **5.2** (Figure 5.12).

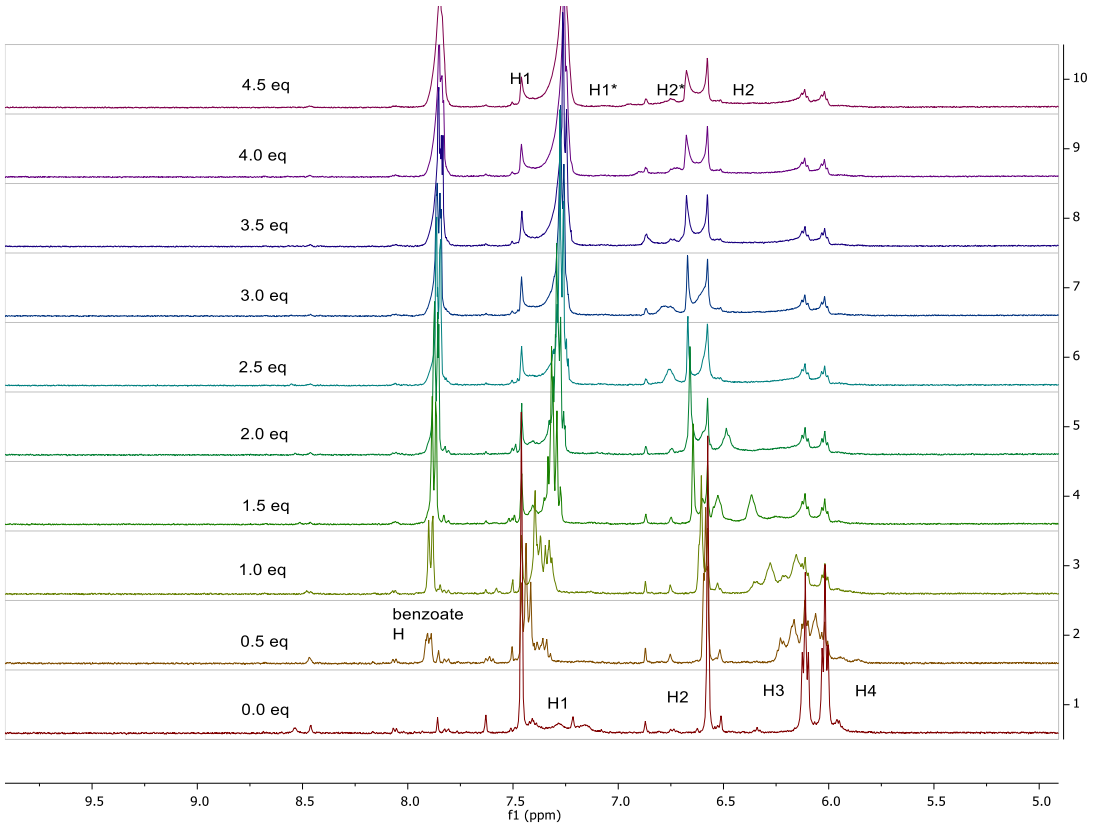

Figure 5.11 Stack plot showing the ^{1}H NMR spectrum of compound **5.2** in DMSO-d_6 in the presence of benzoate ion as tetrabutylammonium salt.

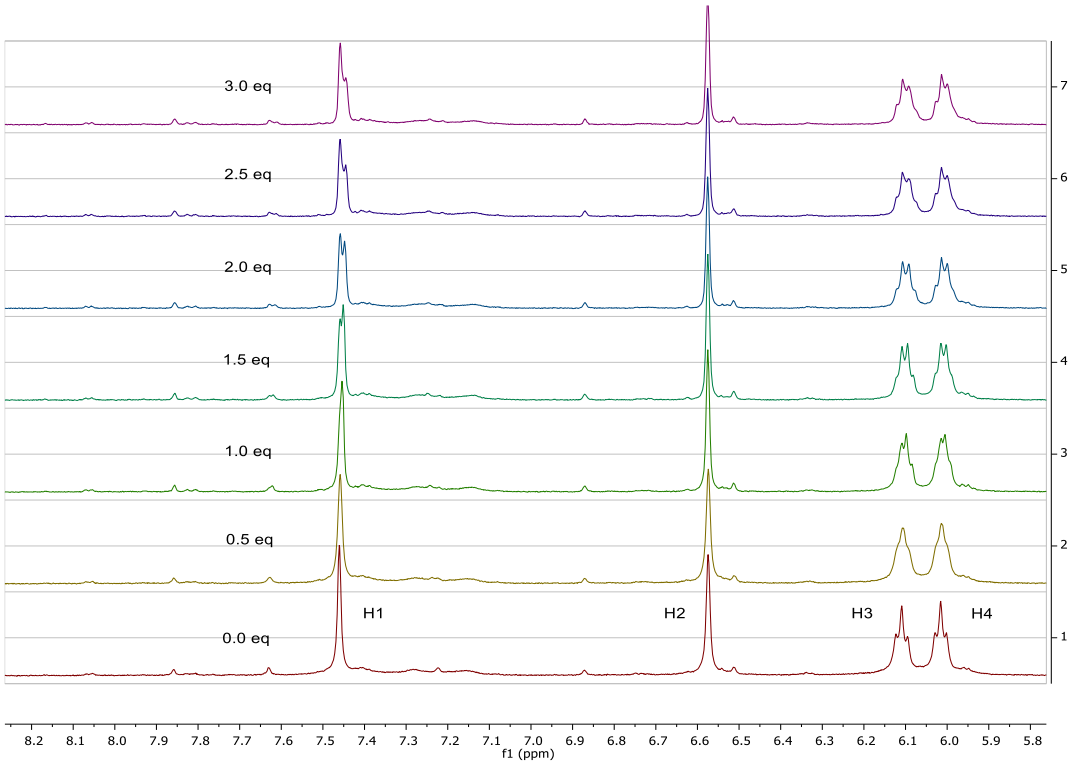

Figure 5.12 Stack plot showing the ^{1}H NMR spectrum of compound **5.2** in DMSO-d_6 in the presence of hydrogen sulphate ion as tetrabutylammonium salt.

On the other hand, the anion binding experiment also has been performed on the ruthenium(II) complexes (**5.3**) containing imidazole with an aromatic ring (ligand **2.4**) to assess the influence of the aromatic group towards the anion binding. The titration experiment has been performed in DMSO-d_6 due to the limitation on the solubility of the complex. Similar to complex **5.2**, imidazole protons, H1 and H2 as well as urea protons H3 and H4 were followed during the titration. For the first titration with chloride ion, the addition of 0.25 equivalent of chloride ion (as tetrabutylammonium salts) has caused the splitting of imidazole H1 and urea H3 proton signals, while the chemical shift of imidazole H2 and urea H4 proton signals remained unchanged (Figure 5.13).

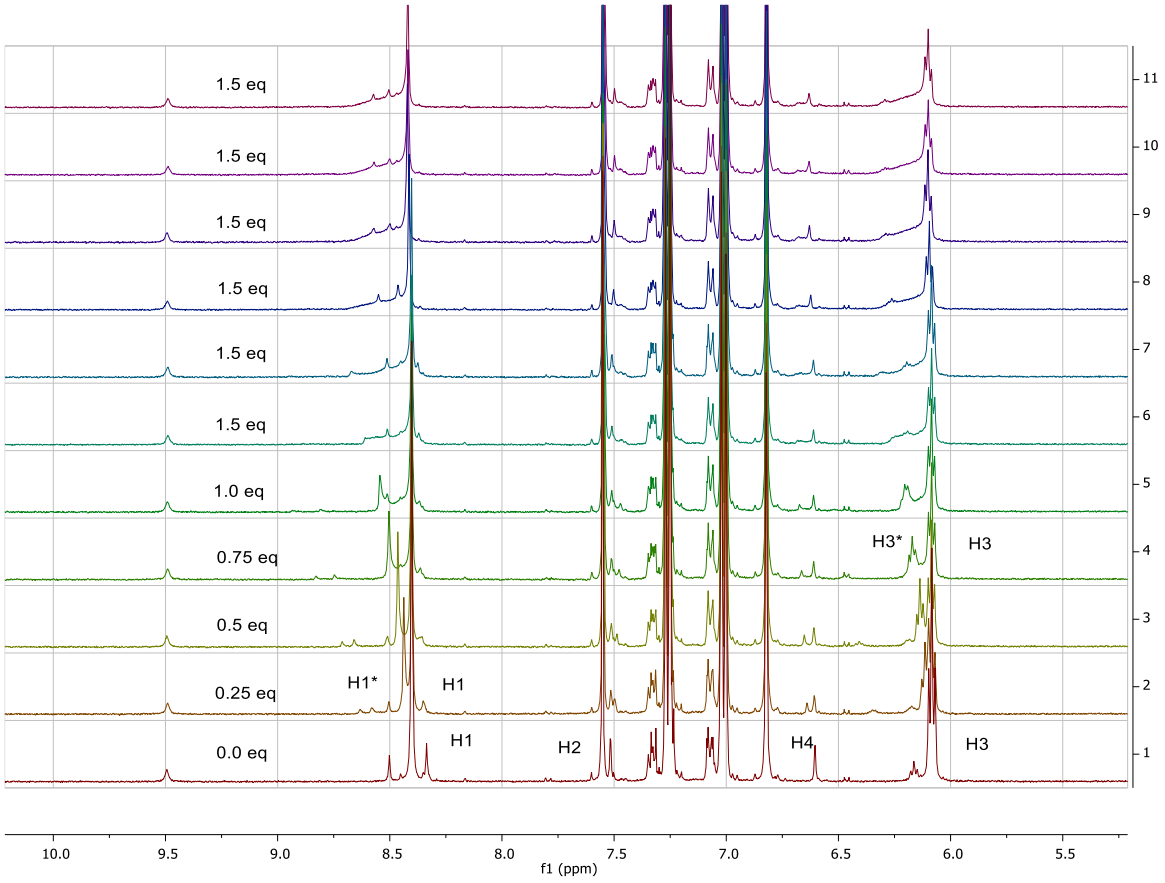

Figure 5.13 Stack plot showing the ^{1}H NMR spectrum of complex **5.3** in DMSO-d_6 in the presence of chloride as tetrabutylammonium salt.

On the other hand, titration experiment of complex **5.3** with larger halide anions such as bromide and iodide (as tetrabutylammonium salt), did not result in any significant changes on the chemical shift of all the designated protons, H1 and H2 of imidazole

protons and H3 and H4 protons of urea although with the addition of excess anions, which were added up to three equivalents (Figure 5.14 and 5.15).

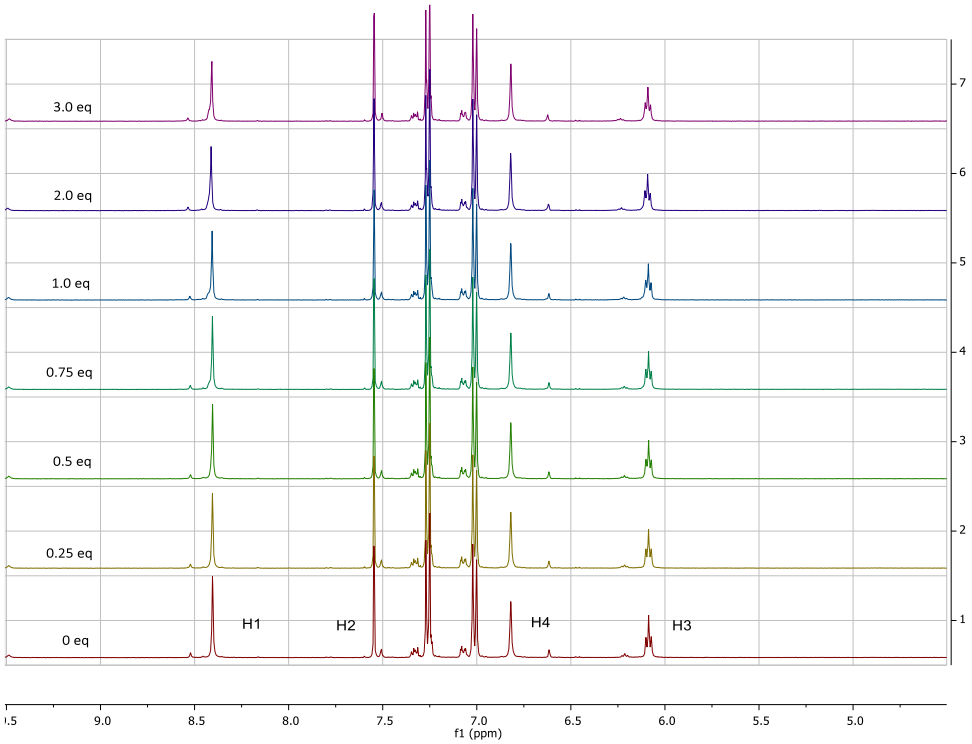

Figure 5.14 Stack plot showing the ^{1}H NMR spectrum of compound **5.3** in DMSO-d_6 in the presence of bromide ion as tetrabutylammonium salt.

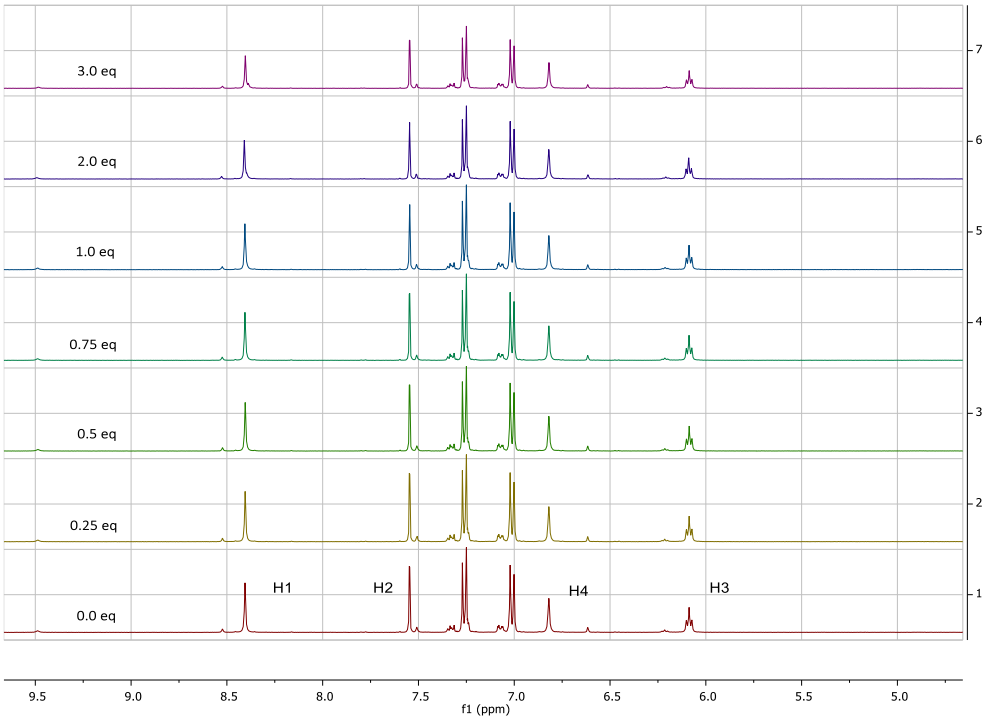

Figure 5.15 Stack plot showing the ^{1}H NMR spectrum of compound **5.3** in DMSO-d_6 in the presence of iodide ion as tetrabutylammonium salt.

Titration experiments of complex **5.3** with different types of basic anions such as fluoride, acetate, benzoate and hydrogen phosphate have also been performed in DMSO-d_6. Figure 5.16 shows that the addition of 0.50 equivalent of fluoride ion results in the broadening of H1 and H3 protons while there is no change on the chemical shift of H2 proton. It is also observed that H4 proton has completely disappeared from the spectrum due to the deprotonation.

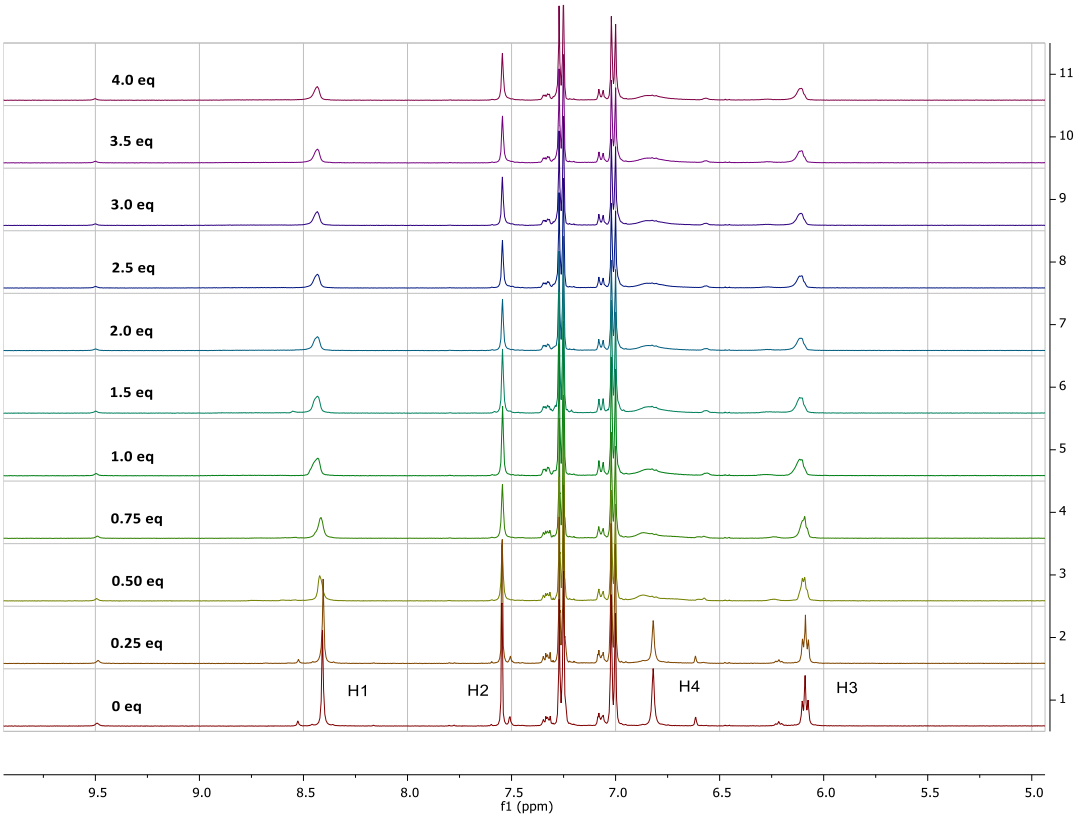

Figure 5.16 Stack plot showing the ^{1}H NMR spectrum of compound **5.3** in DMSO-d_6 in the presence of fluoride ion as tetrabutylammonium salt.

Likewise, the addition of acetate ion results in the downfield shift of H1 and H3 proton resonances ($\Delta\delta$ 0.10 ppm) up to 3 equivalent of acetate ion. The excess amount of acetate ion does not cause any significant changes to the designated proton signal. In contrast to fluoride ion, the addition of acetate ion does not cause the disappearance of H4 proton signal, but instead, the peak broadened (Figure 5.17). Titration of complex **5.3** with benzoate ion also results in the similar pattern with acetate, in which both H1 and H3 protons shifted downfield ($\Delta\delta$ 0.09 ppm), while H2 proton unaffected and the H3 proton peak broadened (Figure 5.18). The downfield shift induced by acetate and benzoate ions is common for urea-based receptors due to the high basicity and complementary Y shape of these anions with the urea group.[14,15]

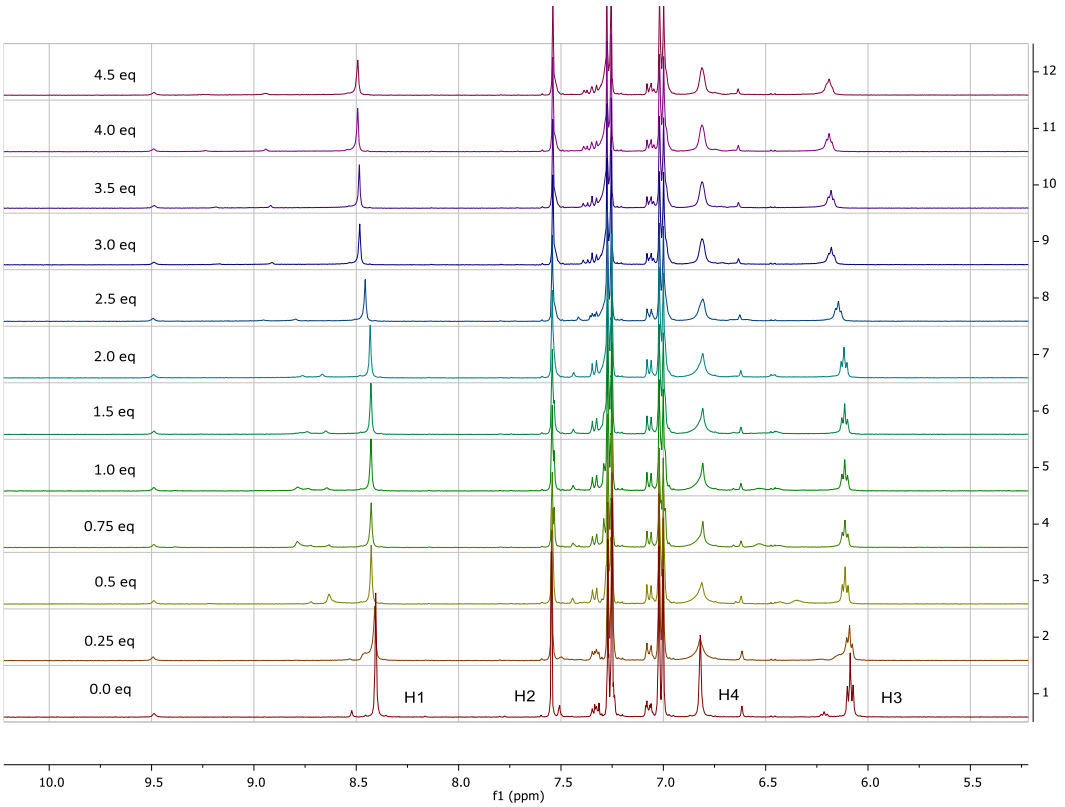

Figure 5.17 Stack plot showing the ^{1}H NMR spectrum of compound **5.3** in DMSO-d_6 in the presence of acetate ion as tetrabutylammonium salt.

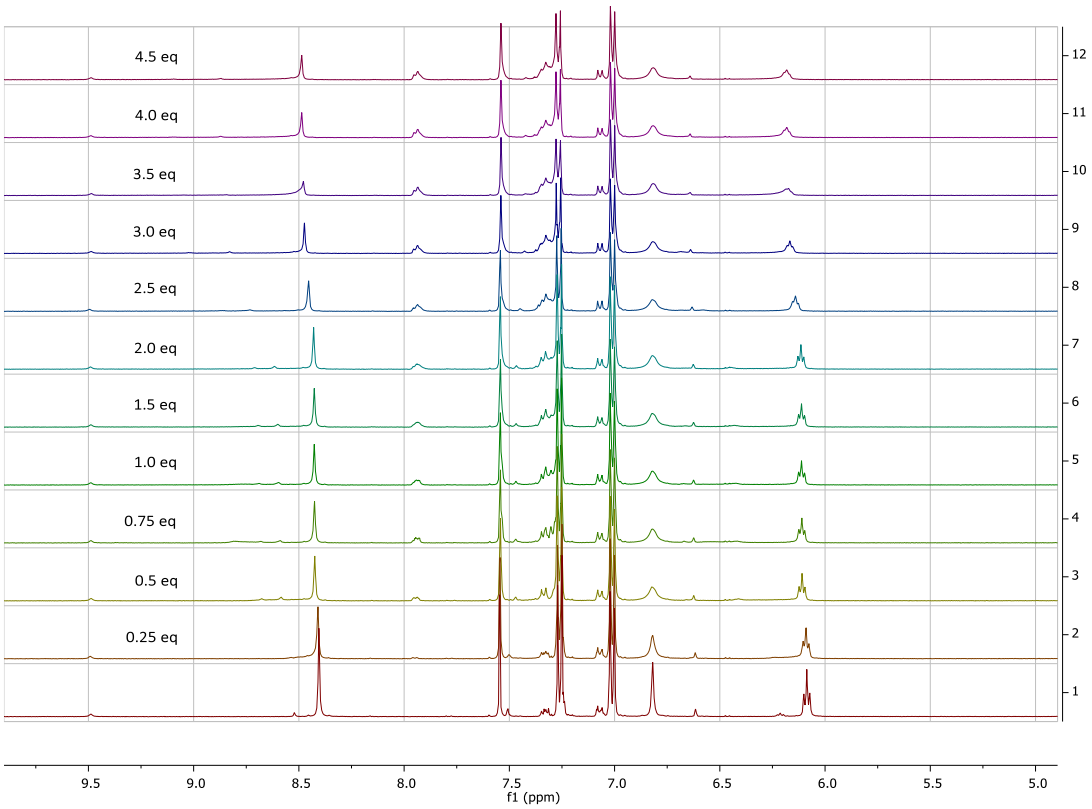

Figure 5.18 Stack plot showing the ^{1}H NMR spectrum of compound **5.3** in DMSO-d_6 in the presence of benzoate ion as tetrabutylammonium salt.

Likewise, the addition of hydrogen phosphate ion also results in the slight downfield of H1 and H3 proton signals but there are no changes on the H2 and H4 signals (Figure 5.19).

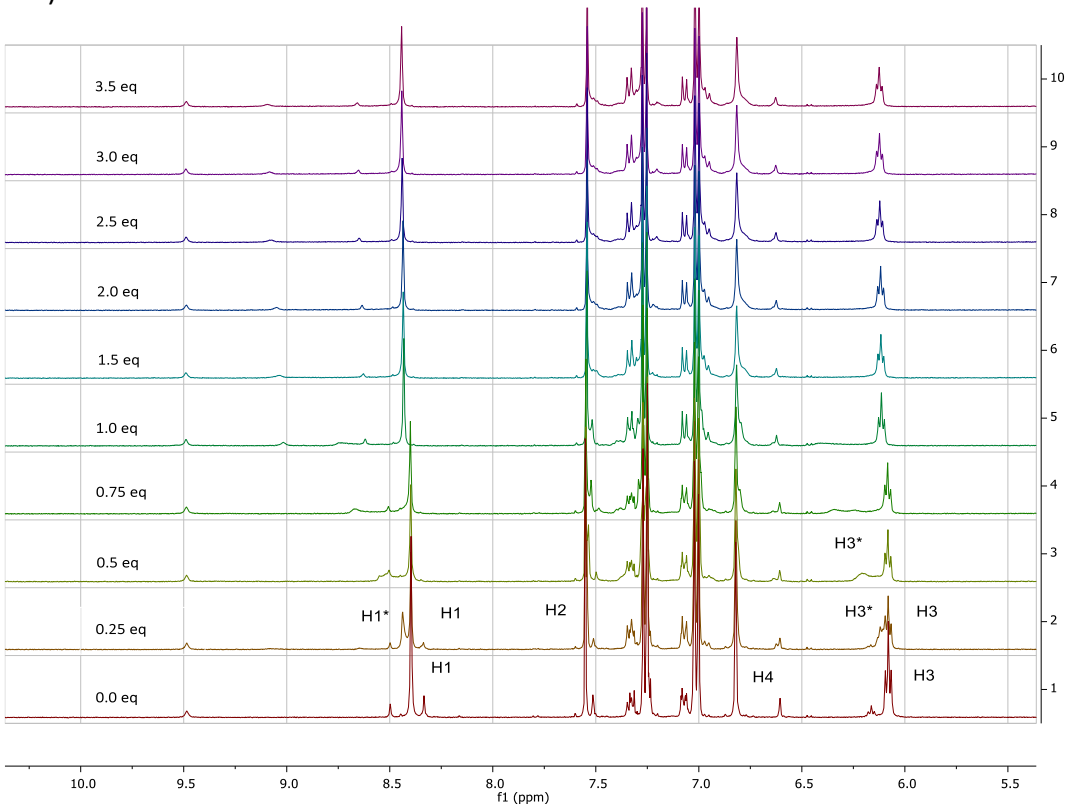

Figure 5.19 Stack plot showing the ^{1}H NMR spectrum of compound **5.3** in DMSO-d_6 in the presence of hydrogen phosphate ion as tetrabutylammonium salt.

The response of complex **5.3** towards chloride fluoride, acetate, benzoate and hydrogen phosphate ion is in agreement with the Hofmeister series (Table 5.2), in which weakly hydrated anions show more significant changes on the proton signals of the complex.[16]

Table 5.2 The Hofmeister Series.

Weakly hydrated (hydrophobic) Strongly hydrated(hydrophilic)

Anions: organic anions > ClO_4^- > I^- > SCN^- > NO_3^- > ClO_3^- > Br^- > Cl^- >> F^-, IO_3^- > $CH_3CO_2^-$, CO_3^{2-} > HPO_4^{2-}, SO_4^{2-} > citrate^{3-}

5.3 Summary

A series of Ruthenium(II) based tripodal hosts, **5.1** – **5.3** have been synthesised from the reaction of [9]ane-S_3-capped ruthenium precursor with respective imidazole urea ligands, **2.1**, **2.3** and **2.4**. ^{1}H NMR titration experiment of complex **5.2** with chloride fluoride, acetate, benzoate and hydrogen sulphate ions (as NBu_4^+ salt) has been performed in DMSO-d_6 and host **5.2** only responds to fluoride, acetate and benzoate ions. In the case of fluoride, deprotonation reaction occurred after the addition of one equivalent of fluoride ion which later causes the disappearances of all the designated proton signals, H1-H4. However, in the case of the titration of complex **5.2** with acetate and benzoate ions, similar patterns have been observed. The addition of both anions at 1.5 equivalent caused the splitting of all proton (H1-H4) signals into two different set at 1:1 ratio suggesting that there might be two different species in the solution, one that responds to the anions, while the other does not. After 2.0 equivalent, the new set of the peak gradually disappeared suggesting deprotonation reaction has taken place.

On the other hand, for complex **5.3**, chloride is the only ion that can cause the splitting of the H1-H4 protons signals after the addition of 0.25 equivalents. The addition of larger anions such as bromide and iodide does not affect the chemical shift of complex **5.3**. In the case of basic anions, only fluoride ion caused the disappearance of H2 proton signal after 0.5 equivalent of fluoride ion added. Titration with other basic anions such as acetate, benzoate and hydrogen phosphate does not result in any significant changes in the proton signals. These findings suggest that this system might not be a suitable system for anion sensing, at least not in a competitive solvent.

5.4 Experimental

All solvents used in the synthesis and purification were of analytical reagent grade. Anhydrous solvents were prepared on an SPS solvent purification system. Commercial reagents were used as supplied, without further purification.

5.5.1 Instrumentation and Analytical Measurements

All NMR spectra were obtained from a Bruker Avance 400 at a frequency of 400 MHz for ^{1}H and 100 MHz for ^{13}C, while ^{1}H, ^{13}C, ^{1}H-^{1}H COSY, ^{1}H-^{1}C HSQC and ^{1}H-^{13}C HMBC spectra were obtained from a Varian INOVA 500 spectrometer at a frequency of 500 MHz for ^{1}H and 125 MHz for ^{13}C. All chemical shifts are reported in parts per million (δ) relative to tetramethylsilane as an internal reference. Electrospray ionisation (ESI) mass spectrometry was recorded on a TQD mass spectrometer instrument. Fourier transforms infrared spectra were recorded with a Perkin-Elmer Spectrum 100 FT-IR spectrometer in which for each spectrum, 64 scans were conducted over a spectral range of 4000 to 600 cm^{-1} with a resolution of 4 cm^{-1}. Elemental analysis was performed using an Exeter Analytical CE-400 Elemental Analyser.

5.5.2 General Procedure for ^{1}H NMR Spectroscopic Titrations

All chemical shifts are reported in ppm relative to residual solvent, DMSO-d_6. A solution of the host species of known concentration typically 0.5-1.5mM, was made up in an NMR tube using the appropriate deuterated DMSO (0.5 ml). Solutions of the anions, as TBA salts (1 ml) were made ten times the concentration of the host solution. The guest solution was typically added in 10 µl aliquots, representing 0.25 equivalents of the guest with respect to the host. Larger aliquots were used in some cases where no inflection of the trace was evident. Spectra were recorded after each addition and the trace was followed simultaneously.

5.5.3 Synthesis of the ruthenium complexes

Synthesis of ([9]ane-S_3)$RuCl_2$.DMSO

In 2 ml of DMSO, $RuCl_3 \cdot 3H_2O$ (1.0 g, 3.8 mmol) was dissolved and heated to boiling to remove any water from the solution. After the DMSO solution cooled to room temperature, acetone (25 ml) was added, leading to precipitation of a dark orange material. Filtration of this material left an orange solution which gave the desired $RuCl_2(DMSO)_4$ as yellow crystals upon drying. Repeated dissolution of the dark orange precipitate with more DMSO/acetone with heating produced more of the yellow product.[10] Yield 1.5 g, 3.1 mmol, 82%. Anal. Calc. for $C_8H_{24}S_4O_4RuCl_2$: C, 19.83; H, 4.99. Found: C, 19.84; H, 4.90.

This $RuCl_2(DMSO)_4$ (0.48 g, 1 mmol) was then dissolved in $CHCl_3$ (25 ml) in a round-bottomed flask fitted with a reflux condenser. 1,4,7-trithiacyclononane ([9]ane-S_3) (0.2 g, 1.1 mmol) was added and the solution heated to reflux for 90 mins with stirring, leading to the precipitation of the capped ([9]ane-S_3)$RuCl_2$.DMSO as a yellow-orange solid. Yield 0.36 g, 0.84 mmol, 84%. Anal. Calc. for $C_8H_{18}S_4ORuCl_2$: C, 22.32; H, 4.21. Found: C, 22.05; H, 4.08.

Synthesis of ([9]ane-S_3)Ru(1-[2-(1*H*-imidazol-4-yl)ethyl]-3-(4-butyl)urea)$_3$.2PF_6^- (**5.1**)

Formation of the ([9]ane-S_3)Ru$(PF_6)_2$.DMSO intermediate was achieved via by stirring ([9]ane-S_3)$RuCl_2$.DMSO (0.22 g, 0.5 mmol) with silver hexafluorphosphate (0.25 g, 1 mmol) for 2 hours in methanol (100 mL) in the dark at room temperature. AgCl precipitate formed was removed by filtration through celite. The yellow filtrate was then degassed for 2 hours before subsequent addition of 1-[2-(1*H*-imidazol-4-yl)ethyl]-3-(4-butyl)urea (0.3 g, 1.5 mmol). The mixture was then stirred and heated to 75 ^oC for 6

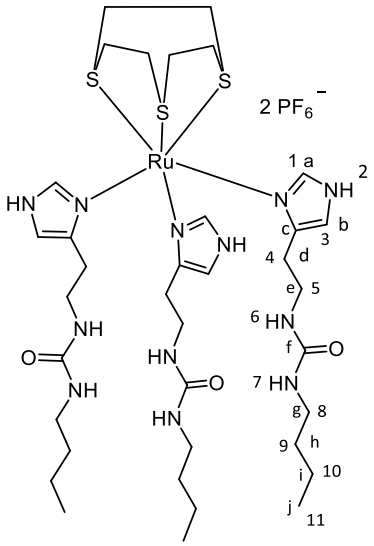

5.1

days. Cooling and removal of the solvent led to the formation of the crude product as an orange viscous liquid.

Purification was achieved by column chromatography using alumina as the stationary phase and gradient eluent system starting from diethyl ether:methanol (9:1) up to 100% methanol. Removal of the solvent from the desired fraction resulted in the formation of final product as orange viscous liquid (0.39 g, 0.33 mmol, 65%). **^{1}H NMR:** δ_H (400 MHz; DMSO-d_6; Me_4Si) 12.64 (1 H, br s, *H2*), 8.47 (1 H, d, *J* 1.1, *H1*), 6.40 (1 H, s, *H3*), 5.84 (1 H, t, *J* 5.6, *H6*), 5.74 (1 H, t, *J* 5.6, *H7*), 3.17 (2 H, m, *H5*), 3.02 (2 H, m, *H8*), 2.66-2.71 (m, *H thioether*), 2.52 (2 H, t, *J* 7.1 *H4*), 1.12 (2 H, m, *H9*), 1.06 (2 H, m, *H10*) , 0.65 (3 H, t, *J* 8.0, *H11*). **^{13}C {^{1}H} NMR:** δ_C {^{1}H} (101 MHz; DMSO) 158.50 (*Cf*), 138.37 (*Ca*), 38.76 (*Cc*), 39.36 (*Cb*), 32.59 (*Ce* and *Cg*), 32.53 (*Cd*), 26.47 – 26.24 (*Thioether C*), 19.95 (*Ch* and *Ci*), 14.18 (*Cj*). **FTIR:** ν_{max}/cm^{-1} 3376 (NH), 1644 (CO), 1568 and 1464 (imid. ring), m/z (ESI-MS) 456.6 $[(M-2PF_6)/2]^{2+}$, m/z (HRMS) 456.1 $[(M-2PF_6)/2]^{2+}$. Due to the impurity of the sample, elemental analysis did not give usable information.

Synthesis of ([9]ane-S_3)Ru(1-[2-(1*H*-imidazol-4-yl)ethyl]-3-(4-dodecyl)urea)$_3$.2PF_6^- **(5.2)**:

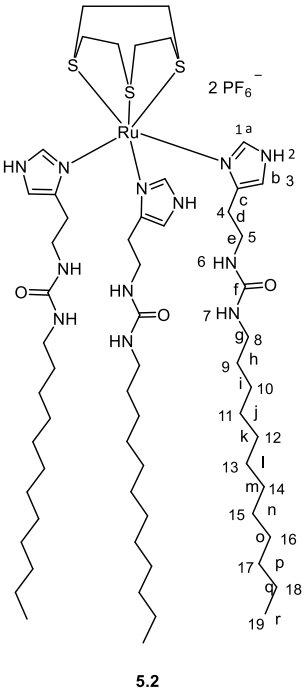

5.2

Formation of the ([9]ane-S_3)Ru(PF_6)$_2$.DMSO intermediate was achieved by stirring ([9]ane-S_3)$RuCl_2$.DMSO (0.22 g, 0.5 mmol) with silver hexafluorophosphate (0.25 g, 1 mmol) for 2 hours in methanol (100 mL) in the dark at room temperature. AgCl precipitate formed was removed by filtration over celite. The yellow filtrate was then degassed for 2 hours before subsequent addition of 1-[2-(1*H*-imidazol-4-yl)ethyl]-3-(4-butyl)urea (0.64 g, 2 mmol). The mixture was then stirred and heated to 75 ^{o}C for 6 days. Cooling and removal of the solvent led to the formation of the crude product as yellow powder. Purification was achieved by column chromatography using alumina as the stationary phase and gradient eluent system starting from diethyl ether: methanol (9:1) up to 100% methanol.

Removal of the solvent from the desired fraction resulted in the formation of final product as light yellow solid (0.48 g, 0.31 mmol, 62%). **^{1}H NMR:** δ_H (400 MHz; DMSO-d_6; Me_4Si) 12.77 (1 H, s, *H2*), 7.32 (1 H, s, *H1*), 6.44 (1 H, s, *H3*), 5.96 (1 H, t, *J* 5.6, *H6*), 5.85 (1 H, t, *J* 5.6, *H7*), 3.06 (2 H, dt, *H5*), 2.79 (2 H, q, *H8*), 2.55 (m, *H thioether*), 2.37 (2 H, t, *J* 7.1 *H4*), 1.09 (20 H, m, *H9-H18*), 0.70 (3 H, t, *J* 8.0, *H19*). **^{13}C {^{1}H} NMR:** δ_C {^{1}H} (101 MHz; DMSO) 158.52 (*Cf*), 138.37 (*Ca*), 130.87 (C*b*), 39.78 (*Cd*), 32.99 (*Ce*), 31.73 (C*g*), 30.50 (C*h-l*), 29.51 (C*m*), 29.30 (C*n*), 28.15 (*Co*), 26.87 (*thioether C*), 26.22 (C*p*), 22.53 (C*q*), 14.37 (C*r*). **FTIR:** ν_{max}/cm^{-1} 3332 (NH), 1621 (CO), 1570 and 1462(imid. ring). m/z (ESI-MS) 625.5 $[(M-2PF_6)/2]^{2+}$, m/z (HRMS) 625.2 $[(M-2PF_6)/2]^{2+}$. Due to the impurity of the sample, elemental analysis did not give usable information.

Synthesis of ([9]ane-S_3)Ru(1-[2-(1*H*-imidazol-4-yl)ethyl]-3-(4-methylphenyl) urea)$_3$.2$CF_3SO_3^-$ **(5.3)**:

Formation of the ([9]ane-S_3)Ru$(PF_6)_2$.DMSO intermediate was achieved by stirring ([9]ane-S_3)$RuCl_2$.DMSO (0.22 g, 0.5 mmol) with silver trifluoromethanesulphonate (0.26 g, 1 mmol) for 2 hours in methanol (100 mL) in the dark at room temperature. AgCl precipitate formed was removed by filtration over celite. The yellow filtrate was then degassed for 2 hours before subsequent addition of 1-[2-(1*H*-imidazol-4-yl)ethyl]-3-(4-methylphenyl)urea (0.98 g, 4 mmol). The mixture was then stirred and heated to 75 ^{o}C for 6 days. Cooling and removal of the solvent led to the formation of the crude product as a brown powder.

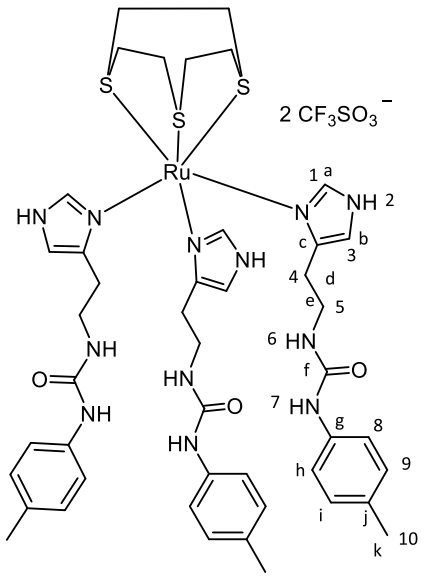

5.3

Purification was achieved by fractional recrystallisation of this brown powder with acetonitrile to remove the remaining reactants. The final product was a lighter shade of brown than the crude (0.45 g, 0.34 mmol, 68%). **^{1}H NMR:** δ_H (400 MHz; DMSO-d_6; Me_4Si) 8.26 (1 H, s, *H1*), 7.40 (1 H, d, *J* 1.1, *H3*), 7.10 (2 H, m, *H8*), 6.85 (2 H, m, *H9*), 6.67 (1 H, br s, *H7*), 5.95 (1 H, t, *J* 5.7, *H6*), 1.13 (2 H, dt, *H5*), 2.55 (m, *H thioether*), 2.36 (2 H, t, *J*

6.9, *H4*), 2.05 (3 H, s, *H10*). **^{13}C {^{1}H} NMR:** δ_C {^{1}H} (101 MHz; DMSO) 155.68 (*Cf*), 138.43 (*Cb*), 135.12 (*Ce*), 130.07 (*Cg*), 129.44 (*Ch*), 118.74 (*Cj*), 118.13 (*Ci*), 39.67 (*Cd*), 28.04 (thioether C), 20.71 (*Ck*). **FTIR:** ν_{max}/cm^{-1} 3337 (NH), 1637 (CO), 1559 and 1451 (imid. ring). m/z (ESI-MS) 507.15 $[(M\text{-}2CF_3SO_3)/2]^{2+}$, m/z (HRMS) 507.15 $[(M\text{-}2\ CF_3SO_3)/2]^{2+}$. Due to the impurity of the sample, elemental analysis did not give usable information.

5.5 **References**

(1) Maity, D.; Bhaumik, C.; Mondal, D.; Baitalik, S. *Inorg. Chem.* **2013**, *52* (24), 13941–13955.

(2) Saha, D.; Das, S.; Maity, D.; Baitalik, S. *Indian J. Chem.* **2011**, *50*, 1418–1428.

(3) Chowdhury, B.; Sinha, S.; Ghosh, P. *Chem. Eur. J.* **2016**, *22* (50), 18051–18059.

(4) Das, S.; Karmakar, S.; Mardanya, S.; Baitalik, S. *Dalton Trans.* **2014**, *43* (9), 3767–3782.

(5) Mo, H.-J.; Niu, Y.-L.; Zhang, M.; Qiao, Z.-P.; Ye, B.-H. *Dalton Trans.* **2011**, *40* (32), 8218–8225.

(6) He, X.; Herranz, F.; Cheng, E. C.-C.; Vilar, R.; Yam, V. W.-W. *Chem. Eur. J.* **2010**, *16* (30), 9123–9131.

(7) Pérez, J.; Riera, L. *Chem. Soc. Rev.* **2008**, *37* (12), 2658–2667.

(8) Mishra, A.; Vajpayee, V.; Kim, H.; Lee, M. H.; Jung, H.; Wang, M.; Stang, P. J.; Chi, K.-W. *Dalton Trans.* **2012**, *41* (4), 1195–1201.

(9) Dickson, S. J.; Paterson, M. J.; Willans, C. E.; Anderson, K. M.; Steed, J. W. *Chem. Eur. J.* **2008**, *14* (24), 7296–7305.

(10) Todd, A. M.; Swinburne, A. N.; Goeta, A. E.; Steed, J. W. *New J. Chem.* **2013**, *37* (1), 89.

(11) Ion, L.; Morales, D.; Nieto, S.; Pérez, J.; Riera, L.; Riera, V.; Miguel, D.; Kowenicki, R. A.; McPartlin, M. *Inorg. Chem.* **2007**, *46* (7), 2846–2853.

(12) Graça O Santana-Marques, M.; Amado, F. M. L.; Ferrer Correia, A. J.; Lucena, M.; Madureira, J.; Goodfellow, B. J.; Félix, V.; Santos, T. M. *J. Mass Spectrom.* **2001**, *36* (5), 529–537.

(13) Shan, N.; Hawxwell, S. M.; Adams, H.; Brammer, L.; Thomas, J. A. *Inorg. Chem.* **2008**, *47* (24), 11551–11560.

(14) Hao, Y.; Jia, C.; Lia, S.; Huang, X.; Yang, X. J.; Janiak, C.; Wu, B. *Supramol Chem* **2012**, *24*, 88–94.

(15) Gomez, D. E.; Fabrizzi, L.; Licchelli, M.; Monzani, E. *Org. Biomol. Chem* **2005**, *3*, 1495–1500.

(16) Steed, J. W.; Atwood, J. L. *Supramolecular Chemistry, 2nd edition*; John Wiley & Sons, Ltd, 2009.

Chapter 6

Self-assembly of Platinum(II) and Palladium(II) complexes of imidazole compounds containing urea derivatives and their interaction with anions

6.1 Background and Project Aims

Platinum and Palladium are both d-block metals which are commonly found in oxidation states of +2 or +4. Platinum(II) and palladium(II) complexes are typically four coordinate while platinum(IV) and palladium(IV) are typically 6-coordinate.[1] Theoretically, 4-coordinate d^8 platinum(II) and palladium(II) complexes could show either a tetrahedral or square planar geometry, but in reality, they are almost always square planar which can be explained in detail by crystal field theory.[1] The Yam group has reported the anion binding behaviour of platinum-based host due to the hosts' useful spectroscopic and luminescence properties.[2] This work has been reviewed in detailed in Chapter 1 section 1.3.3.

Recently, several square planar complexes based on Pt(II) and Au(III) have been extensively studied as supramolecular polymer precursors due to their ability to aggregate into discrete nanostructure linked by various non-covalent interactions.[3–6] Such aggregation has been reported by the Manners' group, in which the platinum(II) complexes of polyethylene glycol-based ligands, **6.1** self-assemble forming functional (1D) supramolecular architectures.[7] This assembly was facilitated by several interactions including metallophilic, hydrogen bonding and π-π interactions. In order to determine the Pt…Pt and π-π overlap in the complexes, various characterisation techniques including AFM microscopy, small-angle X-ray Scattering (SAXS), wide-angled X-ray scattering (WAXS) and selected area diffraction (SAED) techniques have been employed. The characterisation techniques revealed the presence of narrow diameter fibers and the Pt…Pt stacking in the complexes has been confirmed by SAED, that showed a distinct reflection with a spacing of 0.323 nm, attributed to the known range of spacing for Pt…Pt stacking.[8,9] These self-assembled materials possess interesting properties including electronic and emissive properties,[3] resistance to

photobleaching[10] and near IR excitation properties,[4] which could be very useful in various applications particularly in the development of artificial photosynthesis,[11,12] solar cell applications[13,14] and organic light-emitting diodes (OLEDs).[15,16]

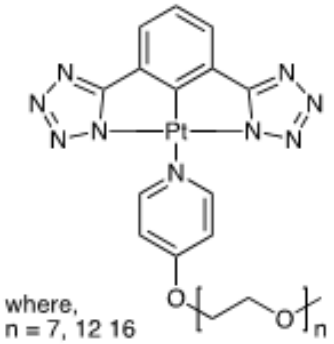

6.1

Single-crystal X-ray diffraction analysis provides the most reliable structural information in the solid-state but, unfortunately, suitable crystals of supramolecular assemblies are often not easily obtained. Moreover, packing-forces may result in solid-state structures different from those existing in solution, where, additionally, equilibria between different stoichiometries may occur. Thus, in the absence of good single crystals suitable for X-ray crystallography, the self-assembly properties of metal complexes can also be studied using Diffusion-ordered Spectroscopy (DOSY), a well-established NMR technique that permits the separation of the NMR signals in a multicomponent mixture based on based on the translational diffusion of each chemical species in solution.[17]

Since the 1990s, the dramatic development of the diffusion-ordered NMR spectroscopy (DOSY) technique, has made the investigation of aggregates in solution became much more accessible. This method enables the resolution of NMR spectra along a diffusion axis, thereby arraying resonances of aggregates by weight, as larger, higher molecular mass complexes diffuse more slowly than lower mass complexes thus giving a lower diffusion coefficient value. This technique is highly dependent on the size and shape of the molecule, as well as the physical properties of the surrounding environment such as viscosity, temperature, etc. There is a large volume of published studies utilising DOSY NMR techniques to characterise the aggregates that form in the solution mixture.[18–21]

For instance, Zheng and co-workers has developed a drug delivery supramolecular complex using coordination-driven self-assembly concept, in which a hexanuclear Pt(II) cage acts as the delivery vehicle with Pt(IV) prodrugs as the cargo.[22] In this work, DOSY NMR was used to measure the size of the resulting supramolecular complex. Using the equation developed by Stang group,[23] the diffusion coeffiecient (*D*) obtained from the DOSY was used to estimate the size of the structure. Results from DOSY NMR analysis has confirmed the encapsulation of the Pt(IV) drugs within the cage by comparing the diffusion coefficient (*D*) values of the cage alone (1.30 x 10^{-10} m^2s^{-1}) and the cage with the drugs (1.60 x 10^{-10} m^2s^{-1}).

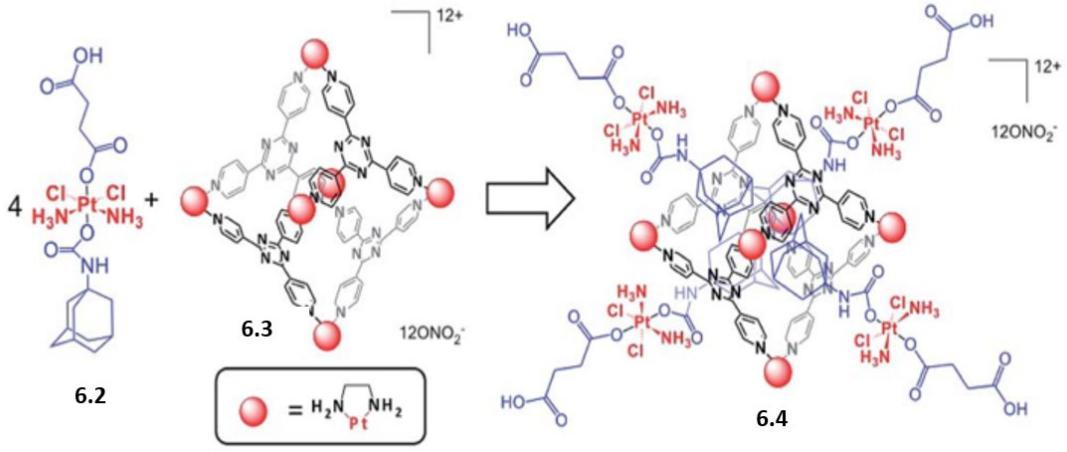

Figure 6.1 Representation of the host–guest complex (**6.4**) assembled from the Pt(IV) prodrug (**6.2**) and the Pt(II) cage (**6.3**). Reproduced with permission from reference 22.

Undoubtedly, for coordination complexes, an appropriate NMR technique such as DOSY is of vital importance to monitor and distinguish mononuclear and polynuclear derivatives that form in the solution *in situ* as exemplified in the work of Ananikov and co-workers.[24] With the advent of DOSY NMR, the identification of intermediate complexes in the catalytic carbon-sulfur bond formation reaction, $[Pd(SPh)_2(PPh_3)_2]$ and $[Pd_2(SPh)_4(PPh_3)_2]$ as mononuclear and polynuclear derivatives, respectively has been made possible. Other techniques such as ^1H NMR and ^{31}P NMR cannot be used to distinguish the nature of the palladium complexes in the mixture. Similarly, X-Ray crystallography analysis, while a powerful technique for structural characterisation of metal complexes, requires very high quality crystals that might only represent the most stable complexes, not the intermediates that form in the solution.

In another example, the DOSY NMR technique was employed to investigate the self-association of $[Pt^{II}(phen)(L^1\text{-}S,O)]^+$ cations that form dimer aggregates in acetonitrile solution and water–acetonitrile mixtures of up to 30% (v/v) D_2O–CD_3CN.[18] This self-association was driven by cation–π stacking interactions as illustrated in Figure 6.2. It was found that by increasing the water content from >30% to 100% (v/v) D_2O–CD_3CN, the extent of aggregation also increased as a function of $[Pt^{II}(phen)(L^1\text{-}S,O)]Cl$ concentration. These aggregations result in the formation of nano-sized structures consisting of up to *ca*. 735 mononuclear as determined by diffusion coefficients obtained from DOSY NMR.

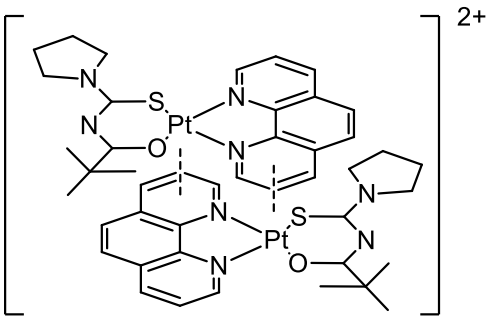

Figure 6.2 Postulated 'average' structure of a {[PtII(phen)(L1 -S,O)]+ }2 dimer aggregate in solution based on ^1H NMR shielding trends as a function of concentration.

In this chapter we aim to produce platinum(II) and palladium(II) complexes of imidazole urea ligands and investigate their interaction with various anions. To study the interaction with the anions, the pincer-type complexes are required to form in *cis*-configuration so that the urea groups can converge and hydrogen bond with the incoming anions. This can be achieved by using a combination of different types of *cis*-blocking ligands such ethylenediamine (en), cyclohexanediamine (cyen) and 1,2-bis(diphenylphosphino)ethane (dppe) with imidazole urea ligands to pre-organise the complex into a *cis* configuration. The use of chelating *cis*-blocked ligands has been exemplified in the work of many researchers.[25,26]

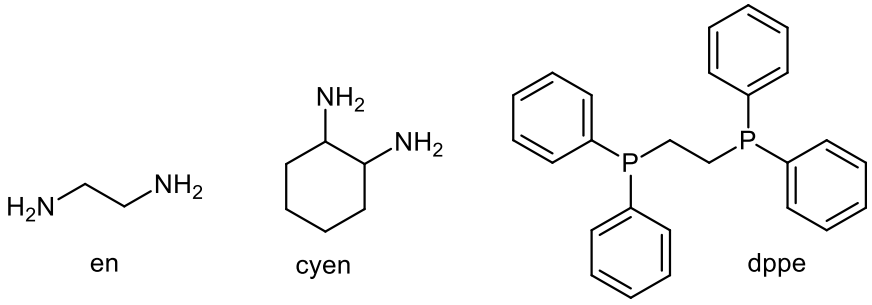

6.2 Results and Discussion

6.2.1 Synthesis and characterisation of Platinum(II) and Palladium(II) complexes

Cis-[Pt(en)Cl_2] **6.5**, prepared from K_2PtCl_4 and ethylenediamine, was converted to [Pt(en)$(CF_3SO_3)_2$] in methanol solution (20 °C, 2 hours, in the dark) by using two equivalent of $AgCF_3SO_3$. After the removal of the greyish precipitate by filtration over celite, the yellow solution obtained was bubbled under a continuous nitrogen stream for 2 hours. Two equivalent of ligand **2.1** was then added to the solution and heated at 75 °C for three days in 2-propanol to afford complex **6.9** (Scheme 6.1).

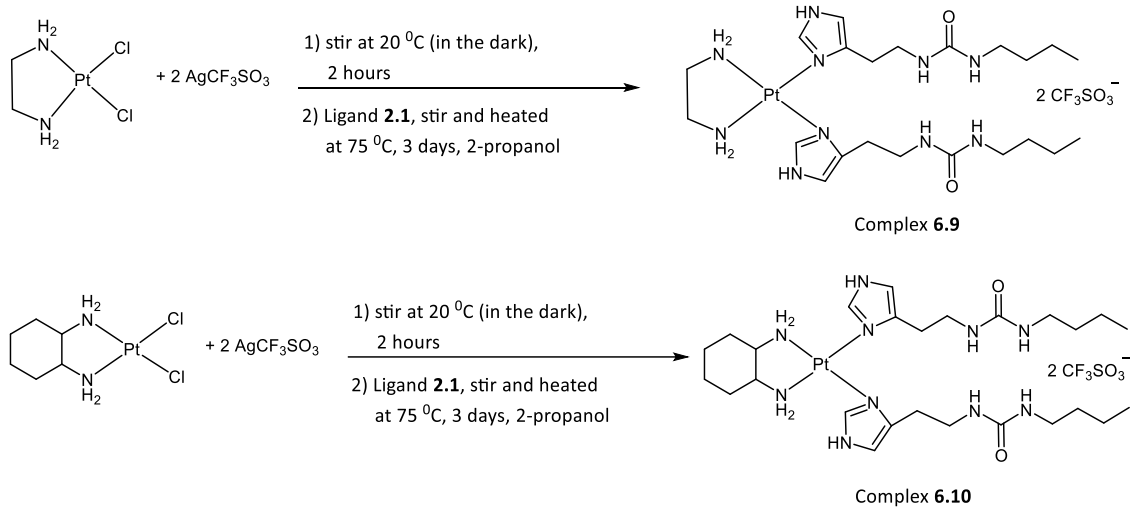

Scheme **6.1** Synthesis pathway of the preparation of mixed-ligands Platinum(II) complexes.

Complex **6.9** was obtained as a brown viscous solid or gum after multiple recrystallisations with different solvents and is soluble in acetone, acetonitrile, methanol, ethanol as well as dimethylsulfoxide. Complex **6.9** has been characterised by ESI-mass spectrometry as a doubly charged ion, $[M\text{-}2(CF_3SO_3)^-]^{2+}$, m/z_{exptl} 337.88 due to the loss of the two CF_3SO_3 counter ions. Complex **6.9** also has been identified using High-Resolution Mass Spectrometry, in which the experimental value of *m/z* is consistent with the simulated *m/z* (Figure 6.3).

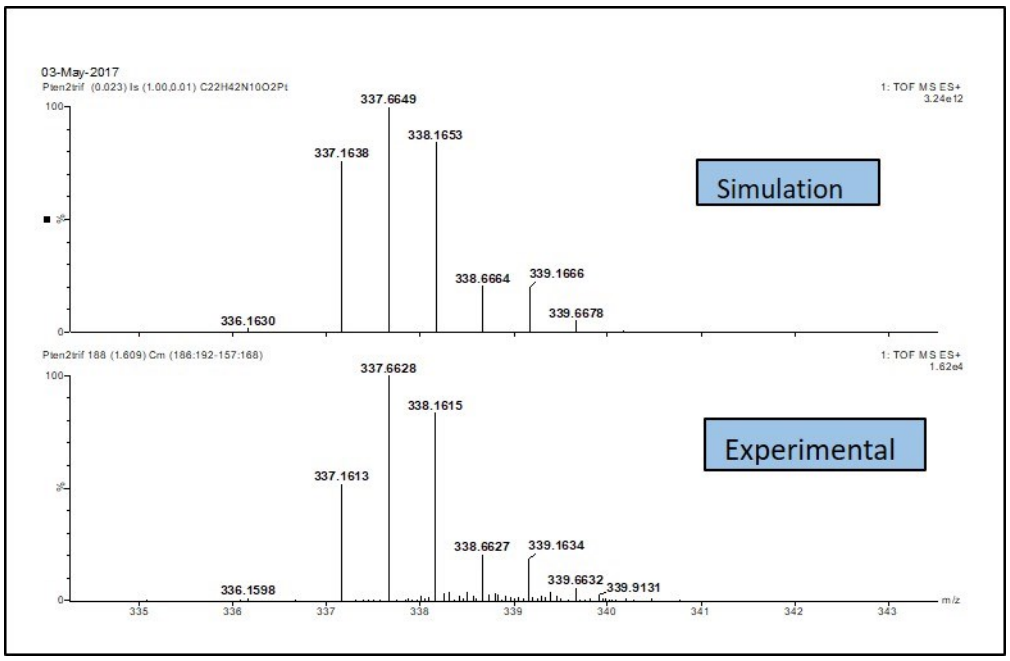

Figure 6.3 High-Resolution Mass Spectrometry data of complex **6.9**.

To our surprise, characterisation of complex **6.9** using ^{1}H NMR spectroscopy in three different deuterated solvents namely MeOH-d_4, DMSO-d_6 and CD_3CN revealed the presence of more than one species in solution. Initially, the first attempt of this reaction was carried out without the presence of nitrogen gas which suggested that the platinum(II) metal ion might have been oxidised to platinum(IV) ion resulting in the octahedral complexes, that could explain the presence of multiple products. Therefore, to eliminate the possibility in the formation of Pt(IV) complexes, for the second attempt, the reaction was performed under continuous nitrogen stream to eliminate the presence of oxygen that might contribute to the oxidation. Nevertheless, even with the absence of oxygen, the reaction still produced an apparent mixture of compounds which was confirmed by ^{1}H NMR spectroscopy, showing ten proton signals assigned to the imidazole CH protons (in the 6.5 to 8.5 ppm region), very different from our expectation of only two resonances attributed to imidazole CH protons (Figure 6.4). The assignment of the signals is also challenging particularly in the methylene proton regions as most of the signals are overlapping with each other. While it is clear from the ^{1}H NMR spectrum of complex **6.9** that there are several species present, their assignment cannot be made on the basis of this one-dimensional data alone.

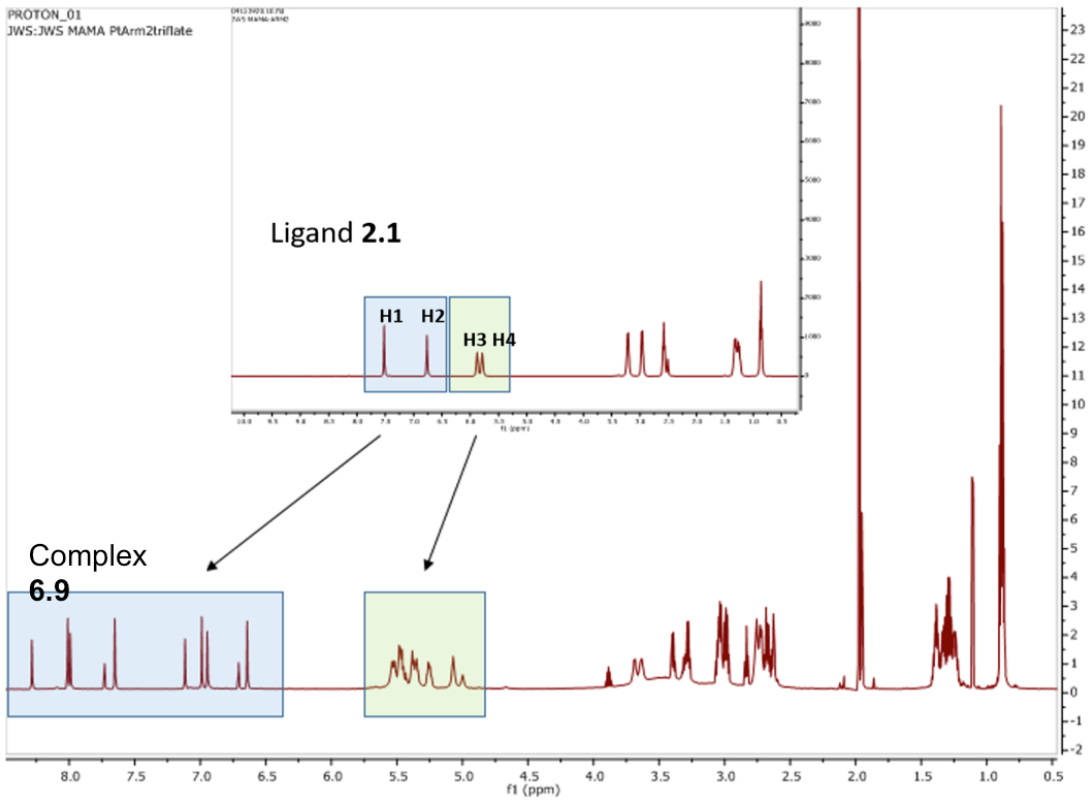

Figure 6.4 ^{1}H NMR spectrum of complex **6.9** comparable to its free ligand **2.1** (inset picture).

The ^{1}H DOSY NMR experiment in CD_3CN established the coexistence of four different compounds present in the solution mixture of complex **6.9**, evident from four distinct layers of imidazole CH proton signals that are well-separated from each other (Figure 6.5). In contrast, the rest of the proton signals are not well resolved as they are exchanging with one another. Using the diffusion coefficient equation developed by Morris group,[27] the molecular weight of each species have been estimated (Table 6.1).

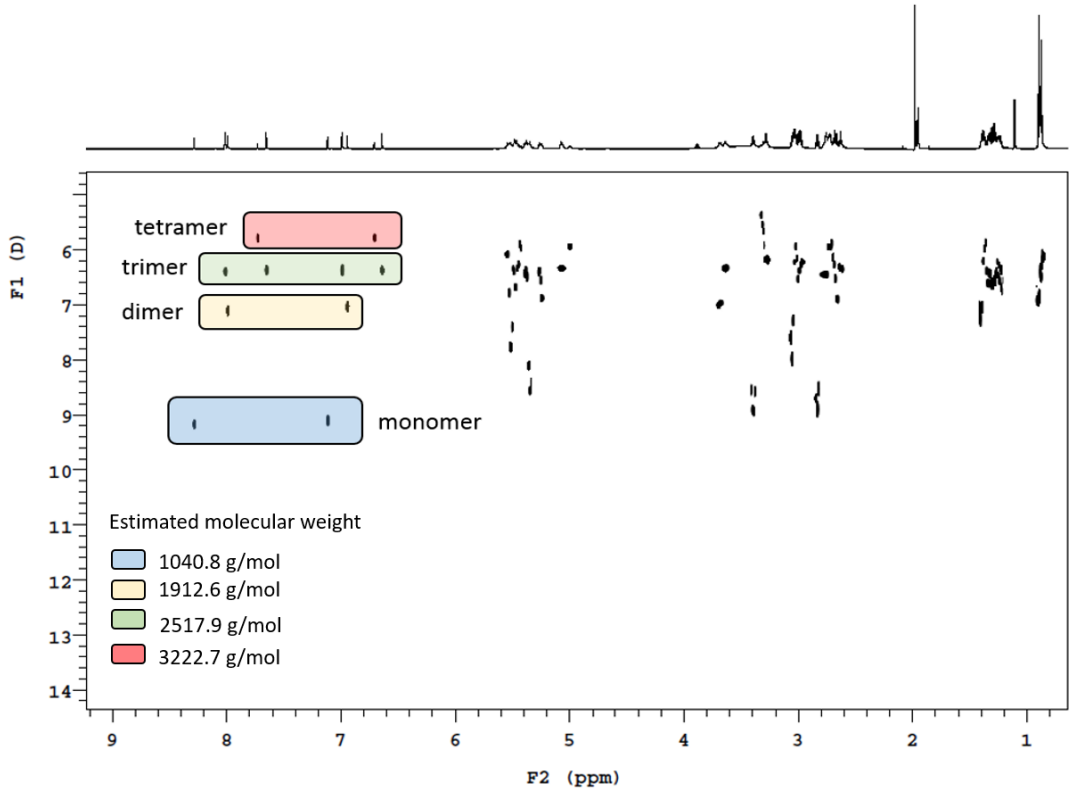

Figure 6.5 ^{1}H DOSY NMR spectrum of complex **6.9** in CD_3CN.

The CD_3CN was chosen as the solvent for DOSY NMR because there is no appreciable proton exchange of the imidazole protons with residual solvents, unlike the exchange that has been observed in the DOSY spectra of complex **6.9** in MeOH-d_4 and DMSO-d_6,. From the DOSY spectra of complex **6.9** in MeOH-d_4, the CH1 and CH2 proton signals of the monomer show higher diffusion coefficients, 7.84×10^{-10} compared to the value in CD_3CN most likely due to the exchange with the residual solvents. The higher diffusion coefficient value results from the average diffusion coefficients between those of the exchanging sites (Figure 6.6).

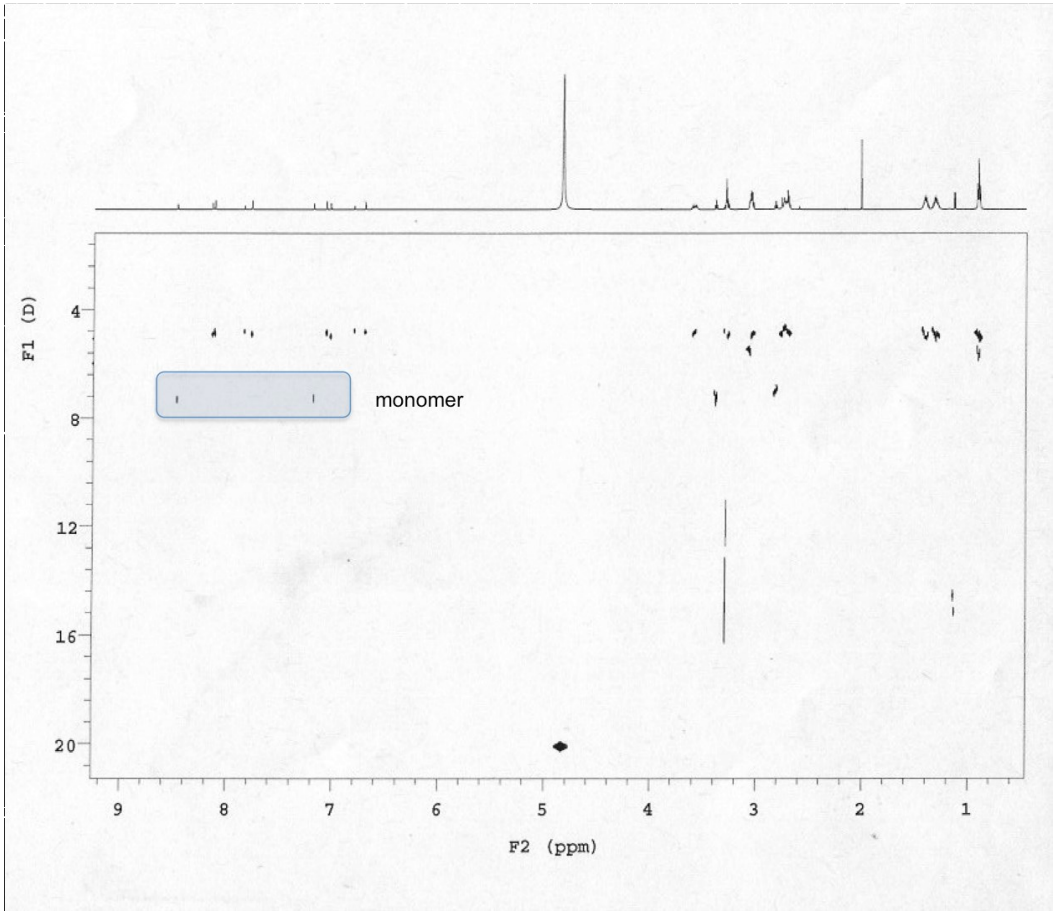

Figure 6.6 ^{1}H DOSY NMR spectrum of complex **6.9** in MeOH-d_4.

Table 6.1 Estimated molecular mass (g/mol) of the components of the mixtures found in the CD_3CN solution of complex **6.9**.

Layer	Diffusion Coefficient, D_{obs} (m^2s^{-1})	Estimated molecular mass (g/mol)	Expected/theoretical molecular mass (g/mol)	Difference (%)
1	9.15×10^{-10}	1040.8	973.23	6.86
2	7.13×10^{-10}	1912.6	1946.46	1.74
3	6.39×10^{-10}	2517.9	2919.69	13.76
4	5.80×10^{-10}	3222.7	3892.92	17.21

Based on the estimated molecular mass (g/mol) obtained from the calculation, it is suggested that four different oligomers of Platinum(II) complexes have been formed. Layer 1 (the bottom layer) represents the monomer as it has smaller molecular weight and diffuses the fastest among all the oligomers. The subsequent layers represent the dimer, followed by the trimer and tetramer, respectively. From the ESI-MS spectrum of complex **6.9** in acetonitrile, several sets of peaks centred around m/z 339, 674, 1012

and 1347 are observed that are assigned to doubly charged ions of the monomer, dimer, trimer and tetramer, respectively (Figure 6.7).

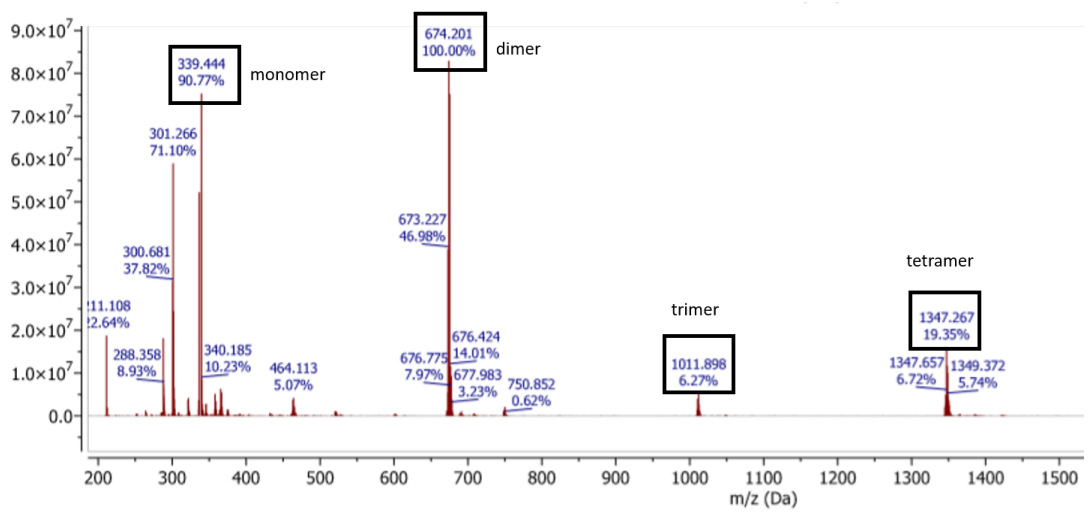

Figure 6.7 ESI-MS spectrum of complex **6.9** showing the presence of oligomers in the acetonitrile solution.

The formation of these oligomers is possibly driven by Pt…Pt interactions and π-π stacking of the imidazole group as shown in previous reports.[26,28] Variable temperature (VT) NMR spectroscopy was also performed to observe or rule out possible conformational changes within the complex or exchange between the different species. The NMR spectrum was recorded at 25°C, 50°C and 80°C (Figure 6.8). However, no appreciable change was observed on the chemical shifts of all protons of complex **6.9** nor in the overall appearance of the spectrum suggesting that the observation of multiple peaks does not arise from the presence of conformers able to exchange on the NMR timescale.

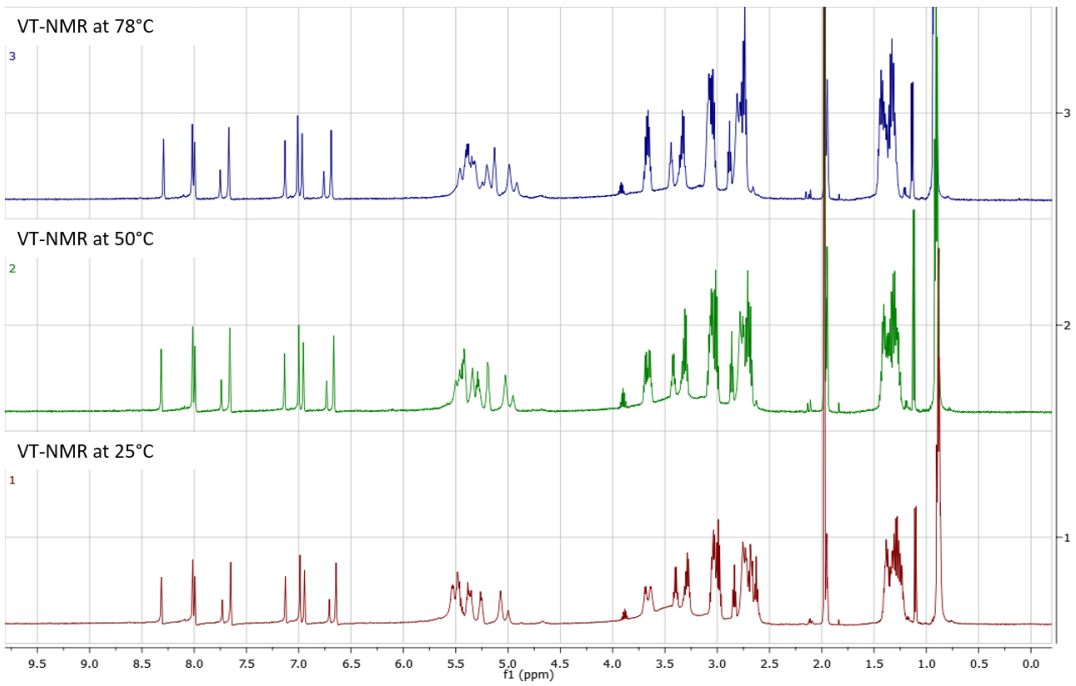

Figure 6.8 VT-NMR spectra of complex **6.9**.

We sought insight the role of ethylenediamine in the self-assembly of the complex by replacing the ethylenediamine ligand with R,R-1,2-cyclohexanediamine, to give complex **6.10**. The precursor, *cis*-[Pt(cyclohexanediamine)Cl_2] **6.6**, prepared from K_2PtCl_4 and cyclohexanediamine, was converted to [Pt(cyclohexanediamine) $(CF_3SO_3)_2$] in methanol solution (20 °C, 2 hours, in the dark) using two equivalent of $AgCF_3SO_3$. After the removal of the light grey precipitate by filtration over celite, the yellow solution obtained was bubbled under a continuous nitrogen stream for 2 hours. Two equivalents of ligand **2.1** was then added to the solution and the mixture heated at 75 °C for three days to afford complex **6.10**. Similar to complex **6.9**, this compound also soluble in the same solvents, namely acetone, acetonitrile, methanol, ethanol as well as dimethylsulfoxide. Characterisation by ESI-mass spectrometry has confirmed the formation of complex **6.10** as doubly charged ion, $[(M\text{-}2(CF_3SO_3^-)]^{2+}$, m/z_{exptl} 364.68 due to the loss of the two CF_3SO_3 counter ions. Complex **6.10** also has been identified using High-Resolution Mass Spectrometry, in which the experimental profile is consistent with the simulated spectrum (Figure 6.9).

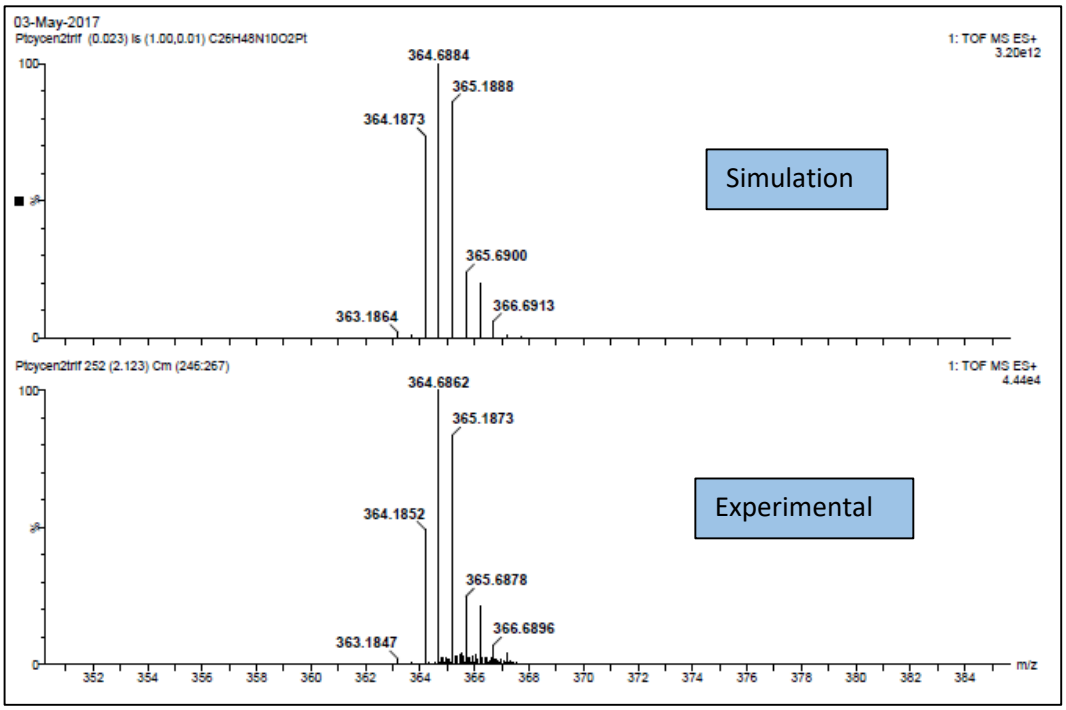

Figure 6.9 High-Resolution Mass Spectrometry data for complex **6.10**.

Characterisation of complex **6.10** using ^{1}H NMR spectroscopy was carried out in CD_3CN similar with complex **6.9**. ^{1}H NMR spectrum of complex **6.10** also shows the presence of more than one species in the solution, similar to complex **6.9** (Figure 6.10).

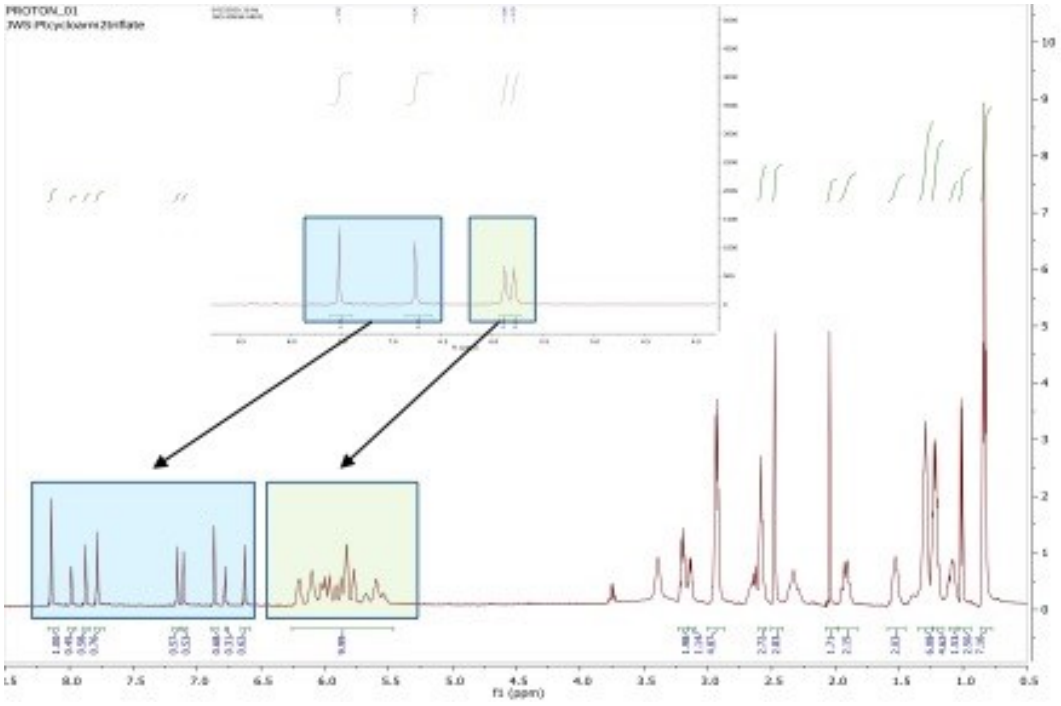

Figure 6.10 ^{1}H NMR spectrum of complex **6.10** comparable to its free ligand **2.1** (inset picture).

A ^{1}H DOSY NMR experiment established the presence of three different species in the solution mixture of complex **6.10** evident from three distinct layers of imidazole CH proton signals that are well-separated from each other (Figure 6.11). The lowest layer is labelled as layer 1 while the rest of the layers are labelled accordingly. Based on the molecular mass calculated from the diffusion coefficient, the first layer corresponds to the trimer of complex **6.10**, followed by pentamer and heptamer for the other two respective layers. While there are distinct signals observed in the imidazole region, the urea protons and methylene protons are not well resolved as they are exchanging with each other. Using the same equation as complex **6.9**, an estimate of the molecular weight of each of the species has been calculated (Table 6.2).

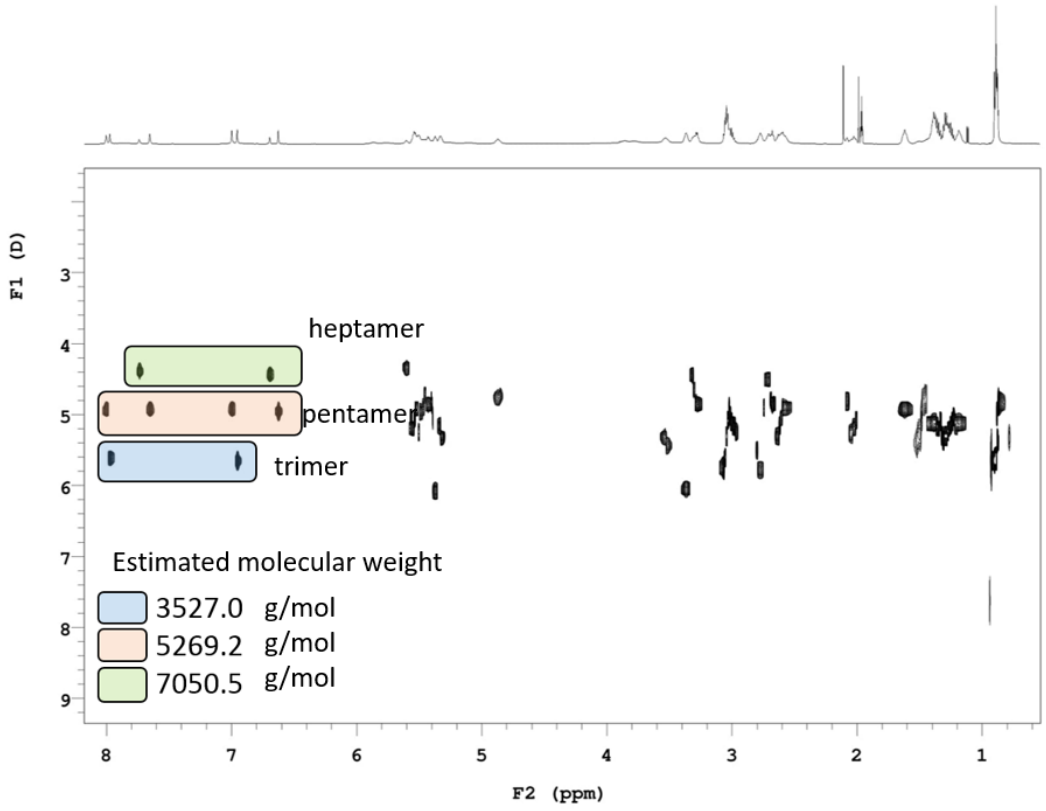

Figure 6.11 ^{1}H DOSY spectrum of complex **6.6** in CD_3CN.

Table 6.2 Estimated molecular mass (g/mol) of both mixtures found in the CD_3CN solution of complex **6.10**.

Layer	Diffusion Coefficient, D_{obs} (m^2s^{-1})	Estimated molecular mass (g/mol)	Expected molecular mass (g/mol)	Difference (%)
1	5.6×10^{-10}	3527.0	1027.28*3 = 3081.84	14.4
2	5.0×10^{-10}	5269.2	1027.28*5 = 5136.40	2.6
3	4.4×10^{-10}	7050.5	1027.28*7 = 7190.96	1.9

Note: Expected molecular mass for layer 1, 2 and 3 correspond to the molecular mass of trimer, pentamer and heptamer.

From the ESI-MS spectrum of complex **6.10** in acetonitrile, several sets of peaks centred around m/z 366, 728, 1092 and 1455 are observed that might correspond to doubly charged ions of the monomer, dimer, trimer and tetramer, respectively. However, there is no ion mass related to the pentamer and heptamer suggesting that the ions of higher molecular weight oligomers might be fragmented into smaller ions during the experiment (Figure 6.12).

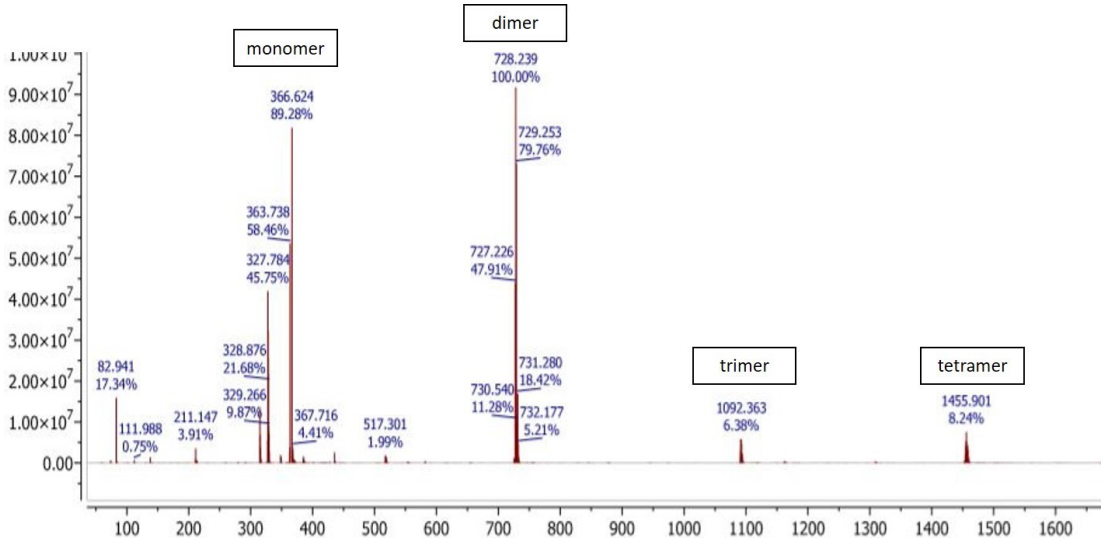

Figure 6.12 ESI-MS spectrum of complex **6.10** showing the ion mass peaks correspond to the oligomers in the acetonitrile solution.

From the data of complex **6.9** and **6.10**, it is suggested that the aggregation of the complexes could be due to the synergistic effect of Pt-Pt stacking, π-π stacking and van der Waals interactions.[29] To examine the effect of Pt-Pt stacking, a palladium analogue, complex **6.11** was synthesised. Complex **6.11** was synthesised from $[Pd(en)Cl_2]$ and the tert-butyl analogue, ligand **2.8** to give a bulkier terminal group. Pd(II) metal was chosen

because it is also a d^8 metal which can give complexes of the same geometry as Pt(II). We hypothesised that replacing Pt(II) with Pd(II) could prevent or at least minimise the aggregation of the complex as the metallophilic (M-M) interaction in Pd(II) is weaker than Pt(II).[30] Introducing the tert-butyl chain to the complex also could prevent van der Waals forces at the alkyl chain and inhibit the formation of the aggregates. Complex **6.11** was prepared using a similar procedure as complex **6.9** and **6.10**, but the reaction time was shortened to 24 hours as Pd(II) metal is more labile compared to Pt(II). The synthesis pathway of complex **6.11** is illustrated in Scheme 6.2.

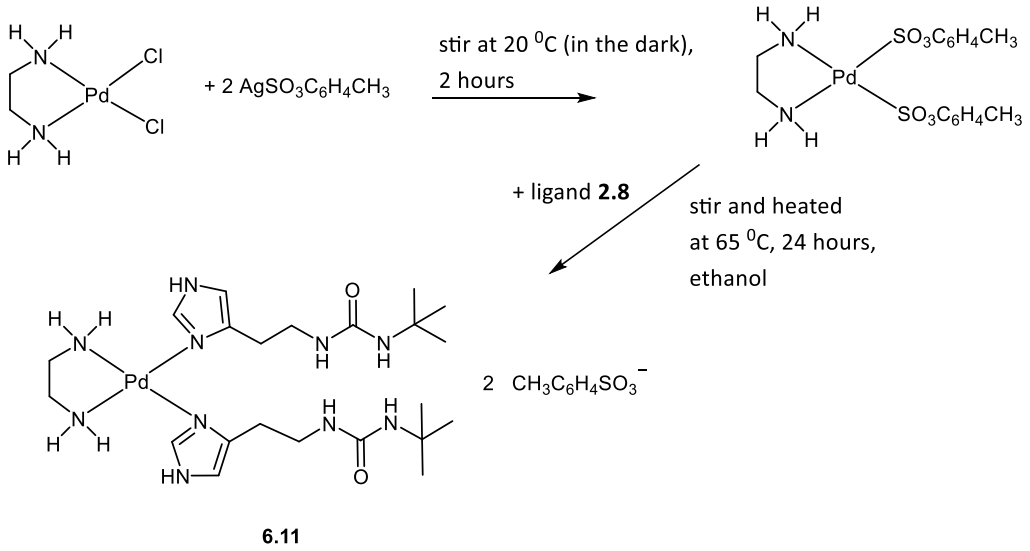

Scheme 6.2 Synthetic pathway of complex **6.11** from $[Pd(en)Cl_2]$ precursor.

After 24 hours reaction, complex **6.11** was isolated as brown sticky solid, dried under vacuum and purified from multiple recrystallisations in nitromethane and acetonitrile. ESI-mass spectrometry data shows a mass peak, m/z_{exptl} 421.28 which is difficult to assign but could be the doubly charged ion, $[M/2 + 2\ ACN + H^+]^+$ of complex **6.11**, (ACN is acetonitrile). To further confirm the mass of complex **6.11**, an HR-MS experiment was performed and the data shows that there is no mass peak at 421.28 or 294.14 (theoretical mass of triply charged ion of complex **6.11**) suggest the targetted compound might not have formed (Figure 6.13).

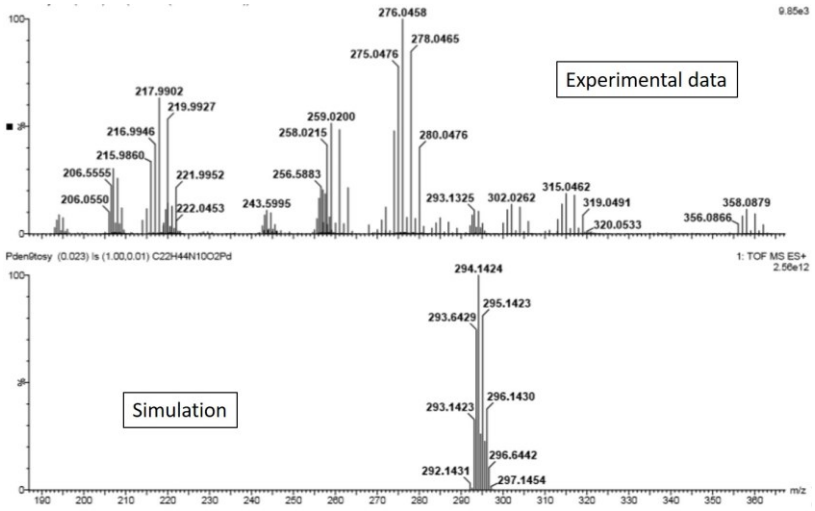

Figure 6.13 HR-MS spectrum of complex **6.11**.

Complex **6.11** was also characterised by ^{1}H and ^{13}C NMR spectroscopy. The appearance of urea NH signals at the region of 5.88 to 5.60 ppm confirms the presence of ligand **2.8**. However, in the ^{1}H NMR spectrum of complex **6.11** three sets of resonances are observed for the imidazole CH1 and CH2 protons as well as three sets of urea NH3 and NH4 peaks (Figure 6.14). This suggests that the complex might also aggregate to form oligomers, similar to complex **6.9** and **6.10**. In contrast with complex **6.9** and **6.10**, complex **6.11** is only partially soluble in acetonitrile and hence the ^{1}H DOSY NMR experiment cannot be performed.

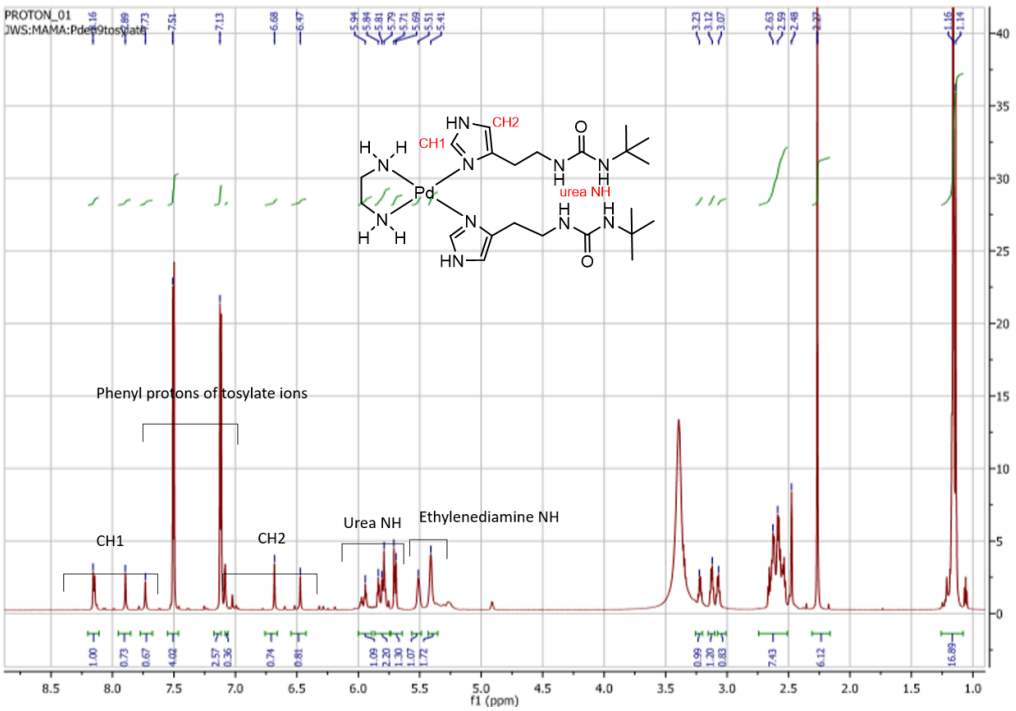

Figure 6.14 ^{1}H NMR spectrum of complex **6.11**.

From the data of complex **6.9**, **6.10** and **6.11**, it is suggested that the *cis*-blocking ligands, ethylenediamine and cyclohexanediamine could play some role in the aggregation of the complexes. To test this hypothesis, we attempted to synthesise another Pd(II) complex using *cis*-block ligand without an amine group, 1,2-bis(diphenylphosphino)ethane (dppe). The precursor, [Pd(dppe)Cl_2] (**6.8**) was synthesised by reacting K_2PdCl_4 in concentrated HCl with dppe for 6 hours at 90 °C.[31] Metathesis on precursor **6.8** was performed using silver(I) tosylate to replace the chloride ion. Silver chloride formed was then filtered over celite and the remaining filtrate was degassed under nitrogen for 2 hours. Ligand **2.8** was added to the solution and the mixture was heated to reflux for 24 hours in methanol. After 24 hours reaction, complex **6.12** was isolated as brown solid, dried under vacuum and purified from multiple recrystallisation in nitromethane and acetonitrile. From the ESI-MS spectrum of complex **6.12**, no mass peak associated to the complex was observed. Meanwhile, from the ^{1}H NMR spectrum (Figure 6.15), appearance of NH urea signals in the range of 5.66 to 5.80 ppm might suggest that complex **6.12** have been successfully synthesised.

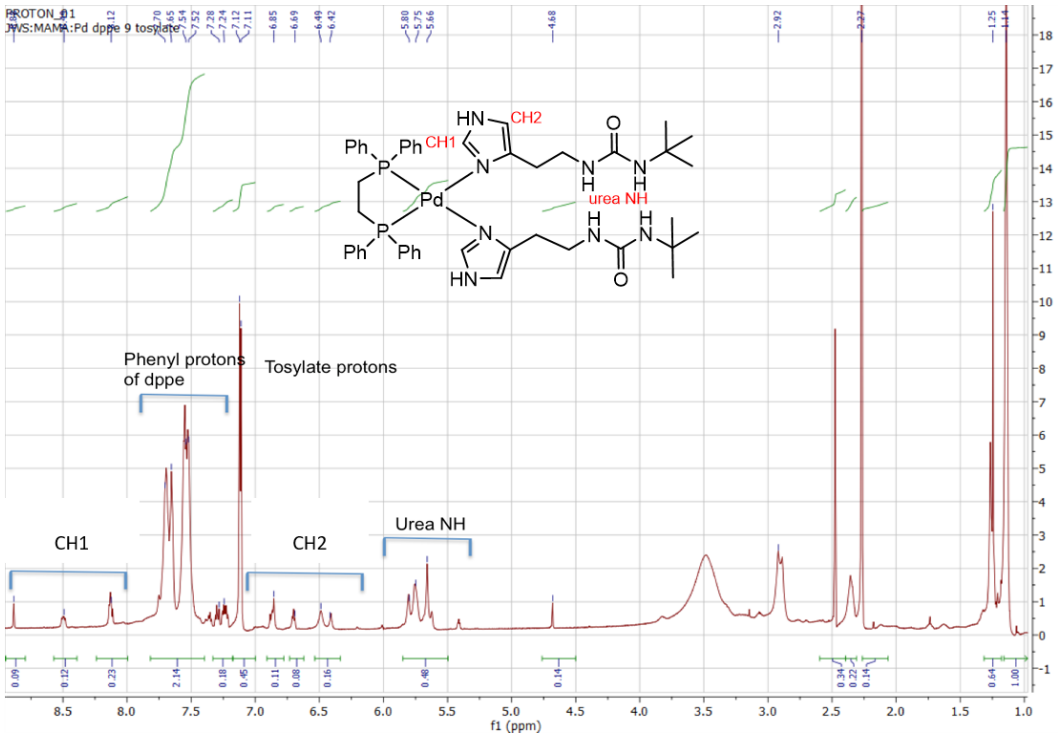

Figure 6.15 ^{1}H NMR spectrum of complex **6.12**.

From the ^{1}H NMR spectrum, at least three sets of each signal, H1 and H2 protons of imidazole and also urea NH can be seen. But unfortunately, complex **6.12** is only partially soluble in acetonitrile, thus ^{1}H DOSY NMR cannot be performed to confirm the presence of oligomers as observed in complex **6.9** and **6.10**. Therefore, there is no solid evidence that can confirm the role of amine (in ethylenediamine and cyclohexanediamine) in the aggregation of the synthesised complexes.

6.2.2 Solution state anion binding studies of Pt(II) and Pd(II) complexes with chloride, fluoride and acetate ions.

The solution state binding properties of complex **6.9** were investigated using ^{1}H NMR spectroscopic titrations in CD_3CN solvent with chloride, fluoride and acetate ion as tetrabutylammonium salts. This study was performed to show whether this complex can be used for anion sensing. During the titration, important signals namely the CH1 and CH2 protons of imidazole as well as NH3 and NH4 protons of urea were followed to investigate the anion binding behaviour of the respective compounds. The first titration experiment was performed using chloride as the tetrabutylammonium salt. The addition of up to 4 equivalents of chloride does not impart any significant changes to the chemical shifts of the CH1, CH2, NH3 and NH4 protons (Figure 6.16). A plausible reason could be associated to the size of chloride ion that does not allow it to penetrate into the supramolecular network of complex **6.9**. In many cases, the binding strength decreases with the increase of ion size.[32] Since complex **6.9** is not responsive to chloride ion, titration with larger, less strongly hydrogen bond accepting halide ions such as bromide and iodide was not carried out.

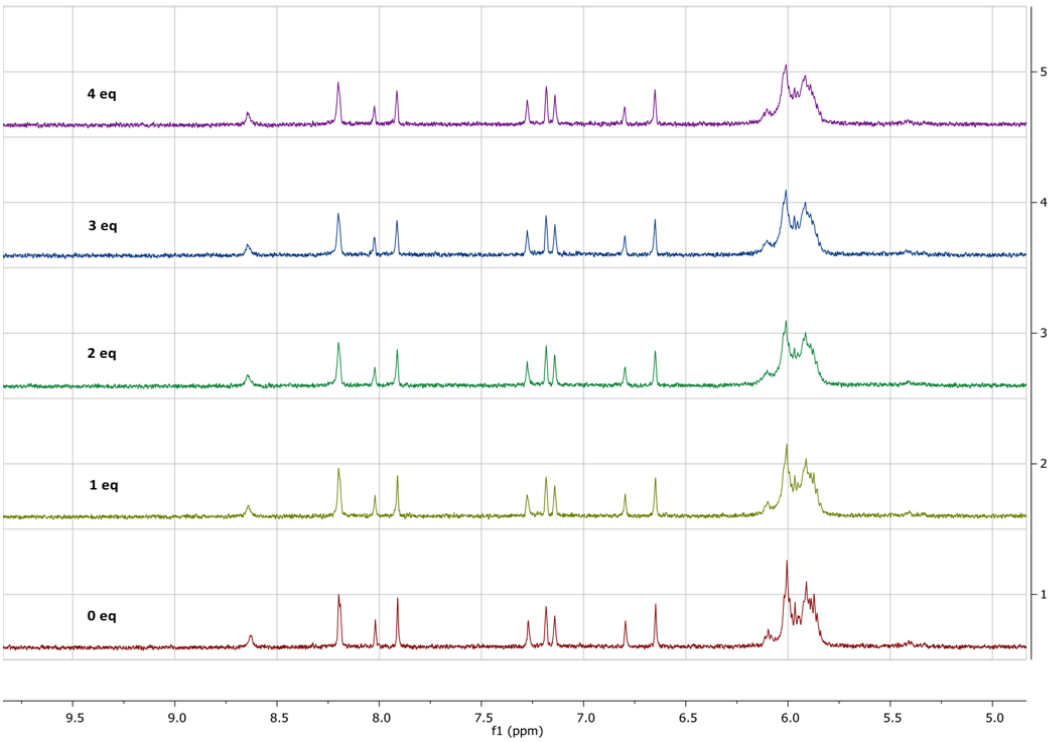

Figure 6.16 Stack plot showing the ^{1}H NMR spectrum of compound **6.9** in CD_3CN in the presence of chloride ion as tetrabutylammonium salt.

Another titration experiment with fluoride (as the tetrabutylammonium salt) was also carried out. From the previous chapters, all of the synthesised hosts including the free ligands interact with fluoride ion though acid-base interaction, in which the synthesised host play their role as acid versus the highly basic fluoride ion. Since complex **6.9** comprises different oligomers, the H1 and H2 protons of the imidazole group are labelled accordingly and followed throughout titration experiments. H1a and H2a represent chemical shifts of the monomer, H1b and H2b is attributed to the chemical shifts of the dimer, H1c1, H1c2, CH2c1 and CH2c2 chemical shifts belongs to the trimer and finally CH1d and CH2d represent chemical shifts of the tetramer. Upon the addition of one equivalent of fluoride ion, peaks of H1d (tetramer) and H1c2 (trimers) start to broaden, meanwhile peak of H1b (dimer) becomes broad and shifts upfield. On the other hand, the addition of one equivalent of fluoride ion does not cause any significant changes on the chemical shifts of the urea NH protons (Figure 6.17). Addition of two equivalents of fluoride ion cause the peaks of H1d and H1c2 to move further upfield. At this point too, the urea protons peaks start to broaden and overlap with each other. Subsequently, three equivalents of fluoride ion added results

in the broadening of the H1c1, H1b and H1d peaks into the baseline. After four equivalents, all imidazole protons have completely deprotonated leaving only H1c2 and H2b, although both of these peaks broadens after the addition of five equivalents of fluoride. The urea proton signals also reduced in the intensity and start to disappear as well upon addition of more equivalents of fluoride. These data have shown that when fluoride ion was introduced to the complex, it deprotonates the imidazole protons of the larger oligomers first, namely the tetramer and trimer. Fluoride only deprotonates the imidazole protons of the dimer and monomer after three equivalents of fluoride has been added. This could suggest that higher molecular weight oligomers are more acidic and prone to deprotonation reaction with fluoride ion over lower molecular weight oligomers.

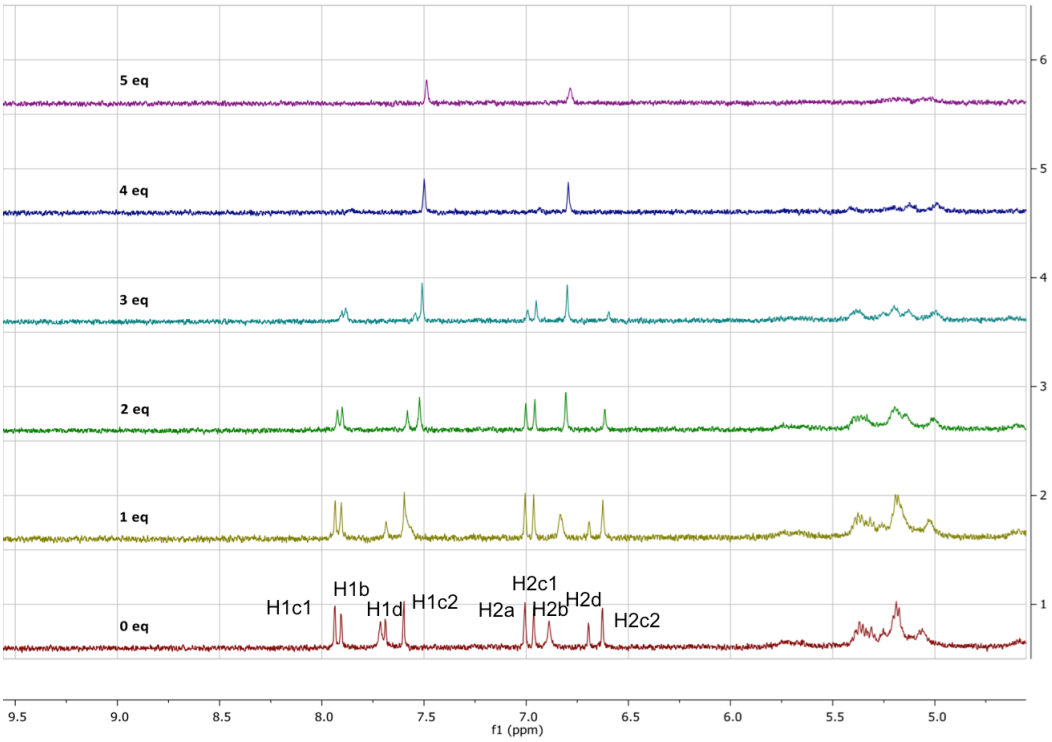

Figure 6.17 Stack plot showing the ^{1}H NMR spectrum of compound **6.9** in CD_3CN in the presence of fluoride ion as the tetrabutylammonium salt.

Complex **6.9** was also titrated with acetate as tetrabutylammonium salt in CD_3CN. Similar to the titration with fluoride ion, the H1 and H2 protons of the imidazole were followed throughout the titration experiments. Addition of one equivalent of acetate ion results in the broadening of H1c1 and H1b signals, while H1d signal split into two separate peaks. On the other hand, upfield shifts were observed for H1c2, H2b, H2d

and H2c2. Subsequent addition of two equivalents of acetate led to the disappearance of one of the split peaks while the rest of the imidazole protons decrease in their intensity possibly indicative of their involvement in hydrogen bonding with the acetate ion. The complete disappearances of all imidazole proton signals except H1c2 and H2b indicate deprotonation. Meanwhile, incremental addition of acetate ion led to the broadening of urea NH peaks (Figure 6.18).

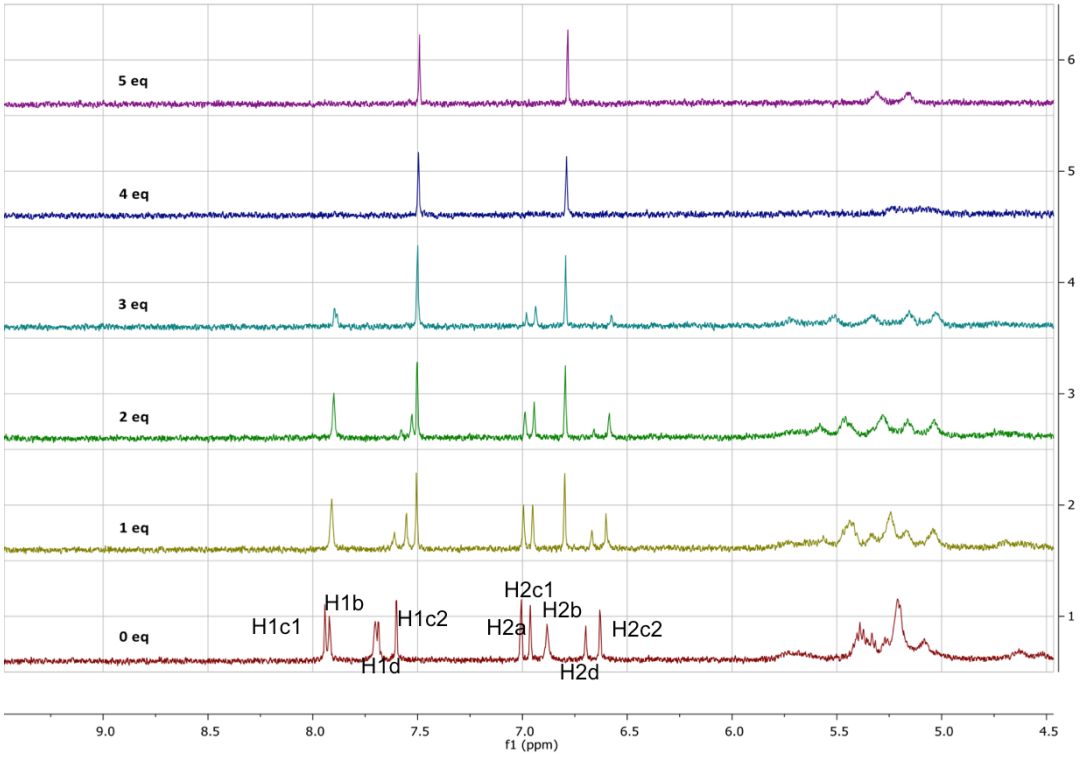

Figure 6.18 Stack plot showing the ^{1}H NMR spectrum of compound **6.9** in CD_3CN in the presence of acetate ion as tetrabutylammonium salt.

Similar to complex **6.9**, a titration experiment of complex **6.10** was carried out in CD_3CN. Complex **6.10** was titrated only with fluoride and acetate as tetrabutylammonium salts. Similar to complex **6.9**, the H1 and H2 protons of imidazole in complex **6.10** were followed throughout the titration experiments. H1a and H2a represent theresonances of the trimer, H1b1, H1b2, H2b1 and H2b2 is attributed to the the pentamer, while H1c and H2c belongs to the heptamer. Addition of one equivalent of fluoride ion cause the broadening of H1c peak as well as slight upfield shift of H2a peak (Figure 6.19). The H1c peak shifts upfield and H2c signal has diminished after the addition of two equivalent of fluoride ion. All signals except H1b2

and H2a disappeared after four equivalent of fluoride ion added indicating deprotonation. Gradual addition of fluoride ion also cause deprotonation on urea NH.

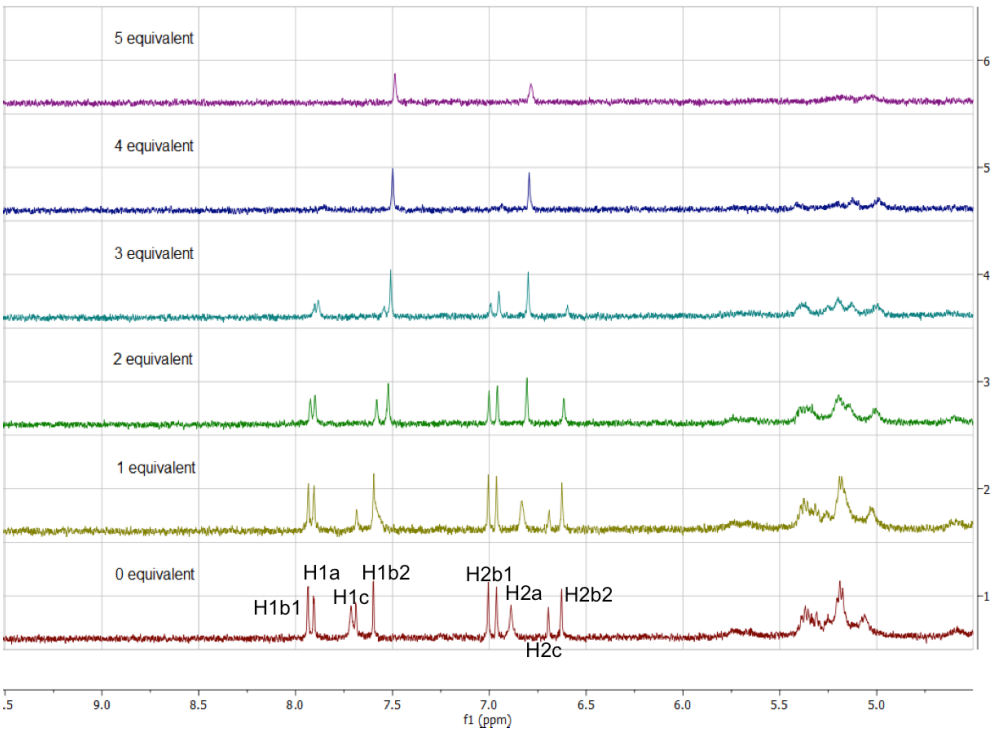

Figure 6.19 Stack plot showing the ^{1}H NMR spectrum of compound **6.10** in CD_3CN in the presence of fluoride ion as tetrabutylammonium salt.

The same pattern has been obtained from the titration experiment of complex **6.10** with acetate (Figure 6.20). This is possibly due to the basic nature of fluoride and acetate ion that allow acid-base reaction to occur.

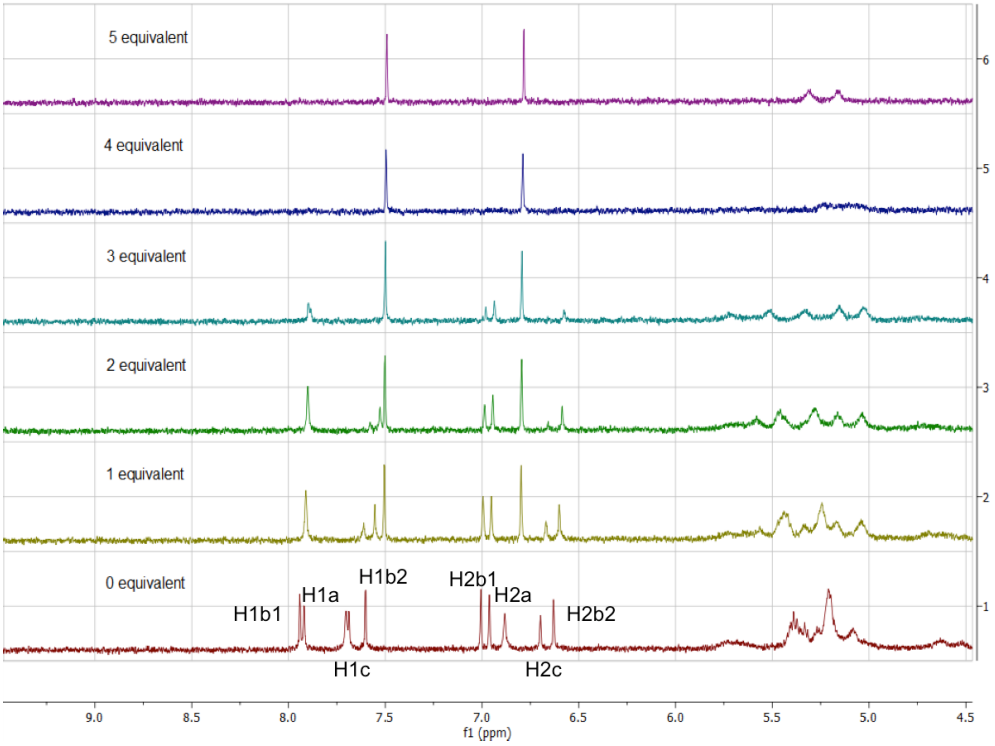

Figure 6.20 Stack plot showing the ^{1}H NMR spectrum of compound **6.10** in CD_3CN in the presence of acetate ion as tetrabutylammonium salt.

Anion binding studies were also performed on complex **6.11** in DMSO-d_6 since complex **6.11** is partially soluble in CD_3CN. Complex **6.11** was titrated with three anions; fluoride, chloride and acetate as tetrabutylammonium salts. The titration experiment was performed only until 1.5 equivalent as complex **6.11** does not show any response to the addition of these anions (Figure 6.21 – 6.23). This could be the result of using a more competitive solvent, DMSO-d_6 that hinders the interaction between the complex and the anions.

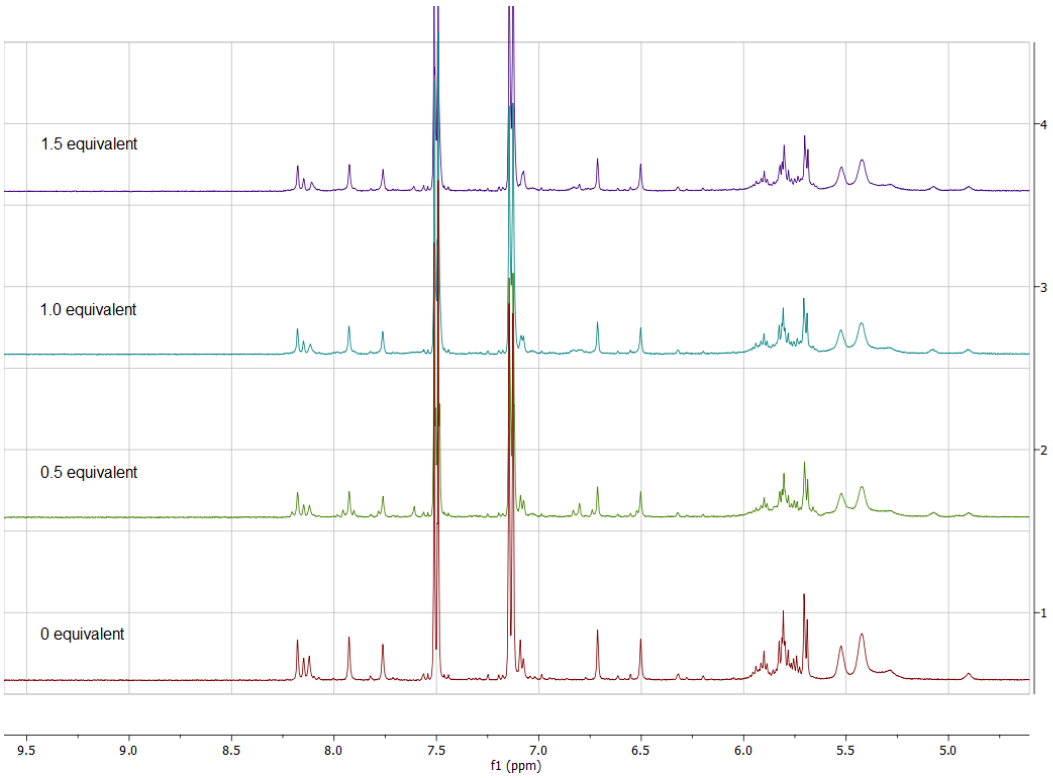

Figure 6.21 Stack plot showing the ^{1}H NMR spectrum of complex **6.11** in DMSO-d_6 in the presence of chloride ion as tetrabutylammonium salt

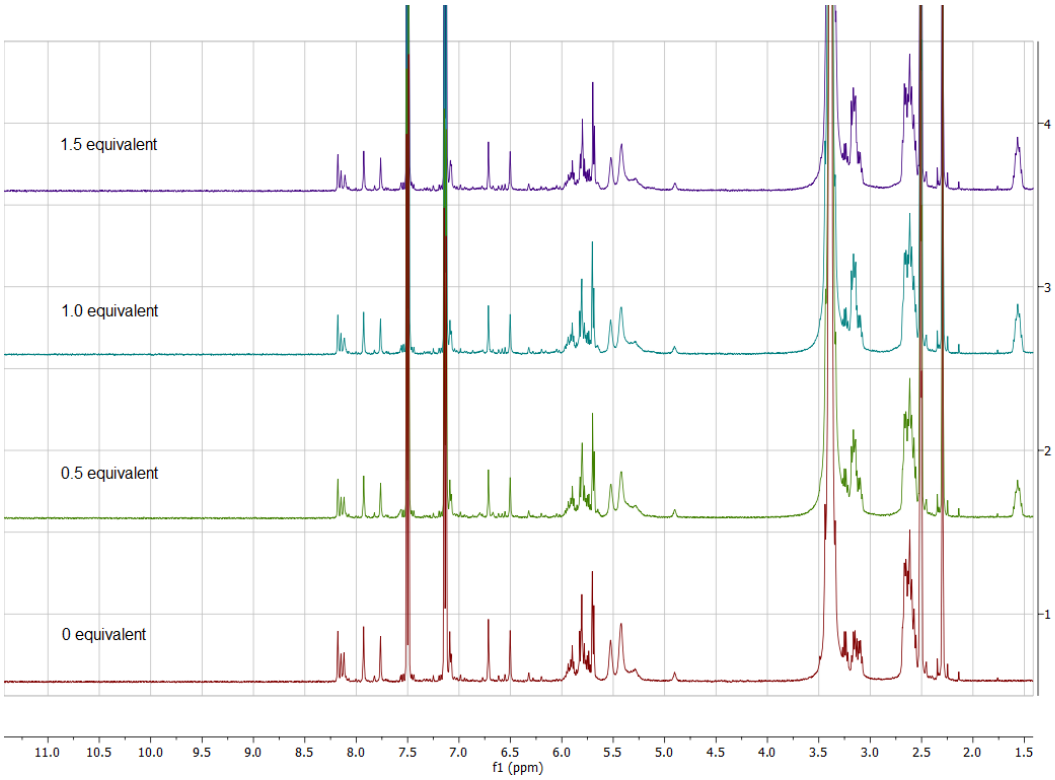

Figure 6.22 Stack plot showing the ^{1}H NMR spectrum of complex **6.11** in DMSO-d_6 in the presence of fluoride ion as tetrabutylammonium salt

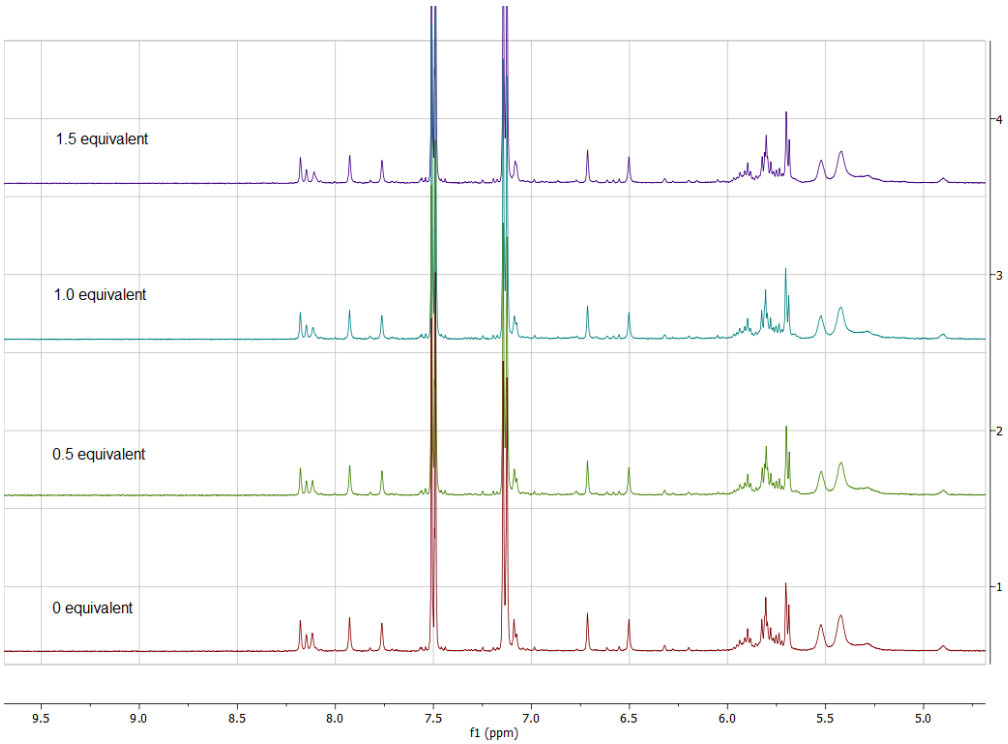

Figure 6.23 Stack plot showing the ^{1}H NMR spectrum of complex **6.11** in DMSO-d_6 in the presence of acetate ion as tetrabutylammonium salt.

6.3 Summary

A series of Pt(II) and Pd(II) complexes, **6.9** – **6.12** have been synthesised from the reaction of [Pt(en)Cl_2] with ligand **2.1**, Pt(cyclohexanediamine)Cl_2 with ligand **2.1**, [Pd(en)Cl_2] with ligand **2.8** and [Pd(dppe)Cl_2] with ligand **2.8**, respectively. ^{1}H DOSY NMR experiments have confirmed the presence of oligomers in complex **6.9** and **6.10**. In acetonitrile solution complex **6.9** exists as a mixture of monomer, dimer, trimer and tetramer. Meanwhile, DOSY NMR data suggests that complex **6.10** comprises of larger size oligomers; trimer, pentamer and heptamer although these are not observed by mass spectrometry. On the other hand, the presence of oligomers in complex **6.11** and **6.12** cannot be proved since both of the complexes are only partially soluble in acetonitrile and hence cannot be studied by DOSY NMR spectroscopy. It is suggested that the aggregation observed in these complexes is driven by metallophilic interactions, hydrogen bonding interaction and π-π stacking.

Anion binding studies have been performed on complex **6.9**, **6.10** and **6.11** towards three anions; chloride, fluoride and acetate as tetrabutylammonium in CD_3CN and

DMSO-d_6 (only for complex **6.11**), respectively. Complex **6.9** has been found to interact with fluoride and acetate ion through deprotonation mechanism but was not responsive towards chloride ion. Complex **6.10** also interacts with fluoride and acetate ion in the same manner as complex **6.9**. In contrast, complex **6.11** does not respond to all three anions. In a nutshell, these complexes might not be suitable for anion sensing, at least in competitive solvents but the aggregation behaviour of these complexes might be interesting for other application such as in the development of supramolecular gelators or photoluminescence materials.

6.4 Experimental

All solvents used in the synthesis and purification were of analytical reagent grade. Anhydrous solvents were prepared on an SPS solvent purification system. Commercial reagents were used as supplied, without further purification.

6.4.1 Instrumentation and Analytical Measurements

All NMR spectra were obtained from a Bruker Avance 400 at a frequency of 400 MHz for ^{1}H and 100 MHz for ^{13}C, while ^{1}H, ^{13}C, ^{1} H-^{1} H COSY, ^{1}H-^{1} C HSQC and ^{1}H-^{13}C HMBC spectra were obtained from a Varian INOVA 500 spectrometer at a frequency of 500 MHz for ^{1}H and 125 MHz for ^{13}C. All chemical shifts are reported in parts per million (δ) relative to tetramethylsilane as an internal reference. Electrospray ionisation (ESI) mass spectrometry was recorded on a TQD mass spectrometer instrument. Fourier transforms infrared spectra were recorded with a Perkin-Elmer Spectrum 100 FT-IR spectrometer in which for each spectrum, 64 scans were conducted over a spectral range of 4000 to 600 cm^{-1} with a resolution of 4 cm^{-1}. Elemental analysis was performed using an Exeter Analytical CE-400 Elemental Analyser.

6.4.2 General Procedure for ^{1}H NMR Spectroscopic Titrations

All chemical shifts are reported in ppm relative to residual solvent, DMSO-d_6. A solution of the host species of known concentration typically 0.5-1.5mM, was made up in an NMR tube using the appropriate deuterated DMSO (0.5 ml). Solutions of the anions, as TBA salts (1 ml) were made ten times the concentration of the host solution. The guest solution was typically added in 10 µl aliquots, representing 1 equivalents of the guest with respect to the host. Larger aliquots were used in some cases where no inflection of the trace was evident. Spectra were recorded after each addition and the trace was followed simultaneously.

6.4.3 Synthesis of the Platinum(II) and Palladium(II) complexes

Synthesis of [Pt(ethylenediamine)Cl_2] (**6.5**)

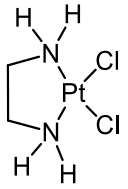

To a solution of K_2PtCl4 (3.688 g, 8.85 mmol) in 0.01 M HCl solution (60 mL), a solution of ethylene diamine (0.6 mL, 8.85 mmol) in 0.01 M HCl (60 mL) was added. The mixture was then stirred for 12 h at 55-60 °C under reflux. After 2 h, a yellow-green solid started to precipitate. The solution was allowed to cool, and the compound formed, [Pt(en)Cl_2], was filtered off, washed carefully with small amounts of water, ethanol, and diethyl ether, and dried under vacuum to give analytically pure material. Yield: 275 mg (0.894 mmol, 73%). Anal. Calcd for $C_2H_8Cl_2N_2Pt$: C, 7.36; H, 2.47; N, 8.59. Found: C, 7.35; H, 2.47; N, 8.62.

Synthesis of [Pt(cyclohexanediamine)Cl_2] (**6.6**)

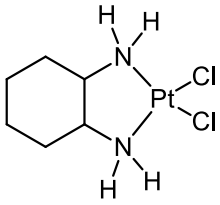

To a solution of K_2PtCl4 (3.688 g, 8.85 mmol) in 0.01 M HCl solution (60 mL), a solution of cyclohexane diamine (0.6 mL, 8.85 mmol) in 0.01 M HCl (60 mL) was added. The mixture was then stirred for 12 h at 55-60 °C under reflux. After 2 h, a yellow-green solid started to precipitate. The solution was allowed to cool, and the compound formed, [Pt(cyclohexanediamine)Cl_2], was filtered off, washed carefully with small amounts of water, ethanol, and diethyl ether, and dried under vacuum to give analytically pure material. Yield: 2.74 g (8.4 mmol, 95%). Anal. Calcd for $C_6H_{14}Cl_2N_2Pt$: C, 18.96; H, 7.31; N, 7.37. Found: H, 18.93; C, 3.67; N, 7.32.

Synthesis of [Pd(ethylenediamine)Cl_2] (**6.7**)

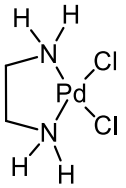

To a solution of K_2PdCl4 (2.614 g, 8 mmol) in 0.1 M HCl solution (25 mL), a solution of ethylenediamine (0.58 mL, 8 mmol) in 0.05 M HCl (150 mL) was added. The mixture was then stirred for 1 h at 62 °C under reflux. After 1 h, a yellow-orange precipitate was obtained. The solution was allowed to cool, and the compound formed, [Pd(ethylenediamine)Cl_2], was filtered off, washed carefully with small amounts of water, ethanol, and diethyl ether, and dried under vacuum to give analytically pure material. Yield: 0.83 g (7 mmol, 87%). Anal. Calcd for $C_2H_8Cl_2N_2Pd$: C, 10.12; H, 3.40; N, 11.80. Found: H, 10.12; C, 3.36; N, 11.71.

Synthesis of [Pd(1,2-Bis(diphenylphosphino)ethane)Cl_2] (**6.8**)

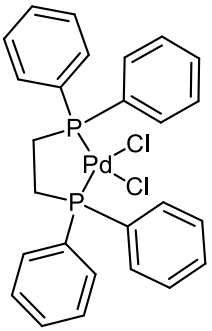

To a solution of K_2PdCl4 (1.62 g, 4.96 mmol) in concentrated HCl solution (60 mL), a solution of 1,2-Bis(diphenylphosphino)ethane (2 g, 4.96 mmol) in ethanol (40 mL) was added. The mixture was then stirred for 6 h at 90 °C under reflux. After 6 h, a light yellow precipitate was obtained. The solution was allowed to cool, and the compound formed, [Pd(1,2-Bis(diphenylphosphino)ethane)Cl_2], was filtered off, washed carefully with small amounts of water, ethanol, and diethyl ether, and dried under vacuum to give analytically pure material. Yield: 2.43 g (4.22 mmol, 85%). Anal. Calcd for $C_{26}H_{24}Cl_2P_2Pd$: C, 54.24; H, 4.20. Found: C, 54.24; H, 4.17.

Synthesis of of [(ethylenediamine)Pt(1-[2-(1*H*-imidazol-4-yl)ethyl]-3-(4-butyl)urea)$_2$].2$CF_3SO_3^-$ (**6.9**)

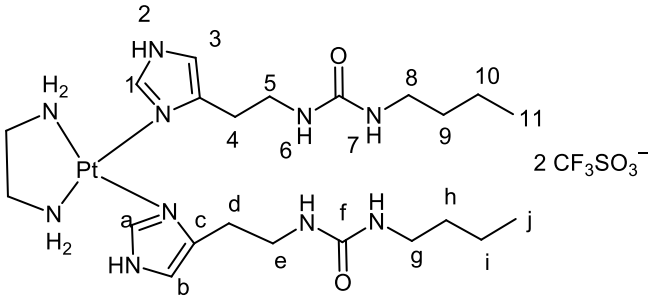

Formation of the [(ethylenediamine)Pt(CF_3SO_3)$_2$] intermediate was achieved via by stirring compound **6.1** (0.81 g, 2.5 mmol) with silver trifluoromethanesulfonate (0.64 g, 2.5 mmol) for 2 hours in methanol (100 mL) in the dark at room temperature. AgCl precipitate formed was removed by filtration over celite. The yellow filtrate was then degassed for 2 hours before subsequent addition of 1-[2-(1*H*-imidazol-4-yl)ethyl]-3-(4-butyl)urea (0.53 g, 2.5 mmol). The mixture was then stirred and heated to 70 ^oC for 3 days. Cooling and removal of the solvent led to the formation of the product as a brown viscous liquid. (1.27 g, 1.88 mmol, 75%). **^{1}H NMR:** δ_H (400 MHz; DMSO-d_6;

Me_4Si) 12.64 (1 H, br s, *H2*), 8.47 (1 H, d, *J* 1.1, *H1*), 6.40 (1 H, s, *H3*), 5.84 (1 H, t, *J* 5.6, *H6*), 5.74 (1 H, t, *J* 5.6, *H7*), 3.17 (2 H, m, *H5*), 3.02 (2 H, m, *H8*), 2.52 (2 H, t, *J* 7.1 *H4*), 1.12 (2 H, m, *H9*), 1.06 (2 H, m, *H10*) , 0.65 (3 H, t, *J* 8.0, *H11*). **^{13}C {^{1}H} NMR:** δ_C {^{1}H} (101 MHz; DMSO) 158.50 (*Cf*), 138.37 (*Ca*), 38.76 (*Cc*), 39.36 (*Cb*), 32.59 (*Ce* and *Cg*), 32.53 (*Cd*), 19.95 (*Ch* and *Ci*), 14.18 (*Cj*). **FTIR:** ν_{max}/cm^{-1} 3371 (NH), 1654 (CO), 1599 and 1432 (imid. ring), m/z (ESI-MS) 337.88 [(M-2(CF_3SO_3)$^-$)/2 + H$^+$]$^+$, m/z (HRMS) 337.88 [(M-2(CF_3SO_3)$^-$)]$^{2+}$. Anal. Calcd for $C_{24}H_{44}F_6N_{10}O_8PtS_2$: C, 29.60; H, 4.55; N, 14.38. Found: H, 29.99; C, 4.59; N, 14.24.

Synthesis of [(cyclohexanediamine)Pt(1-[2-(1*H*-imidazol-4-yl)ethyl]-3-(4-butyl) urea)$_2$].2$CF_3SO_3^-$ (**6.10**)

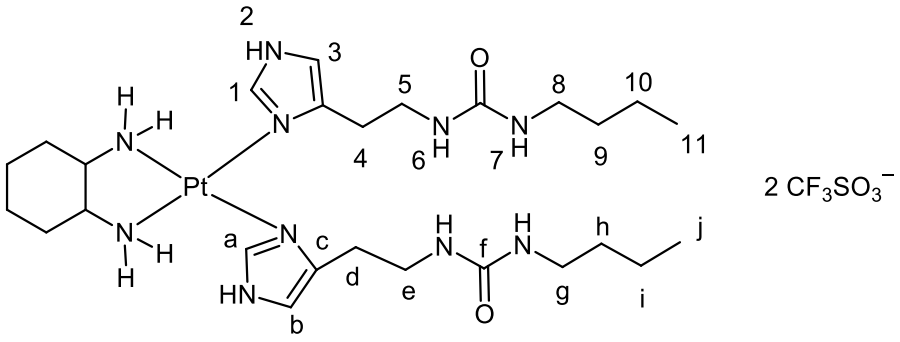

Formation of the [(cyclohexanediamine)Pt(CF_3SO_3)$_2$] intermediate was achieved via by stirring compound **6.2** (0.95 g, 2.5 mmol) with silver trifluoromethanesulfonate (0.81 g, 2.5 mmol) for 2 hours in methanol (100 mL) in the dark at room temperature. AgCl precipitate formed was removed by filtration over celite. The yellow filtrate was then degassed for 2 hours before subsequent addition of 1-[2-(1*H*-imidazol-4-yl)ethyl]-3-(4-butyl)urea (0.53 g, 2.5 mmol). The mixture was then stirred and heated to 70 ^{o}C for 3 days. Cooling and removal of the solvent led to the formation of the crude product as an brown solid (1.25 g, 1.7 mmol, 68%). **^{1}H NMR:** δ_H (400 MHz; DMSO-d_6; Me_4Si) 12.64 (1 H, br s, *H2*), 8.47 (1 H, d, *J* 1.1, *H1*), 6.40 (1 H, s, *H3*), 5.84 (1 H, t, *J* 5.6, *H6*), 5.74 (1 H, t, *J* 5.6, *H7*), 3.17 (2 H, m, *H5*), 3.02 (2 H, m, *H8*), 2.52 (2 H, t, *J* 7.1 *H4*), 1.12 (2 H, m, *H9*), 1.06 (2 H, m, *H10*) , 0.65 (3 H, t, *J* 8.0, *H11*). **^{13}C {^{1}H} NMR:** δ_C {^{1}H} (101 MHz; DMSO) 158.50 (*Cf*), 138.37 (*Ca*), 38.76 (*Cc*), 39.36 (*Cb*), 32.59 (*Ce* and *Cg*), 32.53 (*Cd*), 19.95 (*Ch* and *Ci*), 14.18 (*Cj*). **FTIR:** ν_{max}/cm^{-1} 3372 (NH), 1655 (CO), 1599 and 1496 (imid. ring), m/z (ESI-MS) 364.68 [(M-2($CF_3SO_3^-$)]$^{2+}$m/z (HRMS) 364.68 [(M-

$2(CF_3SO_3)^-)/2 + H^+]^+$. Anal. Calcd for $C_{28}H_{50}F_6N_{10}O_8PtS_2 \cdot 2CH_3CN$: C, 34.62; H, 5.08; N, 15.14. Found: H, 34.45; C, 5.13; N, 14.17.

Synthesis of [(cyclohexanediamine)Pd(1-[2-(1*H*-imidazol-4-yl)ethyl]-3-(4-tert-butyl)urea)$_2$]. $2CH_3C_6H_4SO_3^-$ (**6.11**)

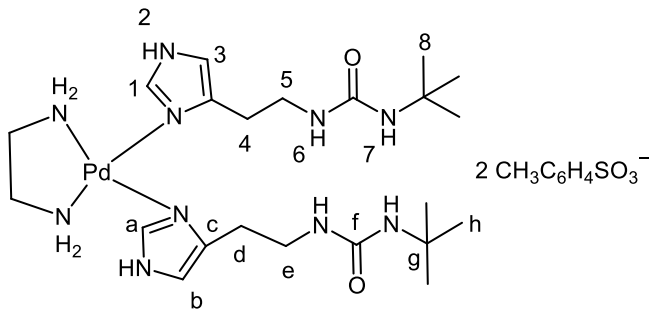

Formation of the [(ethylenediamine)Pt$(CF_3SO_3)_2$] intermediate was achieved via by stirring compound **6.3** (0.81 g, 2.5 mmol) with silver tosylate (0.70 g, 2.5 mmol) for 2 hours in methanol (100 mL) in the dark at room temperature. AgCl precipitate formed was removed by filtration over celite. The yellow filtrate was then degassed for 2 hours before subsequent addition of 1-[2-(1*H*-imidazol-4-yl)ethyl]-3-(4-tert-butyl)urea (0.53 g, 2.5 mmol). The mixture was then stirred and heated to 70 ^oC for 24 h. Cooling and removal of the solvent led to the formation of the product as a beige solid (1.85 g, 1.8 mmol, 72%). **^{1}H NMR:** δ_H (400 MHz; DMSO-d_6; Me_4Si) 12.64 (1 H, br s, *H2*), 8.47 (1 H, d, *J* 1.1, *H1*), 6.40 (1 H, s, *H3*), 5.84 (1 H, t, *J* 5.6, *H6*), 5.74 (1 H, t, *J* 5.6, *H7*), 3.17 (2 H, m, *H5*), 3.02 (2 H, m, *H8*), 2.52 (2 H, t, *J* 7.1 *H4*), 1.12 (2 H, m, *H9*), 1.06 (2 H, m, *H10*) , 0.65 (3 H, t, *J* 8.0, *H11*). **^{13}C {^{1}H} NMR:** δ_C {^{1}H} (101 MHz; DMSO) 158.50 (*Cf*), 138.37 (*Ca*), 38.76 (*Cc*), 39.36 (*Cb*), 32.59 (*Ce* and *Cg*), 32.53 (*Cd*), 19.95 (*Ch* and *Ci*), 14.18 (*Cj*). **FTIR:** ν_{max}/cm^{-1} 3383 (NH), 1655 (CO), 1599 and 1496 (imid. ring), Anal. Calcd for $C_{36}H_{58}O_8N_{10}PdS_2 \cdot 2H_2O$: C, 44.78; H, 6.47; N, 14.51. Found: H, 44.58; C, 6.11; N, 14.09.

Synthesis of of [(1,2-Bis(diphenylphosphino)ethane)Pd(1-[2-(1*H*-imidazol-4-yl)ethyl]-3-(4-tert-butyl)urea)$_2$]. 2$CH_3C_6H_4SO_3^-$ (**6.12**)

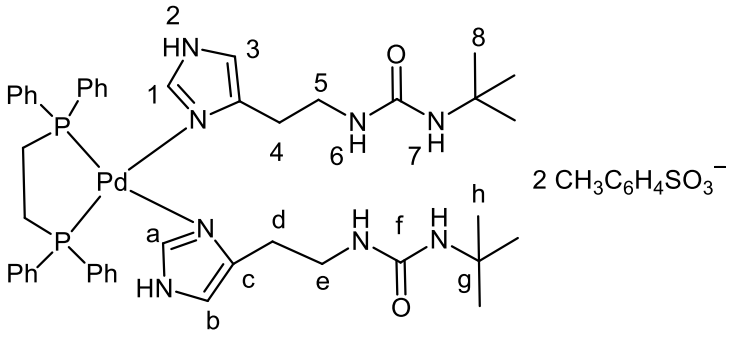

Formation of the [(1,2-bis(diphenylphosphino)ethane)Pt] $(CF_3SO_3)_2$ intermediate was achieved via by stirring compound **6.4** (1.4 g, 2.5 mmol) with silver tosylate (0.69 g, 2.5 mmol) for 2 hours in methanol (100 mL) in the dark at room temperature. AgCl precipitate formed was removed by filtration over celite. The yellow filtrate was then degassed for 2 hours before subsequent addition of 1-[2-(1*H*-imidazol-4-yl)ethyl]-3-(4-tert-butyl)urea (g, 2.5 mmol). The mixture was then stirred and heated to 70 ^oC for 24 h. Cooling and removal of the solvent led to the formation of the product as a beige solid. (1.95 g, 1.55 mmol, 62%). **^{1}H NMR:** δ_H (400 MHz; DMSO-d_6; Me_4Si) 12.64 (1 H, br s, *H2*), 8.47 (1 H, d, *J* 1.1, *H1*), 6.40 (1 H, s, *H3*), 5.84 (1 H, t, *J* 5.6, *H6*), 5.74 (1 H, t, *J* 5.6, *H7*), 3.17 (2 H, m, *H5*), 3.02 (2 H, m, *H8*), 2.52 (2 H, t, *J* 7.1 *H4*), 1.12 (2 H, m, *H9*), 1.06 (2 H, m, *H10*) , 0.65 (3 H, t, *J* 8.0, *H11*). **^{13}C {^{1}H} NMR:** δ_C {^{1}H} (101 MHz; DMSO) 158.50 (*Cf*), 138.37 (*Ca*), 38.76 (*Cc*), 39.36 (*Cb*), 32.59 (*Ce* and *Cg*), 32.53 (*Cd*), 19.95 (*Ch* and *Ci*), 14.18 (*Cj*). **FTIR:** ν_{max}/cm^{-1} 3371 (NH), 1652 (CO), 1597 and 1436 (imid. ring), Anal. Calcd for $C_{60}H_{74}O_8N_8P_2PdS_2 \cdot 2H_2O$: C, 55.27; H, 6.03; N, 8.59. Found: H, 55.18; C, 5.87; N, 8.49.

6.5 References

(1) Rourke, J.; Overton, T.; Weller, M.; Armstrong, F. *Inorganic Chemistry*; 7th Editio.; Oxford Uiversity Press: New York, 2018.

(2) Chung, C. Y. S.; Yam, V. W. W. *Chem. Eur. J.* **2014**, *20*, 13016–13027.

(3) Yam, V. W.-W.; Au, V. K.-M.; Leung, S. Y.-L. *Chem. Rev.* **2015**, *115*, 7589–7728.

(4) Mauro, M.; Aliprandi, A.; Septiadi, D.; Kehr, N. S.; De Cola, L. *Chem. Soc. Rev.* **2014**, *43*, 4144–4166.

(5) Strassert, C. A.; Mauro, M.; De Cola, L. *Adv. Inorg. Chem* **2011**, *63*, 47–103.

(6) Fu, T. F.; Ao, L.; Gao, Z. C.; Zhang, X. L.; Wang, F. *Chin. Chem. Lett.* **2016**, *27*, 1147–1154.

(7) Robinson, M. E.; Nazemi, A.; Lunn, D. J.; Hayward, D. W.; Boott, C. E.; Hsiao, M. S.; Harniman, R. L.; Davis, S. A.; Whittell, G. R.; Richardson, R. M.; De Cola, L.; Manners, I. *ACS Nano* **2017**, *11*, 9162–9175.

(8) Yam, V. W. W.; Wong, K. M. C.; Zhu, N. *J. Am. Chem. Soc.* **2002**, *124*, 6506–6507.

(9) Yam, V. W. W.; Chan, K. H. Y.; Wong, K. M. C.; Zhu, N. *Chem. Eur. J.* **2005**, *11*, 4535–4543.

(10) Zhang, X.; Wright, A. M.; Deyonker, N. J.; Hollis, T. K.; Hammer, N. I.; Webster, C. E.; Valente, E. J. *Organometallics* **2012**, *31*, 1664–1672.

(11) Mayo, E. I.; Kilsa, K.; Tirrell, T.; Djurovich, P. I.; Tamayo, A.; Thompson, M. E.; Lewis, N. S.; Gray, H. B. *Photochem. Photobiol. Sci.* **2006**, *5*, 871–873.

(12) Helgesen, M.; Sondgaard, R.; Krebs, F. C. *J. Mater. Chem* **2010**, *20*, 36–60.

(13) Chakraborty, S.; Wadas, T. J.; Hester, H.; Schmehl, R.; Eisenberg, R. *Inorg. Chem.* **2005**, *44*, 6865–6878.

(14) Hambourger, M.; Moore, G. F.; Kramer, O. M.; Gust, D.; Moore, A. L.; Moore, T. A. *Chem. Soc. Rev.* **2009**, *38*, 25–35.

(15) Bauer, R.; Finkenzeller, W. J.; Bogner, U.; Thompson, M. E.; Yersin, H. *Org. Electron* **2008**, *9*, 641–648.

(16) Zhong, C. M.; Duan, C. H.; Huang, F.; Wu, H. B.; Cao, Y. *Chem. Mater.* **2011**, *23*, 326–340.

(17) Pastor, A.; Martínez-Viviente, E. *Coord. Chem. Rev.* **2008**, *252*, 2314–2345.

(18) Kotze, I. A.; Gerber, W. J.; Wu, Y.-S.; Koch, K. R. *Dalton Trans.* **2013**, *42*, 3791–3801.

(19) Zapata, F.; Caballero, A.; White, N. G.; Claridge, T. D. W.; Costa, P. J.; Félix, V.; Beer, P. D. *J. Am. Chem. Soc.* **2012**, *134*, 11533–11541.

(20) Avram, L.; Cohen, Y. *Chem. Soc. Rev.* **2015**, *44*, 586–602.

(21) Barnard, A.; Dickson, S. J.; Paterson, M. J.; Todd, A. M.; Steed, J. W. *Org. Biomol. Chem.* **2009**, *7*, 1554–1561.

(22) Zheng, Y.-R.; Suntharalingam, K.; Johnstone, T. C.; Lippard, S. J. *Chem. Sci.* **2014**, *6*, 1189–1193.

(23) Megyes, T.; Jude, H.; Grosz, T.; Bako, I.; Radnai, T.; Tarkanyi, G.; Palinkas, G.; Stang, P. J. *J. Am. Chem. Soc.* **2005**, *127*, 10731–10738.

(24) Annanikov, V. P.; Zalessky, S. S.; Kachala, V. V.; Beletskaya, I. P. *J. Organomet. Chem.* **2011**, *699*, 400–405.

(25) He, X.; Herranz, F.; Cheng, E. C.-C.; Vilar, R.; Yam, V. W.-W. *Chem. Eur. J.* **2010**, *16*, 9123–9131.

(26) Yu, S.-Y.; Fujita, M.; Yamaguchi, K. *J. Chem. Soc. Dalt. Trans.* **2001**, *105*, 3415–3416.

(27) Evans, R.; Deng, Z.; Rogerson, A. K.; McLachlan, A. S.; Richards, J. J.; Nilsson, M.; Morris, G. A. *Angew. Chem.* **2013**, *52*, 3199–3202.

(28) Ray, S.; Das, A. *J. Mol. Struct.* **2015**, *1089*, 146–152.

(29) Yu-Lut Leung, S.; Wing-Wah Yam, V. *Chem. Sci.* **2013**, *4*, 4228.

(30) Sluch, I. M.; Miranda, A. J.; Elbjeirami, O.; Omary, M. A.; Slaughter, L. M. *Inorg. Chem.* **2012**, *51*, 10728–10746.

(31) Sabounchei, S. J.; Ahmadi, M.; Nasri, Z.; Shams, E.; Salehzadeh, S.; Gholiee, Y.; Karamian, R.; Asadbegy, M.; Samiee, S. *Comptes Rendus Chim.* **2013**, *16*, 159–175.

(32) Juwarker, H.; Lenhardt, J. M.; Castillo, J. C.; Zhao, E.; Krishnamurthy, S.; Jamiolkowski, R. M.; Kim, K. H.; Craig, S. L. *J. Org. Chem.* **2009**, *74*, 8924–8934.

Chapter 7

Conclusion

The main aims of this work were to synthesise novel imidazole urea-based anion receptor compounds using both organic and transition metal cores. A series of imidazole urea ligands, comprising of different terminal groups ranging from aliphatic, branched and aromatic groups have been synthesised and characterised. Imidazole urea was chosen due to the availability of its cation binding site (imidazole nitrogen) and anion binding site (urea NH) that allows the interaction of these compounds with transition metal ions such as Cu(II), Co(II), Ni(II), Ag(I), Ru(II), Pt(II) and Pd(II) and anions such as halides, nitrate, acetate and benzoate. In Chapter 2, free imidazole urea ligands have been shown to form complexes in unidentate fashion with Cu(II), Co(II) and Ni(II). Crystal structures of these complexes also suggested that the anions such as chloride from the metal salts used form hydrogen bonds with the urea NH groups which influence how the molecules are packed. Halide binding experiments on the imidazole urea ligands show that the anion binding behaviour of these ligands was influenced by urea conformation along with imidazole tautomerism. Titration of ligands **2.6** and **2.7** (imidazole urea bearing aromatic terminal group) with halide ions suggests the presence of isomers in which one of the isomers responds to the halide ion while the other one does not. This behaviour, however was only seen in imidazole urea bearing aromatic group but not in imidazole urea with aliphatic terminal groups. The ability of these compounds to interact with cations and anions has led us to use these compounds as metal and anion binding sites in synthesising preorganised anion receptor compounds based on organic and metal-organic scaffolds.

In Chapter 3, these imidazole ureas have been reacted with silver salts of different counter ions such as silver(I) nitrate, silver(I) hexafluorophosphate, silver(I) tetrafluoroborate and silver(I) perchlorate. When silver(I) salts (except silver(I) nitrate) were added to the solution of 10 mg of ligand **2.3** (imidazole urea with dodecyl group) in 0.5 mL THF, THF: H_2O (8:2), THF: H_2O (7:3) and DMSO, after brief heating and sonicate, the solution turned into a gel instantaneously. The formation of a gel could be facilitated by the symmetrical hydrogen bonding between complexes as well as van der Waals

interactions of the hydrophobic alkyl chains. The obtained gel is not thermoreversible but it is stable for a period of weeks as long as it is stored in the dark. However, upon exposure to light, silver nanoparticles form as evidenced by a UV-Vis absorption band that develops at around 430 nm corresponded to typical surface plasmon absorption of silver nanoparticles. Addition of anions such as Cl^-, Br^-, NO_3^-, acetate, HSO_4^-, $H_2PO_4^-$ and oxalate interrupts the hydrogen bonding between the urea thus induced the transition from gel to solution.

In Chapter 4, a series of preorganised hosts have been prepared using triethylbenzene and mesitylcalixarene cores. Titration of one of the tripodal hosts, **4.2** prepared using ligand **2.3** with chloride ion (as the tetrabutylammonium salt) in DMSO-d_6 did not cause any significant changes to the chemical shift of the urea protons NH3 and NH4 although the free ligand itself, **2.3** shows moderate binding to the urea NH in CD_3CN. In contrast, when titrated with fluoride and acetate ions in DMSO-d_6, tripodal host, **4.2** showed colour changes of the solution from yellow to pink suggesting the deprotonation of imidazole protons, H1 and H2 by these strongly basic anions. A similar observation was also recorded for tripodal host **4.3** suggesting that this system might not be a suitable system for anion sensing, at least not in a competitive solvent. Another organic-based host, **4.6** based on a mesitylcalixarene core does not show any interaction with chloride, acetate and nitrate ions (as tetrabutylammonium salts). However, when the tetrabutylammonium salts were replaced with zinc salts, such as zinc(II) chloride, zinc(II) acetate and zinc(II) nitrate, there are some changes in the chemical shift of imidazole and urea protons observed in the ^1H NMR spectra. A plausible explanation for this result could be that when the zinc metal coordinates to the imidazole nitrogen atom, while the anions of the salt disrupt the hydrogen-bonding network formed by the imidazole moiety.

Apart from organic-based hosts, transition metal-based hosts have also been prepared using Ru(II), Pt(II) and Pd(II) precursors (Chapters 5 and 6). Three [9]ane-S_3-capped Ru(II) complexes of imidazole ureas, **5.1**-**5.3** have been synthesised and characterised. The interaction of these complexes with anions such as chloride, fluoride, acetate, benzoate

and hydrogen sulphate ions have been studied using ^{1}H NMR spectroscopy in DMSO-d_6. Complex **5.2** containing a dodecyl terminal group only responds to basic anions such as fluoride, acetate and benzoate. Addition of fluoride induces deprotonation of complex **5.2**, while the addition of acetate and benzoate separates the proton NMR signals into two different sets, in which one set shows a response to the ions while the other does not. In contrast, complex **5.3** with a methylphenyl terminal group, only interacts with chloride and fluoride ion. Chloride ions form hydrogen bonding with the urea NH while fluoride ion deprotonates the urea NH. The results suggest that these complexes too might not be suitable for anion sensing purposes at least in a competitive solvent such as DMSO-d_6.

On the other hand, a series of Pt(II) and Pd(II) complexes, **6.9** – **6.12** have been synthesised from the reaction of [Pt(en)Cl_2] with ligand **2.1**, Pt(cyclohexanediamine)Cl_2 with ligand **2.1**, [Pd(en)Cl_2] with ligand **2.8** and [Pd(dppe)Cl_2] with ligand **2.8**, respectively. Complexes **6.9** and **6.10** have been shown to form a mixture of oligomers, evidence from the ^{1}H DOSY NMR spectra. Complex **6.9** self-assembles in acetonitrile solution forming monomer, dimer, trimer and tetramer while complex **6.10** self-assembled and formed larger oligomers; trimer, pentamer and heptamer. Complex **6.11** also shows different sets of proton NMR signals which might result from oligomerisation although this behaviour was not confirmed by ^{1}H DOSY NMR. The aggregation observed in these complexes could possibly be driven by metallophilic interactions, hydrogen bonding interaction and π-π stacking. The interaction of complex **6.9** - **6.11** with chloride, fluoride and acetate ions was studied using ^{1}H NMR spectroscopy in CD_3CN (for complex **6.9** and **6.10**) and DMSO-d_6 (for complex **6.11**). The result shows that complexes **6.9** and **6.10** only interact with fluoride and acetate ion through deprotonation mechanism but were not responsive towards chloride ion, while complex **6.11** does not interact with any of the three ions studied.